UNIVERSITY OF SOUTHAMPTON

TIME DOMAIN SIMULATION OF SHIP MOTIONS IN WAVES

EDWARD JOHN BALLARD

A THESIS SUBMITTED FOR THE DEGREE OF
DOCTOR OF PHILOSOPHY

THE FACULTY OF ENGINEERING AND APPLIED SCIENCE,

SCHOOL OF ENGINEERING SCIENCES,

SHIP SCIENCE.

April 2002

UNIVERSITY OF SOUTHAMPTON

ABSTRACT

FACULTY OF ENGINEERING AND APPLIED SCIENCE
SCHOOL OF ENGINEERING SCIENCES,
SHIP SCIENCE

Doctor of Philosophy

TIME DOMAIN SIMULATION OF SHIP MOTIONS IN WAVES

by Edward John Ballard.

A time domain mathematical model is presented for the prediction of ship motions in waves. This mathematical model incorporates convolution integrals, allowing fluid memory effects to be included in the modelling of ship responses to arbitrary excitation. The required impulse response functions are calculated from transforms of frequency domain data evaluated using a three dimensional potential flow analysis. The wave excitation impulse response functions include a negative time component, accounting for the influence of a particular wave before it reaches the reference point at midships.

Impulse response functions are calculated with reference to both equilibrium and body fixed axis systems. Using reverse transforms, it is shown that certain frequency domain data, referenced to equilibrium axes, appears to be unsuitable for the calculation of impulse response functions. To test the effects of using impulse response functions referenced to either axis system, time domain simulations are performed using equations of motion referenced to both axis systems. Comparisons with frequency domain predictions show that the numerical implementation of the model referenced to body fixed axes is more accurate.

Subsequently, non-linear incident wave and restoring force/moment contributions are included in the mathematical model referenced to body fixed axes. These contributions are accounted for by considering the instantaneous underwater portion of the hull at each time step of the simulations. Predictions for this partly non-linear model are compared to both linear predictions and experimental models for a range of wave amplitudes. A number of vessel types are considered, including vessels with flared hull forms and multihulls.

Contents

List of Tables

List Of Figures

Acknowledgements

My time here would not have been possible without funding from the University, and I am grateful to have been given such an opportunity. My supervisor Professor Penny Temarel has provided valuable assistance during the past three and a bit years. His attention to detail and willingness to match my efforts with his own have been much appreciated.

I must also thank Dr Philip Bailey, especially for putting up with all my questions when I first started. I consider myself lucky to have Phil's assistance for a least part of my time here in Southampton. Thanks also to Dr Dominic Hudson, whos door has always been open, whether for information or a chat. There have been many others within the Ship Science community at the University who have been of assistance and I thank you all.

Of course, these acknowledgements could not go without mentioning my wife Hūia. Her encouragement and patience have been invaluable over the last three years. Never again will I head off to the other side of the world without her!

Big thanks must also go to all of my family in New Zealand, especially my parents. Over the years they have always supported my endeavours, for which I am grateful. Being so far away from one's family is hard and being able come home twice during the past three years has made all the difference.

I also wish to thank all the friends I have made during my time here, especially my friends in the University Canoe Club. There's nothing like a weekend of playing hard to making working hard that much easier.

Notation

$O\xi\eta\zeta$	Equilibrium axis system, origin at O.
A_{ij}	Added mass coefficient in ith direction due to unit motion in the jth mode, referenced to the $O\xi\eta\zeta$ equilibrium axis system.
A^0_{ij}	Zero speed added mass coefficient in ith direction due to unit motion in the jth mode, referenced to the $O\xi\eta\zeta$ equilibrium axis system.
B_{ij}	Damping coefficient in ith direction due to unit motion in the jth mode, referenced to the $O\xi\eta\zeta$ equilibrium axis system.
B^0_{ij}	Zero speed damping coefficient in ith direction due to unit motion in the jth mode, referenced to the $O\xi\eta\zeta$ equilibrium axis system.
$Cxyz$	Body fixed axis system, origin at centre of gravity C.
$CXYZ$	Equilibrium axis system, origin at equilibrium position of centre of gravity C.
C_{ij}	Restoring coefficient in ith direction due to unit motion in the jth mode, referenced to the $O\xi\eta\zeta$ equilibrium axis system.
F_n	Froude number, $F_n = \overline{U}/\sqrt{(Lg)}$.
(F_X, F_Y, F_Z)	External forces acting on ship, referenced to $CXYZ$ equilibrium axis system (N).
g	Acceleration due to gravity, 9.81m/s.
(G_X, G_Y, G_Z)	External moments acting on ship, referenced to $CXYZ$ equilibrium axis system (Nm).

$h_{ij}(\tau)$	ith force/moment impulse response function due to motion in the jth mode, referenced to the $O\xi\eta\zeta$ equilibrium axis system.
$h_{i\alpha}(\tau)$	ith exciting force/moment impulse response function, referenced to the $O\xi\eta\zeta$ equilibrium axis system.
(H_1, H_2, H_3)	External force acting on ship, referenced to $O\xi\eta\zeta$ equilibrium axis system (N).
$(\overline{H}_1, \overline{H}_2, \overline{H}_3)$	External force acting on ship, excluding wave excitation, referenced to $O\xi\eta\zeta$ equilibrium axis system (N).
(H_4, H_5, H_6)	External moment acting on ship, referenced to $O\xi\eta\zeta$ equilibrium axis system (Nm).
$(\overline{H}_4, \overline{H}_5, \overline{H}_6)$	External moment acting on ship, excluding wave excitation, referenced to $O\xi\eta\zeta$ equilibrium axis system (Nm).
$H(i\omega_e)$	Complex transfer function $= H^R(\omega_e) + iH^I(i\omega_e)$.
$(\mathbf{i}, \mathbf{j}, \mathbf{k})$	Unit vectors defined in the $Cxyz$ body fixed axis system.
$(\mathbf{I}, \mathbf{J}, \mathbf{K})$	Unit vectors defined in the $O\xi\eta\zeta$ equilibrium axis system.
$(\mathbf{I_O}, \mathbf{J_O}, \mathbf{K_O})$	Unit vectors defined in the $O_OX_OY_OZ_O$ spatial axis system.
$(\mathbf{I_C}, \mathbf{J_C}, \mathbf{K_C})$	Unit vectors defined in the $CXYZ$ equilibrium axis system.
I_{44},I_{55},I_{66}	Inertia in roll, pitch and yaw, referenced to $Cxyz$ body fixed axis system (kgm^2).
I_{45},I_{46},I_{54}, I_{56},I_{64},I_{65}	Cross products of inertia, referenced to $Cxyz$ body fixed axis system (kgm^2).
I_{XX},I_{YY},I_{ZZ}	Inertia in roll, pitch and yaw, referenced to $CXYZ$ body fixed axis system (kgm^2).
I_{XY},I_{XZ},I_{YX}, I_{YZ},I_{ZX},I_{ZY}	Cross products of inertia, referenced to $CXYZ$ body fixed axis system (kgm^2).
$k_i(\tau)$	Roll impulse response function, referenced to $Cxyz$ body fixed axis system, where i is a motion variable.
$k_\alpha(\tau)$	Roll excitation force impulse response function, referenced to $Cxyz$ body fixed axis system, where i is a motion variable.

$\tilde{K}_i$	Roll oscillatory derivative, where i is a velocity or acceleration, referenced to $Cxyz$ body fixed axis system.
(K, M, N)	External moment acting on ship, referenced to $Cxyz$ body fixed axis system (Nm).
$(\overline{K}, \overline{M}, \overline{N})$	External moment acting on ship, excluding wave excitation, referenced to $Cxyz$ body fixed axis system (Nm).
L	Ship length (m).
LCG	ship length between perpendiculars (m).
m	Mass of the ship (kg).
$m_i(\tau)$	Pitch impulse response function, referenced to $Cxyz$ body fixed axis system, where i is a motion variable.
$m_\alpha(\tau)$	Pitch excitation force impulse response function, referenced to $Cxyz$ body fixed axis system, where i is a motion variable.
$\tilde{M}_i$	Pitch oscillatory derivative, where i is a velocity or acceleration, referenced to $Cxyz$ body fixed axis system.
$n_i(\tau)$	Yaw impulse response function, referenced to $Cxyz$ body fixed axis system, where i is a motion variable.
$n_\alpha(\tau)$	Yaw excitation force impulse response function, referenced to $Cxyz$ body fixed axis system, where i is a motion variable.
$\tilde{N}_i$	Yaw oscillatory derivative, where i is a velocity or acceleration, referenced to $Cxyz$ body fixed axis system.
$O_O X_O Y_O Z_O$	Earth fixed spatial axis system
$(P, Q, R), (p, q, r)$	Angular velocity of ship, referenced to $Cxyz$ body fixed axis system, where lower case refers to small quantities.
S	Wetted surface of hull.
$\overline{S}$	Mean wetted surface of hull.
t	Time (s).
$\overline{U}$	Velocity of the ship (m/s).

(u_X, u_Y, u_Z)	Velocity of the ship, referenced to $CXYZ$ equilibrium axis system (m/s).
$(U, V, W), (u, v, w)$	Velocity of ship, referenced to $Cxyz$ body fixed axis system, where lower case refers to small quantities.
$\mathbf{V}(X_O, Y_O, Z_O)$	Fluid velocity vector, referenced to $O_O X_O Y_O Z_O$ spatial axis system.
$\mathbf{V_s}(X_O, Y_O, Z_O)$	Local velocity of body surface, referenced to $O_O X_O Y_O Z_O$ spatial axis system.
$\overline{W}$	Steady flow velocity of free stream relative to $O\xi\eta\zeta$ equilibrium axis system.
(X, Y, Z)	External force acting on ship, referenced to $Cxyz$ body fixed axis system (N).
$(\overline{X}, \overline{Y}, \overline{Z})$	External force acting on ship, excluding wave excitation, referenced to $Cxyz$ body fixed axis system (N).
(X^*, Y^*, Z^*), (x^*, y^*, z^*)	Position of ship centre of mass relative to the origin of the earth fixed frame, where lower case refers to small quantity.
$x_i(\tau)$	Surge impulse response function, referenced to $Cxyz$ body fixed axis system, where i is a motion variable.
$x_\alpha(\tau)$	Surge excitation force impulse response function, referenced to $Cxyz$ body fixed axis system, where i is a motion variable.
$\tilde{X}_i$	Surge oscillatory derivative, where i is a velocity or acceleration, referenced to the $Cyxz$ body fixed axis system.
$y_i(\tau)$	Sway impulse response function, referenced to $Cxyz$ body fixed axis system, where i is a motion variable.
$y_\alpha(\tau)$	Sway excitation force impulse response function, referenced to $Cxyz$ body fixed axis system, where i is a motion variable.
$\tilde{Y}_i$	Sway oscillatory derivative, where i is a velocity or acceleration, referenced to the $Cxyz$ body fixed axis system.

$z_i(\tau)$	Heave impulse response function, referenced to $Cxyz$ body fixed axis system, where i is a motion variable.
$z_\alpha(\tau)$	Heave excitation force impulse response function, referenced to $Cxyz$ body fixed axis system, where i is a motion variable.
$\tilde{Z}_i$	Heave oscillatory derivative, where i is a velocity or acceleration, referenced to the $Cxyz$ body fixed axis system.
α	Incident wave amplitude (m).
$\overline{\zeta}$	Distance of origin C below origin O (m).
$\overline{\eta}$	Distance of origin C to starboard of origin O (m).
(η_1, η_2, η_3)	Displacement of ship (small quantity), referenced to $O\xi\eta\zeta$ equilibrium axis system (m).
(η_4, η_5, η_6)	Angular displacement of ship (small quantity), referenced to $O\xi\eta\zeta$ equilibrium axis system (rad).
Θ, θ	Euler pitch angle, where lower case refers to small quantity (rad).
$\overline{\xi}$	Distance of origin C forward of origin O (m).
ρ	Water density (km/m^3).
τ	Time variable used for convolution integrals (s).
Φ, ϕ	Euler roll angle, where lower case refers to small quantity (rad).
$\overline{\Phi}(\xi, \eta, \zeta)$	General velocity potential in equilibrium axis system.
$\overline{\phi}(\xi, \eta, \zeta)$	Velocity potential associated with unsteady motion.
χ_0	Heading of ship relative to waves, where 180° is head waves case (deg).
Ψ, ψ	Euler yaw angle, where lower case refers to small quantity (rad).
ω	Wave frequency (rad/s).
ω_e	Wave encounter frequency (rad/s).
ω'_e	Non-dimensional wave encounter frequency = $\omega_e\sqrt{L/G}$.
$(\omega_X, \omega_Y, \omega_Z)$	Angular velocity of the ship, referenced to $CXYZ$ equilibrium axis system (rad/s).
∇	Displacement volume (m^3).

Units for Radiation Hydrodynamic Actions

Motion	Added Mass and Acceleration Derivatives	Damping and Velocity Derivatives	Impulse Response Functions
Pure Surge **Pure Heave** **Pure Sway**	kg	kg/s	kg/s^2
Pure Roll **Pure Pitch** **Pure Yaw**	kgm^2	kgm^2/s	kgm^2/s^2
All Cross Coupled Modes	kgm	kgm/s	kgm/s^2

Units for Wave Excitation Hydrodynamic Actions

Motion	Force/Moment	Impulse Response Functions
Surge **Heave** **Sway**	N	N/s
Roll **Pitch** **Yaw**	Nm	Nm/s

1 Introduction

The desire to model ship motions in waves has resulted in many studies on the nature of the interaction between fluids and structures. The ability to predict the loads and motions experienced by a vessel in waves can be of great benefit when investigating design possibilities and operating potential. For instance, accurate prediction of the loads acting on a ship allows structures to be built in the most efficient and economical manner. Knowledge of the likely motions allows aspects of ship operability to be analysed, such as seasickness among passengers on ferries and the operational effectiveness of weapons systems on board warships. The development of ship motion simulation techniques offers the possibility of avoiding costly scale modelling or trial and error testing at full scale. Such techniques would provide benefits for both the designers and operators of modern ships.

The aim of this thesis is to present methods for the implementation of a time domain simulation technique, applicable for ship-shaped forms in a realistic seaway. It will not be subject to constraints placed on conventional linear techniques which restrict analysis to regular waves of very low amplitude. The use of a convolution integral formulation will allow memory effects to be included in the modelling of ship responses to arbitrary excitation. By taking into account the instantaneous underwater portion of the vessel's hull at each time step, non-linear wave excitation and hydrostatic restoring contributions will be determined. In doing so, it will be possible to perform time domain simulations of rigid body motions in waves of realistic amplitude, enabling comparison of the results of this technique to experiments, thus helping to demonstrate the validity of the method.

Structure and Outcomes

Chapter 2 presents a review of some of the range of theories that have been developed to address the need for reliable prediction of ship motions. These methods have undergone considerable development over time, accelerating particularly in the last 30 years. Originally these methods allowed the prediction of frequency domain responses in regular waves. They were restricted to small amplitude ship motions/waves and zero or low forward speed. Developments to these frequency domain methods saw modifications made that allowed analysis of ships at higher speeds. Later, time domain methods were introduced which offered greater flexibility in terms of the types of problems that could be analysed. Larger and more realistic wave conditions could be simulated with correspondingly increased ship motions. Time domain methods allow for the inclusion of influences due to control surfaces and excitation by random waves. They also allow for the inclusion of fluid memory effects, as exemplified by the generation of motion induced surface waves. Such memory effects introduce a dependence of the fluid forces and moments on past motion/excitation. Additionally, a time domain method opens the possibility for incorporating non-linear components in the formulation, allowing more accurate modelling of certain aspects of the ship motion problem.

The time domain simulation of ship motions in waves requires a means to relate these motions to a known reference. Chapter 3 examines methods of axis system definition, in particular the equilibrium and body fixed axis systems. These axis systems have traditionally been associated with seakeeping and manoeuvring motions, respectively. It is shown that hydrodynamic actions and ship motions defined in either axis system may be related to the other using a series of transformations, as proposed by Bailey et al [6]. The case is made that it is possible that the axis system used to reference ship motions to, be they of either seakeeping or manoeuvring type, need not be that traditionally favoured. Hence, for example, it would be reasonable to use a body fixed axis system to reference for motions conforming to the traditional definition of seakeeping motions.

Chapter 4 examines the techniques used to determine the theoretical hydrodynamic data which forms the basis of the time domain method. Two three dimensional singularity dis-

tribution techniques are used, based on a source distribution over the mean wetted surface of the hull. The first method uses a pulsating source with forward speed correction [45], the second using a translating, pulsating source [26]. Given that both the accuracy and the restrictions applied to these methods are relevant to the subsequent use of the theoretical data they provide, the theoretical basis of these methods is discussed.

Chapter 5 presents methods by which the hydrodynamic data, initially calculated in the frequency domain, may be converted into a form suitable for use in a time domain simulation technique. The use of a convolution integral formulation in the time domain allows for memory effects to be included in the modelling of responses to arbitrary excitation. Convolution integrals require impulse response functions to be determined and relationships are presented for the transformation of frequency domain hydrodynamic coefficients to the corresponding impulse response functions. The radiation impulse response functions are determined using either the real or imaginary parts of the frequency domain data. The wave excitation impulse response functions are unusual in that they include a negative time component. This accounts for the influence of a particular wave prior to its reaching the reference point at the centre of mass of the vessel. These impulse response functions are determined using both the real and imaginary parts of the frequency domain data. The relationships presented are applicable for frequency domain data referenced to both equilibrium and body fixed axes.

Chapter 6 examines the process of evaluating the frequency domain theoretical hydrodynamic data. In particular, the source distribution techniques require the mean wetted surface of the hull to be represented as a series of quadrilateral panels, with a source being placed at the centre of each panel. Methods for achieving this discretisation are examined, with emphasis placed on the effects of changing panel distribution on the calculation of frequency domain hydrodynamic data. The subsequent use of the frequency domain hydrodynamic data for calculation of impulse response functions requires the data to be calculated to comparatively high frequencies. This places constraints on the type of panel distributions that may be used. In addition, the time taken to calculate the frequency domain data is directly related to the number of panels used to represent the hull, requiring a

compromise between accuracy and the time taken for calculation.

Chapter 7 presents a validation of the numerical techniques used to determine the impulse response functions from the corresponding frequency domain hydrodynamic data. The accuracy of the numerical methods is confirmed by comparing the original frequency domain data with that calculated by inverse transform from the corresponding impulse response functions. However, in certain cases it is not possible to accurately transform frequency domain data because of the low frequency characteristics of the data.

Having established methods for the determination of impulse response functions from the corresponding frequency domain data, Chapter 8 presents techniques for the incorporation of this data into a time domain method employing convolution integrals. Equations of motion are developed for both equilibrium and body fixed axis representations. The solution of these equations of motion requires a time stepping scheme, the method chosen being the fourth order Runge-Kutta technique.

Chapter 9 presents results for the linear time domain simulation of ship motions in regular waves. Using theoretical hydrodynamic data, the heave and pitch motions of a *Series 60* model, referenced to both equilibrium and body fixed axes, are compared with frequency domain predictions in order to verify the accuracy of the methods. It is found that the motions referenced to equilibrium axes do not correspond with frequency domain predictions. The differences in the results are shown to be the result of certain frequency domain data sets tending to an infinite value at low frequency, preventing the accurate determination of the corresponding impulse response functions. Hence, subsequent simulations are referenced exclusively to body fixed axes. The symmetric motions of a *Series 60* model at a range of headings in regular waves are simulated in the time domain and the results are found to compare well with frequency domain predictions. Simulations of anti-symmetric motions make it clear that the incorporation of viscous effects is vital for accurate, stable predictions of such motions. A high speed *NPL5b* hull form is examined in both monohull and catamaran configurations, the later being used to examine the effects of changing hull separations on symmetric motions.

Chapter 10 presents an extension to the linear time domain simulation technique, whereby non-linear incident wave and restoring forces/moment contributions are incorporated. These non-linear contributions are determined at each time step of the simulation using the instantaneous underwater portion of the hull. By introducing these effects to an otherwise linear formulation, it becomes possible to account for effects due to changes in hull shape that occur above the waterline, i.e. flared bows, overhanging sterns. This method is applied to a *Series 60* model in head waves and the results compared to linear predictions and experimental results. Anti-symmetric motions are simulated for the *Series 60* both with and without viscous effects. The method is also applied to a *S175* containership hull form,which displays more features likely to show non-linear effects than the wall sided *Series 60*. Predicted motions in head waves are again compared to linear predictions and experimental results. Other vessels compared using this method include a yacht type hull form and *NPL5b* catamaran models of variable separation.

2 Literature Review

2.1 Frequency Domain Techniques

The first successful studies on the motions of ships in waves were carried out by Froude and Krylov. Froude considered the case of a ship rolling [36], while Krylov investigated the pitching of a ship in a seaway [59]. Krylov later developed a more general theory which encompassed all six degrees of freedom for rigid body ship motions [58]. Both Froude and Krylov based their respective work on the assumption that the presence of the ship did not alter the pressure field of the incident waves. This allowed the incident wave forces acting on the ship to be found by integrating the undisturbed wave pressure over the wetted surface of the vessel. This assumption of an undisturbed incident wave has become known as the Froude-Krylov hypothesis. Whilst on their own these so-called Froude-Krylov forces are insufficient to accurately model to actual forces on a ship in waves, most modern ship motion prediction methods use this theory to determine a significant part of the total wave excitation forces.

In the decades following the publication of the theories of Froude and Krylov, a broader understanding of the physical principles involved in the ship motion problem, as well as the mathematical tools needed to describe them, were developed. In particular, the strip theory developed by Korvin-Kroukovsky [54] and later Korvin-Kroukovsky and Jacobs [55], gave the first practical method for predicting heave and pitch ship motions. This strip theory was based on the assumption that if a ship was sufficiently slender, the fluid perturbation resulting from the oscillatory motions of the ship would be primarily in the transverse plane

to the vessel. Furthermore, it was assumed that, with the exception of surge, all possible oscillations of the ship were presumed to have negligible velocity components in the longitudinal direction. Hence the hull of the ship could be divided into transverse sections or 'strips', for which the hydrodynamic damping and added mass could be calculated. The properties of the entire ship could then be found by integrating the results for the individual strips over the length of the vessel.

2.1.1 Two-Dimensional

The strip theory of Korvin-Kroukovsky used a two-dimensional boundary value problem method to determine the hydrodynamic added mass and damping. A linearised free surface condition was used in conjunction with a body boundary condition which required that the normal component of the fluid velocity on the body equal the normal velocity of the body itself. The first application of the two-dimensional boundary value problem method to a ship-like shape was by Lewis [62]. Lewis's solution employed a conformal mapping technique, based on a two-parameter family of curves. Using this method, the shape of a ship-like section could be mapped to that of a cylinder for which the hydrodynamic properties were more easily calculated. However, Lewis's work was also based upon the assumption of the ship vibrating at infinite frequency, effectively giving a rigid free surface. This did not allow for any study of the frequency dependence arising from the creation of surface waves. Some years later Ursell [94] developed a more complete solution to the problem of a cylinder heaving on the surface with a linearised free surface condition. He used a multipole expansion method that satisfied the frequency dependent free surface condition, Laplace's equation and a condition at infinity.

The so-called Lewis forms have shown enduring popularity due to their simplicity, requiring only the beam/draft ratio and the sectional area coefficient to describe a particular section. However these Lewis forms are limited in their ability to describe more complex ship-like shapes such as bulb and chine sections. To this end, multi-parameter conformal mapping methods were introduced and these offer improved sectional representations as

the number of parameters in the mapping can be increased for more complex sections [60].

The two-dimensional boundary value problem can also be solved using a boundary integral method as first proposed by Frank [35]. In this method the underwater portion of each section is divided into a series of straight line segments. At the centre of each of these segments lies a fundamental singularity. Using Green's second identity, the velocity potential at any point in the fluid may be expressed as the summation of the contributions of these singularities. The singularities used in this method may be either sources or dipoles, or alternatively a combination of the two. Each of the singularities satisfies the zero speed linearised free surface condition, the Laplace equation and an appropriate condition at infinity. By satisfying the body boundary condition at the centre of each of the segments, the strength of each of the singularities can be determined. Knowing the strength of the singularities allows the velocity potential to be calculated, from which the pressures in the fluid and hence the forces may be obtained. In common with other singularity distribution techniques, the boundary-integral method suffers from a mathematical breakdown at certain frequencies if the vessel is surface piercing [50]. Irregular frequencies aside, the advantage of this method over Lewis form methods is in its ability to obtain improved resolution of hull sections with complex geometry, simply by decreasing the size of the line segments.

A comparison of the results obtained using Lewis forms, multi-parameter conformal mapping and Franks boundary-integral method was given by Bishop, Price and Tam [19] for heave and by Bishop, Price and Temarel [20] for sway and roll. Bishop, Price and Tam presented results showing the differences between the mapped forms obtained using the Lewis form method and multiparameter mapping for five ship-like sections: a chine section, rectangular section, triangular section, fine section and a bulbous section. It was found that a much better representation of the sections could be obtained using the multiparameter conformal mapping as opposed to the Lewis fit method. Comparison of the calculated hydrodynamic added mass and damping showed that the multiparameter conformal mapping technique gave a considerable improvement over the Lewis form method. However, they also noted that the boundary-integral method suffered at high frequencies from irregularities and was considerably more computational expensive. Similar results were found by

Bishop, Price and Temarel, using identical ship-like sections to determine sway and roll hydrodynamic coefficients. Again it was found that, provided suitable parameters were chosen for the mapping, the multi-parameter conformal mapping technique could be used to determine hydrodynamic coefficients to the required degree of accuracy.

Korvin-Kroukovsky and Korvin-Kroukovsky and Jacob's so-called 'intuitive' strip theory was the first method by which reasonably accurate predictions could be made for ship motions. The success of this technique lead to efforts to develop more mathematically rigorous strip theory methods. One major objection voiced against the intuitive strip theory was that it did not properly account for forward speed effects. The strips were analysed in isolation and interactions between them were not accounted for. Among these 'improved' strip theories were those of Gerritsma and Beukelman [39] and Ogilvie and Tuck [81]. Ogilvie and Tuck presented a more general strip theory, which now included the solution of the full three-dimensional boundary value problem. This so-called "rational" strip theory was quite computationally intensive and was followed by other less rigorous, but more practical, treatments of the problem.

Salvesen et al [86] praised the accuracy and simplicity of Korvin-Kroukovsky and Jacobs original strip theory, though pointing out that the forward speed terms in the coefficients did not satisfy the symmetry relations proven by Timman and Newman [92]. Using a less complex formulation than Ogilvie and Tuck, Salvesen et al. included additional forward speed dependent terms which satisfied the symmetry relations of Timman and Newman and were able to obtain good results for vessels advancing at constant speed in regular waves.

In order to linearise the potential flow problem, the theory of Salvesen et al., in common with other strip theories, assumed that the wave resistance perturbation potential and all its derivatives were small enough to be ignored. This meant that there was no account taken for the diffracted wave force and its effect on the motions. To include the diffraction contribution, strip theories have had to rely on Haskind relations, determined by Newman [74]. These relations allow for the diffraction potentials, and hence forces, to be determined from the ship motion (radiation) potentials.

An alternative to the strip theory is the slender ship theory which assumes the beam and draft to be small in comparison to the length of the ship [73, 75]. This method has been found to give good agreement with experimental results provided the forward speed is very low [76]. The problem of how to properly include forward speed effects was addressed by the "unified" theory of Newman [77] which combined aspects of strip theory and thin ship theory. This was developed out of a concern that the existing two-dimensional methods had aspects that remained unsatisfactory from a 'rational' point of view. Among the aspects addressed was the mathematical validity of the solution at low frequencies (despite good agreement with experimental results, e.g. Salvesen et al. [86]), the emergence of forward speed effects only as a higher order correction and the difficult nature of the diffraction problem in short incident waves. Whereas earlier strip theory methods determined the hydrodynamic added mass and damping using the Laplace equation, Newman replaced this with a Helmholtz equation, using the longitudinal wave number as a parameter. This change in the formulation provided a correction to the two-dimensional problem to account for the fact that the body was not infinitely long on its longitudinal axis. This method has been shown by Newman and Sclavounos [78] to provide better correlation with experimental results than previous strip theory techniques.

Increasing interest in the use of multi-hulled vessels, in particular catamarans, for commercial purposes meant that methods were sought for estimating the responses of these types of vessels in waves. It was realised that if a strip theory method was to be used on vessels of this type some estimation would have to be made of the interaction between the hulls. Wang and Wahab [99] investigated the oscillation of twin cylinders in the free surface, noting that there were certain frequencies at which the fluid between the cylinders was strongly excited. The application of strip theory to catamaran configurations involving realistic demi-hull-forms was carried out by Lee et al [61], who investigated the effects of changing the separation between the hulls on the resultant motions. Lee noted the inability of a conventional strip theory to correctly account for the interactions between the hulls of a catamaran vessel with forward speed. Given that strip theory was a two-dimensional method, when the vessel had forward speed it would be unable to account for the fact that the waves produced by one section would be likely to interact with another section further

aft. Modifications were required to account for this and prevent over-estimation of the interactions between the hulls.

Kim [51] presented in a strip theory method by which the motions and loads of a catamaran type ship of arbitrary shape could be determined. This method was valid for conventional catamarans with ship-like demi-hulls as well as semi-submersible type ships with catamaran configuration. Results were presented that showed generally good agreement between experimental and theoretical results for both a conventional catamaran type ship and a semi-submersible catamaran. Further work on the problem of catamarans was carried out by Ohkusu and Faltinsen [83]. They investigated the nature of the hydrodynamic forces present when forward speed was included. They noted that experiments had shown [82] that the hydrodynamic interaction effects between the two hulls of a catamaran were not as strong as those predicted by a two-dimensional strip theory method. This difference became greater as the forward speed was increased. Ohkusu and Faltinsen used a theoretical method that included theories relating to the high speed motions of a flat surface piercing plate, the stationary flow around the bow of a ship and the diffraction problem at the bow. The added mass and damping hydrodynamic coefficients calculated compared well to experiments for high Froude number. They also showed that as the forward speed increased the level of interaction between the hulls decreased.

Faltinsen and Zhao [32] attempted to address some of the perceived deficiencies of strip theory in their study of 1991. They produced a two-dimensional method that was able to account for the interaction between the local steady flow and the unsteady flow. The local steady flow contribution was solved using a more complete formulation of the classical linear free surface condition with forward speed than had been used previously for strip theories. The three-dimensional nature of the wave system created by the ships forward motion was modelled starting from the bow and progressing aft along the sections into which the hull had been divided. In this way they were able to include in each section the influences of the sections upstream. This inclusion of three-dimensional effects has seen this method dubbed a $2\frac{1}{2}$-D strip theory. Comparison of the results to experiments showed the non-linear calculation of the local steady flow offered improvements in the calculated

wave profile along the ship. Heave added mass and damping data was also compared to experiments and a satisfactory level of agreement was noted [32].

2.1.2 Three-Dimensional

Whilst strip theories had been shown to provide reasonable agreement with experimental results for conventional ship hull forms, there existed a need to find methods that were subject to less restrictions than strip theory. In particular, there was an increasing need to model the motions of vessels that were not of conventional shape, such as the semi-submersible platforms used in oil exploration. Such cases would require the solution of the three-dimensional boundary value problem. The method employed to solve this problem was similar to that of Frank, with fundamental singularities distributed over the surface of the object. Having assumed that the fluid was invicid, homogeneous and the fluid motion irrotational, the velocity potential throughout the fluid domain could be determined from the sum of the contributions of the singularities.

Initially this method was used only for studies of zero or very low speed cases, meaning that a pulsating source could be used as the singularity. The pulsating source satisfies the Laplace equation throughout the fluid domain, the zero speed free-surface boundary condition and a condition to ensure outward moving waves at infinity. The solution to the practical problem of a floating body in waves is found by dividing the underwater portion of the vessel into panels, with a singularity at the centre of each of the panels. The strength of each source is obtained by satisfying the body-boundary condition at the centre of the panel. By assuming that the source strengths are constant over each of the panels, the fluid pressures can be calculated and hence the forces acting on the vessel. Early examples of the method include Garrison [37] and Faltinsen and Mitchelsen [31]. Faltinsen and Mitchelsen found that when using a simple floating box there was very good agreement between the numerical calculations and experimental results, though subject to the normal limitations of linear theory. It was shown that using a two-dimensional strip theory to calculate the responses of the box shape did not produce acceptable results, leading to the conclusion

that only a three dimensional method would be suitable for problems involving objects that do not conform to the strip theory requirement of being 'thin'.

The introduction of forward speed corrections, similar to those used by Salvesen et al. [86], meant that vessels travelling with forward speed could be considered. Inglis and Price compared the results of a strip theory method using Lewis forms to a three dimensional method with forward speed correction for the calculation of the wave exciting forces and moments [48] and hydrodynamic coefficients [49]. They found that provided the forward speed was low the three dimensional method employing forward speed correction gave good agreement in terms of the predicted motions/response. However, the individual hydrodynamic coefficients and wave excitation forces were not as accurate as those found using method that fully accounted for forward speed effects.

The velocity potential function of a translating, pulsating source, used to solve the three-dimensional problem with forward speed, was first given by Wehausen and Laitone [100]. This formulation is very complicated, involving single and double integrals dependent on the forward speed of the vessel and its frequency of oscillation. The first practical method employing this type of velocity potential was that of Chang [24]. Despite simplifying the formulation, the evaluation of the integrals was still extremely time-consuming. Other attempt to simplify the translating, pulsating source formulation have been made. Inglis and Price [46] employed an exponential integral, which for low values of $\beta = \bar{U}\omega/g$ contained only single integrals. However for $\beta > 0.25$ double integrals remained. Guevel and Bougis [40] presented a method which also employed an exponential integral to simplify the double integrals, though in this case for all values of β. A similar exponential integral method for the simplification of the double integrals over all values of β was presented by Wu and Eatock-Taylor [102]. Bessho [12] presented an alternative simplified translating, pulsating source method which now contained only single integrals, whilst still satisfying the boundary conditions of the method of Wehausen and Laitone [100]. Although there were now only elementary functions in the integrand, it was still very complicated and it was not until Ohkusu and Iwashita [84] that a numerical scheme based on this formulation was presented.

There is not a great deal of published data regarding the effectiveness of translating, pulsating source methods in determining ship motions. Inglis and Price [48, 49] compared the results obtained using two versions of a translating pulsating source method, each with a different body boundary condition, to a pulsating source method with forward speed correction and a strip theory method. They found that while the use of the translating, pulsating source method gave benefits in the calculation of individual hydrodynamic coefficients and wave actions, the differences in the response calculations were quite small. For the relatively low Froude numbers considered (maximum Fn=0.3) the differences between the methods were fairly small and the computational effort required for the translating, pulsating source far outweighed that for the strip theory and pulsating source methods. Another study of a translating, pulsating source method applied to a realistic ship form was that of Squires and Wilson [91], who used a formulation similar to that of Wu and Eatock-Taylor [102] to simplify the Green's function formulation. Comparisons were made with results from Wu and Eatock-Taylor [102] and Inglis and Price [46], showing close agreement between the methods.

Attempts have been made to circumvent the need for the translating, pulsating source altogether, whilst still including forward speed effects, including the studies of Huijsmans and Hermans [44] and Wu and Eatock-Taylor [103]. In particular, Wu and Eatock-Taylor expanded the velocity potential of the pulsating source method as a perturbation series, including the effects of the interaction between the steady and unsteady wave patterns on the hydrodynamic coefficients. This gave the ability to include forward speed effects whilst avoiding the complication of the translating, pulsating source formulation.

2.2 Time Domain Techniques

The need for increased computational efficiency lead to a great deal of effort being expended to improve translating, pulsating source techniques for use in the frequency domain. However, if the three-dimensional boundary value problem is reformulated in the time domain, the computational complexity can be reduced. Green's second identity is still

used, but in the time domain the Green's function is much less complicated, regardless of the velocity of the body.

King et al. [52] presented results obtained using a linear time domain method which accounted for forward speed effects. These were compared to results from a strip theory method (based on that of Salvesen et al. [86]), "unified" strip theory (Sclavounos [88]), three-dimensional methods of Inglis and Price [48], Chang [24], Guevel and Bougis [40] and experimental data. It was found that there was good agreement between all the theoretical methods when calculating the heave added mass and damping, the strip theory and unified theory producing particularly close results to the experimental measurements. The pitch damping results for all methods did not show agreement with the experimental results, strip theory proving particularly poor. King et al. [52] stated that the time domain method came closest to describing the correct general character of the experimental results. The cross-coupling coefficients found using the time domain method showed the best agreement with experimental results of all the theoretical methods, though the authors could not explain why this would be the case when the pure heave and pitch had not been so good.

Another investigation into the ship motion problem in the time domain was carried out by Bingham et al [14], using a transient Green's function method. They presented the results of their time domain method for a Wigley hull, with and without steady forward speed. These results were compared to experiments and frequency domain methods, for which there was found to be a good level of agreement. Further development of this method was detailed by Bingham et al. [13] with results being presented again for a Wigley hull and also the more realistic Series 60 type hull. It was found that the time domain solution suffered from the effects of irregularities in much the same way as frequency domain methods. Comparison was made between the time domain and frequency domain methods. First of all, Fourier transforms were used to evaluate frequency domain hydrodynamic added mass, damping and exciting forces/moments from the time domain impulse response functions. This frequency domain data was used to solve the equations of motion to obtain the response amplitude operators (RAOs). Secondly a time domain simulation was carried out

using the impulse response functions, the RAOs being found using Fourier transforms of the resulting motions. Good agreement was found between the methods, with results for changing speed showing close agreement with experimental measurements.

Performing ship motion predictions in the time domain gives the opportunity to extend the range of motion considered beyond the traditional restrictions of small amplitude. Ships in larger amplitude waves can now be considered, with their correspondingly large motions. This offers the possibility of better simulating realistic conditions in which the possibility of extreme motions/loads is most likely. Lin and Yue [64] presented a time domain method in which the exact body boundary condition was satisfied on the instantaneous underwater surface, while the free-surface boundary conditions remained linearised and on the calm water free surface. This contrasted with previous time domain methods which had continued to use the mean wetted surface of the ship to obtain the hydrodynamic characteristics. The linear free-surface boundary condition still applied, hence incident waves and the waves generated by the ships motion (both radiation and diffraction) were still assumed small. This lead to methods of this type being referred to as "body non-linear". Lin and Yue compared the results of their program *LAMP* (*L*arge *A*mplitude *M*otions *P*rogram) at zero speed to a linearised time domain method, strip theory results based on the method of Salvesen et al. [86] and experimental measurements. It was found that there was good agreement between hydrodynamic coefficients obtained using the *LAMP* method and those found by experiment. The agreement between *LAMP* and experiments was such that the authors suggested that non-linear free surface terms could be of less importance than had been assumed for the prediction of motion coefficients.

Lin and Yue [64] noted that the presence of large amplitude heave motions resulted in significant increases in the added resistance and steady sinkage and trim forces. Also of importance was the finding that with increasing motion amplitude there were considerable changes in the first harmonic (excitation frequency) motion coefficients. In particular, the non-linearly calculated added mass was found to decrease markedly with increasing heave amplitude.

Further work by Lin et al. [63] increased the degree of non-linearity of the *LAMP* program.

Now, in addition to satisfying the body boundary condition on the instantaneous wetted surface of the hull, they linearised the free surface boundary condition about the incident wave. This was done by using the incident wave elevation to transform the body geometry into a computational domain with a deformed body and a flat free surface. In this way they were able to include the true hydrodynamic effects of the underwater portion of the hull as well as the correct hydrostatic and Froude-Krylov forces. Whilst the radiated and diffracted waves remained small, it was said that this method allowed incident waves of arbitrary profile to be used in the analysis. Lin and Yue presented results for a S175 containership found using two methods. In the first the linearised free surface condition was satisfied on the surface of the incident wave (*LAMP4*), the second method using radiation actions found using a linearised free surface condition combined with restoring and Froude-Krylov forces found using the instantaneous underwater portion of the hull (*LAMP2*).

Comparing these two methods to experimental data for a range of wave amplitudes showed that both the *LAMP2* and *LAMP4* methods displayed similar non-linear effects to the experimental results. The pitch predictions using both methods were similar, though lower than the experimental values. The heave value predicted by *LAMP2* were higher than the experimental results, which were more closely matched by the *LAMP4* method. The computation effort required by these two methods was very different, the *LAMP4* method requiring 40 times more computing time than *LAMP2*. Such differences in computation effort are of considerable relevance when considering the possible applications of a technique in commercial design.

2.3 Alternative Three-Dimensional Techniques

Thus far the three-dimensional methods discussed have all employed Green's theorem in conjunction with a distribution of suitable singularities over the hull of the ship to allow the calculation of the velocity potential in the fluid domain. An alternative method is to use the so-called Rankine Panel method. In this method Green's second identity is still used, allowing the problem of obtaining the velocity potential to be reduced from being

the entire fluid domain to the surfaces of the domain. The Green's function used is now a simple $1/R$ singularity. A source of this type does not satisfy either the free-surface condition or the body-boundary condition. This means that the singularities must be distributed over both the body-surface and the free-surface. Without the radiation condition at infinity that is applied to other Green's function methods, the radiation condition must be applied numerically. The strengths of the Rankine sources are determined by applying a dynamic pressure condition to the free-surface and a body-boundary condition. Having evaluated the strengths of the sources, the velocity potential can then be calculated and hence the pressures on the body and the free-surface elevation determined. The computational effort required to evaluate the Green's function used in the Rankine panel approach is considerably less than for the Green's function methods previously described. However, a great deal more singularities are used in Rankine panel methods which leads to additional requirements in terms of the larger matrices which must be inverted. This is due to the fact that in addition to requiring that the body of the vessel be discretised using panels, the free surface to an appropriate distance from the vessel must also be panelled.

As was the case for the previous Green's function methods, the Rankine panel methods were initially applied in the frequency domain. Nakos and Sclavounos [72] compared the results of a frequency domain Rankine panel method to experimental results for a Wigley hull and a Series 60 model, finding good agreement. Sclavounos et al [87] used a frequency domain Rankine panel method to model the seakeeping of SL7 and S175 ship hull and an IACC type yacht form. The purpose of this investigation was to assess the effects of flare and transom sterns. The transom stern issue was addressed by including a strip of panels to form a 'wake' behind the ship. It was observed that if the shape of the wave profile along the ship was not accounted for (i.e. only examined the mean wetted surface), the heave and pitch responses were over estimated. However if the wave profile along the ship was accounted for, thus including contributions from flared and overhanging portions of the hull to the instantaneous underwater area, the predicted responses were in much better agreement with experiments.

Formulation of the Rankine panel method in the time domain was first achieved by Maskew

[66]. Numerical solutions to this method have been found using the Euler-Lagrange method [9]. This method uses a time stepping approach which requires two major tasks to be carried out at each time step. The first of these to solve the linear field equation in the Eulerian frame, the second being to track the individual Lagrangian points on the free surface using a fully non-linear boundary condition in order to update their position and potential values. This method has been used for two-dimensional cases from the late 1970's and more recently for three-dimensional cases. Three dimensional situations are much more computationally difficult due to the large number of unknowns required. This has meant that their successful use has been reliant on the availability of sufficient computing power.

In their 1994 paper, Beck et al. [9] solved the mixed boundary value problem using a desingularised integral method. This allowed the body motions and free-surface elevation to be non-linear. A solution was obtained by using an integration surface outside of the fluid domain. By distributing the singularities on a surface slightly removed from the control surface, the kernel in the resulting integral equation was desingularised. This meant that simple numerical summation techniques could be used to evaluate the integrals over the panels, greatly reducing computational effort. Results were presented for a Wigley hull form, which were found to give better agreement with experimental results than linear strip theory and three-dimensional methods.

There have also been efforts made to develop less computationally intensive methods which still allow accurate simulation of the motions of ships. These methods take advantage of the fact that performing ship motion simulations in the time domain allows for the inclusion of certain non-linear effects in an otherwise linear formulation. It has been most common to account for non-linear effects by allowing the shape of the underwater portion of the hull be time dependent, allowing the calculation of the instantaneous Froude-Krylov and restoring forces at each time step of the simulation. Fonseca and Guedes-Soares [34] presented a method where the non-linear Froude-Krylov and restoring forces were calculated using the instantaneous underwater portion of the hull. The radiation and diffraction forces were represented using frequency dependent coefficients found using a strip theory method. Their time domain solution employed a convolution method to account for memory effects. They

represented the linear radiation forces using impulse response functions, infinite frequency added masses and what they referred to as a "radiation restoring coefficient". The diffraction forces were calculated at each instant using frequency domain transfer functions. The combination of linear and non-linear expressions in a single method requires some care. It was noted by Fonseca and Guedes-Soares that to use a frequency dependent expression to directly calculate the radiation forces associated with non-linear motions was not correct, since the non-linear system would not respond in a unique and known frequency. In addition, it has been shown [29] that the so-called radiation restoring coefficient is always equal to zero and any non-zero value is simply the result of numerical errors.

Other methods which have used a partially non-linear formulation include the study by Kring et al [56] who used a Rankine panel method to determine the linear radiation and diffraction contributions. To these linear components non-linear Froude-Krylov and restoring forces were added. It was found that there was a considerable improvement in the results found using the partially non-linear method over a linear method when compared to experimental measurements for a vessel with overhangs and flare. Further results using a combination of linear radiation and diffraction calculated using a Rankine panel method and non-linear Froude-Krlyov and restoring forces are presented by Kring et al [57] and Huang and Sclavounos [42]. Kring et al. examined the case of a high speed Lewis form catamaran and Huang and Sclavounos examined monohull vessels with flare above the waterline. In both cases it was found that inclusion of non-linear components into an otherwise linear formulation gave considerable improvements over entirely linear methods.

2.4 Application of Seakeeping Analysis

The previous sections of this review have given coverage to a range of methods that are available for the numerical analysis of the seakeeping characteristics of ships. Through the history of their development there has been an increase in the numerical sophistication and the physical correctness of these methods. Yet, despite these developments, the most popular method used today for the analysis of seakeeping is still the strip theory method.

This can be attributed to the fact that strip theory has been shown to reliably produce results that are sufficiently accurate for most purposes, require only sectional data to describe the hull form (which is easily obtained) and are extremely quick to implement.

Hearn et al. [41] argued that there was little doubt that the design of ships could be improved if designers were to use seakeeping analysis as a tool in preliminary design. They stated that, using cause and effect relationships, the benefits of changing design parameters could be analysed in a scientific way. Such a process would require the repeated application of seakeeping analysis methods in order to ascertain the characteristics of each design iteration. It is this need for repeated application that makes speed of calculation one of the most important aspects in gaining acceptance of seakeeping analysis as a viable tool for design. Strip theory has been regarded as the only method which offers calculation speeds that are sufficiently fast to encourage its use. However, as has been noted previously in this review, strip theories do not correctly account for many increasingly common characteristics of modern vessels. High speed craft, multi-hulls and craft with unconventional hull forms such as semi-submersibles and SWATHs (*S*mall *W*aterplane *A*rea *T*win *H*ull ships) are not well served by strip theories and the increasing use of these types of craft means that efficient alternative methods for evaluating their seakeeping responses are required.

3 Axis Systems and Equations of Motion

The development of methods for the mathematical description of ship motions requires a means to relate these motions to a defined reference system. In ship motion simulation, these reference systems take the form of spacial axis systems, which may be fixed in space or within the vessel. In the latter case the axes may either perform the motions of the vessel or translate with the vessel and remain unaffected by its perturbations.

The context in which the simulation of ship motions occurs has traditionally been the deciding factor for the type of axis system which is used. For the study of the seakeeping motions of vessels, where the ship in question maintains a constant speed and heading in a defined seaway, an equilibrium axis system has been favoured. However, if the manoeuvring characteristics of a vessel are being investigated, such as assessing the dynamic response to prescribed actions e.g. circle and zig-zag manoeuvres, the motions have normally been referenced to a body fixed axis system.

The traditional choice of axis system for particular circumstances does not result from the fundamental unsuitability of either method for the description of certain types of motions. Indeed, it has been shown by Bishop and Price [18] and later Bailey et al. [6] that the theories of seakeeping and manoeuvring may be related by a series of transformations to provide a "unified" theory. Hence the possibility exists that the choice of axis system might not necessarily be based on the nature of the motions of interest, but rather on other factors present in the mathematical problem, as will be shown in later chapters.

In the following sections of this chapter, the mathematical basis of both the equilibrium and body fixed axis systems are developed. They are developed along parallel lines so that it becomes possible to directly compare the two systems. This leads to the formulation of relations which allow transformation of data between axis systems, enabling direct comparisons of results obtained from a variety of theoretical and experimental methods.

3.1 Equilibrium Axes Representation

Seakeeping theory has traditionally referenced the rigid body motions of a vessel to equilibrium axes. This axis system moves with the ship but remains unaffected by the vessel's parasitic motions.

Figure 3.1 shows the axis systems traditionally associated with the equilibrium axis representation of ship motions. Two axis systems are defined within the vessel. The first of these is the axis system $O\xi\eta\zeta$ which has its origin at the point O, which is at the height of the calm water surface. The ζ-axis is positive upwards and the ξ- and η- axes lie in the plane of the calm water surface. This $O\xi\eta\zeta$ axis system translates with the same velocity $\overline{U}$ as the ship, but remains unaffected by its parasitic motions.

The axis system $CXYZ$ has its origin at C, the equilibrium position of the centre of mass. With the ship in its equilibrium position, the Z-axis points vertically upwards and the X- and Y- axes lie in a plane parallel to the calm water surface. The $CXYZ$ axis system is fixed within the ship and performs its parasitic motions.

Lastly there is the space fixed axis system $O_OX_OY_OZ_O$. The position of this axis system coincides with that of the equilibrium axis system $O\xi\eta\zeta$ at time $t = 0$.

The process of describing the forces and moments acting on the ship and the subsequent motions that occur is aided by describing a series of unit vectors as follows,

(i) $\mathbf{I}, \mathbf{J}$ and $\mathbf{K}$ along $O\xi$, $O\eta$ and $O\zeta$ respectively and

(ii) $\mathbf{I_C}$, $\mathbf{J_C}$ and $\mathbf{K_C}$ along CX, CY and CY respectively.

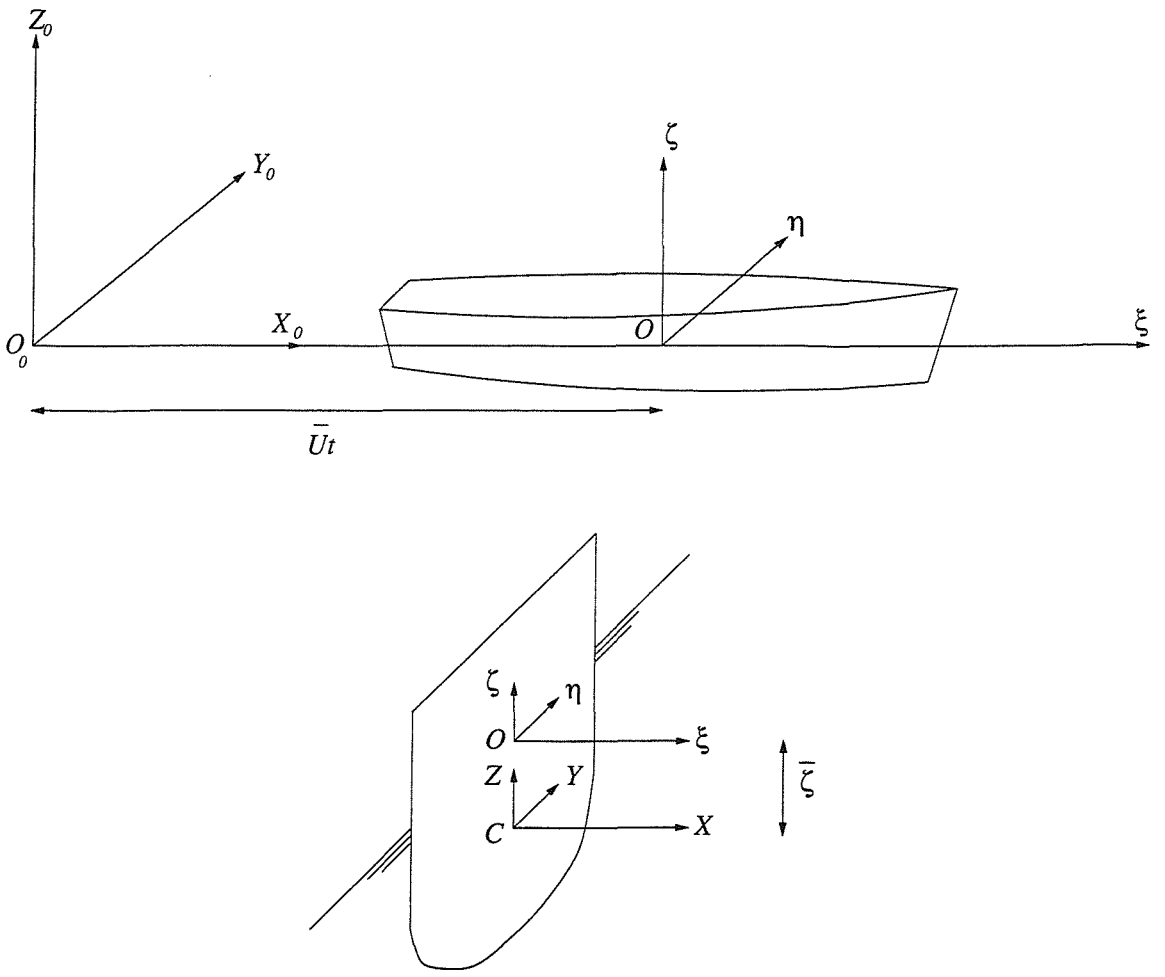

Figure 3.1: Equilibrium axis system.

Hence it becomes possible to define the total force acting on the vessel as [18]

$$\mathbf{F_C} = F_X\mathbf{I_C} + F_Y\mathbf{J_C} + F_Z\mathbf{K_C}.$$

Similarly, the total moment of the external forces acting about the centre of mass is

$$\mathbf{G_C} = G_X\mathbf{I_C} + G_Y\mathbf{J_C} + G_Z\mathbf{K_C}.$$

In addition, one may now express the velocity and angular velocity of the vessel, both referenced to the $CXYZ$ axis system, as

$$\mathbf{U} = U_X\mathbf{I_C} + U_Y\mathbf{J_C} + U_Z\mathbf{K_C}$$

$$\boldsymbol{\Omega} = \Omega_X\mathbf{I_C} + \Omega_Y\mathbf{J_C} + \Omega_Z\mathbf{K_C}.$$

Because in a seakeeping analysis one is considering the case of a vessel performing small parasitic motions whilst moving forward with steady speed, it is possible to specify,

$$\begin{bmatrix} U_X \\ U_Y \\ U_Z \end{bmatrix} = \begin{bmatrix} \bar{U} + u_X \\ u_Y \\ u_Z \end{bmatrix} \qquad \begin{bmatrix} \Omega_X \\ \Omega_Y \\ \Omega_Z \end{bmatrix} = \begin{bmatrix} \omega_X \\ \omega_Y \\ \omega_Z \end{bmatrix}$$

$$\begin{bmatrix} F_X \\ F_Y \\ F_Z \end{bmatrix} = \begin{bmatrix} \Delta F_X \\ \Delta F_Y \\ \Delta F_Z \end{bmatrix} \qquad \begin{bmatrix} G_X \\ G_Y \\ G_Z \end{bmatrix} = \begin{bmatrix} \Delta G_X \\ \Delta G_Y \\ \Delta G_Z \end{bmatrix}$$

where the lower case and Δ values are small quantities.

In the case of a generic ship, without port/starboard symmetry, the small net force and net moment required to displace the ship from its straight line equilibrium motion are given by

$$\begin{aligned} \Delta\mathbf{F_C} &= \Delta F_X \mathbf{I_C} + \Delta F_Y \mathbf{J_C} + \Delta F_Z \mathbf{K_C} = m\dot{U} \\ &= m(\dot{u}_X \mathbf{I_C} + \dot{u}_Y \mathbf{J_C} + \dot{u}_Z \mathbf{K_C}), \end{aligned} \tag{3.1}$$

and

$$\Delta\mathbf{G_C} = \Delta G_X \mathbf{I_C} + \Delta G_Y \mathbf{J_C} + \Delta G_Z \mathbf{K_C} = \begin{bmatrix} I_{XX} & -I_{XY} & -I_{XZ} \\ -I_{YX} & I_{YY} & -I_{ZY} \\ -I_{ZX} & -I_{ZY} & I_{ZZ} \end{bmatrix} \begin{bmatrix} \dot{\omega}_X \\ \dot{\omega}_Y \\ \dot{\omega}_Z \end{bmatrix}, \tag{3.2}$$

where I_{XX},I_{XY} etc. represent the inertias of the ship about the $CXYZ$ axis system.

The motions of the vessel in the equilibrium axis system are referenced to the $O\xi\eta\zeta$ axis system as follows

(i) small translations $\eta_1(t)$, $\eta_2(t)$ and $\eta_3(t)$, parallel to the axes $O\xi$, $O\eta$ and $O\zeta$ respectively,

(ii) small rotations $\eta_4(t)$, $\eta_5(t)$ and $\eta_6(t)$, about the axes $O\xi$, $O\eta$ and $O\zeta$ respectively.

Thus one requires a method by which the velocities and accelerations calculated with respect to the body fixed $CXYZ$ axis can be referenced to the equilibrium axes. In the

general case the alignment between the $O\xi\eta\zeta$ and the $CXYZ$ axis systems is illustrated in Figure 3.2 where the axes are aligned and the translations between them in the X,Y and Z directions are $\bar{\xi}$, $\bar{\eta}$ and $\bar{\zeta}$ respectively.

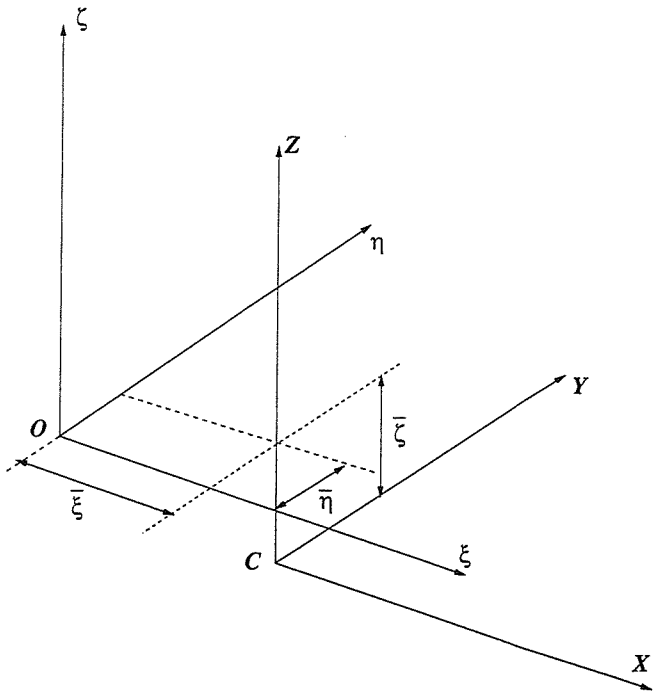

Figure 3.2: Generalised relationship between equilibrium axis systems $O\xi\eta\zeta$ and $CXYZ$.

Hence the position of C within the equilibrium axis system $O\xi\eta\zeta$ can be written as

$$\mathbf{R}_{OC} = \bar{\xi}\mathbf{I} + \bar{\eta}\mathbf{J} + (-\bar{\zeta})\mathbf{K}.$$

The angular velocities and accelerations referenced to the $O\xi\eta\zeta$ and the $CXYZ$ axis systems are thus related as follows [17],

$$\mathbf{\Omega} = \begin{bmatrix} \omega_X \\ \omega_Y \\ \omega_Z \end{bmatrix} = \begin{bmatrix} \dot{\eta}_4 \\ \dot{\eta}_5 \\ \dot{\eta}_6 \end{bmatrix} \quad \text{and} \quad \dot{\mathbf{\Omega}} = \begin{bmatrix} \dot{\omega}_X \\ \dot{\omega}_Y \\ \dot{\omega}_Z \end{bmatrix} = \begin{bmatrix} \ddot{\eta}_4 \\ \ddot{\eta}_5 \\ \ddot{\eta}_6 \end{bmatrix}. \tag{3.3}$$

The displacement of the ship's centre of gravity is referenced to the $O\xi\eta\zeta$ axis system by

$$\mathbf{R}_{OC} = (\eta_1 + \bar{\xi})\mathbf{I} + (\eta_2 + \bar{\eta})\mathbf{J} + (\eta_3 - \bar{\zeta})\mathbf{K},$$

hence, it is possible to show that the perturbation velocities of the ship, as defined in the $O\xi\eta\zeta$ and the $CXYZ$ axis systems are related as follows [7],

$$\begin{bmatrix} u_X \\ u_Y \\ u_Z \end{bmatrix} = \begin{bmatrix} \dot{\eta}_1 - \bar{\zeta}\dot{\eta}_6 - \bar{\eta}\dot{\eta}_6 \\ \dot{\eta}_2 + \bar{\zeta}\dot{\eta}_4 - \bar{\xi}\dot{\eta}_6 \\ \dot{\eta}_3 + \bar{\eta}\dot{\eta}_4 - \bar{\xi}\dot{\eta}_5 \end{bmatrix} \quad \text{and} \quad \begin{bmatrix} \dot{u}_X \\ \dot{u}_Y \\ \dot{u}_Z \end{bmatrix} = \begin{bmatrix} \ddot{\eta}_1 - \bar{\zeta}\ddot{\eta}_6 - \bar{\eta}\ddot{\eta}_6 \\ \ddot{\eta}_2 + \bar{\zeta}\ddot{\eta}_4 - \bar{\xi}\ddot{\eta}_6 \\ \ddot{\eta}_3 + \bar{\eta}\ddot{\eta}_4 - \bar{\xi}\ddot{\eta}_5 \end{bmatrix}. \tag{3.4}$$

Therefore, if the net force and moment required to perturb the ship from its equilibrium position are referenced to the $O\xi\eta\zeta$ axis system as

$$\Delta F_O = \Delta H_1\mathbf{I} + \Delta H_2\mathbf{J} + \Delta H_3\mathbf{K}$$

and

$$\Delta G_O = \Delta H_4\mathbf{I} + \Delta H_5\mathbf{J} + \Delta H_6\mathbf{K},$$

then it can be shown that they are related to forces and moments referenced to the $CXYZ$ axis system in the following way

$$\begin{bmatrix} \Delta H_1 \\ \Delta H_2 \\ \Delta H_3 \end{bmatrix} = \begin{bmatrix} \Delta F_X \\ \Delta F_Y \\ \Delta F_Z \end{bmatrix} \tag{3.5}$$

and

$$\begin{bmatrix} \Delta H_4 \\ \Delta H_5 \\ \Delta H_6 \end{bmatrix} = \begin{bmatrix} \Delta G_X + \bar{\zeta}\Delta F_Y + \bar{\eta}\Delta F_Z \\ \Delta G_Y - \bar{\xi}\Delta F_Z - \bar{\zeta}\Delta F_X \\ \Delta G_Z + \bar{\xi}\Delta F_Y - \bar{\eta}\Delta F_X \end{bmatrix}. \tag{3.6}$$

For a ship with the equilibrium axis system on the centreline and vertically above the centre of mass, $\bar{\xi} = \bar{\eta} = 0$, $I_{45} = I_{54} = I_{56} = I_{65} = 0$ and it becomes possible to split the equations of motion into symmetric and anti-symmetric parts. Hence, it can be shown [7] that the equations of motion referenced to an equilibrium axis may be written as follows for symmetric motions

$$\begin{bmatrix} \Delta H_1 \\ \Delta H_3 \\ \Delta H_5 \end{bmatrix} = \begin{bmatrix} m & 0 & -m\bar{\zeta} \\ 0 & m & 0 \\ -m\bar{\zeta} & 0 & (I_{55} + m\bar{\zeta}^2) \end{bmatrix} \begin{bmatrix} \ddot{\eta}_1 \\ \ddot{\eta}_3 \\ \ddot{\eta}_5 \end{bmatrix}, \tag{3.7}$$

and for antisymmetric motions.

$$\begin{bmatrix} \Delta H_2 \\ \Delta H_4 \\ \Delta H_6 \end{bmatrix} = \begin{bmatrix} m & m\bar{\zeta} & 0 \\ m\bar{\zeta} & (I_{44} + m\bar{\zeta}^2) & -I_{46} \\ 0 & -I_{64} & I_{66} \end{bmatrix} \begin{bmatrix} \ddot{\eta}_2 \\ \ddot{\eta}_4 \\ \ddot{\eta}_6 \end{bmatrix}, \tag{3.8}$$

The net actions in equations 3.7 and 3.8 can be further expanded as follows,

$$\begin{bmatrix} \Delta H_1 \\ \Delta H_3 \\ \Delta H_5 \end{bmatrix} = \begin{bmatrix} \Delta H_{1rad} + H_1(t) \\ \Delta H_{3rad} - C_{33}\eta_3 - C_{35}\eta_5 + H_3(t) \\ \Delta H_{5rad} - C_{53}\eta_3 - C_{55}\eta_5 + H_5(t) \end{bmatrix} \tag{3.9}$$

$$\begin{bmatrix} \Delta H_2 \\ \Delta H_4 \\ \Delta H_6 \end{bmatrix} = \begin{bmatrix} \Delta H_{2rad} + H_2(t) \\ \Delta H_{4rad} - C_{44}\eta_4 + H_4(t) \\ \Delta H_{6rad} + H_6(t) \end{bmatrix}. \tag{3.10}$$

In Equations 3.9 and 3.10 the subscript "rad" refers to the radiation actions, the terms C_{ij} are restoring terms and the terms $H_j(t)$ refer to the time dependent forces and moments which includes wave excitation contributions. The determination of these time dependent oscillatory actions is examined in Chapter 4.

3.2 Body Fixed Axis Representation

The use of a body fixed axis system has normally been associated with the investigation of ship manoeuvring characteristics. Studies of manoeuvring have focused primarily on the assessment of the dynamic stability of the vessel from a prescribed motion, i.e. constant speed, zero rudder angle etc. Focus has been given primarily to the antisymmetric motions of sway and yaw, with the assumption that the coupling of these motions to all others are insignificant and can be ignored.

Conventionally, the orientation of the body fixed axis has been as shown in Figure 3.3, with a set of axes $Cxyz$ fixed to the body with the origin C at the centre of mass. $Cxyz$ lies in the plane of port/starboard symmetry. The body fixed axis moves relative to a space fixed system $O_0X_0Y_0Z_0$, having started at time $t = 0$ in parallel with each other.

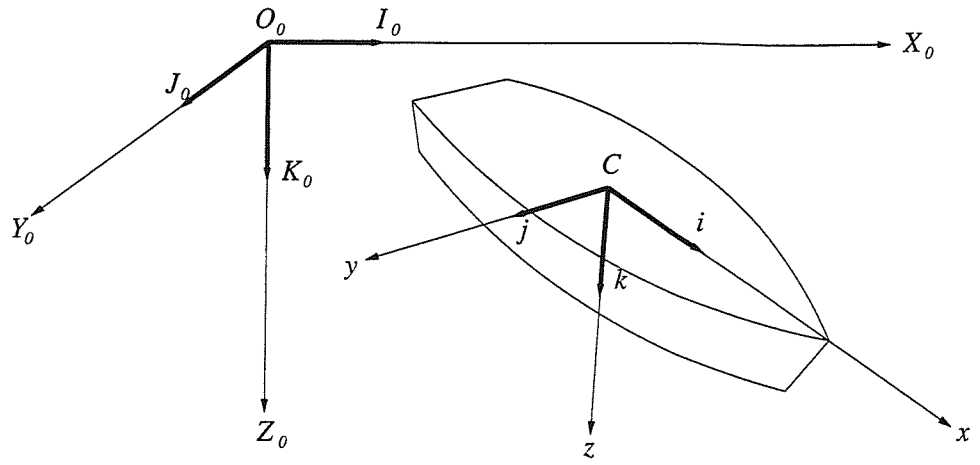

Figure 3.3: Conventional body fixed axis representation

The standard practice in manoeuvring dynamics has been to have the Cz and O_OZ_0 pointing downwards. However, Bishop and Price [18] showed that to enable comparisons with equilibrium axis representations, an upright right handed frame of reference is more convenient for the description of body fixed motions. In this frame of reference the Cz and O_OZ_0 axes point positive upwards. This axis system is shown in Figure 3.4.

In this upright body fixed axis representation, two sets of unit vectors are defined as follows

(i) $\mathbf{i}, \mathbf{j}$, and $\mathbf{k}$ along the axes Cx, Cy and Cz respectively and

(ii) $\mathbf{I_O}$, $\mathbf{J_O}$, and $\mathbf{K_O}$ along the axes O_OX_O, O_OY_O and O_OZ_O respectively.

In the theory of body axes, a vessel is brought to its actual orientation by imposing a series of Euler angle orientations. These are a swing (or yaw) Ψ, a tilt (or pitch) Θ and a heel (or roll) Φ in that specific order [18].

If an arbitrarily chosen vector can be written as,

$$\mathbf{A} = A\mathbf{I_O} + B\mathbf{J_O} + C\mathbf{K_O} = a\mathbf{i} + b\mathbf{j} + c\mathbf{k},$$

then,

$$\begin{bmatrix} A \\ B \\ C \end{bmatrix} = \mathbf{T} \begin{bmatrix} a \\ b \\ c \end{bmatrix},$$

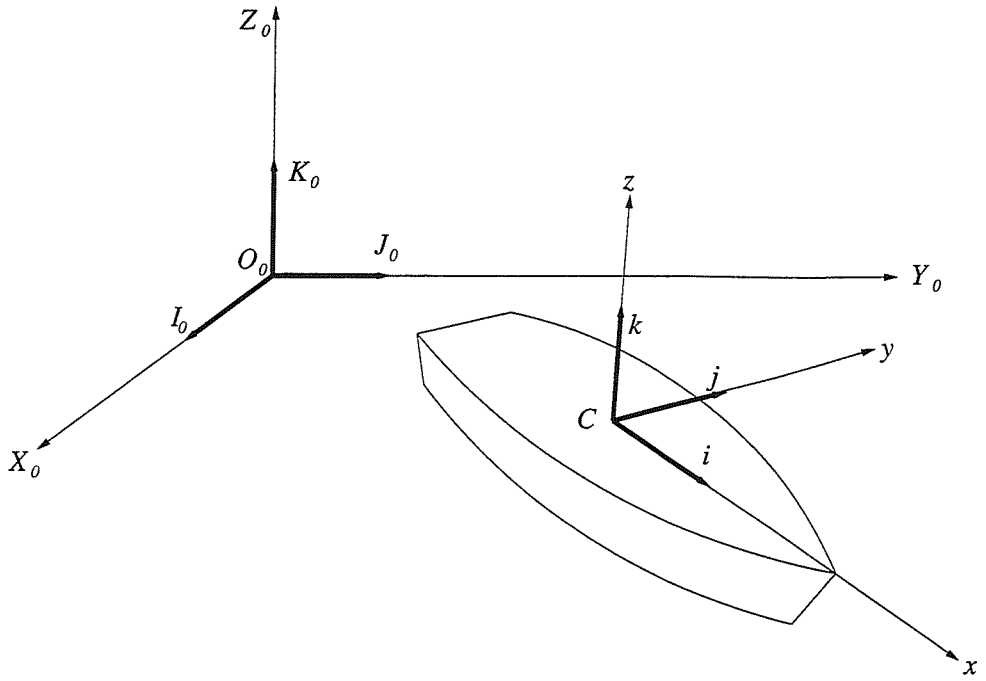

Figure 3.4: Inverted body fixed axis representation

where $\mathbf{T}$ is the orthogonal (3×3) matrix,

$$\mathbf{T} = \begin{bmatrix} \cos\Psi\cos\Theta & \begin{pmatrix} \cos\Psi\sin\Theta\sin\Phi \\ -\sin\Psi\cos\Theta \end{pmatrix} & \begin{pmatrix} \cos\Psi\sin\Theta\cos\Phi \\ +\sin\Psi\sin\Theta \end{pmatrix} \\ \sin\Psi\cos\Theta & \begin{pmatrix} \sin\Psi\sin\Theta\sin\Phi \\ +\cos\Psi\cos\Theta \end{pmatrix} & \begin{pmatrix} \sin\Psi\sin\Theta\cos\Phi \\ -\cos\Psi\sin\Theta \end{pmatrix} \\ -\sin\Theta & \cos\Theta\sin\Phi & \cos\Theta\cos\Phi \end{bmatrix}. \tag{3.11}$$

If one defines the ship's velocity as,

$$\mathbf{U} = U_O\mathbf{I_O} + V_O\mathbf{J_O} + W_O\mathbf{K_O} = U\mathbf{i} + V\mathbf{j} + W\mathbf{k},$$

and the angular velocity of the ship as,

$$\boldsymbol{\Omega} = P_O\mathbf{I_O} + Q_O\mathbf{J_O} + R_O\mathbf{K_O} = P\mathbf{i} + Q\mathbf{j} + R\mathbf{k},$$

then it is possible to use the transformation matrix $\mathbf{T}$ to relate these expressions as follows,

$$\begin{bmatrix} U_O \\ V_O \\ W_O \end{bmatrix} = \mathbf{T}\begin{bmatrix} U \\ V \\ W \end{bmatrix}, \quad \begin{bmatrix} P_O \\ Q_O \\ R_O \end{bmatrix} = \mathbf{T}\begin{bmatrix} P \\ Q \\ R \end{bmatrix}. \tag{3.12}$$

Furthermore, Bishop and Parkinson [17] showed that it is possible to relate the angular velocity of the vessel to the time derivatives of the Euler angles as,

$$\begin{bmatrix} P \\ Q \\ R \end{bmatrix} = \mathbf{S} \begin{bmatrix} \dot{\Phi} \\ \dot{\Theta} \\ \dot{\Psi} \end{bmatrix},$$

where the non-orthogonal matrix $\mathbf{S}$ is,

$$\mathbf{S} = \begin{bmatrix} 1 & 0 & -\sin\Theta \\ 0 & \cos\Phi & \cos\Theta\sin\Phi \\ 0 & -\sin\Phi & \cos\Theta\cos\Phi \end{bmatrix}. \tag{3.13}$$

In the body fixed axis representation the total force acting on the vessel is given by,

$$\mathbf{F} = X\mathbf{i} + Y\mathbf{j} + Z\mathbf{k} - mg\mathbf{K_O}.$$

where the weight of the vessel has been separated to leave only external forces. The weight contribution has components along each of the body fixed axes as follows,

$$-mg\mathbf{K_O} = (mg\sin\Theta)\mathbf{i} + (-mg\cos\Theta\sin\Phi)\mathbf{j} + (-mg\cos\Theta\cos\Phi)\mathbf{k}.$$

The total external moment acting on the ship about its centre of gravity is expressed as,

$$\mathbf{G} = K\mathbf{i} + M\mathbf{j} + N\mathbf{k} = \begin{bmatrix} I_{44} & -I_{45} & -I_{46} \\ -I_{54} & I_{55} & -I_{56} \\ -I_{64} & -I_{65} & I_{66} \end{bmatrix} \begin{bmatrix} \dot{P} \\ \dot{Q} \\ \dot{R} \end{bmatrix}.$$

If the products of motion variables are negligibly small, Bishop and Parkinson [17] showed that the inertias I_{44}, I_{45} etc. referenced to body fixed axis are equal to the inertias I_{XX}, I_{XY} etc. referenced to equilibrium axes.

In the case where the ship is undergoing am equilibrium straight line motion, where it makes small departures from the steady course, one may specify that

$$\begin{bmatrix} \dot{U} \\ \dot{V} \\ \dot{W} \end{bmatrix} = \begin{bmatrix} \dot{u} \\ \dot{v} \\ \dot{w} \end{bmatrix} \qquad \begin{bmatrix} U \\ V \\ W \end{bmatrix} = \begin{bmatrix} \bar{U} + u \\ v \\ w \end{bmatrix}$$

$$\begin{bmatrix} \dot{P} \\ \dot{Q} \\ \dot{R} \end{bmatrix} = \begin{bmatrix} \dot{p} \\ \dot{q} \\ \dot{r} \end{bmatrix} \qquad \begin{bmatrix} P \\ Q \\ R \end{bmatrix} = \begin{bmatrix} p \\ q \\ r \end{bmatrix} \qquad \begin{bmatrix} \Psi \\ \Theta \\ \Phi \end{bmatrix} = \begin{bmatrix} \psi \\ \theta \\ \phi \end{bmatrix}$$

where the lower case variables are small quantities. Additionally, the external forces and moments can now be expressed as

$$\begin{aligned} X &= \bar{X} + \Delta X \qquad & K &= \bar{K} + \Delta K \\ Y &= \bar{Y} + \Delta Y \qquad & M &= \bar{M} + \Delta M \\ Z &= \bar{Z} + \Delta Z \qquad & N &= \bar{N} + \Delta N \end{aligned} \tag{3.14}$$

where the overbar refers to steady quantities and the Δ refers to the small forces and moments required to perturb the ship from its reference motion. In the case of the reference motion at constant velocity, the steady forces are all equal to zero, apart from $\bar{Z}$, which is equal to the weight of the ship. This gives the buoyancy contribution $\bar{Z} = mg$.

Hence it is possible to show that the equations of motion for symmetric motions may be defined as follows,

$$\begin{bmatrix} m & 0 & 0 \\ 0 & m & 0 \\ 0 & 0 & I_{55} \end{bmatrix} \begin{bmatrix} \dot{u} \\ \dot{w} \\ \dot{q} \end{bmatrix} + \begin{bmatrix} 0 & 0 & 0 \\ 0 & 0 & -m\bar{U} \\ 0 & 0 & 0 \end{bmatrix} \begin{bmatrix} u \\ w \\ q \end{bmatrix} = \begin{bmatrix} \Delta X + mg\theta \\ \Delta Z \\ \Delta M \end{bmatrix}, \tag{3.15}$$

and for anti-symmetric motions as,

$$\begin{bmatrix} m & 0 & 0 \\ 0 & I_{44} & -I_{46} \\ 0 & -I_{64} & I_{66} \end{bmatrix} \begin{bmatrix} \dot{v} \\ \dot{p} \\ \dot{r} \end{bmatrix} + \begin{bmatrix} 0 & 0 & m\bar{U} \\ 0 & 0 & 0 \\ 0 & 0 & 0 \end{bmatrix} \begin{bmatrix} v \\ p \\ r \end{bmatrix} = \begin{bmatrix} \Delta Y - mg\phi \\ \Delta K \\ \Delta N \end{bmatrix}. \tag{3.16}$$

In a similar manner to Equations 3.9 and 3.10, the net actions in Equations 3.15 and 3.16 can be expressed as

$$\begin{bmatrix} \Delta X + mg\theta \\ \Delta Z \\ \Delta M \end{bmatrix} = \begin{bmatrix} \Delta X_{rad} + X(t) + mg\theta \\ \Delta Z_{rad} + Z_{z^*} z^* + Z_\theta \theta + Z(t) \\ \Delta M_{rad} + M_{z^*} z^* + M_\theta \theta + M(t) \end{bmatrix}, \tag{3.17}$$

$$\begin{bmatrix} \Delta Y - mg\phi \\ \Delta K \\ \Delta N \end{bmatrix} = \begin{bmatrix} \Delta Y_{rad} + Y(t) - mg\phi \\ \Delta K_{rad} + K_\phi \phi + K(t) \\ \Delta N_{rad} + N(t) \end{bmatrix}. \tag{3.18}$$

Again, in a similar manner to the equilibrium axis case, the subscript "rad" denotes a frequency dependent hydrodynamic action (analogous to the radiation actions of a seakeeping theory), restoring coefficients are described by terms such as Z_{z^*} and K_ϕ and additional excitations (e.g. wave or rudder excitation) are given by terms such as $X(t)$.

Given that it has been assumed that the ship in question is performing an equilibrium straight line motion, with the body and spacial axes initially aligned, the relative orientation of the body fixed axes at any time is defined by the small Euler angles ψ, θ and ϕ.

In the body fixed equations of motion, the velocities, accelerations and external actions are referenced to the upright body axes. However, the displacements are more difficult to define, since displacements of the body relative to these axes are meaningless since the axes move with the body. Hence the position and orientation of the vessel is the integration of component velocities along each of the body axes from a known starting position. For example,

$$\begin{aligned} X^* &= \int_0^t \left(u + \bar{U}\right) dt \\ y^* &= \int_0^t \left(v + \bar{U}\psi\right) dt \\ z^* &= \int_0^t \left(w - \bar{U}\theta\right) dt \end{aligned}$$

where the displacements signified with a lower case letter are small values.

The task of comparing equilibrium and body fixed axes is greatly assisted by the assumption of small Euler angles. For instance, it is possible to reduce the transformation matrix **T** to

$$\mathbf{T} = \begin{bmatrix} 1 & -\psi & \theta \\ \psi & 1 & -\phi \\ -\theta & \phi & 1 \end{bmatrix}, \tag{3.19}$$

by assuming small angles and ignoring the products of small quantities. Hence it becomes possible to relate the velocity and angular velocity of the ship to the spacial axis system $OX_OY_OZ_O$ as follows

$$\begin{bmatrix} U_O \\ V_O \\ W_O \end{bmatrix} = \mathbf{T} \begin{bmatrix} \bar{U} + u \\ v \\ w \end{bmatrix} = \begin{bmatrix} \bar{U} + u \\ v + \psi\bar{U} \\ w - \theta\bar{U} \end{bmatrix}$$

and

$$\begin{bmatrix} P_O \\ Q_O \\ R_O \end{bmatrix} = \mathbf{T} \begin{bmatrix} p \\ q \\ r \end{bmatrix} = \begin{bmatrix} p \\ q \\ r \end{bmatrix}.$$

3.3 Kinematic Relationships Between Equilibrium and Body Fixed Axis Systems

The previous sections in this chapter have shown that it is possible to formulate the equations of motion in either an equilibrium or a body fixed axis system. Bishop and Price [18] showed that simplified relationships between the two systems can be determined, provided that it is assumed that the body fixed axis system moves only a small amount relative to the equilibrium system. This corresponds with the idea of a ship performing small oscillations about a steady course which has been used in the development of the equilibrium and body fixed axis system equations of motion in Sections 3.1 and 3.2.

In the case where the $Cxyz$ body fixed axes and the $CXYZ$ equilibrium axis are initially aligned, the subsequent perturbed position of the vessel relative to the equilibrium axes will be defined by the small Euler rotations ψ, θ and ϕ. If the $CXYZ$ equilibrium axis system is chosen to be aligned with the $OX_OY_OZ_O$ space fixed system, the transformation matrix $\mathbf{T}$, defined in Equation 3.19 can be used to relate the elements of the equilibrium and body fixed systems.

Hence, it can be shown that the net forces and moments acting on the ship in the body fixed

$Cxyz$ and equilibrium $CXYZ$ axis system can be related by

$$\begin{bmatrix} \Delta F_X \\ \Delta F_Y \\ \Delta F_Z \end{bmatrix} = \begin{bmatrix} \Delta X + mg\theta \\ \Delta Y - mg\phi \\ \Delta Z \end{bmatrix}$$

$$\begin{bmatrix} \Delta G_X \\ \Delta G_Y \\ \Delta G_Z \end{bmatrix} = \begin{bmatrix} \Delta K \\ \Delta M \\ \Delta N \end{bmatrix}$$

Given that the equilibrium axis system representation references forces and moments to the $O\xi\eta\zeta$ axis system, using Equations 3.5 and 3.6 for $\overline{\zeta} = 0 = \overline{\eta}$, the relationships between body fixed and equilibrium axis systems are

$$\begin{aligned} \Delta F_X = \Delta X + mg\theta &= \Delta H_1 & \qquad \Delta G_X = \Delta K &= \Delta H_4 - \bar{\zeta}\Delta H_2 \\ \Delta F_Y = \Delta Y - mg\phi &= \Delta H_2 & \qquad \Delta G_Y = \Delta M &= \Delta H_5 + \bar{\zeta}\Delta H_1 \\ \Delta F_Z = \Delta Z &= \Delta H_3 & \qquad \Delta G_Z = \Delta N &= \Delta H_6 \end{aligned} \tag{3.20}$$

Furthermore, the linear velocities and accelerations referenced to the $Cxyz$ body fixed axis system can be related to those referenced to the $CXYZ$ equilibrium axis system by

$$\begin{bmatrix} \bar{U} + u_X \\ u_Y \\ u_Z \end{bmatrix} = \begin{bmatrix} \bar{U} + u \\ v + \psi\bar{U} \\ w - \theta\bar{U} \end{bmatrix} \quad \text{and} \quad \begin{bmatrix} \dot{u}_X \\ \dot{u}_Y \\ \dot{u}_Z \end{bmatrix} = \mathbf{T} \begin{bmatrix} \dot{u} \\ \dot{v} \\ \dot{w} \end{bmatrix} \tag{3.21}$$

and for the angular velocities and accelerations

$$\begin{bmatrix} \omega_X \\ \omega_Y \\ \omega_Z \end{bmatrix} = \begin{bmatrix} p \\ q \\ r \end{bmatrix} \quad \text{and} \quad \begin{bmatrix} \dot{\omega}_X \\ \dot{\omega}_Y \\ \dot{\omega}_Z \end{bmatrix} = \begin{bmatrix} \dot{p} \\ \dot{q} \\ \dot{r} \end{bmatrix} \tag{3.22}$$

Hence it is possible to determine any variable in a particular axis system using its equivalents in the other axis representation. The complete listing of the relationships is given in Appendix A.1, where each acceleration, velocity and displacement variable in both equilibrium and body fixed axis systems is expressed in terms of variables in the alternative axis system.

4 Determination of Theoretical Hydrodynamic Data

This chapter provides an introduction to the theoretical methods that are used to determine the hydrodynamic data that will form the basis for methods enabling the modelling of ship motions in the time domain. As noted in the literature review in Chapter 2, there are a number of methods that have been developed for the determination of theoretical hydrodynamic data. It is frequency domain three dimensional singularity distribution techniques that form the theoretical building blocks for the time domain methods that are to be presented in this thesis (see Section 2.1.2).

The theoretical methods that are to be used employ an appropriate singularity and assume that the fluid motion can be represented by a velocity potential function satisfying the Laplace equation throughout the fluid domain. A solution to the Laplace equation is found by sub-dividing the velocity potential into a linear summation of contributions [11]. These contributions are a potential due to the steady translation, an unsteady potential due to the incident waves, an unsteady potential due to the diffracted waves and a radiation potential due to motions in each of the six degrees of freedom.

The first method uses a pulsating source distribution and uses numerical methods originally developed by Inglis [45]. As noted in Section 2.1.2, in a method of this type, forward speed effects are included by way of a correction to the zero speed solution. The second method uses a translating, pulsating source distribution and has been developed by Du [26]. In contrast to the pulsating source method, the translating, pulsating source method implicitly accounts for forward speed effects, making it more appropriate for use in the analysis of

high speed vessels.

Fully accounting for forward speed effects makes the translating, pulsating source method considerably more computationally expensive than the pulsating source method. To give an example, calculating data at 50 frequencies for a vessel idealised using 1000 panels takes approximately 40 minutes running the pulsating source method on a PC with Pentium III 650 MHz processor. Using the same model with the translating, pulsating source method would result in a computational time of around 6-7 days.

Whenever using theoretical methods, a certain level of confidence must exist in the accuracy of the methods. In a scientific context the usual way to achieve such satisfaction in a particular method is to undertake a process of validation. Such a process will involve the comparison of results from a number of acknowledged sources. In will then become apparent how the results of the particular technique compare to similar methods.

The two theoretical methods used to calculate frequency domain hydrodynamic data for use in this study have recently been subjected to rigourous validation processes, the results of which may be found in the literature [1, 3, 6, 27, 28]. These results give confidence that the methods satisfactorily solve the posed problem, subject to the constraints imposed by the mathematical model used. Given that the mathematical constraints that these methods are subject to are of considerable relevance to the subsequent phases of this work, they will be elaborated upon in the following sections.

4.1 General Formulation of the Ship Motion Problem

The theoretical methods determine hydrodynamic data referenced to an equilibrium axis system, as discussed in Section 3.1. The equilibrium axes are identical to those described in Section 3.1, being made up of a space fixed axis system $O_O X_O Y_O Z_O$, a translating equilibrium axis system $O\xi\eta\zeta$ and an axis system $CXYZ$, where O lies in the calm waterplane and on the same vertical line as the centre of mass C.

The vessel travels at a constant forward speed $\overline{U}$ with an arbitrary angle χ_0 between the di-

rection of the vessel and the wave, such that $\chi_0 = 180°$ is head seas. The vessel encounters regular deep water sinusoidal waves with amplitude α and frequency ω. The frequency of encounter between vessel and waves, in water of infinite depth, is defined by

$$\omega_e = \omega - \left(\frac{\bar{U}\omega^2}{g}\right)\cos\chi_0. \tag{4.1}$$

It has been shown [77] that the problem of a rigid ship oscillating in waves can be described as a boundary value problem incorporating velocity potential functions. Ideal fluid assumptions must be made, whereby it is assumed that the fluid is invicid, incompressible and irrotational. Given these assumptions the total fluid potential may be represented by the function $\Phi(X_O, Y_O, Z_O, t)$, which satisfies Laplace's equation $\nabla^2\Phi = 0$, throughout the fluid domain.

To obtain a solution for the unknown velocity potential, appropriate boundary conditions must be applied to the system domain. These boundary conditions are as follows

- **Radiation Condition at Infinity** : Ensures that the wave energy produced by the disturbance of the vessel is travelling away from the vessel.
- **Sea Floor Condition** : Enforces the condition that the sea floor is a rigid boundary through which there is assumed to be no flow.
- **Body Surface Condition** : Ensures that the velocity component of the fluid normal to the body surface is the same as the velocity of the body. This condition is imposed on the mean wetted surface of the vessel and means that there can be no flow through the surface of the body.
- **Free Surface Condition** : A kinematic and dynamic boundary condition is imposed such that the particles on the free surface remain on the surface and move with it. Also, because the position of the free surface is unknown, it is assumed that the pressure on the free surface is atmospheric.

4.2 Practical Solution of the Ship Motion Problem

The complete formulations of the body boundary and free surface conditions are complex non-linear functions. To aid calculation, these conditions are linearised and simplified. For example, the body boundary condition in its complete form is given by,

$$(\mathbf{V}_s - \mathbf{V}) \cdot \mathbf{n} = 0 \quad \text{on} \quad S \tag{4.2}$$

Here $\mathbf{V_S}$ is the velocity of the body surface, which may be expressed as

$$\mathbf{V}_s = \mathbf{U} + \dot{\alpha}$$

where $\mathbf{U} = (\overline{U}, 0, 0)$, $\alpha = (\xi - X_O, \eta - Y_O, \zeta - Z_O)$, the fluid velocity $\mathbf{V}$ is defined by $\mathbf{V}(X_0, Y_0, Z_0, t) = \nabla\Phi(X_0, Y_0, Z_0, t)$ and S is the instantaneous underwater portion of the hull and $\mathbf{n}$ is the normal to the hull surface.

The steady flow relative to the moving reference frame $O\xi\eta\zeta$ may be defined as [45]

$$\mathbf{W} = \overline{U}\nabla(\overline{\phi}(\xi, \eta, \zeta) - \xi)$$

which satisfies the relationship

$$\mathbf{W} \cdot \mathbf{n} = 0 \quad \text{on} \quad S$$

and where the velocity potential $\overline{\phi}$ describes the steady forward motion of the ship in the space fixed inertial frame of reference. Timman and Newman [92] showed that it is possible to simplify the body boundary condition and express it as

$$\frac{\partial\overline{\phi}}{\partial n} = [\dot{\alpha} + \nabla \times (\alpha \times \mathbf{W})] \cdot \mathbf{n} \quad \text{on} \quad \overline{S} \tag{4.3}$$

where $\overline{S}$ is the mean wetted surface of the vessel. This formulation of the body boundary condition is suitable for conditions where the displacement of the body is assumed small and is used for both pulsating and translating, pulsating source methods.

The complete form of the free surface condition, neglecting second order terms, is given by

$$\frac{\partial^2\Phi}{\partial t^2} + g\frac{\partial\Phi}{\partial Z_0} = 0 \quad \text{on} \quad Z_0 = 0. \tag{4.4}$$

Ignoring the second order terms means that the free surface condition is applied on the undisturbed water surface.

If the vessel has forward speed it then becomes possible to express the velocity potential as a summation of contributions due to the steady forward motion and the unsteady oscillatory motion. Hence

$$\Phi(\xi,\eta,\zeta,t) = \overline{U}\,\overline{\phi}(\xi,\eta,\zeta) + \phi(\xi,\eta,\zeta,t) \tag{4.5}$$

where the velocity potential is now referenced to the equilibrium axis system $O\xi\eta\zeta$, $\overline{\phi}$ is the potential due to the steady forward motion and ϕ is the unsteady velocity potential.

If one assumes that the disturbance of the steady flow due to the forward speed may be neglected, then $\mathbf{W} = (-\overline{U}, 0, 0)$. This can be justified if the ship is thin or flat or is travelling at low speed. This allows one to derive the free surface condition as used in the translating, pulsating source method of Du [26],

$$\left(i\omega_e - \overline{U}\frac{\partial}{\partial\xi}\right)^2 \phi + g\frac{\partial\phi}{\partial\zeta} = 0 \qquad \text{on} \quad \zeta = 0.$$

This expression of the free surface condition may be further expanded to give

$$\overline{U}\frac{\partial^2\phi}{\partial\xi^2} - 2i\omega_e\overline{U}\frac{\partial\phi}{\partial\xi} - \omega_e^2\phi + g\frac{\partial\phi}{\partial\zeta} = 0 \qquad \text{on} \quad \zeta = 0. \tag{4.6}$$

In the case of the pulsating source method, the free surface condition is further simplified by assuming the forward speed is very low and there is a high frequency of oscillation. Hence Equation 4.6 may be simplified to give the free surface condition specified by Inglis [45],

$$-\omega_e^2\phi + g\frac{\partial\phi}{\partial\zeta} = 0 \qquad \text{on} \quad \zeta = 0. \tag{4.7}$$

It can be seen that, as previously noted, the pulsating source method does not account for forward effects. Account for these effects is made via forward speed corrections, similar to those used for strip theory (see Section 4.3.1).

4.2.1 Decomposition of the Velocity Potential

If the unsteady oscillatory motions are assumed small, the velocity potential due to the incident waves, the diffraction of the incident waves and the rigid body motions in six degrees of freedom may be decomposed linearly as follows

$$\Phi = (\phi_O + \phi_D + \sum_{k=1}^{6} \eta_k \phi_k) e^{i\omega_e t} \tag{4.8}$$

where ϕ_O = incident wave potential

ϕ_D = potential due to diffracted wave

ϕ_k = velocity potential associated with kth mode of motion

η_k = displacement due to kth mode of motion

The incident and diffraction potentials satisfy the following condition,

$$\frac{\partial}{\partial n}(\phi_O + \phi_D) = 0 \qquad \text{on} \quad \overline{S},$$

and the boundary condition on the hull surface for the radiation potentials ϕ_k, derived from Equation 4.3 by Ogilvie and Tuck [81], is given by:

$$\frac{\partial \phi_k}{\partial n} = i\omega_e n_j + \overline{U} m_j \qquad \text{on} \quad \overline{S} \tag{4.9}$$

where $(n_1, n_2, n_3) = \mathbf{n}$ $\qquad \overline{U}(m_1, m_2, m_3) = -(\mathbf{n} \cdot \nabla)\mathbf{W}$

$(n_4, n_5, n_6) = (\mathbf{r} \times \mathbf{n})$ $\qquad \overline{U}(m_4, m_5, m_6) = -(\mathbf{n} \cdot \nabla)(\mathbf{r} \times \mathbf{W})$

$(\xi, \eta, \zeta) = \mathbf{r}$

From Equation 4.9 it is clear that the boundary condition for the unsteady velocity potentials ϕ_k is dependent on the speed of the vessel via the definition of $\mathbf{W}$. As noted earlier, if one ignores the disturbance of the fluid due to the steady forward motion, then $\mathbf{W} = (-\overline{U}, 0, 0)$. Consequently, the m_j terms from Equation 4.9 reduce to

$$m_1 = 0 = m_2 = m_3 = m_4; \qquad m_5 = n_3; \qquad m_6 = -n_2.$$

4.3 Determination of Forces and Moments Acting on the Vessel

The pressure at any point in the fluid is able to be calculated using Bernoulli's equation, where

$$p(X_O, Y_O, Z_O, t) = -\rho\left(\frac{\partial\Phi}{\partial t} + \frac{1}{2}\mathbf{V}^2 + gZ_O\right) + P_a \tag{4.10}$$

where P_a is the atmospheric pressure. By substituting the equation for the velocity potential into Equation 4.10 and neglecting second order terms in Φ, it is possible to obtain the following equation for the fluid pressure,

$$p = -\rho\left(\frac{\partial\Phi}{\partial t} + \mathbf{W}\cdot\nabla\phi + \frac{1}{2}\mathbf{W}^2 + gZ_O\right). \tag{4.11}$$

In this new pressure equation the last two terms are time independent contributions, the first due to wavemaking drag and dynamic lift and the second due to the buoyancy force contribution. Due to their time independence, these components may be ignored for the calculation of the oscillatory forces. The total oscillatory force is found by integrating the unsteady pressure over the underwater portion of the hull. Whilst, strictly speaking, this integration should be taken over the instantaneous underwater portion of the hull, in practice this is very difficult and so the mean wetted surface is used. Hence the total oscillatory force is given by,

$$H_j = -\rho\iint_{\overline{S}} n_j\left(\frac{\partial\Phi}{\partial t} + \mathbf{W}\cdot\nabla\phi\right)\,dS. \tag{4.12}$$

Here H_j $(j = 1, 2, 3)$ represents the force components along the $O\xi$,$O\eta$ and $O\zeta$ axes and H_j $(j = 4, 5, 6)$ the moments about those axes, respectively. Equation 4.12 ignores the term $\rho\{\frac{1}{2}\mathbf{W}^2 + gZ_O\}$ which gives a force proportional to the unsteady displacement of the ship [77].

Substitution of Equation 4.8 into Equation 4.12 allows the total force to be described as

$$H_j = F_j + E_j$$

where F_j is the exciting force and moment due to the incident waves,

$$F_j = -\rho \iint_{\overline{S}} n_j (i\omega_e + \mathbf{W} \cdot \nabla)(\phi_O + \phi_D)\, dS \tag{4.13}$$

and E_j is the exciting force and moment due to the bodily motions of the vessel and is given by,

$$\begin{aligned} E_j &= -\rho \iint_{\overline{S}} n_j (i\omega_e + \mathbf{W} \cdot \nabla) \sum_{k=1}^{6} \eta_k \phi_k \, dS \\ &= \sum_{k=1}^{6} T_{jk} \eta_k \quad \text{for} \quad j = 1, 2, \ldots, 6 \ , \end{aligned}$$

where,

$$\begin{aligned} T_{jk} &= \omega_e^2 A_{jk} - i\omega_e B_{jk} \\ &= -\rho \iint_{\overline{S}} n_j (i\omega_e + \mathbf{W} \cdot \nabla) \phi_k \, dS \end{aligned} \tag{4.14}$$

The term T_{jk} represents the hydrodynamic force and moment in the jth direction due to a unit motion in the kth mode. The forward speed and frequency dependent terms A_{jk} and B_{jk} are conventionally known as added mass and damping hydrodynamic coefficients respectively.

4.3.1 Hydrodynamic Coefficients Determined Using Pulsating Source Method

As was noted earlier, the pulsating source method does not implicitly account for forward speed in its formulation. Hence the hydrodynamic added mass and damping coefficients calculated using this method are not speed dependent, unlike the general case given in Equation 4.14. Instead, a correction is made to the zero speed solution to account for the forward speed effects. This correction is similar to those used for strip theories [11], where if the zero speed hydrodynamic coefficients are denoted with a superscript 0, the added

mass and damping coefficients predicted by the pulsating source method are [86],

$$
\begin{aligned}
A_{11}(\omega_e) &= A^0_{11}(\omega_e) & B_{11}(\omega_e) &= B^0_{11}(\omega_e)\\
A_{13}(\omega_e) &= A^0_{13}(\omega_e) & B_{13}(\omega_e) &= B^0_{13}(\omega_e)\\
A_{15}(\omega_e) &= A^0_{15}(\omega_e) - (\overline{U}/\omega_e^2)B^0_{13}(\omega_e) & B_{15}(\omega_e) &= B^0_{15}(\omega_e) + \bar{U}A^0_{13}(\omega_e)\\
A_{22}(\omega_e) &= A^0_{22}(\omega_e) & B_{22}(\omega_e) &= B^0_{22}(\omega_e)\\
A_{24}(\omega_e) &= A^0_{24}(\omega_e) & B_{24}(\omega_e) &= B^0_{24}(\omega_e)\\
A_{26}(\omega_e) &= A^0_{26}(\omega_e) + (\overline{U}/\omega_e^2)B^0_{22}(\omega_e) & B_{26}(\omega_e) &= B^0_{15}(\omega_e) - \overline{U}A^0_{22}(\omega_e)\\
A_{31}(\omega_e) &= A^0_{31}(\omega_e) & B_{31}(\omega_e) &= B^0_{31}(\omega_e)\\
A_{33}(\omega_e) &= A^0_{33}(\omega_e) & B_{33}(\omega_e) &= B^0_{33}(\omega_e)\\
A_{35}(\omega_e) &= A^0_{35}(\omega_e) - (\overline{U}/\omega_e^2)B^0_{33}(\omega_e) & B_{35}(\omega_e) &= B^0_{35}(\omega_e) + \overline{U}A^0_{33}(\omega_e)\\
A_{42}(\omega_e) &= A^0_{42}(\omega_e) & B_{42}(\omega_e) &= B^0_{42}(\omega_e)\\
A_{44}(\omega_e) &= A^0_{44}(\omega_e) & B_{44}(\omega_e) &= B^0_{44}(\omega_e)\\
A_{46}(\omega_e) &= A^0_{46}(\omega_e) + (\overline{U}/\omega_e^2)B^0_{24}(\omega_e) & B_{46}(\omega_e) &= B^0_{46}(\omega_e) - \overline{U}A^0_{24}(\omega_e)\\
A_{51}(\omega_e) &= A^0_{51}(\omega_e) + (\overline{U}/\omega_e^2)B^0_{31}(\omega_e) & B_{51}(\omega_e) &= B^0_{51}(\omega_e) - \overline{U}A^0_{13}(\omega_e)\\
A_{53}(\omega_e) &= A^0_{53}(\omega_e) + (\overline{U}/\omega_e^2)B^0_{33}(\omega_e) & B_{53}(\omega_e) &= B^0_{53}(\omega_e) - \overline{U}A^0_{33}(\omega_e)\\
A_{55}(\omega_e) &= A^0_{55}(\omega_e) + (\overline{U}/\omega_e)^2A^0_{33}(\omega_e) & B_{55}(\omega_e) &= B^0_{55}(\omega_e) + (\overline{U}/\omega_e)^2B^0_{33}(\omega_e)\\
A_{62}(\omega_e) &= A^0_{62}(\omega_e) - (\overline{U}/\omega_e^2)B^0_{22}(\omega_e) & B_{62}(\omega_e) &= B^0_{62}(\omega_e) + \overline{U}A^0_{22}(\omega_e)\\
A_{64}(\omega_e) &= A^0_{64}(\omega_e) - (\overline{U}/\omega_e^2)B^0_{24}(\omega_e) & B_{64}(\omega_e) &= B^0_{64}(\omega_e) + \overline{U}A^0_{24}(\omega_e)\\
A_{66}(\omega_e) &= A^0_{66}(\omega_e) + (\overline{U}/\omega_e)^2A^0_{22}(\omega_e) & B_{66}(\omega_e) &= B^0_{66}(\omega_e) + (\overline{U}/\omega_e)^2B^0_{22}(\omega_e).
\end{aligned}
$$

4.4 Equations of Motions Referenced to Equilibrium Axes

In Chapter 3 it was shown that the basic equations of motion for a rigid ship referenced to an equilibrium axis system could be described by Equations 3.7, 3.8, 3.9 and 3.10. These equations of motion included terms with the subscript "rad" which signified radiation contributions due to the body motions. The hydrodynamic added mass and damping terms found using the theoretical methods which have been described thus far in this chapter may be substituted for this radiation term in the equations of motion. For example, consider the case of heave motions, where the radiation actions can be expressed in terms of

added mass and damping coefficients as follows

$$\Delta H_{3rad} = -A_{31}(\omega_e)\ddot{\eta}_1 - B_{31}(\omega_e)\dot{\eta}_1 - A_{33}(\omega_e)\ddot{\eta}_3 - B_{33}(\omega_e)\dot{\eta}_3 \\ -A_{35}(\omega_e)\ddot{\eta}_5 - B_{35}(\omega_e)\dot{\eta}_5.$$

Using a similar argument for all of the remaining symmetric and anti-symmetric motions allows for the complete equations of motion to be expressed as follows, for symmetric motions

$$\begin{bmatrix} m & 0 & -m\bar{\zeta} \\ 0 & m & 0 \\ -m\bar{\zeta} & 0 & (I_{55} + m\bar{\zeta}^2) \end{bmatrix} \begin{bmatrix} \ddot{\eta}_1 \\ \ddot{\eta}_3 \\ \ddot{\eta}_5 \end{bmatrix} = \begin{bmatrix} \Delta H_1(t) \\ \Delta H_3(t) \\ \Delta H_5(t) \end{bmatrix}$$
$$= -\begin{bmatrix} A_{11} & A_{13} & A_{15} \\ A_{31} & A_{33} & A_{35} \\ A_{51} & A_{53} & A_{55} \end{bmatrix} \begin{bmatrix} \ddot{\eta}_1 \\ \ddot{\eta}_3 \\ \ddot{\eta}_5 \end{bmatrix} - \begin{bmatrix} B_{11} & B_{13} & B_{15} \\ B_{31} & B_{33} & B_{35} \\ B_{51} & B_{53} & B_{55} \end{bmatrix} \begin{bmatrix} \dot{\eta}_1 \\ \dot{\eta}_3 \\ \dot{\eta}_5 \end{bmatrix}$$
$$-\begin{bmatrix} 0 & 0 & 0 \\ 0 & C_{33} & C_{35} \\ 0 & C_{53} & C_{55} \end{bmatrix} \begin{bmatrix} \eta_1 \\ \eta_3 \\ \eta_5 \end{bmatrix} + \begin{bmatrix} H_1(t) \\ H_3(t) \\ H_5(t) \end{bmatrix} \tag{4.15}$$

and for antisymmetric motions

$$\begin{bmatrix} m & m\bar{\zeta} & 0 \\ m\bar{\zeta} & (I_{44} + m\bar{\zeta}^2) & I_{46} \\ 0 & I_{64} & I_{66} \end{bmatrix} \begin{bmatrix} \ddot{\eta}_2 \\ \ddot{\eta}_4 \\ \ddot{\eta}_6 \end{bmatrix} = \begin{bmatrix} \Delta H_2(t) \\ \Delta H_4(t) \\ \Delta H_6(t) \end{bmatrix}$$
$$= -\begin{bmatrix} A_{22} & A_{24} & A_{26} \\ A_{42} & A_{44} & A_{46} \\ A_{62} & A_{64} & A_{66} \end{bmatrix} \begin{bmatrix} \ddot{\eta}_2 \\ \ddot{\eta}_4 \\ \ddot{\eta}_6 \end{bmatrix} - \begin{bmatrix} B_{22} & B_{24} & B_{26} \\ B_{42} & B_{44} & B_{46} \\ B_{62} & B_{64} & B_{66} \end{bmatrix} \begin{bmatrix} \dot{\eta}_2 \\ \dot{\eta}_4 \\ \dot{\eta}_6 \end{bmatrix}$$
$$-\begin{bmatrix} 0 & 0 & 0 \\ 0 & C_{44} & 0 \\ 0 & 0 & 0 \end{bmatrix} \begin{bmatrix} \eta_2 \\ \eta_4 \\ \eta_6 \end{bmatrix} + \begin{bmatrix} H_2(t) \\ H_4(t) \\ H_6(t) \end{bmatrix}. \tag{4.16}$$

4.5 Equations of Motion Referenced to Body Fixed Axes

The equations of motion referenced to body fixed axes use a slightly different representation of the hydrodynamic actions than is found when using an equilibrium axis representation. Instead of using frequency dependent hydrodynamic coefficients, the radiation actions are described in terms of oscillatory derivatives. In Equations 3.17 and 3.18 it was shown that the equations of motion referenced to a body fixed axis system included radiation terms, denoted by the subscript "rad". In a similar fashion to the equilibrium axis case these radiation actions may be expanded, for example for heave motions, as follows,

$$\Delta Z_{rad} = \tilde{Z}_{\dot{u}}(\omega_e)\dot{u} + \tilde{Z}_{u}(\omega_e)u + \tilde{Z}_{\dot{w}}(\omega_e)\dot{w} + \tilde{Z}_{w}(\omega_e)w + \tilde{Z}_{\dot{q}}(\omega_e)\dot{q} + \tilde{Z}_{q}(\omega_e)q, \quad (4.17)$$

where the frequency dependent terms such as $\tilde{Z}_{\dot{u}}(\omega_e)$ and $\tilde{Z}_{w}(\omega_e)$ are referred to as oscillatory derivatives. The terms $\tilde{Z}_{\dot{u}}(\omega_e)$, $\tilde{Z}_{\dot{w}}(\omega_e)$ and $\tilde{Z}_{\dot{q}}(\omega_e)$ are acceleration derivatives and $\tilde{Z}_{u}(\omega_e)$, $\tilde{Z}_{w}(\omega_e)$ and $\tilde{Z}_{q}(\omega_e)$ are velocity derivatives.

As was the case for the equilibrium axis representation, this expansion of the radiation terms may be applied in a similar manner for each of the six degrees of freedom to give the complete equations of motion. For symmetric motions,

$$\begin{aligned}
&\begin{bmatrix} m & 0 & 0 \\ 0 & m & 0 \\ 0 & 0 & I_{yy} \end{bmatrix} \begin{bmatrix} \dot{u} \\ \dot{w} \\ \dot{q} \end{bmatrix} + \begin{bmatrix} 0 & 0 & 0 \\ 0 & 0 & -m\bar{U} \\ 0 & 0 & 0 \end{bmatrix} \begin{bmatrix} u \\ w \\ q \end{bmatrix} = \begin{bmatrix} \Delta X(t) \\ \Delta Z(t) \\ \Delta M(t) \end{bmatrix} \\
&= \begin{bmatrix} \tilde{X}_{\dot{u}} & \tilde{X}_{\dot{w}} & \tilde{X}_{\dot{q}} \\ \tilde{Z}_{\dot{u}} & \tilde{Z}_{\dot{w}} & \tilde{Z}_{\dot{q}} \\ \tilde{M}_{\dot{u}} & \tilde{M}_{\dot{w}} & \tilde{M}_{\dot{q}} \end{bmatrix} \begin{bmatrix} \dot{u} \\ \dot{w} \\ \dot{q} \end{bmatrix} + \begin{bmatrix} \tilde{X}_{u} & \tilde{X}_{w} & \tilde{X}_{q} \\ \tilde{Z}_{u} & \tilde{Z}_{w} & \tilde{Z}_{q} \\ \tilde{M}_{u} & \tilde{M}_{w} & \tilde{M}_{q} \end{bmatrix} \begin{bmatrix} u \\ w \\ q \end{bmatrix} \\
&+ \begin{bmatrix} 0 & 0 & 0 \\ 0 & Z_{z^*} & Z_{\theta} \\ 0 & M_{z^*} & M_{\theta} \end{bmatrix} \begin{bmatrix} x^* \\ z^* \\ \theta \end{bmatrix} + \begin{bmatrix} X(t) \\ Z(t) \\ M(t) \end{bmatrix}
\end{aligned} \quad (4.18)$$

and for anti-symmetric motions,

$$\begin{bmatrix} m & 0 & 0 \\ 0 & I_{xx} & -I_{xz} \\ 0 & -I_{zx} & I_{zz} \end{bmatrix} \begin{bmatrix} \dot{v} \\ \dot{p} \\ \dot{r} \end{bmatrix} + \begin{bmatrix} 0 & 0 & m\bar{U} \\ 0 & 0 & 0 \\ 0 & 0 & 0 \end{bmatrix} \begin{bmatrix} v \\ p \\ r \end{bmatrix} = \begin{bmatrix} \Delta Y(t) \\ \Delta K(t) \\ \Delta N(t) \end{bmatrix}$$

$$= \begin{bmatrix} \tilde{Y}_{\dot{v}} & \tilde{Y}_{\dot{p}} & \tilde{Y}_{\dot{r}} \\ \tilde{K}_{\dot{v}} & \tilde{K}_{\dot{p}} & \tilde{K}_{\dot{r}} \\ \tilde{N}_{\dot{v}} & \tilde{N}_{\dot{p}} & \tilde{N}_{\dot{r}} \end{bmatrix} \begin{bmatrix} \dot{v} \\ \dot{p} \\ \dot{r} \end{bmatrix} + \begin{bmatrix} \tilde{Y}_{v} & \tilde{Y}_{p} & \tilde{Y}_{r} \\ \tilde{K}_{v} & \tilde{K}_{p} & \tilde{K}_{r} \\ \tilde{N}_{v} & \tilde{N}_{p} & \tilde{N}_{r} \end{bmatrix} \begin{bmatrix} v \\ p \\ r \end{bmatrix}$$

$$+ \begin{bmatrix} 0 & 0 & 0 \\ 0 & K_{\phi} & 0 \\ 0 & 0 & 0 \end{bmatrix} \begin{bmatrix} y^* \\ \phi \\ \psi \end{bmatrix} + \begin{bmatrix} Y(t) \\ K(t) \\ N(t) \end{bmatrix}. \tag{4.19}$$

4.6 Relationships Between Hydrodynamic Actions in Equilibrium and Body Fixed Axis Systems

It has been shown that it is possible to represent the equations of motion for a rigid ship using either an equilibrium axis or body fixed axis representation. However, because the theoretical data available for use in this study is referenced only to an equilibrium axis system, one requires relations for the transformation of hydrodynamic data between the two systems.

Consider, as an example, the case of heave motions. In the equilibrium axis representation found in Equation 4.15, the net heave force in terms of hydrodynamic coefficients is given by

$$\Delta H_3 = -A_{31}(\omega_e)\ddot{\eta}_1 - B_{31}(\omega_e)\dot{\eta}_1 - A_{33}(\omega_e)\ddot{\eta}_3 - B_{33}(\omega_e)\dot{\eta}_3$$
$$-A_{35}(\omega_e)\ddot{\eta}_5 - B_{35}(\omega_e)\dot{\eta}_5 - C_{33}\eta_3 - C_{35}\eta_5 + H_3(t).$$

When referenced to a body fixed axis system, as in Equation 4.18, the net heave force in terms of oscillatory derivatives is

$$\Delta Z = \tilde{Z}_{\dot{u}}(\omega_e)\dot{u} + \tilde{Z}_{u}(\omega_e)u + \tilde{Z}_{\dot{w}}(\omega_e)\dot{w} + \tilde{Z}_{w}(\omega_e)w$$
$$+\tilde{Z}_{\dot{q}}(\omega_e)\dot{q} + \tilde{Z}_{q}(\omega_e)q + Z_{z^*}z^* + Z_{\theta}\theta + Z(t)$$

It is possible to express the oscillatory derivatives in terms of the hydrodynamic coefficients by using relations from Equation 3.20 and Appendix A.2. Hence the equilibrium axis system motion variables η_1, η_3 and η_5 may be replaced with the equivalent body fixed axis system motion variables to give,

$$\begin{aligned}\Delta H_3 &= -A_{31}(\omega_e)\left\{\dot{u}+\bar{\zeta}\dot{q}\right\} - B_{31}(\omega_e)\left\{u+\bar{\zeta}q\right\} \\ &\quad -A_{33}(\omega_e)\left\{\dot{w}-\bar{U}q\right\} - B_{33}(\omega_e)\left\{w-(\bar{U}/\omega_e^2)\dot{q}\right\} - C_{33}\left\{z^*\right\} \\ &\quad -A_{35}(\omega_e)\left\{\dot{q}\right\} - B_{35}(\omega_e)\left\{q\right\} - C_{35}\left\{\theta\right\}.\end{aligned}$$

Hence,

$$\begin{aligned}\Delta Z &= \tilde{Z}_{\dot{u}}(\omega_e)\dot{u} + \tilde{Z}_u(\omega_e)u + \tilde{Z}_{\dot{w}}(\omega_e)\dot{w} + \tilde{Z}_w(\omega_e)w \\ &\quad +\tilde{Z}_{\dot{q}}(\omega_e)\dot{q} + \tilde{Z}_q(\omega_e)q + Z_{z^*}z^* + Z_\theta\theta + Z(t) \\ &= \Delta H_3 \\ &= \left\{-A_{31}(\omega_e)\right\}\dot{u} + \left\{-B_{31}(\omega_e)\right\}u \\ &\quad +\left\{-A_{33}(\omega_e)\right\}\dot{w} + \left\{-B_{33}(\omega_e)\right\}w + \left\{-C_{33}\right\}z^* \\ &\quad +\left\{-\bar{\zeta}A_{31}(\omega_e) - (\bar{U}/\omega_e^2)B_{33}(\omega_e) - A_{35}(\omega_e)\right\}\dot{q} \\ &\quad +\left\{-\bar{\zeta}B_{31}(\omega_e) + \bar{U}A_{33}(\omega_e) - B_{35}(\omega_e)\right\}q.\end{aligned}$$

Comparing coefficients gives the following relations between body fixed axis system heave oscillatory derivatives and equilibrium axis system hydrodynamic coefficients,

$$\begin{aligned}\tilde{Z}_{\dot{u}}(\omega_e) &= -A_{31}(\omega_e) \\ \tilde{Z}_u(\omega_e) &= -B_{31}(\omega_e) \\ \tilde{Z}_{\dot{w}}(\omega_e) &= -A_{33}(\omega_e) \\ \tilde{Z}_w(\omega_e) &= -B_{33}(\omega_e) \\ \tilde{Z}_{\dot{q}}(\omega_e) &= -\bar{\zeta}A_{31}(\omega_e) - (\bar{U}/\omega_e^2)B_{33}(\omega_e) - A_{35}(\omega_e) \\ \tilde{Z}_q(\omega_e) &= -\bar{\zeta}B_{31}(\omega_e) + \bar{U}A_{33}(\omega_e) - B_{35}(\omega_e) \\ Z_{z^*} &= -C_{33} \\ Z_\theta &= -C_{35}.\end{aligned} \tag{4.20}$$

It is possible to repeat this process for each of the six degrees of freedom, giving the results which can be found in Appendix A.2.

The development of these relationships between the equilibrium axis system and body fixed axis system means that it is now possible to compare hydrodynamic data referenced

to either axis system. The original source of particular data is no longer important, as the transformations defined in this chapter and Appendix A allow it to be expressed in either a body fixed or equilibrium representation, greatly aiding the process of comparison. This ability will be taken advantage of when time domain methods are considered.

5 Functional Representation of Fluid Actions

It has been shown experimentally by Burcher [22] that the motion dependent hydrodynamic actions of a ship are dependent upon the previous actions of the vessel. The cause of this dependence may be described as a "memory effect" and has been linked to the creation of motion generated waves and/or vortices by both Cummins [25] and Brard [21], the latter of whom examined the effects of vortices on the manoeuvring of a submerged body. Both surface waves and vortices are dependent upon the motions of the body and the effects produced by a particular motion will alter the subsequent actions on the ship for a finite period of time. It is clear physically that surface waves resulting from ship motions will move away from the body with time and any vortices will eventually shed from the hull. Therefore the influence of past motions on the present actions will diminish over time.

Conventional frequency domain methods consider only motions that are steady state sinusoidal or slow. In the case of steady state sinusoidal motions, the vessel is considered to have been undergoing a steady motion for a long period of time. Hence, it may be assumed that physical effects, such as surface waves, have reached a fully developed state. Thus it is assumed that memory effects will no longer be apparent and may be ignored, allowing constant, frequency dependent, coefficients to be used to describe the fluid actions. Whilst this assumption of sinusoidal waves and responses aids the tractability of the ship motion problem, it is clear that this assumed model does not accurately represent the motions of a ship in realistic seaways. To do so requires a method which, in addition to allowing memory effects to be accounted for, permits the use of arbitrary excitation.

5.1 Impulse Response Functions and Convolution Integrals

The convolution integral and impulse response function have been used widely to model the response of a linear system to arbitrary or random inputs [68]. In its most general form, for an input $v(t)$, output $f(t)$ and impulse response function $h(\tau)$, the convolution integral takes the form

$$f(t) = \int_{-\infty}^{\infty} h(\tau)v(t-\tau)d\tau \tag{5.1}$$

where $h(\tau) = 0 \quad \text{for } \tau < 0$

and $v(t-\tau) = 0 \quad \text{for } \tau > t.$

The impulse response function $h(\tau)$ is the response of the system to a unit impulsive input applied at time $\tau = 0$. In the general case a condition of realisability is imposed, whereby the value of $h(\tau)$ is zero for $\tau < 0$. This condition reflects the fact that there may be no response before the input is applied. Hence the lower limit in Equation 5.1 may be set to zero without any change to the value of $f(t)$. In addition, because $v(t-\tau)$ is only considered for positive values, the upper limit on the integral may be replaced by t, again without changing the value of $f(t)$.

The convolution integral may be considered to consist of an infinite summation of the responses of a system to impulsive inputs. Hence each of the past impulsive inputs will have a particular effect at the present moment. If one were to consider an impulsive input of amplitude $v(t-\tau)$ which was applied for a time $\Delta\tau$ some τ seconds ago, the response at the present time t due to that particular input would be given by

$$\Delta f(t) = h(\tau)v(t-\tau)\Delta\tau.$$

Hence the convolution integral described in Equation 5.1 may be seen to represent an infinite summation of responses such as this. In effect, the impulse response function may be seen as a term which controls the amplitude of the response which is sustained after a given period. As the time between the application of a particular impulsive force and the present time increases, the effect of that input on the response at the present time will

decrease. It is clear that this characteristic of the convolution integral formulation makes it ideal for the modelling of fluid memory effects in the ship motion problem.

Price and Bishop [85] demonstrated that a convolution integral formulation employing impulse response functions could be used as part of a 'black box' type system, whereby for a given wave disturbance 'input', the resulting ship motions were the 'output'. Such a system would be subject to two important restrictions:

i) **Linearity** : If the input was scaled by a particular amount then the output would be scaled by an identical amount, i.e. doubling the input will always result in doubling of the output.

ii) **Time Invariance** : An impulsive input applied at time t produces the same output at time $t + \tau$ as an impulsive input applied at time $t + \sigma$ gives at $t + \sigma + \tau$. In the context of ship motions calculations this means that the ship characteristics must remain constant.

5.2 Use of Convolution Integrals to Describe Fluid Actions

Cummins [25] was the first to suggest using impulse response functions to model memory effects in the ship motion problem. Initially the ship system was described in terms of a simple function which related a particular motion response $x(t)$ to an arbitrary force $f(t)$ as follows

$$x(t) = \int_0^\infty R(\tau) f(t-\tau)\, d\tau$$

where $R(t)$ is the motion response to a unit excitation applied at time $t = 0$. Hence, if $\{f_j(t)\}(j = 1, 2, \ldots, 6)$ were an arbitrary set of forcing functions, the corresponding responses could be described by

$$x_k(t) = \sum_{j=1}^{6} \int_0^\infty R_{jk}(\tau) f_j(t-\tau)\, d\tau$$

where the matrix $\{R_{jk}(t)\}$ completely characterises the response of the ship to arbitrary excitation. In addition, Cummins noted that for certain modes, in particular those without restoring force (i.e. surge, sway and yaw), the impulse response function $R_{jk}(t)$ would asymptotically approach a non-zero value.

However, Cummins [25] suggested that it was generally preferable to consider the various components that made up the complete equations of motion, rather than simply a universal transfer function for each motion. To accomplish this, Cummins expressed the motion dependent velocity potential in terms of a convolution integral. Hence, the following equations of motion were developed for a ship with non-zero forward speed,

$$\sum_{j=1}^{6}\left[(m_j\delta_{jk}+m_{jk})\ddot{x}_j+b_{jk}\dot{x}_j+c_{jk}x_j+\int_{-\infty}^{t}K_{jk}(t-\tau)\dot{x}_j(\tau)\,d\tau\right]=f_k(t) \qquad (5.2)$$

where m_j = inertia of the ship in the jth mode,

$c_{jk}x_j$ = hydrostatic force in the kth mode due to displacement x_j in the jth mode,

$\delta_{jk} = 1$ if $j = k$, otherwise $\delta_{jk} = 0$ if $j \neq k$.

The constants m_{jk} and b_{jk} are functions of the instantaneous potential and $K_{jk}(t)$ is the kernel which introduces a dependence on the history of the potential. As noted in Chapter 4, the use of a velocity potential function requires the assumption of irrotational flow, hence memory effects due to vorticity are ignored and the primary source of the memory effects is the generation of surface waves.

The importance of fluid memory effects, originally acknowledged by Cummins [25], means that they continue to form an important part in theoretical formulations of motion dependent hydrodynamic actions. Section 2.2 discussed some of the methods for the calculation of time dependent velocity potentials. Such methods will invariably use a formulation which includes a convolution integral formulation as part of the equations of motion. King [52] uses a similar equation of motion to that suggested by Cummins [25] which involves memory functions to describe both radiation and wave excitation (incident wave and diffraction) contributions. Similar formulations may be found in the methods of Beck

and Liapis [10], Bingham et al. [13, 14], Korsmeyer and Bingham [53] and Yi and Hsiung [104], to list but a few.

As noted in Chapter 4, the theoretical methods available for this study to calculate hydrodynamic data are frequency domain methods. In addition, experimental hydrodynamic data determined using devices such as planar motion mechanisms (PMM) is also in the frequency domain. Neither method accounts for fluid memory effects. Given the importance of including memory effects in any realistic method of determining ship motions, one requires a means to express the hydrodynamic data, available in the frequency domain from either theoretical or experimental methods, in a form that is able to account for such memory effects.

Ogilvie [80] showed that there was a relationship between the representation of fluid actions using convolution integrals and the equivalent frequency domain data. This relationship may be used to allow the data from the existing, extensively validated, theoretical frequency domain methods, as well as experiments, to be used as part of a time domain method.

5.3 Relationship Between Functional and Frequency Domain Representations

Chapter 4 detailed the methods by which theoretical hydrodynamic data may be determined using frequency domain methods, referenced to either the equilibrium or body fixed axis systems. To successfully use this data in a time domain method employing convolution integrals, one requires the means to convert the frequency domain data to a time domain impulse response function representation. The methods that follow allow such a transformation to be performed.

The Fourier transform of an convolution integral of the form found in Equation 5.1 is the

product of the Fourier transforms of the convoluted variables. That is to say,

$$F(i\omega_e) = \mathcal{F}\{f(\tau)\} = \int_{-\infty}^{\infty} f(\tau)e^{-i\omega_e\tau}\,d\tau = H(i\omega_e)V(i\omega_e)$$

where

$$H(i\omega_e) = \mathcal{F}\{h(\tau)\} = \int_{-\infty}^{\infty} h(\tau)e^{-i\omega_e\tau}\,d\tau$$

and

$$V(i\omega_e) = \mathcal{F}\{v(\tau)\} = \int_{-\infty}^{\infty} v(\tau)e^{-i\omega_e\tau}\,d\tau.$$

The Fourier transform of an arbitrary action is the product of the Fourier transforms of the transfer function and the velocity signal. Hence $H(i\omega_e)$ is the transfer function and is equal to the Fourier transform of the impulse response function. The transfer function may be expressed in terms of real and imaginary parts,

$$H(i\omega_e) = H^R(\omega_e) + iH^I(\omega_e) = \int_{-\infty}^{\infty} h(\tau)\{\cos(\omega_e\tau) - i\sin(\omega_e\tau)\}\,d\tau.$$

Hence, by comparison, it becomes clear the real and imaginary parts of the transfer function may be represented in terms of the impulse response function by

$$H^R(\omega_e) = \int_{-\infty}^{\infty} h(\tau)\cos(\omega_e\tau)\,d\tau \tag{5.3}$$

and

$$H^I(\omega_e) = -\int_{-\infty}^{\infty} h(\tau)\sin(\omega_e\tau)\,d\tau. \tag{5.4}$$

Taking the inverse Fourier transform of the impulse response function gives:

$$h(\tau) = \frac{1}{2\pi}\int_{-\infty}^{\infty} H(i\omega_e)e^{i\omega_e\tau}\,d\omega_e$$

which may be expanded to give

$$h(\tau) = \frac{1}{2\pi}\int_{-\infty}^{\infty}\{H^R(\omega_e)\cos(\omega_e\tau) - H^I(\omega_e)\sin(\omega_e\tau)\}\,d\omega_e + \frac{i}{2\pi}\int_{-\infty}^{\infty}\{H^I(\omega_e)\cos(\omega_e\tau) + H^R(\omega_e)\sin(\omega_e\tau)\}\,d\omega_e$$

It may be argued that if the impulse response function is real the second integration is zero. Also, the symmetry of the integrand (from Equations 5.3 and 5.4) of the first integral suggests that the impulse response function may be written as

$$h(\tau) = \frac{1}{\pi}\int_0^\infty \{H^R(\omega_e)\cos(\omega_e\tau) - H^I(\omega_e)\sin(\omega_e\tau)\}\, d\omega_e \qquad \text{for all} \quad \tau. \tag{5.5}$$

If it is accepted that the impulse response function $h(\tau)$ is equal to zero for $\tau < 0$, then

$$\int_0^\infty \{H^R(\omega_e)\cos(\omega_e\tau) - H^I(\omega_e)\sin(\omega_e\tau)\}\, d\omega_e = 0 \qquad \text{for} \quad \tau < 0.$$

Furthermore, if one introduces a new variable $\tau = -\tau$, then

$$\int_0^\infty \{H^R(\omega_e)\cos(\omega_e\tau) + H^I(\omega_e)\sin(\omega_e\tau)\}\, d\omega_e = 0 \qquad \text{for} \quad \tau > 0$$

and hence it may be shown that,

$$-\int_0^\infty H^I(\omega_e)\sin(\omega_e\tau)\, d\omega_e = \int_0^\infty H^R(\omega_e)\cos(\omega_e\tau)\, d\omega_e \qquad \text{for} \quad \tau > 0. \tag{5.6}$$

Substitution of Equation 5.6 into 5.5 allows the impulse response function for $\tau > 0$ to be written in terms of the either the real or imaginary parts of the transfer function alone,

$$h(\tau) = \frac{2}{\pi}\int_0^\infty H^R(\omega_e)\cos(\omega_e\tau)\, d\omega_e, \tag{5.7}$$

or,

$$h(\tau) = -\frac{2}{\pi}\int_0^\infty H^I(\omega_e)\sin(\omega_e\tau)\, d\omega_e. \tag{5.8}$$

The previous two equations suggest that if the real or imaginary parts of the transfer function are known, then the means exists for the impulse response function to be determined. To apply this formulation to seakeeping applications requires a method by which the frequency dependent coefficients may be related to the transfer function $H(\omega_e)$.

5.4 Relationship Between Impulse Response Functions and Frequency Dependent Radiation Actions

For the determination of the relationship between the impulse response function and the frequency domain radiation coefficients, one returns again to the basic definition of the

convolution integral given in Equation 5.1. For the purposes of illustration, the limits are now between 0 and t. Considering this convolution integral subject to a steady state forced sinusoidal velocity of the form $v(t) = v_o \sin(\omega_e t)$, gives

$$\begin{aligned} f(t) &= \int_0^t h(\tau) v_o \sin(\omega_e t - \omega_e \tau)\, d\tau \\ &= v_o \sin(\omega_e t) \int_0^t h(\tau) \cos(\omega_e \tau)\, d\tau - v_o \cos(\omega_e t) \int_0^t h(\tau) \sin(\omega_e \tau)\, d\tau. \end{aligned}$$

If one allows the upper limit of the integration to tend towards infinity, the transient elements of the equation will tend to zero and the system will be undergoing steady state sinusoidal oscillation. Hence the limiting value of $f(t)$ becomes,

$$\begin{aligned} \lim_{t\to\infty} f(t) &= v_o \sin(\omega_e t) \int_0^\infty h(\tau) \cos(\omega_e \tau)\, d\tau - v_o \cos(\omega_e t) \int_0^\infty h(\tau) \sin(\omega_e \tau)\, d\tau \\ &= f_o(\omega_e) \sin(\omega_e t + \epsilon(\omega_e)). \end{aligned} \tag{5.9}$$

Given that it has been assumed that $h(\tau) = 0$ for $\tau < 0$ the lower limits of integration in Equation 5.9 may be expanded to $-\infty$ without changing the value, giving,

$$\begin{aligned} f_o(\omega_e) \sin(\omega_e t + \epsilon) &= v_o \sin(\omega_e t) \int_{-\infty}^\infty h(\tau) \cos(\omega_e \tau)\, d\tau \\ &\quad - v_o \cos(\omega_e t) \int_{-\infty}^\infty h(\tau) \sin(\omega_e \tau)\, d\tau. \end{aligned} \tag{5.10}$$

For the conventional frequency domain ship motion problem, the linear system is considered to be subject to an input velocity of the form $v(t) = v_0 \sin(\omega_e t)$. In the case where the ship-fluid system has reached a steady state, i.e. the ship has been oscillating for a sufficiently long period of time for all time dependent effects, such as memory effects, to have tended to zero, the frequency domain formulation of the hydrodynamic actions may be written as

$$\begin{aligned} f_0(\omega_e) \sin(\omega_e t + \epsilon(\omega_e)) &= A(\omega_e)\dot{v}(t) + B(\omega_e) v(t) \\ &= A(\omega_e)\omega_e v_0 \cos(\omega_e t) + B(\omega_e) v_0 \sin(\omega_e t), \end{aligned} \tag{5.11}$$

where $A(\omega_e)$ is the hydrodynamic added mass or the acceleration oscillatory derivative depending on which axis system the motions are referenced. Correspondingly, $B(\omega_e)$ is the hydrodynamic damping or the velocity oscillatory derivative depending on axis system.

Hence, comparison of Equations 5.11 and 5.9 yields the following relationships

$$B(\omega_e) = \int_0^\infty h(\tau)\cos(\omega_e\tau)d\tau \tag{5.12}$$

and

$$A(\omega_e)\omega_e = -\int_0^\infty h(\tau)\sin(\omega_e\tau)d\tau. \tag{5.13}$$

Comparison of these relationships to those in Equations 5.3 and 5.4 shows clearly that the damping term is equivalent to the real part of the transfer function and the product of encounter frequency and added mass to the imaginary. Hence the frequency domain hydrodynamic transfer function may be written as,

$$H(i\omega_e) = A(\omega_e)i\omega_e + B(\omega_e). \tag{5.14}$$

This allows one to use Equations 5.7 and 5.8 to calculate the impulse response function for $\tau > 0$ from frequency domain hydrodynamic data in the following way,

$$h(\tau) = \frac{2}{\pi}\int_0^\infty B(\omega_e)\cos(\omega_e\tau)\,d\omega_e, \tag{5.15}$$

or,

$$h(\tau) = -\frac{2}{\pi}\int_0^\infty A(\omega_e)\omega_e\sin(\omega_e\tau)\,d\omega_e. \tag{5.16}$$

These equations provide the tools that are required to successfully use hydrodynamic data that has been determined in the frequency domain as part of a time domain method that employs convolution integrals. However, there are certain aspects of frequency domain hydrodynamic coefficients that require special consideration when converting to a time domain convolution integral representation (see Chapter 7).

5.5 Convolution Integral Representation of Hydrodynamic Actions

The evaluation of Equations 5.15 and 5.16 is complicated by the fact that in many cases the frequency domain hydrodynamic data tends to non-zero values at infinite frequency. To

simplify the problem a method was developed by Bishop, Burcher and Price [16], whereby the frequency dependent terms were expressed as follows

$$\begin{aligned} A(\omega_e) &= A^*(\omega_e) + A(\infty), \\ B(\omega_e) &= B^*(\omega_e) + B(\infty), \end{aligned}$$

where $A(\infty)$ is the asymptotic value of the added mass and $B(\infty)$ is the asymptotic value of the damping and where, as ω_e tends to infinity

$$\begin{aligned} \lim_{\omega_e \to \infty} A^*(\omega_e) &= 0, \\ \lim_{\omega_e \to \infty} B^*(\omega_e) &= 0. \end{aligned}$$

Hence, using the result of Equation 5.14 it may be shown that

$$i\omega_e\{A^*(\omega_e) + A(\infty)\} + \{B^*(\omega_e) + B(\infty)\} = \int_0^\infty h(\tau)e^{-i\omega_e\tau}d\tau.$$

The impulse response function may be divided into two components in a fashion similar to the frequency dependent coefficients to give $h(\tau) = h^*(\tau) + h^\infty(\tau)$, resulting in

$$i\omega_e A^*(\omega_e) + B^*(\omega_e) = \int_0^\infty h^*(\tau)e^{-i\omega_e\tau}d\tau \tag{5.17}$$

and

$$i\omega_e A(\infty) + B(\infty) = \int_0^\infty h^\infty(\tau)e^{-i\omega_e\tau}d\tau. \tag{5.18}$$

Hence in a similar fashion to Equations 5.15 and 5.16, the impulse response function $h^*(\tau)$ for $\tau > 0$ may be evaluated by,

$$h^*(\tau) = \frac{2}{\pi}\int_0^\infty B^*(\omega_e)\cos(\omega_e\tau)d\omega_e, \tag{5.19}$$

$$= -\frac{2}{\pi}\int_0^\infty A^*(\omega_e)\omega_e\sin(\omega_e\tau)d\omega_e. \tag{5.20}$$

Bishop et al. [15] showed that to obtain the constants $A(\infty)$ and $B(\infty)$ from Equation 5.18 the function $h^\infty(\tau)$ must take the form

$$h^\infty(\tau) = -A(\infty)\delta(\tau)\frac{d}{d\tau} + B(\infty)\delta(\tau).$$

Hence the complete form of the impulse response function now becomes

$$h(\tau) = -A(\infty)\delta(\tau)\frac{d}{d\tau} + B(\infty)\delta(\tau) + h^*(\tau).$$

Substitution of this impulse response function equation into the convolution integral equation (of the form of Equation 5.1) gives the following function

$$\begin{aligned} f(t) &= \int_0^t h(\tau)v(t-\tau)\,d\tau \\ &= -A(\infty)\dot{v}(t) + B(\infty)v(t) + \int_0^t h^*(\tau)v(t-\tau)\,d\tau. \end{aligned} \tag{5.21}$$

The form of the previous equation is similar to that found in for formulation of Cummins [25] and others, e.g. Equation 5.2. It contains instantaneous components which are dependent upon the value of the acceleration and velocity and an additional convolution integral which imparts the "memory" effects.

5.6 Wave Excitation Impulse Response Functions

The methods that have been presented for the calculation of radiation impulse response functions are relevant for the calculation of wave excitation impulse response functions as well. Specific differences exist between the two types of data which change the manner in which the impulse response functions are calculated.

In particular, the conditions exist in the ship wave system whereby the ship will experience an exciting force due to a particular wave prior to its reaching the reference point at the centre of gravity. If one considers a single wave approaching the ship from directly ahead, this wave will begin to exert an exciting force/moment on the ship from the moment it reaches the bow.

Figure 5.1 shows a single oncoming wave reaching the bow of the vessel at time $t = \tau - \sigma$. Prior to that time there is no excitation force/moment acting on the ship. However, between $t = \tau - \sigma$ and $t = \tau$ and for a subsequent period of time as $t > \tau$, the wave will be exerting a force/moment on the ship. This presents something of a problem, as it is generally assumed that the "memory" effect relates to the past actions, be they motions or excitations. In the case of wave excitation in the ship-wave system, one requires a means of including "memory" of both past *and* future excitation, prior to reaching the reference point. This provokes a conflict with the condition of physical realisability, which would have it that

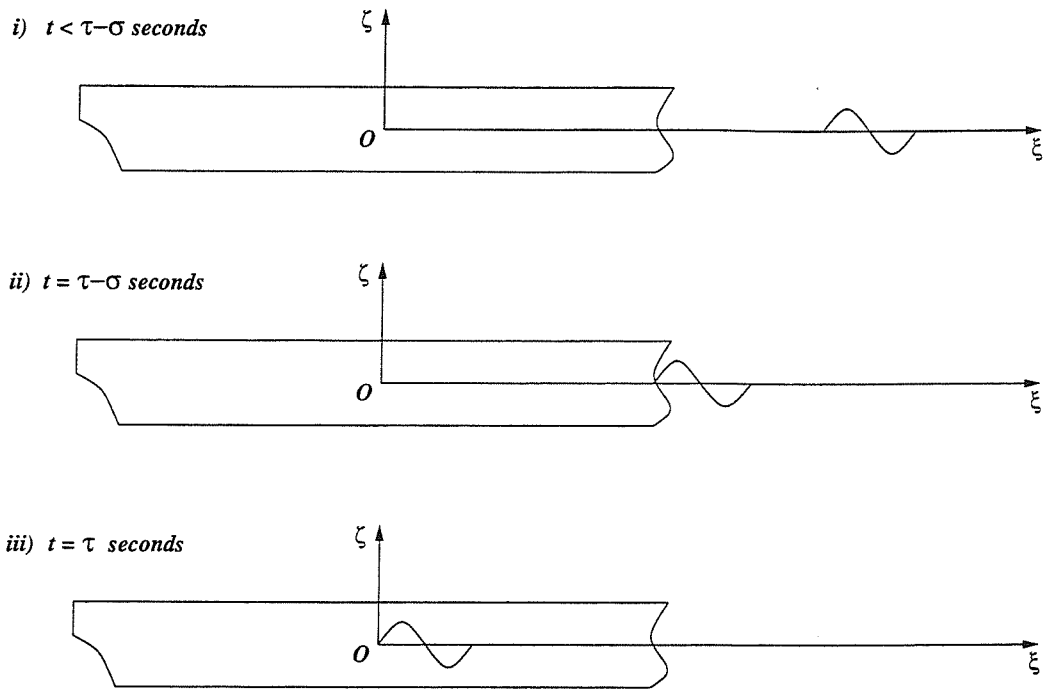

Figure 5.1: Time history of a single wave approaching the vessel. Axis system $O\xi\eta\zeta$ has the origin O on the calm water surface.

there may be no response before the application of an input.

The problem lies in the very nature of the description of the system. The excitation of a ship by waves cannot be accurately represented by a system that exists only at the centre of mass or other reference point within the vessel. A ship has length and breadth and is subject to forces that may act on it some distance from the centre of mass. Hence, to say that a wave may only act on the vessel when it has reached the reference point at the centre of mass is clearly incorrect physically.

It would be possible to move the reference point for the impulse response functions to a point somewhere in front of the vessel. In this way the impulse response functions would include only a positive time component. However, to avoid having to define a different reference point for the calculation, it is convenient to instead allow there to be a negative

time component to the wave excitation impulse response functions. Whilst this could be said to violate the condition of physical realisability, it is in fact simply the result of shifting the reference point for an impulse response function which otherwise satisfies this condition. This concept has been used successfully in other of studies regarding the time domain simulation of ship motions [14, 52, 53].

Determination of wave excitation impulse response functions is, in most respects, similar to the process demonstrated for the motion dependent hydrodynamic actions. Consider for example a sinusoidal excitation $\Xi(i\omega_e)$, where

$$\begin{aligned}\Xi(i\omega_e) &= \Xi^R(\omega_e) + i\Xi^I(\omega_e) \\ &= \int_{-\infty}^{\infty} h_\alpha(\tau)\{\cos(\omega_e\tau) - i\sin(\omega_e\tau)\}\, d\tau.\end{aligned}$$

In a similar fashion to Equations 5.3 and 5.4, it is possible to relate the real and imaginary parts of the transfer function to the impulse response function as follows

$$\Xi^R(\omega_e) = \int_{-\infty}^{\infty} h_\alpha(\tau)\cos(\omega_e\tau)\, d\tau \tag{5.22}$$

and

$$\Xi^I(\omega_e) = -\int_{-\infty}^{\infty} h_\alpha(\tau)\sin(\omega_e\tau)\, d\tau. \tag{5.23}$$

Taking the inverse Fourier transform of the impulse response function $h_\alpha(\tau)$ gives

$$h_\alpha(\tau) = \frac{1}{2\pi}\int_0^{\infty} \Xi(i\omega_e)e^{i\omega_e\tau}\, d\omega_e$$

which expands to give

$$\begin{aligned}h_\alpha(\tau) = \frac{1}{2\pi}\int_0^{\infty}\{\Xi^R(\omega_e)\cos(\omega_e\tau) - \Xi^I(\omega_e)\sin(\omega_e\tau)\}\, d\omega_e + \\ \frac{i}{2\pi}\int_0^{\infty}\{\Xi^I(\omega_e)\cos(\omega_e\tau) + \Xi^R(\omega_e)\sin(\omega_e\tau)\}\, d\omega_e.\end{aligned}$$

Using a similar argument to that used to obtain Equation 5.5, this may be simplified to give

$$h_\alpha(\tau) = \frac{1}{\pi}\int_0^{\infty}\{\Xi^R(\omega_e)\cos(\omega_e\tau) - \Xi^I(\omega_e)\sin(\omega_e\tau)\}\, d\omega_e \qquad \text{for all} \quad \tau. \tag{5.24}$$

Whereas in the case of the motion dependent hydrodynamic actions it was assumed that $h(\tau) = 0$ for $\tau < 0$, allowing the impulse response function to be expressed in terms of

either the real or imaginary part of the transfer function, this is not the case for the wave excitation. Because $h_\alpha(\tau)$ is assumed to be non-zero for $\tau < 0$, no further manipulation is possible and Equation 5.24 represents the final form of the relationship between the frequency domain excitation and the impulse response function. Whereas the motion dependent hydrodynamic actions may be calculated using either the real or imaginary parts of the transfer function, the wave excitation impulse response function requires both the real *and* imaginary parts of the wave excitation.

6 Numerical Evaluation of Frequency Domain Data

The previous chapters, in particular Chapters 4 and 5, have concentrated on the theoretical methods that exist for the determination of hydrodynamic data and the representation of that data in either the frequency or time domains. This chapter and Chapter 7 examine the practical aspects of calculating that data in the frequency domain and subsequently the time domain.

The process of determining the required data for a convolution integral formulation of the ship motion problem involves a series of steps. Firstly, one must model the ship in question using lines plan software. This lines representation is then used to create a panelled representation of the hull surface for use in the three-dimensional source distribution method. Having determined the frequency domain hydrodynamic data numerical methods are required for the Fourier transformation of the frequency domain data into time domain impulse response functions.

6.1 Panel Representation of Hull Surface

The theoretical frequency domain methods described in Chapter 4 involve the distribution of singularities over the surface of the vessel in order to solve a boundary value problem for the fluid potential. This distribution of the singularities is achieved by the discretisation of the hull surface into a finite number of quadrilateral panels, each with a singularity at its

centre.

The process of creating the panel representation of the hull begins with the creation of a hull description using a ship lines software. For this investigation the software package used is *ShipShape*, developed by the Wolfson Unit for Marine Technology and Industrial Aerodynamics [89]. This software uses a network of cubic splines to represent the surface of the ship. The traditional lines plan of waterlines, sections and buttocks is created from this spline network by intersecting the surface of the hull with the appropriate planes.

The panelled representation of the hull surface is determined using the program *panshp* [5]. This method uses the cubic patch representation of the hull output by *ShipShape* to distribute panels around the sections of the hull. The full details of this method will not be elaborated upon here but needless to say this method has been developed to allow considerable flexibility in the manner in which the panel representation of the hull is created. This flexibility means that one must have a clear idea of what represents the best solution to the problem of representing the hull.

It has been shown by Inglis [45] that the aspect ratio of the panels used is important for the calculation of the hydrodynamic added mass and damping coefficients. Inglis concluded that the optimum ratio was as near as practically possible to unity. In the practical application of panelling techniques to realistic ship hulls, there exists the problem of how one addresses the conflicting issues of the accuracy of the representation and the total number of panels, given that the computational time is proportional to the number of panels.

When creating a mesh representation of the surface of a hull, the panels should ideally be concentrated in the regions where the surface changes most rapidly. This allows for a more accurate representation of the changing fluid flow in these areas. Since the geometry of most ships changes more quickly around the girth than along the length, it is often tempting to increase the number of panels around the girth of the ship whilst maintaining the number along the length. In this way the total number of panels is not increased excessively. This conflicting desire for accurate representation without excessive numbers of panels can lead to unfavourable aspect ratios, in particular in the bow and stern where

the section perimeter is reduced. In such cases any advantage obtained through improved geometrical representation may be outweighed by the effects of poor aspect ratio.

The problem of aspect ratio is not the only serious consideration that must be made when panelling the surface of the hull. The time taken for the calculation of the frequency domain data is proportional to the square of the total number of panels. Hence, to ensure reasonable computational time, it is important to ensure that in addition to obtaining an accurate panelled version of the hull shape, the total number of panels used to create that representation is reasonable.

The result of the conflicting issues of accuracy and total number of panels is that there will exist an optimum solution to the problem of creating the panelled representation that will involve a compromise of some sort. A large number of panels will accurately model the hull form but will lead to very long calculation times for the frequency domain methods. On the other hand, being too economical with the number of panels used could result in an insufficiently accurate representation of the hull form and the corresponding frequency domain hydrodynamic data.

The program *panshp* gives the user two option for the distribution of panels over the hull surface. The first of these defines a fixed number of panels around each section and the desired aspect ratio. It will be referred to as the "Fixed Method". The second method requires the user to select the height of the panels as a fraction of the draft as well as the desired aspect ratio. This method results in a variable number of panels around each section. This avoids the dense clustering of panels found in the first method in places where the section perimeter reduces, such as the bow or the stern. This second method will be referred to as the "Variable Method"

6.1.1 Fixed Number of Panels Method

This method requires the user to define the number of panels per section, the aspect ratio and the longitudinal position of the most forward and most aft sections. At the first for-

ward section, the section is divided into an equal number of segments by dividing by the selected number of panels. The distance of the next section aft of the first is then found by multiplying the height of the panels in the first section by the desired aspect ratio. A line parallel to the waterline (constant z) is then traced aft the required distance and the next section line is started from this place. This section line is divided into equal parts in the same manner as the first and the process repeated to determine the distance to the next section. This process continues until the midships point of the ship is reached. Since it is unlikely that the final section will occur at exactly the midships point, the sectioning is carried on beyond the midships point. The distance that the final section overshoots the midship point is then distributed back over the sections, using their longitudinal spacing as a weighting. A second pass is then made from the forward section towards the middle of the ship. The sections determined in the first pass are split into segments of even length, the panel corners being calculated along a constant coordinate line (fixed x).

The same steps are repeated for the aft part of the hull. In this case the sectioning process starts from the aft most section and proceeds towards the midships point. Finally the bow and stern profiles are panelled. In the case of the bow, the distribution of panels between the forward most section and the actual bow is carried out by first of all tracing the profile of the bow from the base of the forward most section up to the maximum height (the constant z value used previously). Panels corners are distributed evenly along this profile line and quadrilateral panels are then formed using these points and the corresponding ones on the forward most section.

6.1.2 Variable Number of Panels Method

The Variable Method provides an alternative panelling scheme to that previously described. This method varies the number of panels around each section, meaning it is possible to avoid unnecessarily dense concentrations of panels in areas where the section perimeter is reduced, such as the bow or stern.

Whereas the Fixed Method requires the user to select the number of panels to be applied

around every section, in the Variable Method an ideal panel height must be specified (as a fraction of the draft), along with a restriction on the maximum and minimum number of panels. By applying a restriction on the maximum and minimum number of panels it is possible to ensure that small perimeter sections have sufficient accuracy, whilst ensuring that the number of panels used to describe larger sections is economical.

The process for panelling the hull is much the same as for the Fixed Method . Starting from the forward end of the ship, the forward most section is divided into segments based on the ideal panel height that has been specified. The position of the next section is then found in an identical method to the previous method, using the aspect ratio multiplied by the height of the panels in the previous section. The Variable Method is more numerically intensive than the Fixed Method due to the fact that if two adjacent sections have a different number of panels around their section then the trace of the section line between them must be divided in panels twice, once for each number of panels. It should also be noted that this method can result in what has been described as "geometrical leaks" [30], where panels do not fit together exactly when adjacent columns have different numbers of panels. However, it has been shown that the frequency domain methods, in which the panelled hull representations are used, are insensitive to such effects [8].

6.1.3 Comparison of Panel Representations

To compare the panelling methods, a *Series 60* ($C_B = 0.7$) type hull form was used. The *Series 60* model was originally developed by Todd [93] to address the need to develop a more systematic collection of information regarding the resistance characteristics of a single screw merchant ship. Subsequently this ship has been used for a variety of seakeeping experiments under the auspices of the International Towing Tank Committee (ITTC). The results of a number of studies performed around the world were brought together in the ITTC proceedings for 1966 by Nakamura [70]. The particulars and body plan of the *Series 60* type vessel are given in Appendix B.1.

Figures 6.1, 6.2, 6.3 and 6.4 show a *Series 60* type hull which has had its mean wetted

surface discretised using the Fixed Method . Figures 6.1 and 6.2 show cases where the number of panels around each section is 6 and the aspect ratios 2 and 1 respectively. It can be seen that reducing the aspect ratio from 2 to 1 doubles the total number of panels from 372 to 744.

Figures 6.3 and 6.4 show the same hull form but now with 10 panels per section, the former having and aspect ratio of 2 and the latter being 1. Again, halving the aspect ratio of the panels nearly doubles the total number of panels, this time from 1040 to 2060.

Figures 6.5, 6.6, 6.7 and 6.8 show the same *Series 60* hull form, this time panelled using the Variable Method . Figures 6.5 and 6.6 have a panel height of 0.35 times the draft of the vessel, which results in the maximum number of panels around any section being 6, which is the same number of panels per section as was used for the equivalent Fixed Method representation. The aspect ratios are again 2 and 1 respectively. Comparison of these two panelled hulls to those in Figures 6.1 and 6.2 shows that the total number of panels now used in the case of either aspect ratio is considerably reduced. There is a reduction in the total number of panels of around 30% in the case where the aspect ratio is 2 and around 45% where the aspect ratio is 1. Visual inspection of the panelled hulls shows that the reduction is due to there being less panels describing the sections nearest the bow and stern, where the section perimeter is smallest.

Figures 6.7 and 6.8 show the *Series 60* hull panelled using the Variable Method , now with panel height equal to 0.2 times the draft. This results in a maximum number of panels per section of 10. Again comparison of these panelled hulls with those calculated using the Fixed Method with a similar number of panels per section, shows that there is a considerable reduction in the total number of panels. In the case of the models with aspect ratio 2, this reduction is in the region of 40%, whilst for aspect ratio 1 the reduction is again close to 40%. It is again obvious that much of the savings in panel numbers is obtained in the region of the bow and the stern where the Variable Method allows the use of less panels when describing sections with smaller perimeter.

Comparison of the total number of panels in Figures 6.5 and 6.7, both with aspect ratio

2, shows that increasing the number of panels around each section from 6 to 10 results in the total number of panels being increased by a factor of nearly 3. Similar increases in the number of panels occur in Figures 6.6 and 6.8 where the aspect ratio is one. Whilst visual inspection of the models with the increased number of panels, be this the result of reducing aspect ratio or increased number of panels per section, suggests a more accurate representation of the hull surface, it is evident that use of these models will result in considerably increased computational time.

The displaced volume, LCB and wetted surface area of each of the panelled hull representations were compared to the results obtained from the original *ShipShape* model. This comparison can be seen in Table 6.1. There is little difference between the calculated values using either panelling method, the variable method giving a slightly worse prediction of the displaced volume. However, the differences are small enough in all cases to make it clear that either method will provide representations that adequately depict the hull form.

Hull Representation		∇ (m^3)	LCB Fwd. of	Wetted Surface
Method	N°. of Panels		Amidships (m)	Area (m^2)
Fixed	372	0.1591 (-1.11)	0.0128 (-14.67)	1.8316 (-0.35)
	744	0.1593 (-0.98)	0.0128 (-14.67)	1.8336 (-0.24)
	1040	0.1607 (-0.14)	0.0133 (-11.33)	1.8467 (0.47)
	2060	0.1606 (-0.16)	0.0143 (-4.67)	1.8352 (-0.15)
Variable	254	0.1576 (-2.06)	0.0103 (-31.33)	1.8197 (-0.99)
	404	0.1584 (-1.56)	0.0115 (-23.33)	1.8265 (-0.63)
	660	0.1604 (-0.32)	0.0127 (-15.33)	1.84396 (0.32)
	1310	0.1605 (-0.24)	0.0127 (-15.33)	1.8455 (0.41)

Table 6.1: Comparison of parameters predicted using different panelling techniques (% difference from *ShipShape* predictions)

It becomes clear that each of the two methods offers its own advantages. The Fixed Method possibly offers a better representation of the hull surface (free of geometric leaks), while the Variable Method allows less panels to be used, reducing the duration of subsequent

frequency domain calculations. Hence the question becomes, "Which of these methods offers the best possible combination of accuracy of solution and speed of calculation?".

6.2 Comparison of Frequency Domain Data Calculated Using Alternative Panelled Hull Forms

In an attempt to clarify the effects of mean wetted surface idealisation on hydrodynamic data, each of the hull representations shown in Figures 6.1 to 6.8 was used to calculate a range of frequency domain data. Added mass and damping coefficients were calculated for encounter frequencies ranging from 0 to 50 rad/s and $F_n = 0.2$ using the pulsating source distribution method. The upper limit was chosen as 50 rad/s due to the need for frequency domain data to be calculated to a high upper limit to enable the accurate determination of the corresponding impulse response functions [7].

6.2.1 Fixed Method

Figures 6.9 to 6.12 show hydrodynamic added mass and damping coefficients calculated using the Fixed Method . The different representations used in each case are identified in the keys of the graphs in the following way: *Fixed(a,b,c)*, where a is the total number of panels, b is the aspect ratio of the panels and c is the number of panels per section. The four panelled models tested for the Fixed Method consist of two with 6 panels per section and two with 10 panels per section. In each pair, one has an aspect ratio of 2 and the other an aspect ratio of 1.

Figure 6.9 shows pure sway and yaw added mass and damping coefficients. The only differences apparent are in the region of the irregular frequency effects which occur in the $A_{22}(\omega_e)$ data. These effects are predicted as having the largest amplitude by the hull representations having the least total number of panels. The damping coefficients $B_{22}(\omega_e)$ and $B_{66}(\omega_e)$ display larger differences in the predicted results at relatively high encounter

frequency. In particular, the irregular frequency effects in the $B_{22}(\omega_e)$ data are again predicted as having the largest amplitude by the hulls having the least total number of panels. In addition, it becomes clear that the damping at high frequencies is not well predicted by the representations with the fewest panels. It can be seen that the hull with a total of 372 panels begins to show large spikes in the predicted response from an encounter frequency of around 16 rad/s. Whilst there are fewer irregular frequency effects evident in the B_{66} data, it can be seen that the representations with 6 panels per section appear to not produce as good results as those with 10 panels per section at the highest frequencies. In particular, it can be seen that these results do not tend toward zero at high frequency, unlike the predictions using the 10 panel per section representations. The consequences of these irregular frequency effects on the calculation of the corresponding impulse response functions are discussed in Chapter 7.

Further evidence of the effect of insufficient total panel number can be seen in Figures 6.10 where the cross-coupled sway-yaw damping coefficients can again be seen to suffer from inaccuracy in the solution at high frequencies when the number of panels around the sections in smallest. Examining Figures 6.11 and 6.12 for the heave and pitch hydrodynamic coefficients, shows the similar tends are observed for these symmetric motions as were seen for the antisymmetric motions. The added mass is predicted well by all the panelled representations while the damping is not well predicted at high frequencies when the total number of panels is low.

6.2.2 Variable Method

As noted in the description of the method in Section 6.1.2, using the Variable Method prevents the accumulation of large numbers of panels in places where the section perimeter is least. This means that the panel sizes are roughly even over the length of the ship and hence the number of panels required to model the complete hull is less than for the Fixed Method using similarly sized panels at the section of greatest perimeter. While achieving a reduced total number of panels is desirable from the point of view of the time taken to

calculate the frequency domain hydrodynamic data, the data found using the fixed number of panels method suggests that savings in the total number of panels might not necessarily be without detriment. In particular, given that one requires frequency domain data to a high frequency in order to calculate the impulse response functions, it needs to be determined whether the advantages gained in terms of reduced panel numbers are rendered irrelevant by the loss of accuracy in the computed data.

Figures 6.13 to 6.16 show anti-symmetric and symmetric added mass and damping coefficients calculated using four different panelled hull representations created using the Variable Method. In a similar fashion to the Fixed Method results, the keys in the graphs describe the panelled representations as follows: *Variable(a,b,c)*, where a is the total number of panels, b is the aspect ratio of the panels and c is the maximum number of panels per section.

Examination of the sway and yaw added mass coefficients in Figure 6.13 shows that there are some differences between the values predicted by the various panelled representations as the frequency is increased. This is in contrast to Figure 6.9, where there was very little difference between the added mass values, even at high frequency, other than at irregular frequencies. The sway and yaw damping coefficients indicate that the representations using the fewest panels suffer from insufficient resolution of the hull form at quite moderate frequencies. As the frequency increases further, the damping coefficients predicted using the smallest total number of panels become particularly poor, as can be seen in the prediction of negative B_{22} and B_{66} values at high frequency. Similar trends can be seen in Figure 6.14 where the damping results using the smallest number of panels appear to be obviously inaccurate.

Considering the symmetric motions, Figure 6.15 shows that for the pure heave and pitch coefficients there is reasonable agreement between the added mass results, but as the frequency is increased considerable differences arise in the damping results. The cross coupled coefficients in Figure 6.16 again show good agreement in the added mass predictions, while the damping coefficients do not agree well as the frequency is increased.

6.2.3 Comparison of Alternative Panelling Methods

It is clear that reducing the total number of panels used to represent the mean wetted surface of the hull can have an undesirable effect on the subsequent calculation of the frequency domain hydrodynamic coefficients. Hence, for each of the two panelling methods, the two representations using the smallest number of panels (Fixed(372,2,6), Fixed(744,1,6), Variable(254,2,6) and Variable(404,1,6)) have been discarded from further consideration. This leaves four representations, two each from either panelling method, all with either a fixed or maximum number of panels per section of 10. As noted in Section 6.1.3, the difference in total number of panels required for the Variable Method is around 30-40% less than for the equivalent models found using the Fixed Method.

The results found using these four representations are compared in Figures 6.17 to 6.20. It can be seen from the pure sway and yaw coefficients in Figure 6.17 that the added mass predictions are virtually identical. The damping coefficients only show a difference at very high frequencies where the Variable Method with larger aspect ratio (Variable(660,2,10)) diverges from the other sets of results for both B_{22} and B_{66}. The cross coupled added mass coefficients in Figure 6.18 show that the results found using the two Variable Method representations diverge both from each other and the Fixed Method at high frequencies. Damping results show a similar trend, the divergence being particularly great for the Variable Method representation with the smallest number of panels.

The symmetric motion coefficients (Figures 6.19 and 6.20) show similar trends for the added mass coefficients. Results for all four representations are very similar for the entire frequency range. However, the two different panelling methods give quite different damping coefficients at high frequencies. Those calculated using the Fixed Method tend towards a constant (zero) value from a reasonably low frequency, while those calculated using the Variable Method show large oscillations at the highest frequencies.

It is believed that this oscillation at high frequencies when using the Variable Method is due to insufficient accuracy in the panelling of the ends of the ship. Inglis [45] recommended that the panel length should ideally be less than one eighth of the incident wave

length. Bailey [7] went further to suggest that in the case where added mass and damping coefficients were of interest, the criterion of panel length should instead be based in the wavelength of the radiated waves. Bailey [7] went on to show that if such a radiated wave criteria was used and panels with aspect ratio 1 were used, the total number required was given by,

$$N \approx S\left(\frac{8}{2\pi g}\right)^2 \omega_e^4.$$

where S is the area of the mean wetted surface. This means that the total number of panels required is related to the encounter frequency to the power of four. Furthermore, panels with aspect ratio greater than one increase this factor by the square of the aspect ratio. It is clear that in order to calculate frequency domain data to a sufficiently high frequency to satisfy the requirements of the transformations given in Equations 5.19 and 5.20, care must be taken in the creation of the panelled hull representation that is to be used.

Hence it is recommended that when frequency domain data is to be calculated to high frequencies, such as would be required for the calculation of impulse response functions, the Fixed Method should be used to create the panelled representation. If one were only interested in frequencies of moderate value it would appear that the Variable Method method offers the method of producing a panelled hull representation which will result in the least computational expense when calculating frequency domain data.

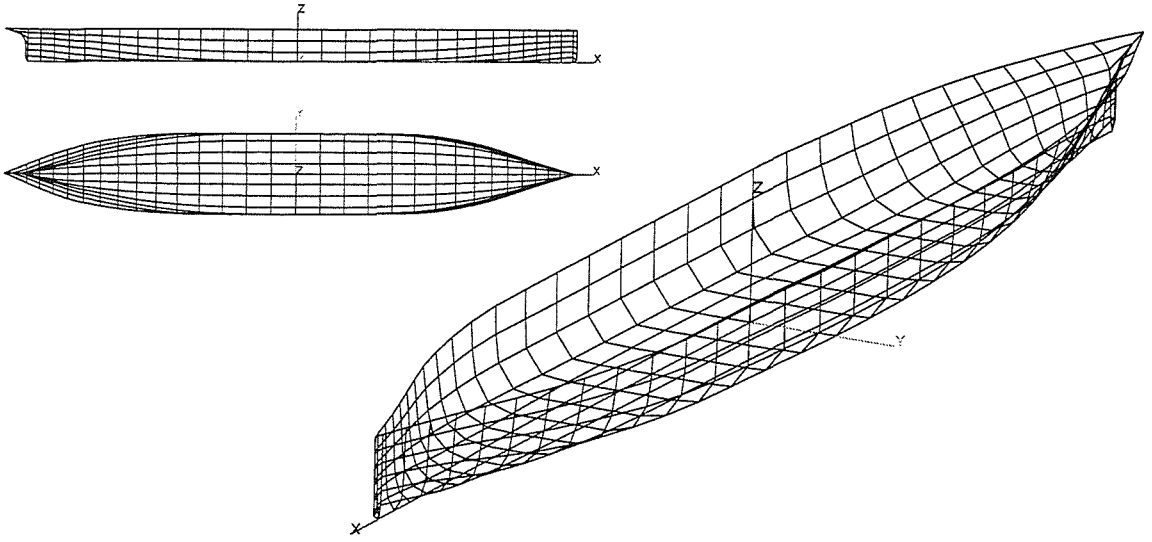

Figure 6.1: Discretisation of underwater surface of *Series 60* model, using a fixed number of panels per section. 6 panels per section, aspect ratio=2.0, total number of panels 372

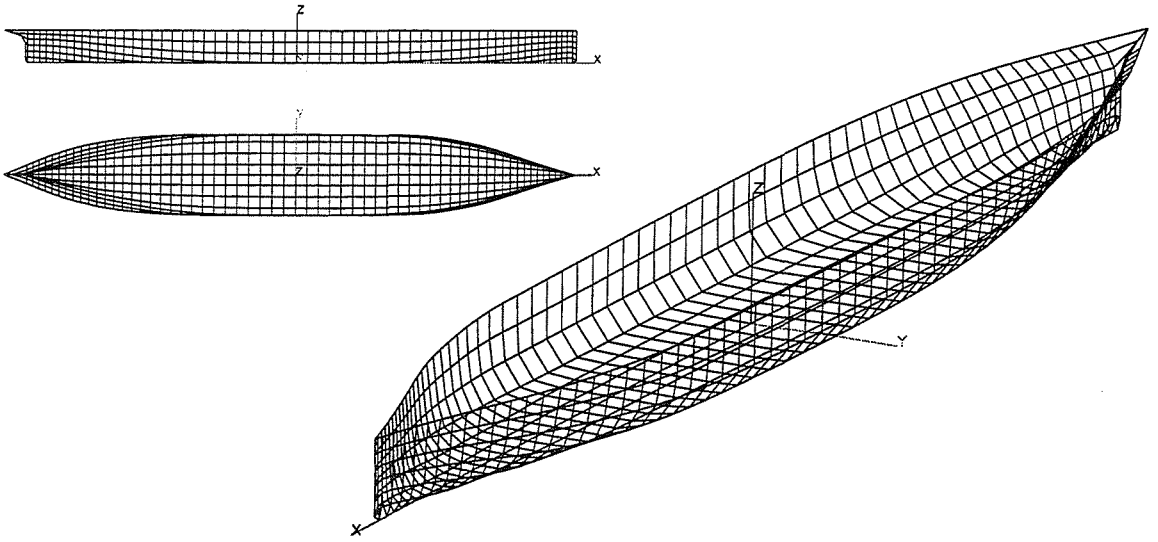

Figure 6.2: Discretisation of underwater surface of *Series 60* model, using a fixed number of panels per section. 6 panels per section, aspect ratio=1.0, total number of panels 744

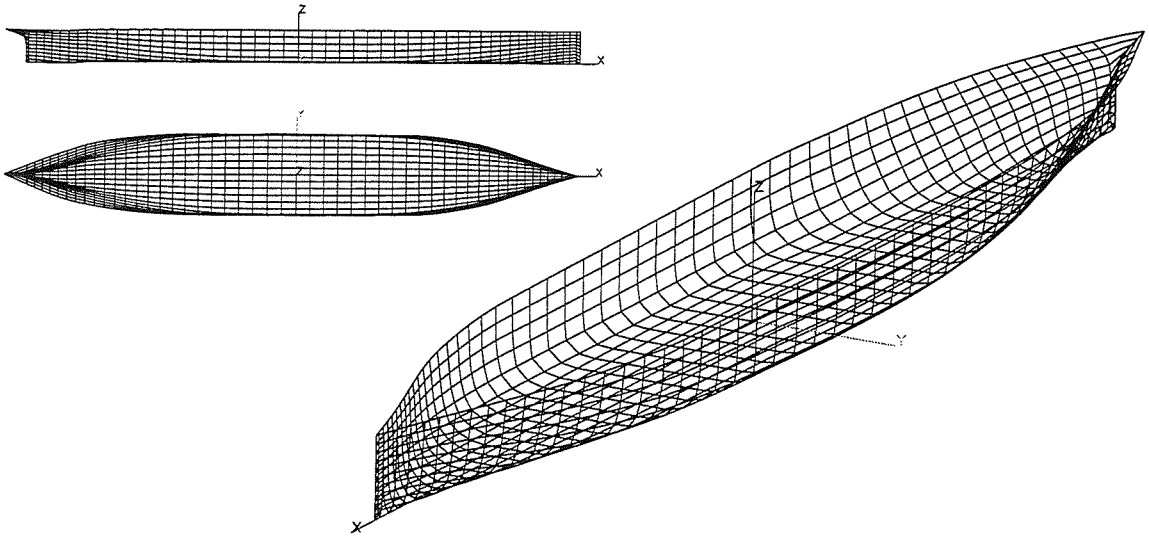

Figure 6.3: Discretisation of underwater surface of *Series 60* model, using a fixed number of panels per section. 10 panels per section, aspect ratio=2.0, total number of panels 1040

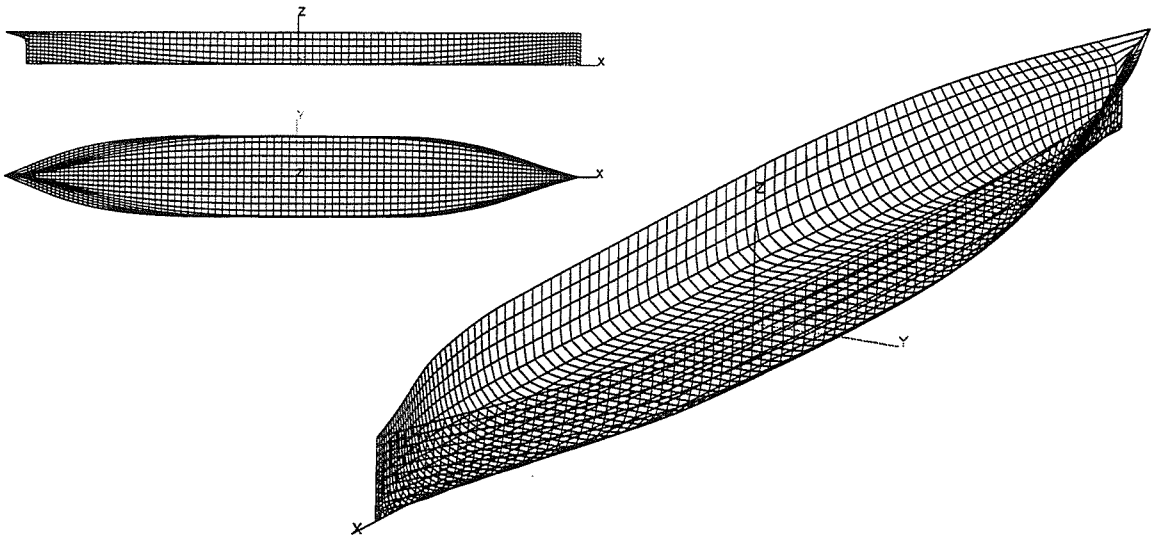

Figure 6.4: Discretisation of underwater surface of *Series 60* model, using a fixed number of panels per section. 10 panels per section, aspect ratio=1.0, total number of panels 2060

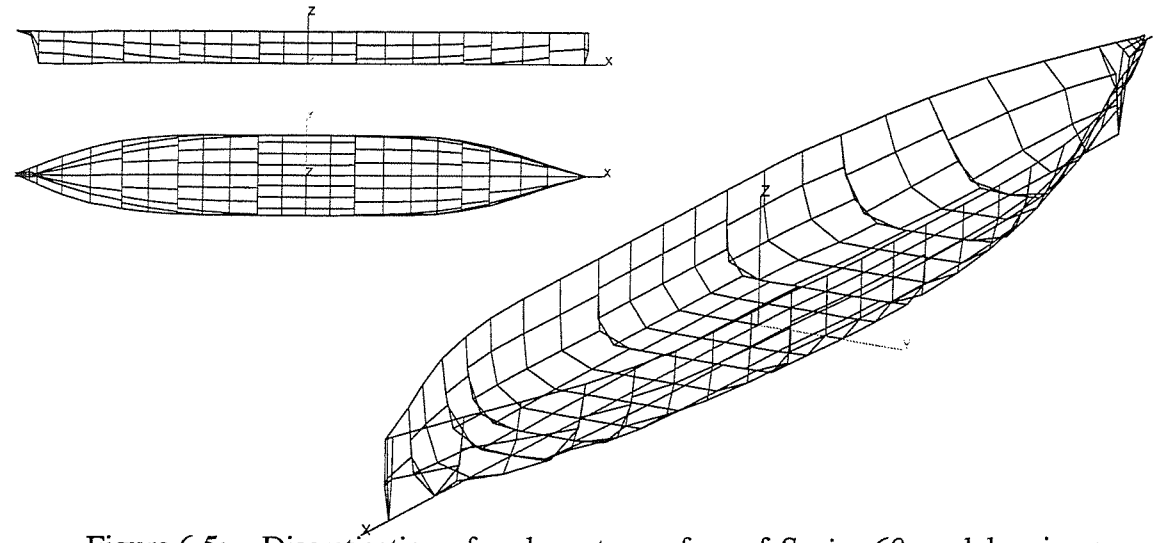

Figure 6.5: Discretisation of underwater surface of *Series 60* model, using a variable number of panels per section. Ideal panel height as a fraction of draft=0.35, aspect ratio=2.0, total number of panels 254

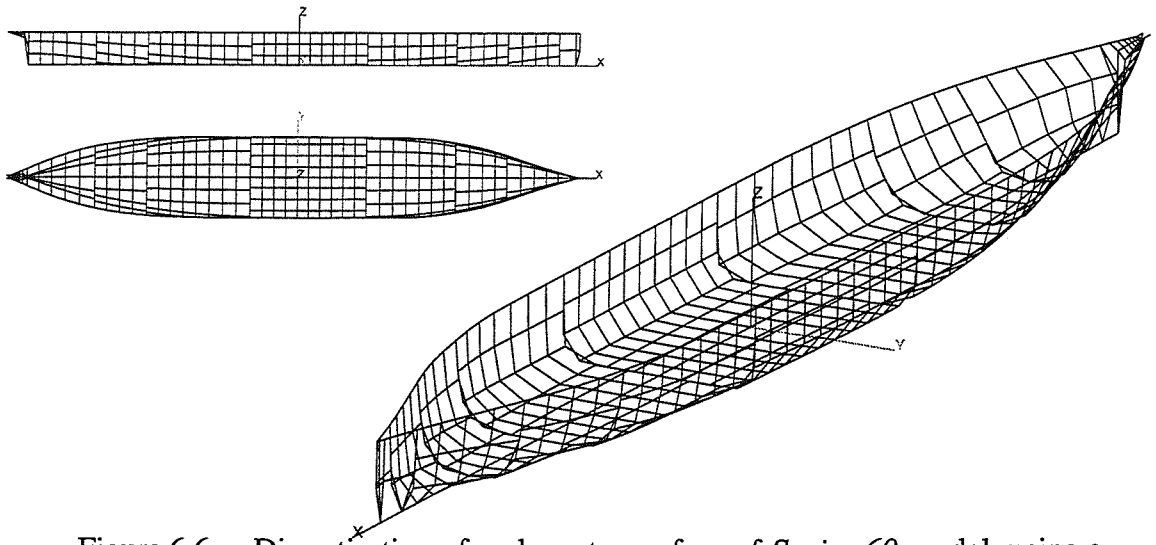

Figure 6.6: Discretisation of underwater surface of *Series 60* model, using a variable number of panels per section. Ideal panel height as a fraction of draft=0.35, aspect ratio=1.0, total number of panels 404

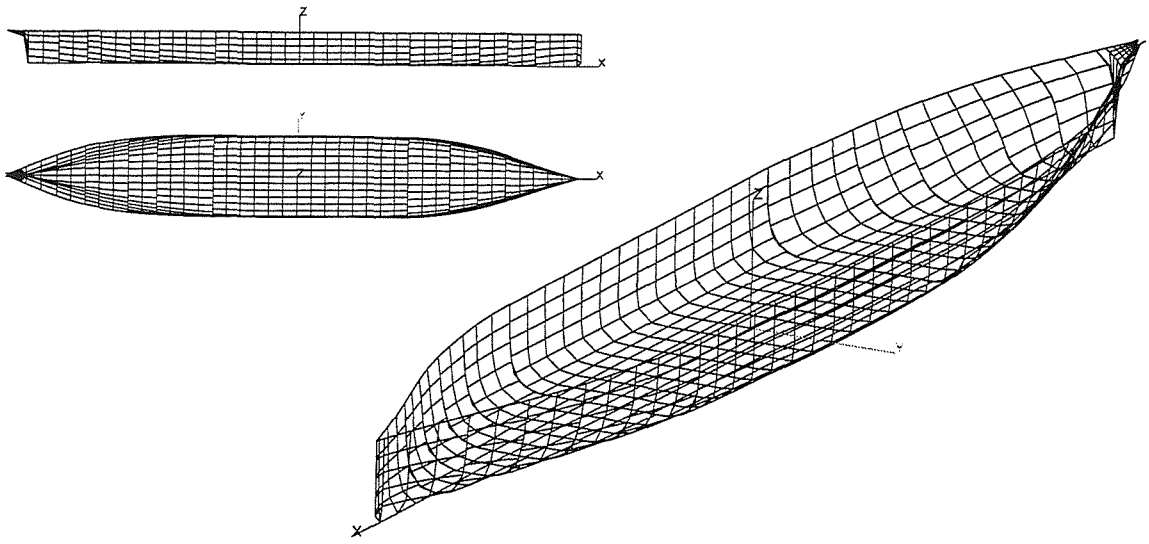

Figure 6.7: Discretisation of underwater surface of *Series 60* model, using a variable number of panels per section. Ideal panel height as a fraction of draft=0.2, aspect ratio=2.0, total number of panels 660

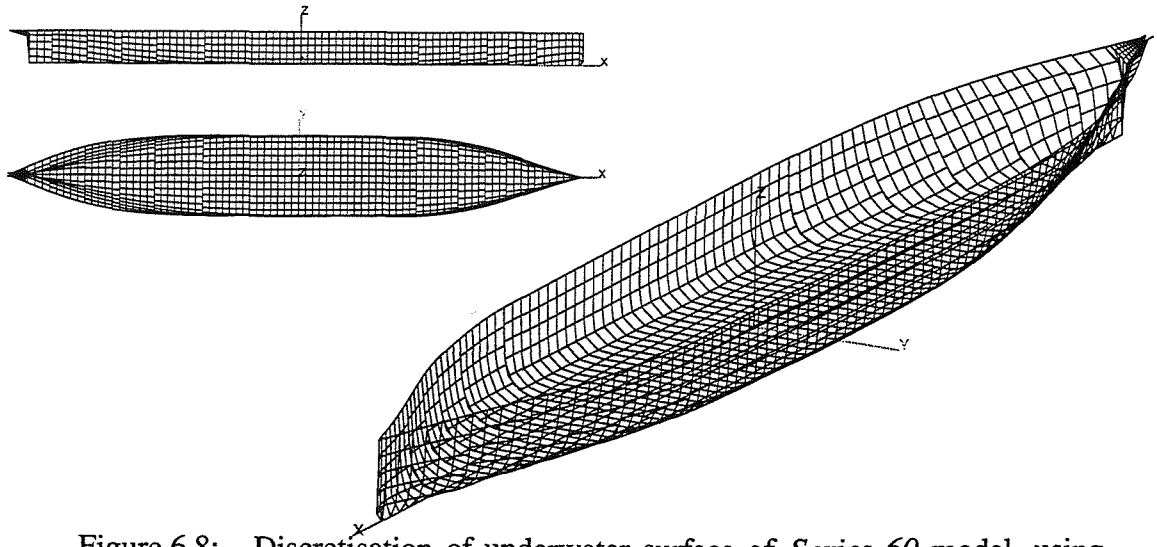

Figure 6.8: Discretisation of underwater surface of *Series 60* model, using a variable number of panels per section. Ideal panel height as a fraction of draft=0.2, aspect ratio=1.0, total number of panels 1310

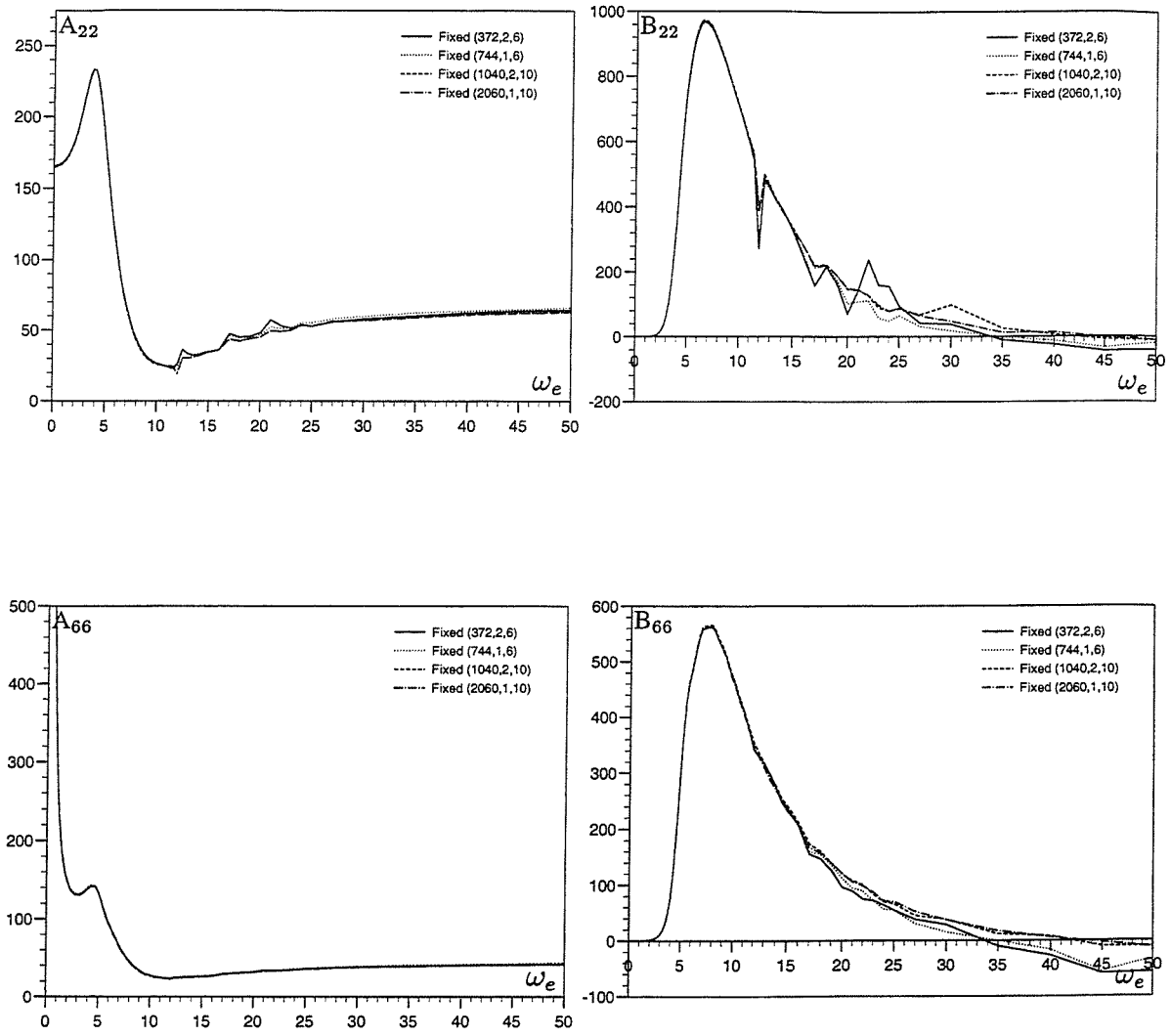

Figure 6.9: Pure sway and pure yaw added mass and damping coefficients found using fixed number of panels per section method to model Series 60 mono-hull, L=3.048m, Fn=0.2.

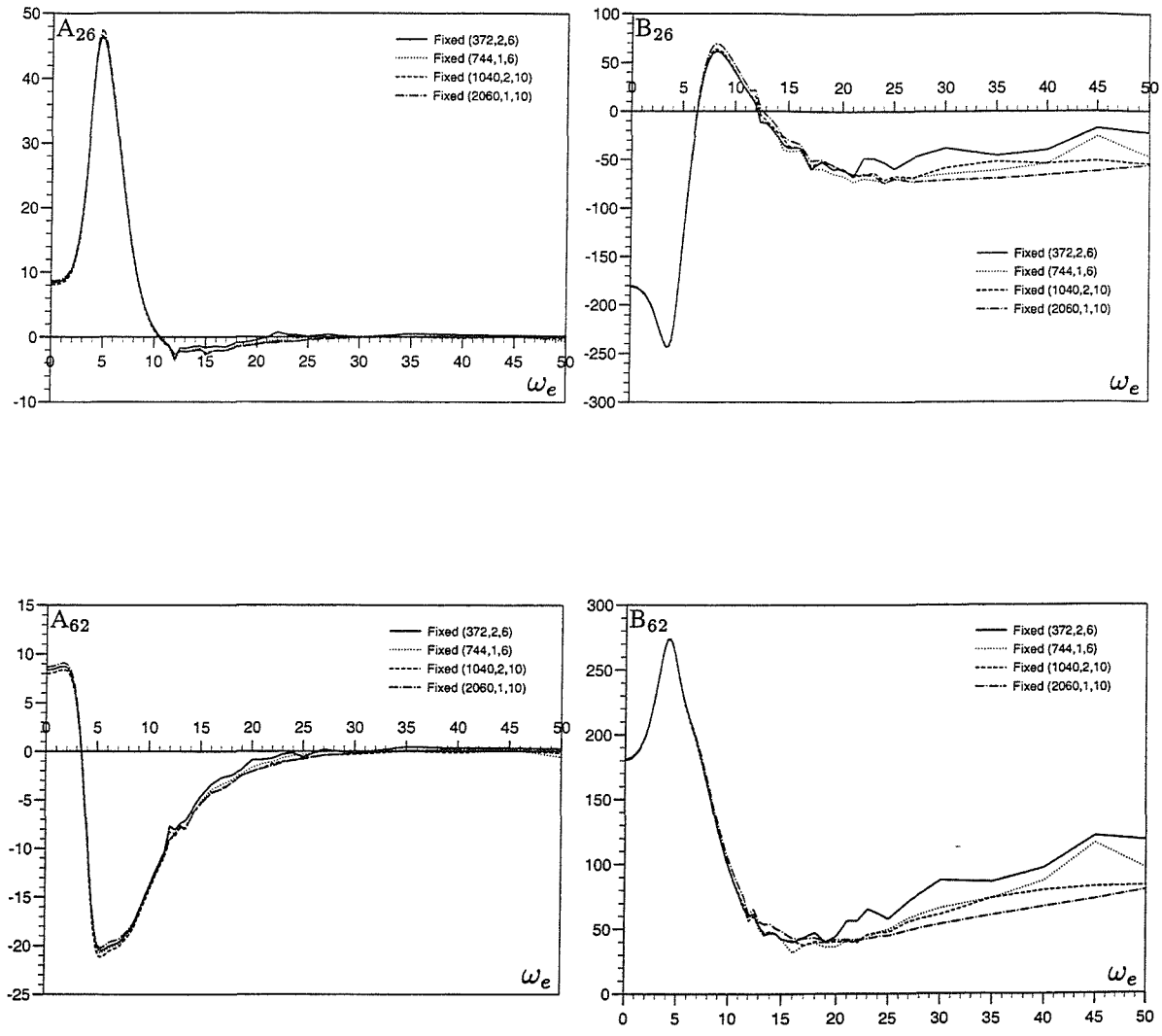

Figure 6.10: Cross coupled sway and yaw added mass and damping coefficients found using fixed number of panels per section method to model Series 60 mono-hull, L=3.048m, Fn=0.2.

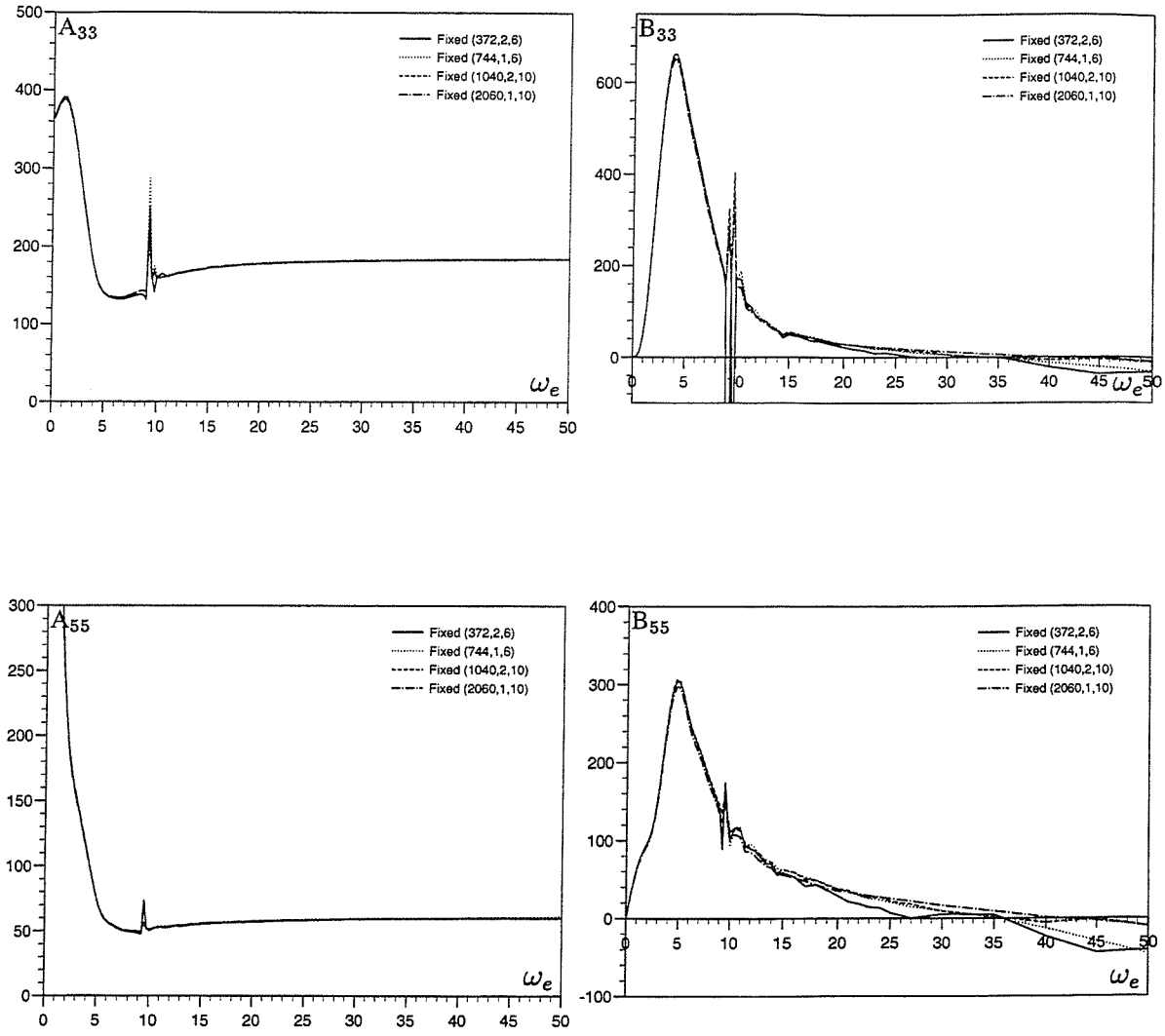

Figure 6.11: Pure heave and pure pitch added mass and damping coefficients found using fixed number of panels per section method to model Series 60 mono-hull, L=3.048m, Fn=0.2.

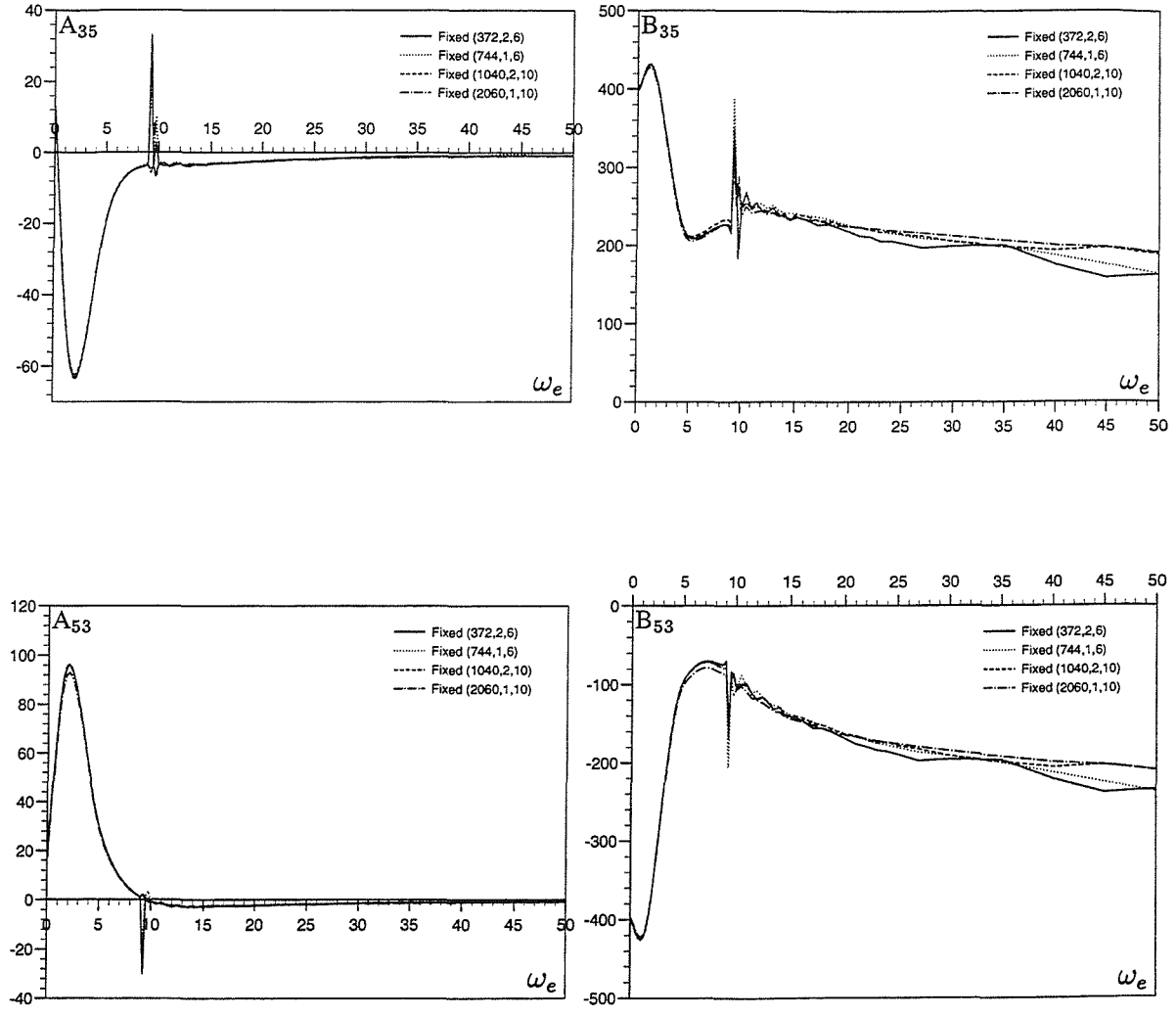

Figure 6.12: Cross coupled heave and pitch added mass and damping coefficients found using fixed number of panels per section method to model Series 60 mono-hull, L=3.048m, Fn=0.2.

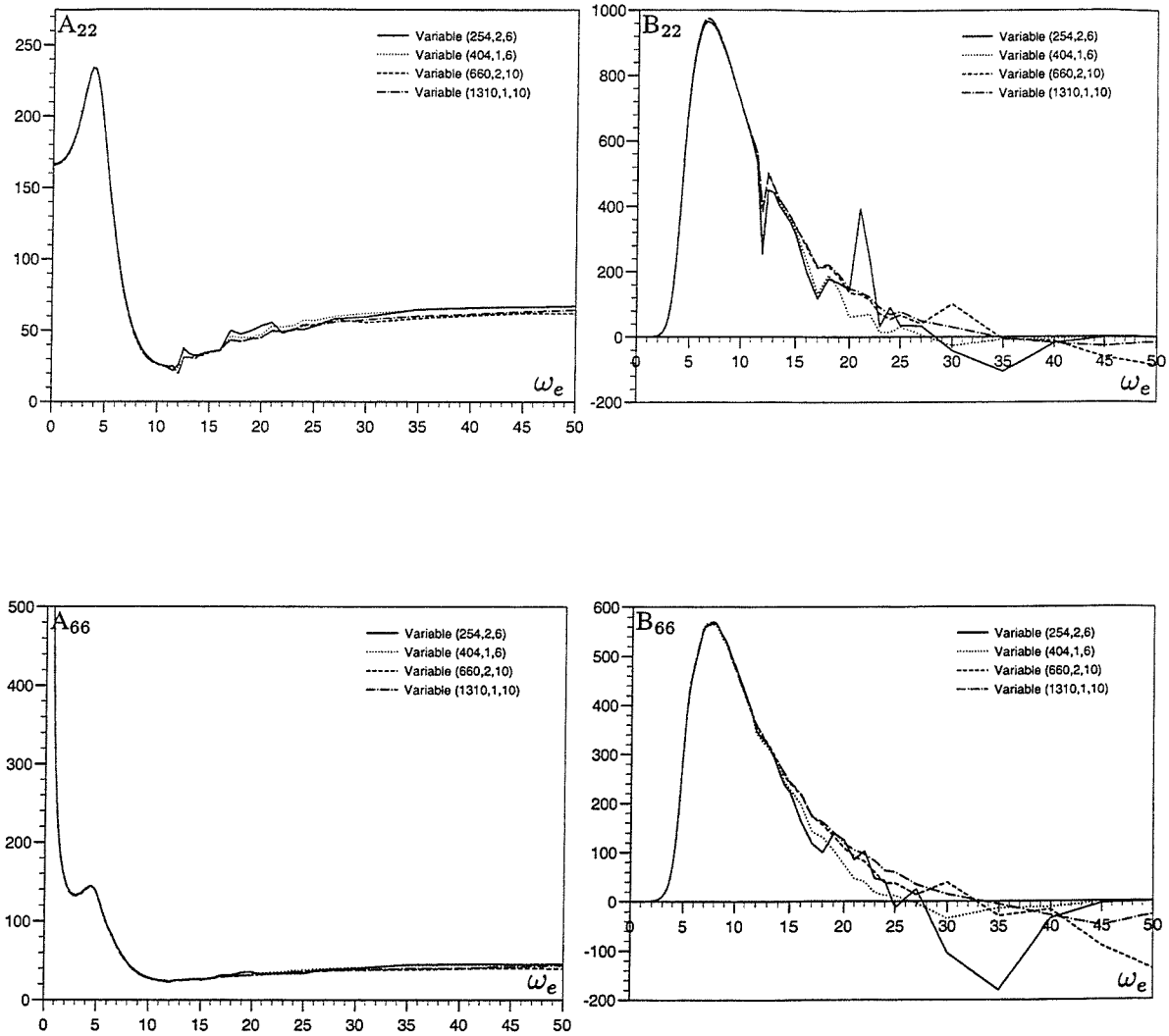

Figure 6.13: Pure sway and pure yaw added mass and damping coefficients found using variable number of panels per section method to model Series 60 mono-hull, L=3.048m, Fn=0.2.

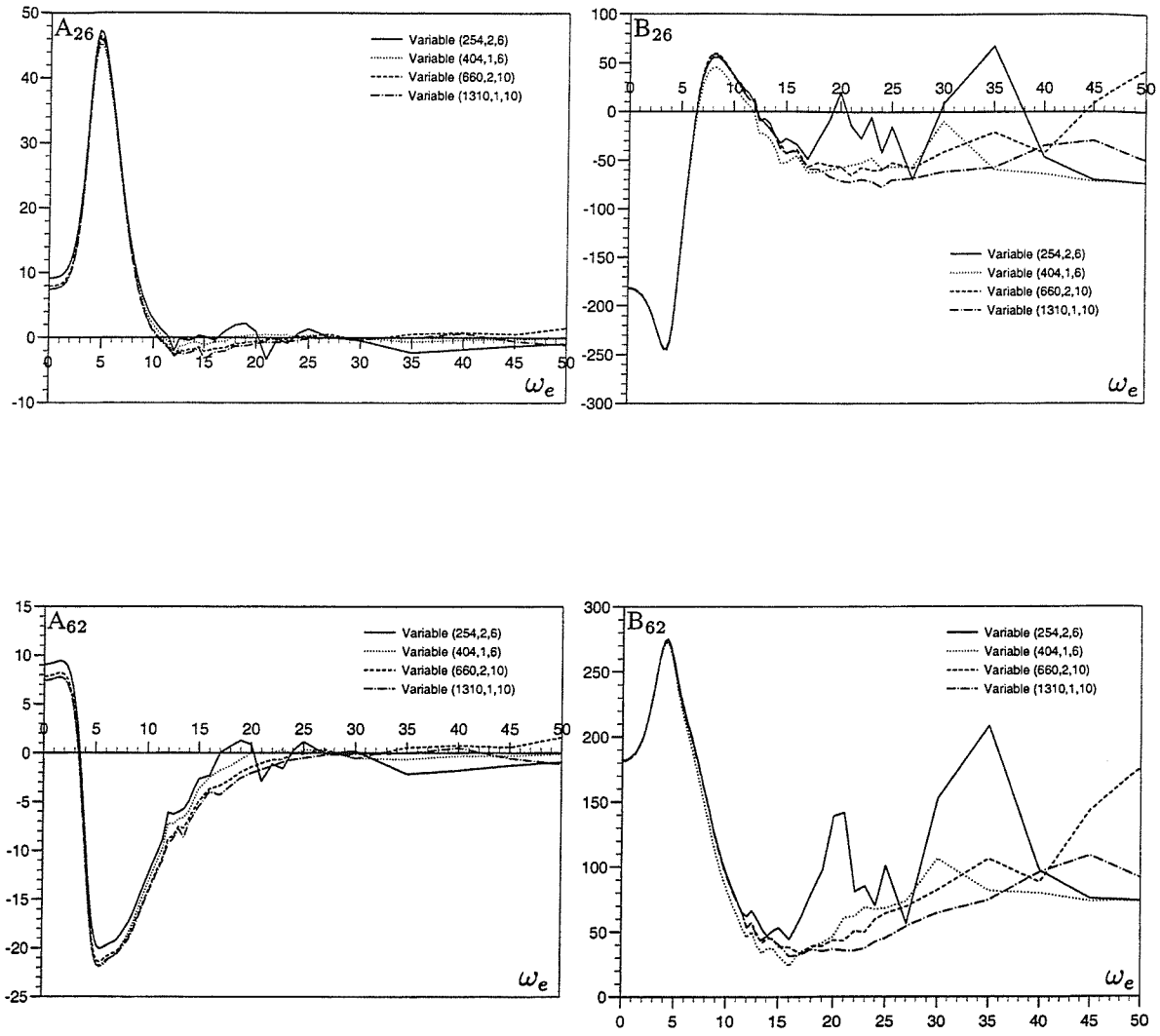

Figure 6.14: Cross coupled sway and yaw added mass and damping coefficients found using variable number of panels per section method to model Series 60 mono-hull, L=3.048m, Fn=0.2.

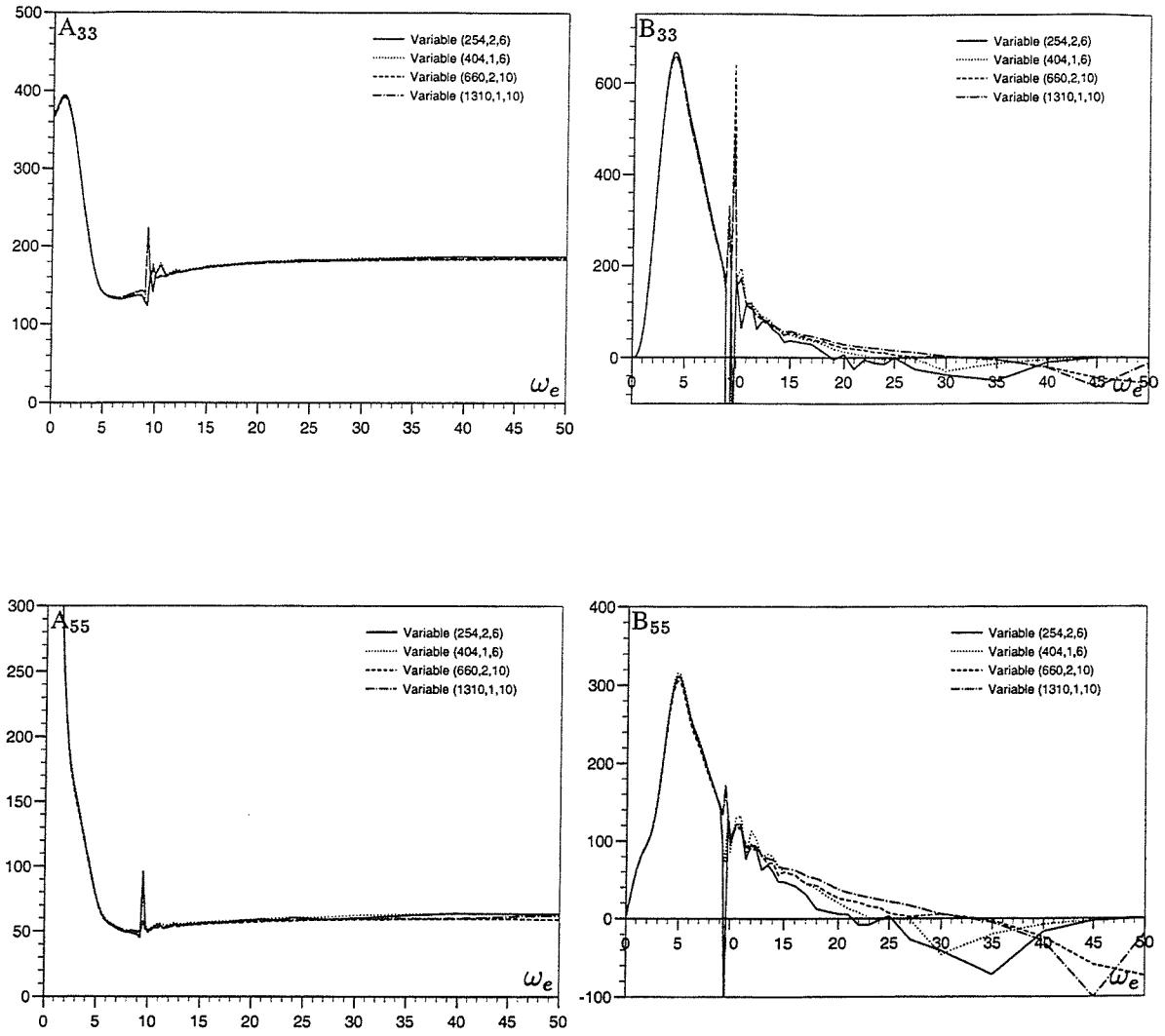

Figure 6.15: Pure heave and pure pitch added mass and damping coefficients found using variable number of panels per section method to model Series 60 mono-hull, L=3.048m, Fn=0.2.

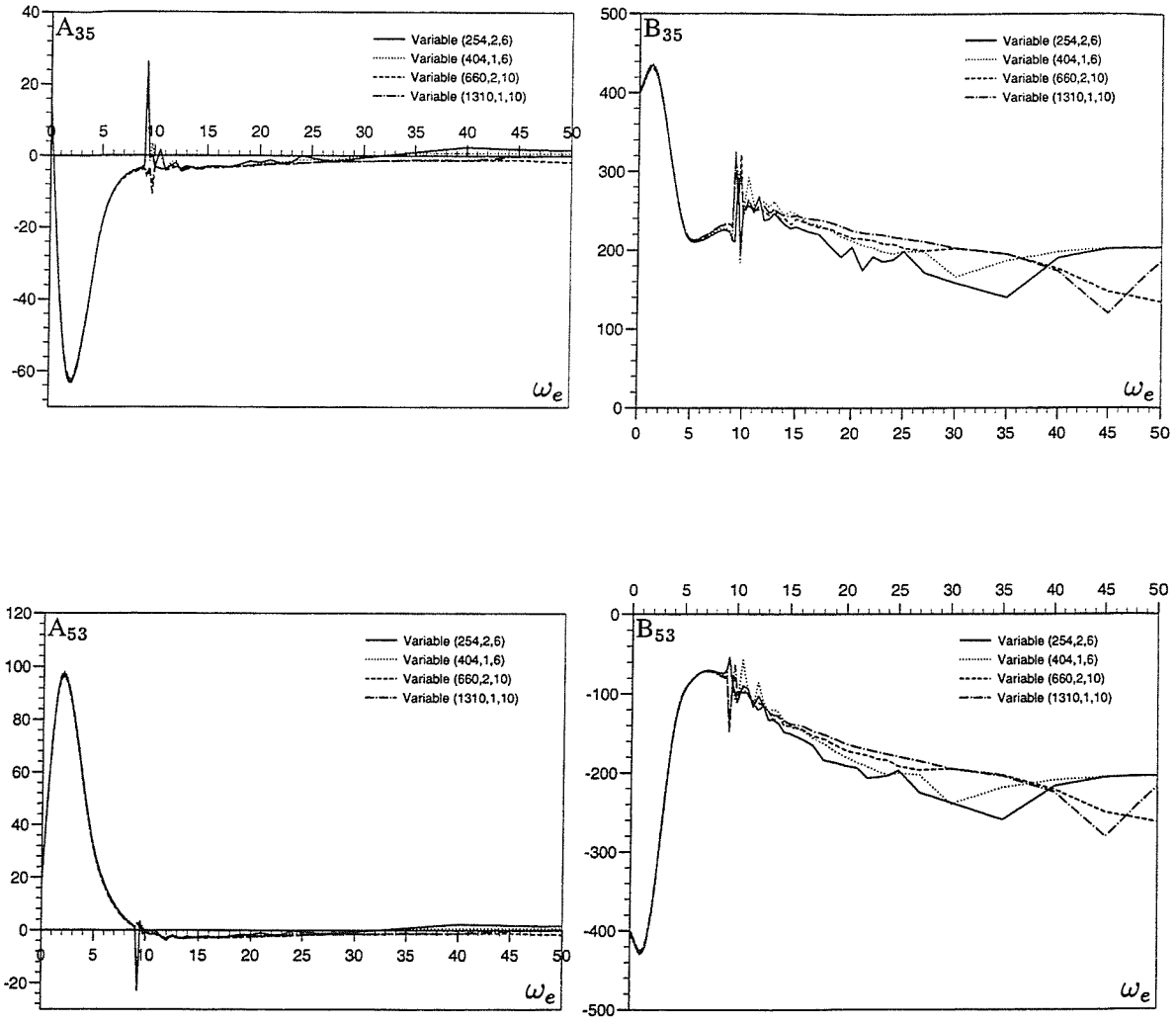

Figure 6.16: Cross coupled heave and pitch added mass and damping coefficients found using variable number of panels per section method to model Series 60 mono-hull, L=3.048m, Fn=0.2.

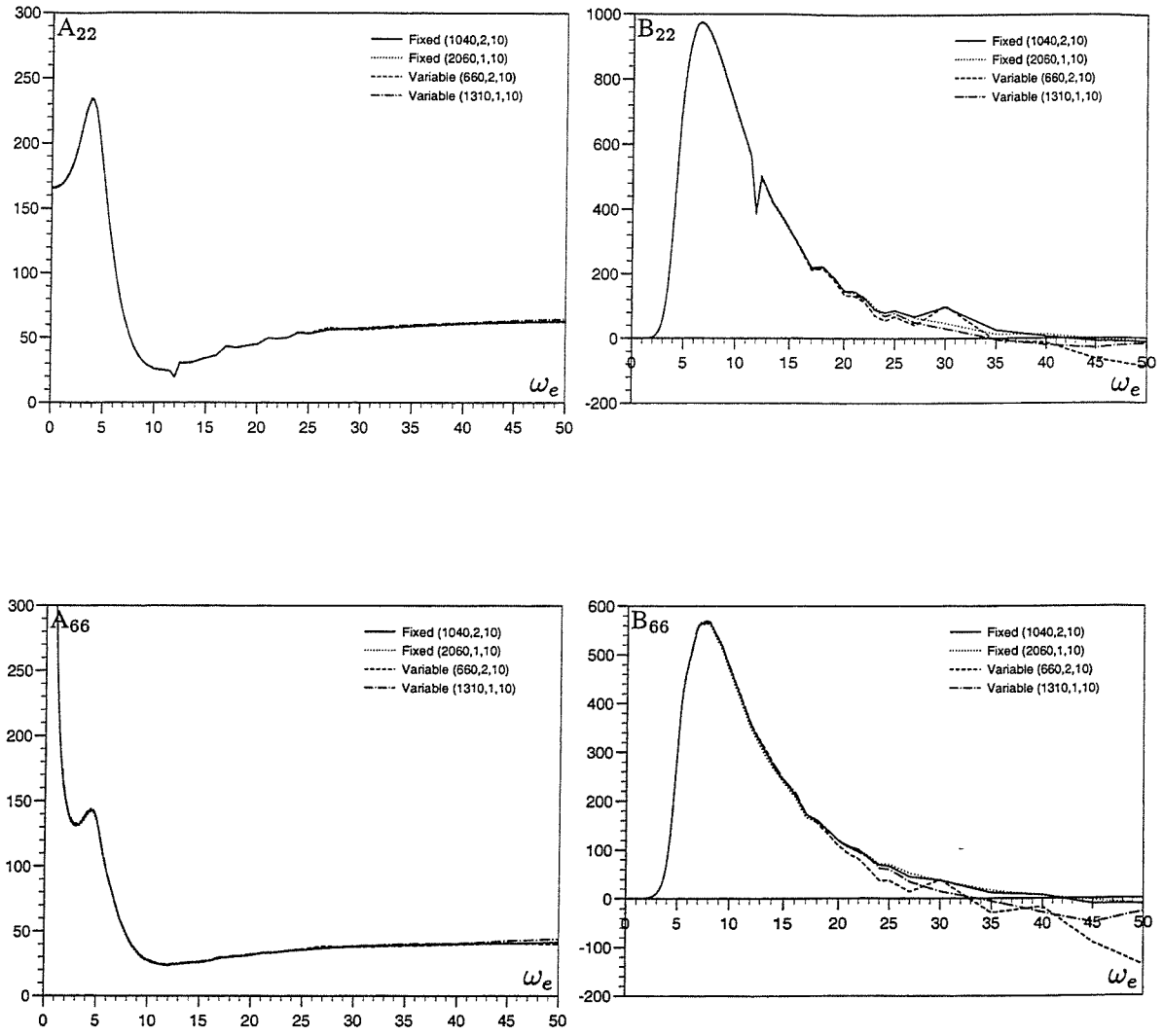

Figure 6.17: A comparison of pure sway and pure yaw added mass and damping coefficients found using Fixed and Variable Methods to panel the hull. Series 60 mono-hull, L=3.048m, Fn=0.2.

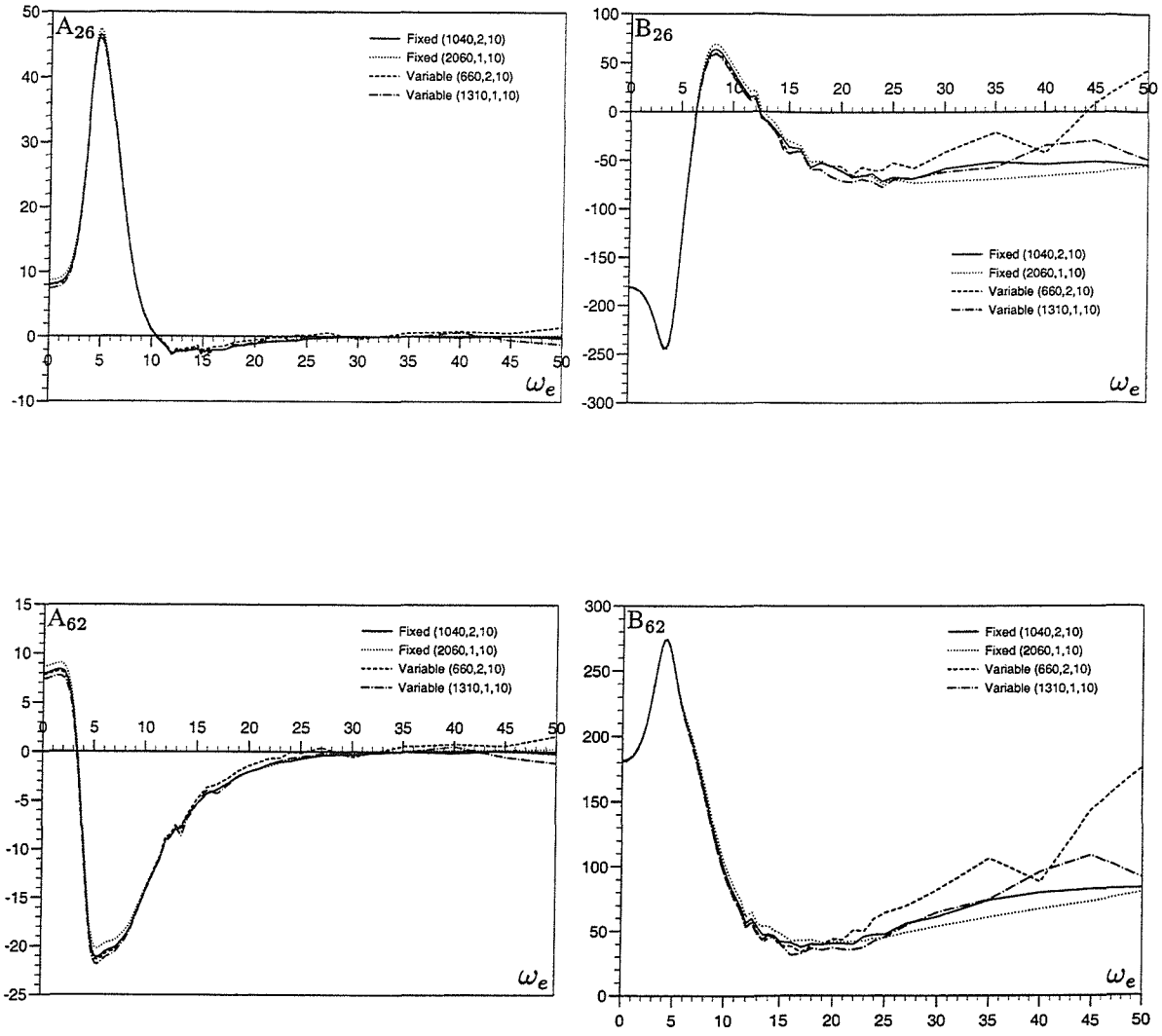

Figure 6.18: A comparison of cross coupled sway and yaw added mass and damping coefficients found using Fixed and Variable Methods to panel the hull. Series 60 mono-hull, L=3.048m, Fn=0.2.

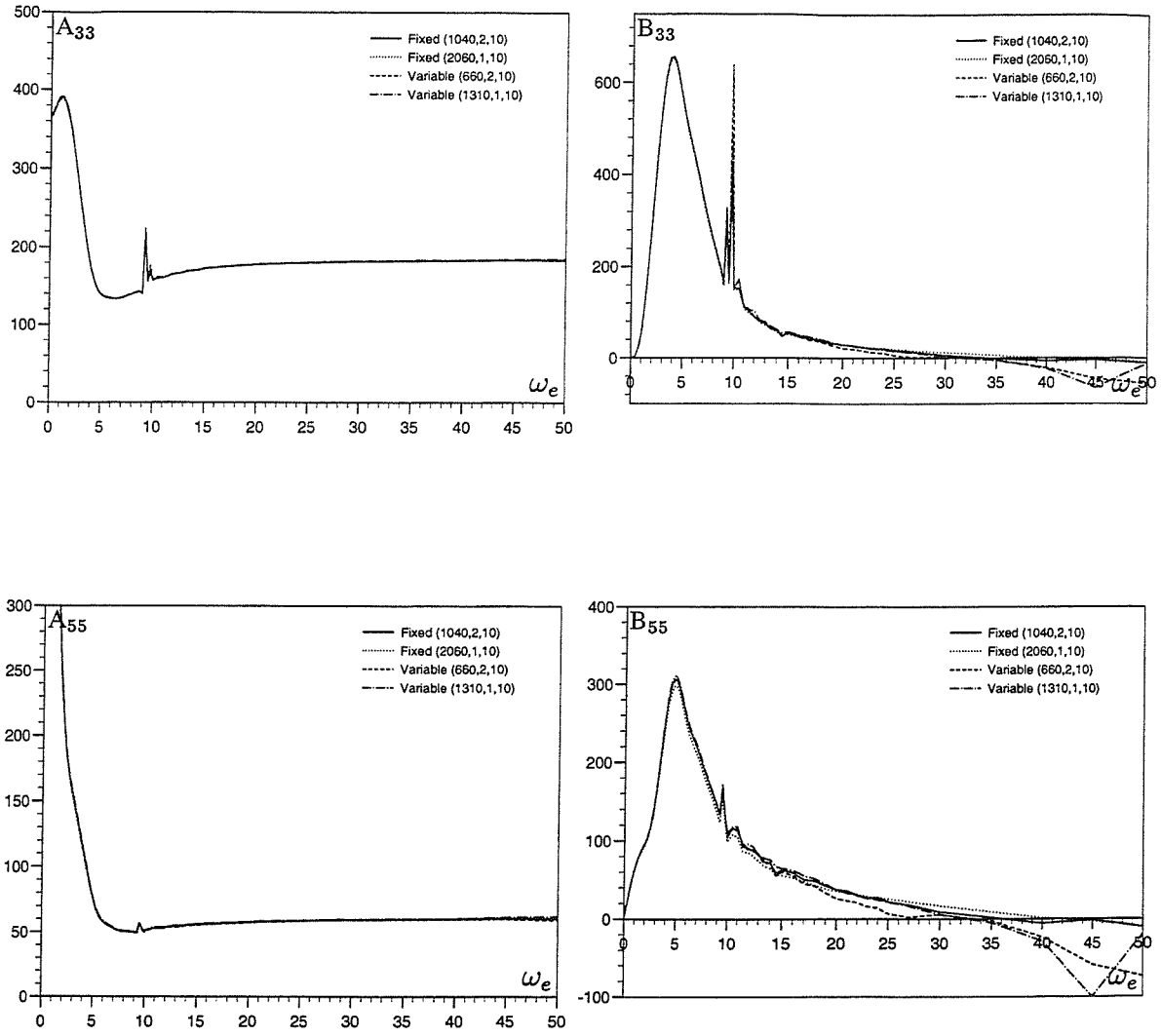

Figure 6.19: A comparison of pure heave and pure pitch added mass and damping coefficients found using Fixed and Variable Methods to panel the hull. Series 60 mono-hull, L=3.048m, Fn=0.2.

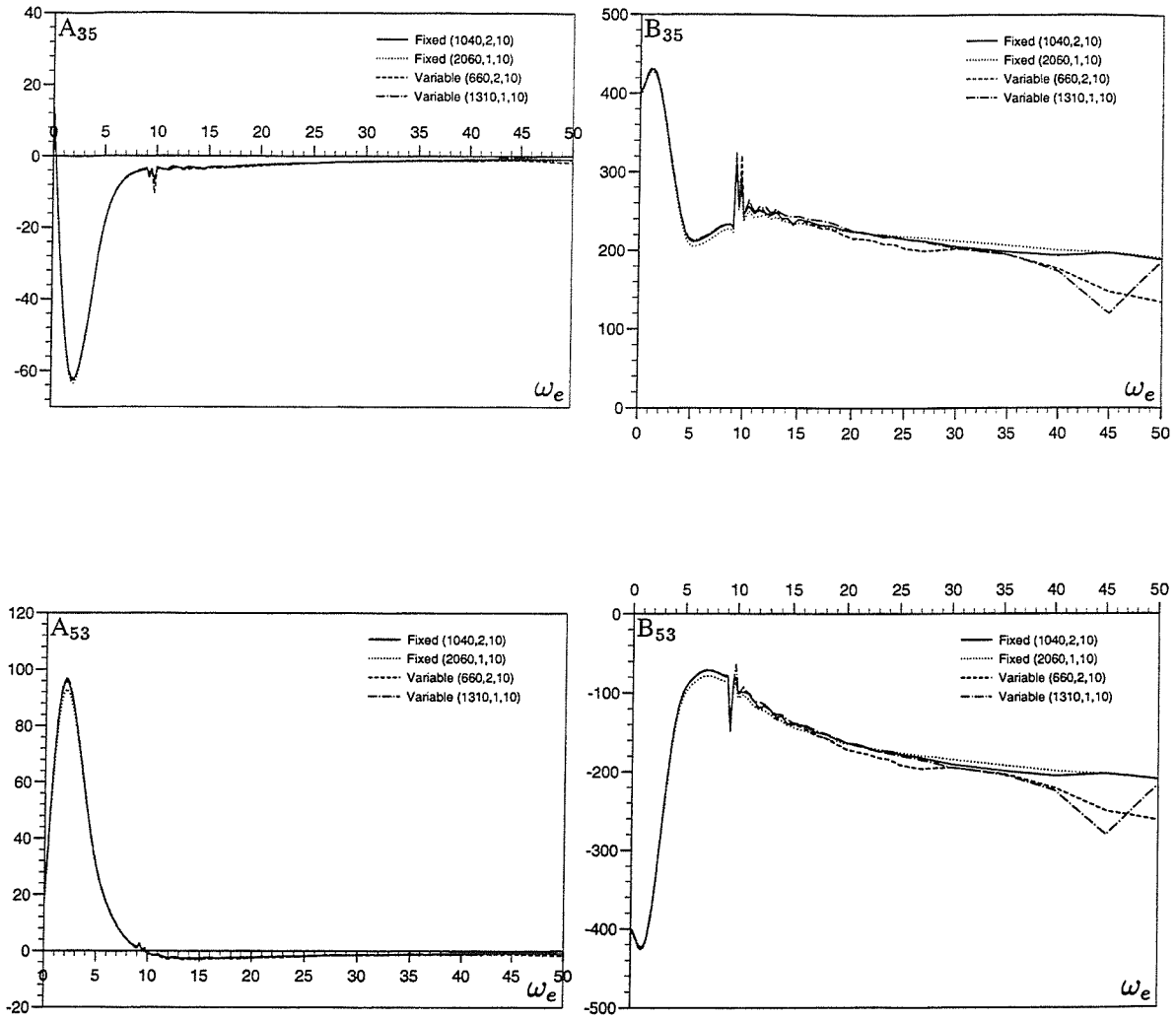

Figure 6.20: A comparison of cross coupled heave and pitch added mass and damping coefficients found using Fixed and Variable Methods to panel the hull. Series 60 mono-hull, L=3.048m, Fn=0.2.

7 Numerical Evaluation of Impulse Response Functions

Having established an accurate methodology for the panelling of ship hulls for use in the calculation of frequency domain hydrodynamic data, methods are required to transform the resultant frequency domain data into the corresponding time domain representation. This chapter will discuss these methods and then attempt verify their accuracy.

In particular, transformations are performed on frequency domain data in order to calculate time domain impulse response functions. In order to verify the numerical transformation methods, these time domain data sets are then inverse transformed to obtain a new set of the corresponding frequency domain data. By comparing the original and transformed frequency domain data sets, the accuracy of the numerical methods that are being used may be confirmed.

7.1 Calculation of Impulse Response Functions from Frequency Domain Data

The calculation of the impulse response functions requires the solution of Equation 5.19 or 5.20 and Equation 5.24. The numerical method used in this study is one developed by Burcher [22] as an improvement upon the trapezoidal method of Solodovnikov [90]. Whereas Solodovnikov's method required visual placement of a small number of trapezoids, Burcher's method, while requiring more trapezoidal elements, removes the need for

visual judgement. This facilitates the creation of computational methods for the evaluation of the impulse response functions.

Consider the case of the calculation of the corresponding impulse response function from the real part of the frequency domain transfer function, which will be referred to as $B^*(\omega_e)$. Equation 5.19 gave the following relationship,

$$h^*(\tau) = \frac{2}{\pi}\int_0^\infty B^*(\omega_e)\cos(\omega_e\tau)d\omega_e \quad \text{for} \quad \tau > 0 \tag{7.1}$$

where, as previously noted, $B^* = (B(\omega_e) - B(\infty))$. Burcher's method of evaluation involves dividing the frequency data into a finite number of trapezoids, such that a function $P_n(\omega_e)$ may defined as follows,

$$P_n(\omega_e) = \begin{cases} B_n^* - B_{n+1}^* & : \ 0 < \omega_e < \omega_{e_n} \\ \frac{(B_n^* - B_{n+1}^*)}{(\omega_{e_{n+1}} - \omega_{e_n})}\left[\omega_{e_{n+1}} - \omega_e\right] & : \ \omega_{e_n} < \omega_e < \omega_{e_{n+1}} \\ 0 & : \ \omega_e > \omega_{e_{n+1}} \end{cases} . \tag{7.2}$$

The frequency dependent coefficient $B^*(\omega_e)$ may be represented as the sum of the trapezoids,

$$B^*(\omega_e) = \sum_{n=1}^{N-1} P_n(\omega_e). \tag{7.3}$$

Substituting Equation 7.1 into Equation 7.3 gives

$$h^*(\tau) = \frac{2}{\pi}\sum_{n=1}^{N-1}\int_0^\infty P(\omega_e)\cos(\omega_e\tau)d\omega_e \qquad \text{for} \quad \tau > 0 \tag{7.4}$$

Hence, substituting Equation 7.2 into Equation 7.4 gives

$$h^*(\tau) \approx \frac{2}{\pi}\sum_{n=1}^{N-1}\left\{ \begin{array}{l} \displaystyle\int_0^{\omega_{e_n}} \left(B_n^* - B_{n+1}^*\right)\cos\omega_e\tau \, d\omega_e \\ \qquad \displaystyle + \int_{\omega_{e_n}}^{\omega_{e_{n+1}}} \left(\frac{B_n^* - B_{n+1}^*}{\omega_{e_{n+1}} - \omega_{e_n}}\right)\left[\omega_{e_{n+1}} - \omega_e\right]\cos\omega_e\tau \, d\omega_e \end{array} \right\},$$

which can be shown to equal,

$$h^*(\tau) \approx \frac{2}{\pi}\sum_{n=1}^{N-1}(B_n^* - B_{n+1}^*)\Omega_n \frac{\sin(\Omega_n\tau)}{\Omega_n\tau}\frac{\sin(\Delta_n\tau)}{\Delta_n\tau}, \tag{7.5}$$

where

$$\Omega_n = \frac{\omega_{e_{n+1}} + \omega_{e_n}}{2} \qquad \text{and} \qquad \Delta_n = \frac{\omega_{e_{n+1}} - \omega_{e_n}}{2}.$$

This method offers an approximation to Equation 7.1 which is numerically easy to implement. Convergence of this method is assured, as for high frequencies $B^*_n - B^*_{n+1}$ tends to zero. Care must be taken in the selection of N, the number of steps and the upper frequency to which the approximation is made to, so as to ensure that the expected convergence does actually occur.

In much the same way, impulse response functions may be calculated using the imaginary part of the transfer function. From Equation 5.20,

$$h^*(\tau) = \frac{-2}{\pi} \int_0^\infty A^*(\omega_e)\omega_e \sin(\omega_e \tau) d\omega_e$$

where, as with the real part of the transfer function, $A^* = (A(\omega_e) - A(\infty))$.

Using similar arguments to those used previously for the real part of the transfer function, a function $Q_n(\omega_e)$ may be defined such that

$$Q_n(\omega_e) = \begin{cases} A^*_n \omega_{e_n} - A^*_{n+1}\omega_{e_{n+1}} & : \ 0 < \omega_e < \omega_{e_n} \\ \frac{(A^*_n \omega_{e_n} - A^*_{n+1}\omega_{e_{n+1}})}{(\omega_{e_{n+1}} - \omega_{e_n})}[\omega_{e_{n+1}} - \omega_e] & : \ \omega_{e_n} < \omega_e < \omega_{e_{n+1}} \\ 0 & : \ \omega_e > \omega_{e_{n+1}} \end{cases} . \tag{7.6}$$

The frequency dependent coefficient $A^*(\omega_e)$ may then be represented as the sum of a series of trapezoids as follows,

$$A^*(\omega_e) = \sum_{n=1}^{N-1} Q_n(\omega_e). \tag{7.7}$$

In a similar fashion to Equation 7.5, the calculation of the impulse response function $h^*(\tau)$ using $A^*(\omega_e)$, is given by

$$h^*(\tau) \approx \frac{-2}{\pi} \sum_{n=1}^{N-1} (A^*_n \omega_{e_n} - A^*_{n+1}\omega_{e_{n+1}})\Omega_n \left\{ \frac{1}{\Omega_n \tau} - \frac{\cos(\Omega_n \tau)}{\Omega_n \tau} \frac{\sin(\Delta_n \tau)}{\Delta_n \tau} \right\}, \tag{7.8}$$

where Ω_n and Δ_n have the same values as previously.

To enable validation of the accuracy of the numerical methods, inverse operations are required to allow determination of frequency domain data from the time domain impulse

response functions. This allows comparison of the original and transformed frequency domain data, which should highlight any deficiencies in the methods used.

The equations for the inverse transformation are very similar in form to the equations for the calculation of the impulse response functions. To calculate the real part of the transfer function from the impulse response function,

$$\begin{aligned} B^*(\omega_e) &= \int_0^\infty h^*(\tau)\cos(\omega_e\tau)d\tau \\ &\approx \sum_{n=1}^{N-1}(h_n^* - h_{n-1}^*)\Omega_n^\tau \frac{\sin(\Omega_n^\tau\omega_e)}{\Omega_n^\tau\omega_e}\frac{\sin(\Delta_n^\tau\omega_e)}{\Delta_n^\tau\omega_e}, \end{aligned} \tag{7.9}$$

and to calculate the imaginary part

$$\begin{aligned} A^*(\omega_e)\omega_e &= -\int_0^\infty h^*(\tau)\sin(\omega_e\tau)d\tau \\ &\approx \sum_{n=1}^{N-1}(h_n^* - h_{n-1}^*)\Omega_n^\tau \left\{\frac{1}{\Omega_n^\tau\omega_e} - \frac{\cos(\Omega_n^\tau\omega_e)}{\Omega_n^\tau\omega_e}\frac{\sin(\Delta_n^\tau\omega_e)}{\Delta_n^\tau\omega_e}\right\}, \end{aligned} \tag{7.10}$$

where for both Equation 7.9 and 7.10

$$\Omega_n^\tau = \frac{\tau_{e_{n+1}} + \tau_{e_n}}{2} \qquad \text{and} \qquad \Delta_n^\tau = \frac{\tau_{e_{n+1}} - \tau_{e_n}}{2}.$$

7.2 Calculation of Radiation Impulse Response Functions

Using the relationships in equations 7.5 and 7.8, frequency domain radiation data, referenced to either equilibrium or body fixed axis system may be transformed into time domain impulse response functions. Although it was shown in Section 5.4 that the radiation impulse response functions could be calculated using either the real or imaginary parts of the radiation transfer function, it has been shown by Bailey [7] that using the real part results in faster convergence of the solution of the impulse response functions. Hence radiation impulse response functions are only calculated using the real part of the transfer function, i.e. using Equation 7.5.

To validate the methods used, transformations were performed from the real part of the frequency domain transfer function to the time domain. These time domain impulse response functions were then used to attempt to recreate the original frequency domain data, both the real and imaginary parts, by reverse transformation. Using a panelled hull representation of a Series 60 model, denoted earlier in Chapter 6 as Fixed(1040,2,10), frequency domain hydrodynamic damping coefficients were calculated. This data, referenced to an equilibrium axis system, was also transformed to a body fixed axis representation, so that the corresponding body fixed axis impulse response functions could be calculated. For the purposes of illustration, only the coefficients relating to heave and pitch are presented.

7.2.1 Equilibrium Axis Data

Figures 7.1 and 7.2 show heave and pitch frequency domain added mass and damping data referenced to an equilibrium axis system. In each of these graphs there is the original frequency domain data (i.e. $A_{JK}(\omega_e)$ and $B_{JK}(\omega_e)$) as calculated by the pulsating source method described in Chapter 4. In addition there is frequency domain data calculated by inverse transform from the corresponding impulse response functions ($A^*_{JK}(\omega_e)$ and $B^*_{JK}(\omega_e)$).

It can be seen that, in general, both the added mass and damping data calculated by reverse transformation show good agreement with the original data. In cases where the original data tends to a non-zero value at high frequency, there is a shift, equal to the infinite frequency value of the original data, between the two data sets. Of interest is the fact that the A_{55} coefficient, which in the original data tends to an infinite value at low frequency, is not well represented in the data calculated by inverse transformation. The recalculated data does not correctly recreate the low frequency tendencies of the original data. This is an important result, the significance of which will be seen when time domain simulations are performed using this data in Chapter 9.

Figure 7.3 shows the impulse response functions calculated from the frequency domain damping data shown in Figures 7.1 and 7.2. Of interest in these impulse response func-

tions is they all exhibit oscillations that are slow to die out. These oscillations are due to the presence of irregular frequency effects in the frequency domain data. The irregular frequencies in the frequency domain data sets take the form of spikes in the data at discrete frequencies. Because these spikes in the data occur over a very small frequency range, it is possible to consider them to be a delta function.

Consider the case of frequency domain added mass and damping data sets which consisted only of a delta function, $\delta(\omega_{e_i})$, which occurred at frequency ω_{e_i}. The added mass and damping functions would be given by $A^*(\omega_e) = A_i\delta(\omega_{e_i})$ and $B^*(\omega_e) = B_i\delta(\omega_{e_i})$. Using Equations 5.19 and 5.20, the resulting impulse response functions may be shown to be

$$\begin{aligned} h^*(\tau) &= \frac{2}{\pi}\int_0^\infty B_i\delta(\omega_{e_i})\cos(\omega_e\tau)\,d\omega_e, \\ \text{or} \qquad h^*(\tau) &= -\frac{2}{\pi}\int_0^\infty A_i\delta(\omega_{e_i})\,\omega_e\sin(\omega_e\tau)\,d\omega_e. \end{aligned}$$

Given that the integral of such a delta function is equal to 1, these equations further simplify to give the following relationships between delta functions in the frequency domain and the corresponding time domain response,

$$\begin{aligned} h^*(\tau) &= \frac{2}{\pi}B_i\cos(\omega_{e_i}\tau) \\ \text{or} \qquad h^*(\tau) &= -\frac{2}{\pi}A_i\,\omega_{e_i}\sin(\omega_{e_i}\tau). \end{aligned}$$

From these last equations it becomes clear that the time domain response corresponding to a frequency domain impulse is sinusoidal in form, where the sharper the impulse, the larger the amplitude of the sinusoidal time domain response. This sinusoidal response can be seen in the impulse response functions in Figure 7.3, being especially prominent in the h_{33} and h_{35} graphs due to the large irregular frequency spikes that may be seen in the frequency domain data from which they were calculated.

However, these oscillations in the impulse response functions do not appear to have any negative effect on the accuracy of the frequency domain data calculated from the impulse response functions . Indeed, it can be seen that when frequency domain data is calculated by inverse transformation, the irregular frequency effects are quite well recreated. This suggests that the numerical methods used are able to correctly account for the effects that arise due to the irregular frequencies.

7.2.2 Body Fixed Axis Data

Figures 7.4 and 7.5 show the frequency domain acceleration and velocity derivatives calculated by transforming the frequency domain data from an equilibrium axis to a body fixed axis representation. From this frequency domain data the corresponding impulse response functions have been calculated, again using the real part of the transfer function, in this case the velocity derivatives. These impulse response functions are shown in Figure 7.6. As was the case for the equilibrium axis data, frequency domain derivatives calculated by reverse transform from the impulse response functions are presented against the original data in order the validate the numerical methods. It can be seen that there is good agreement between the original frequency domain data and that calculated from the impulse response functions, the only exception being the transformed $Z_{\dot{q}}$ data, which does not match the original at very low frequency. There is a shift present if the original frequency domain data did not tend to zero at high frequency, but otherwise agreement between the two data sets in each case is good. In particular, it should be noted that because all of the original frequency domain data sets tend to finite values at low frequency, there are not the inaccuracies that were seen in the case of the A_{55} data calculated from the h_{55} impulse response function.

Because irregular frequency effects are still apparent in the body fixed axis frequency domain data, there are oscillations in the impulse response functions calculated from this data. Also, when frequency domain data is calculated by inverse transformation from the impulse response functions, the irregular frequencies are recreated well, appearing to have no effect on the surrounding data.

7.3 Wave Excitation Data

The verification of the numerical methods for the calculation of the wave excitation impulse response functions was carried out in the same manner as for the radiation data. Although both real and imaginary parts of the frequency domain transfer function are required for

the calculation of the impulse response function (see Equation 5.24), the inverse transform of either the real or imaginary part from the impulse response function is identical to that used for the radiation data (compare Equations 5.22 and 5.23 for the wave excitation with Equations 5.12 and 5.13 for the radiation actions).

Again using only symmetric modes of motion to illustrate the verification process, Figure 7.7 shows frequency domain wave excitation data referenced to an equilibrium axis system. It can be seen that frequency domain data calculated by inverse transform from the impulse response functions is virtually indistinguishable from the original data. The wave excitation impulse response functions calculated from the original frequency domain data, which include a negative time component, are shown in Figure 7.8.

Similarly, frequency domain data referenced to a body fixed axis system is shown in Figures 7.9 and 7.10. It can be seen that the similarity of the original frequency domain data to that calculated by transformation from the impulse response functions is as good was found for the equilibrium axis data, as would be expected, given the similarity of the two data sets.

7.4 Conclusions Regarding Numerical Methods

Through the use of inverse transforms, it has been possible to assess the accuracy of the numerical methods used for the calculation of time domain impulse response functions from the corresponding frequency domain hydrodynamic data. Both radiation and total wave excitation data have been examined. In general the comparisons carried out show that the numerical methods used are very accurate. The exception to this is the case of the $A_{55}(\omega_e)$ added mass coefficient, for which it was not possible in the current research to perform ($A_{66}(\omega_e)$ will be similar). This inaccuracy was the result of the numerical method not being able to adequately represent the tendency of the original frequency domain data to tend to very high values at low frequency.

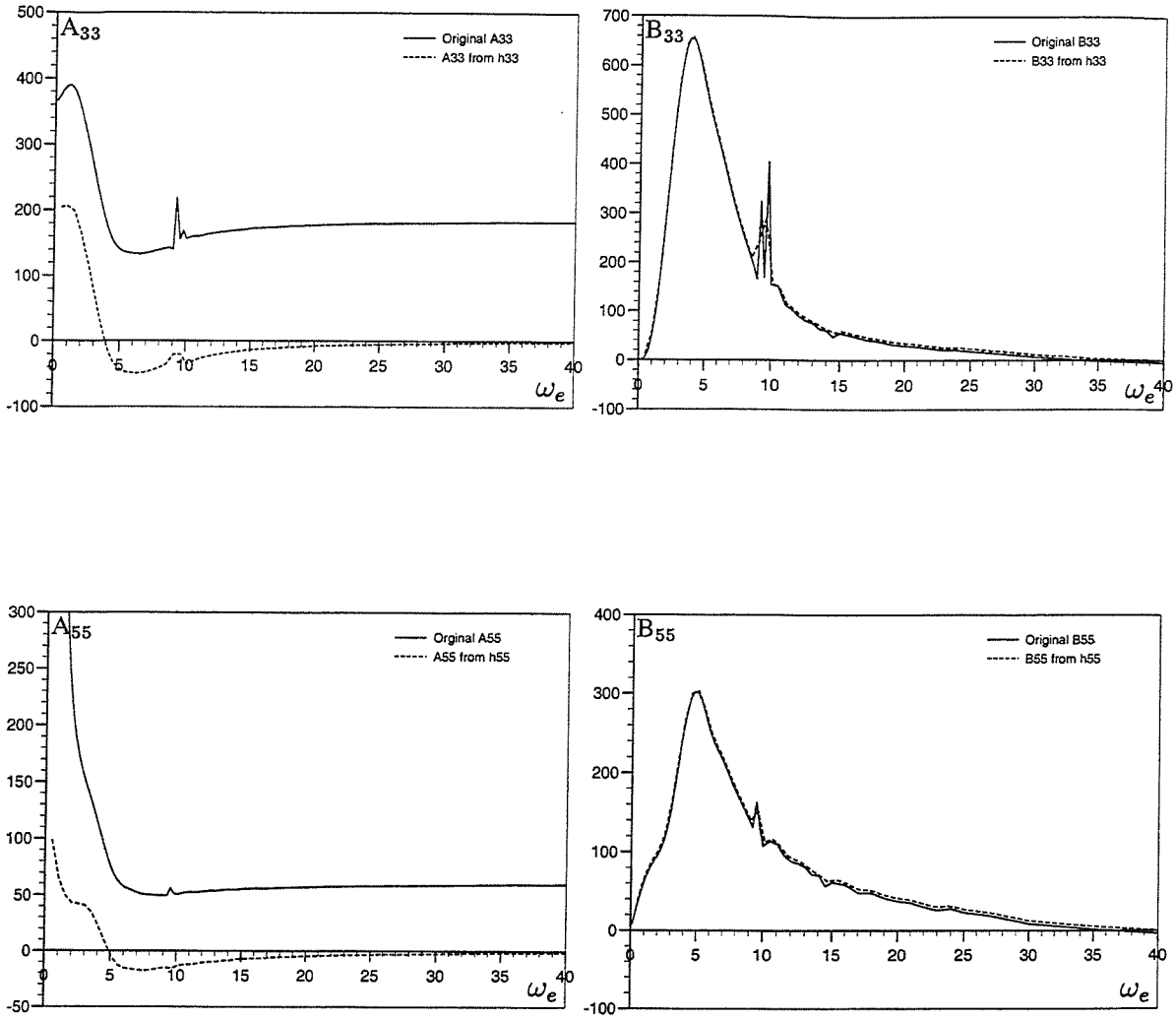

Figure 7.1: Pure heave and pitch frequency domain coefficients calculated directly and by reverse transformation from impulse response functions. Series 60 mono-hull, L=3.048m, Fn=0.2.

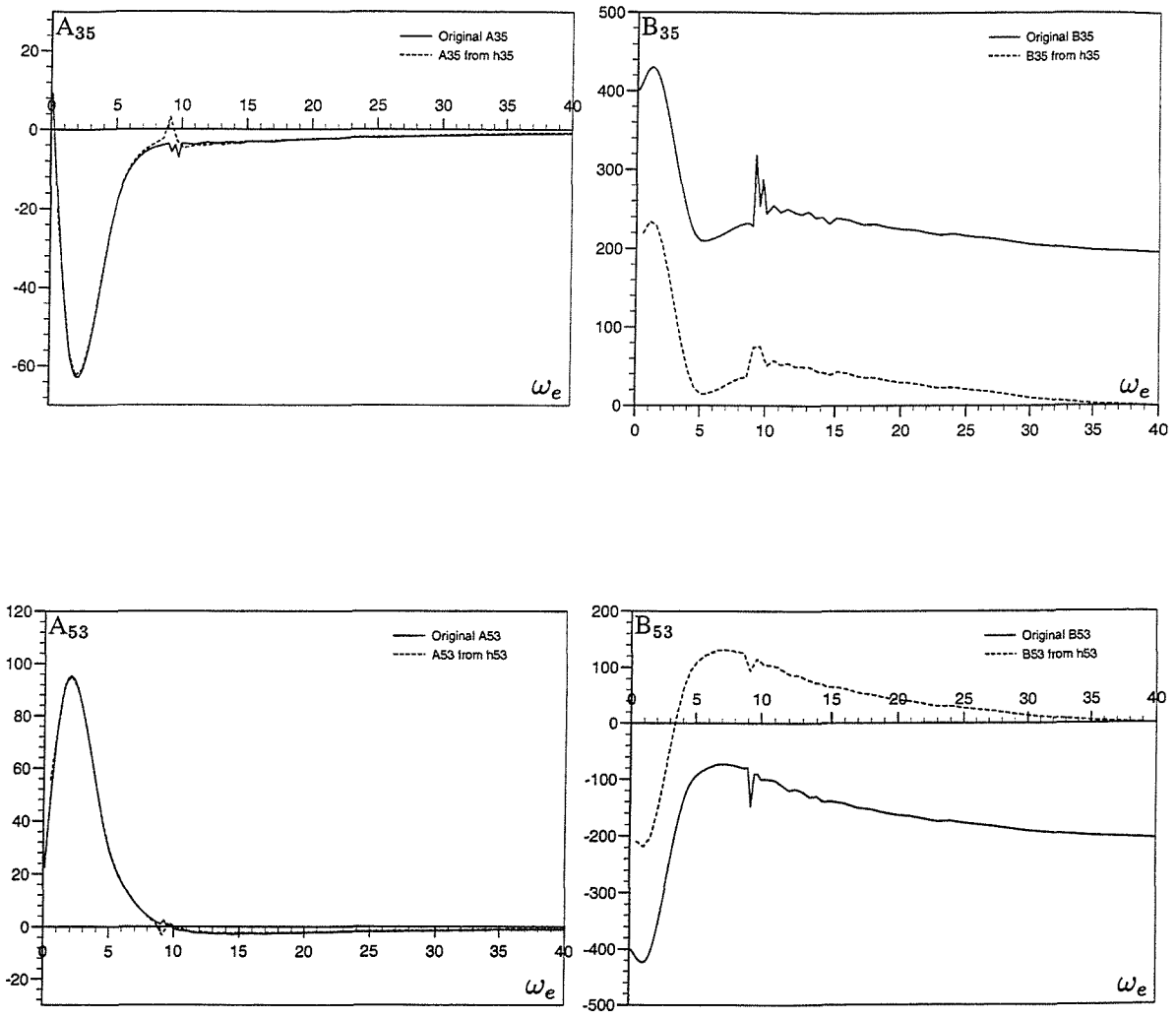

Figure 7.2: Cross coupled heave and pitch frequency domain coefficients calculated directly and by reverse transformation from impulse response functions. Series 60 mono-hull, L=3.048m, Fn=0.2.

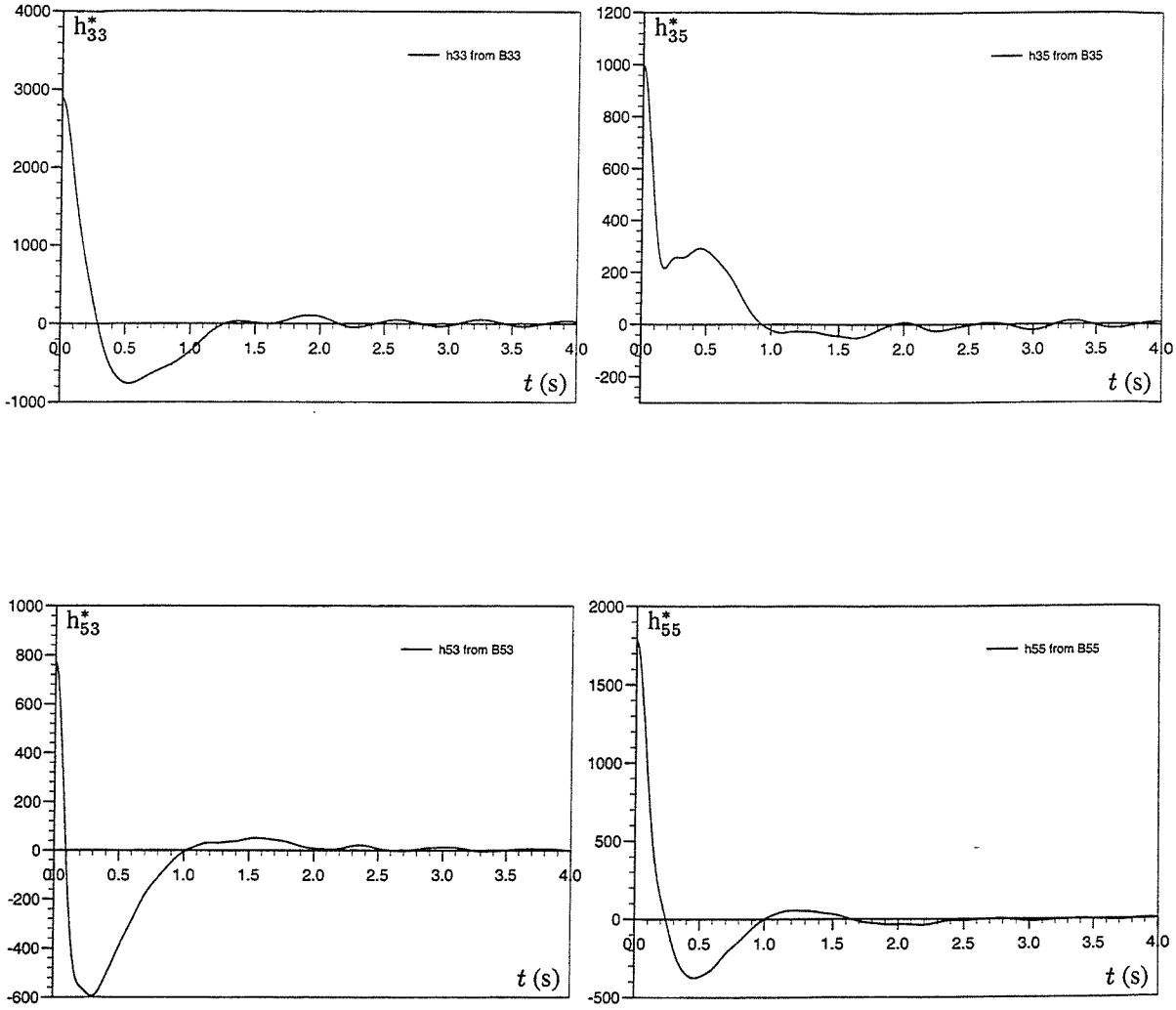

Figure 7.3: Impulse response functions calculated using hydrodynamic damping coefficients. Series 60 mono-hull, L=3.048m, Fn=0.2.

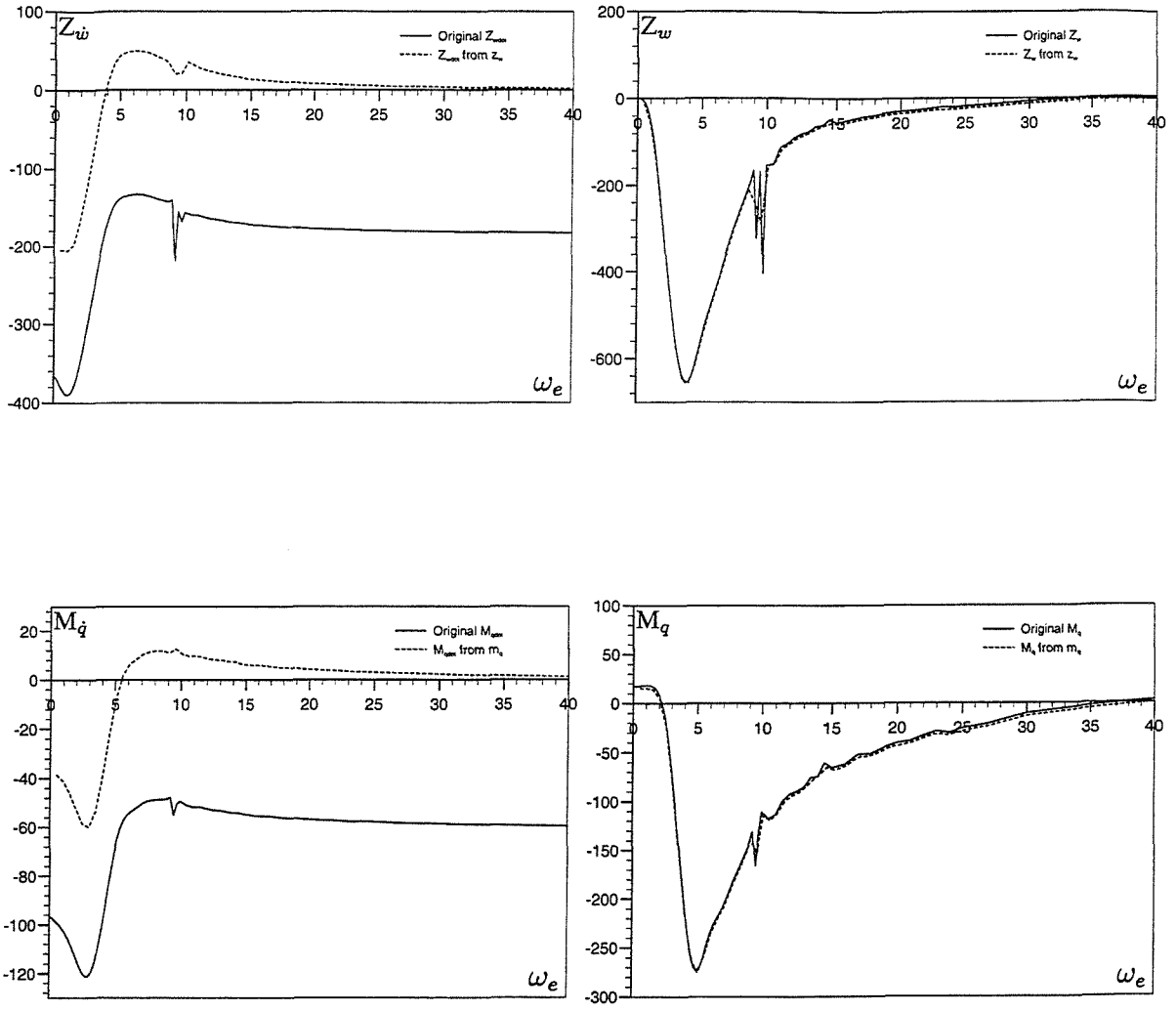

Figure 7.4: Pure heave and pitch frequency domain derivatives calculated directly and by reverse transformation from impulse response functions. Series 60 mono-hull, L=3.048m, Fn=0.2.

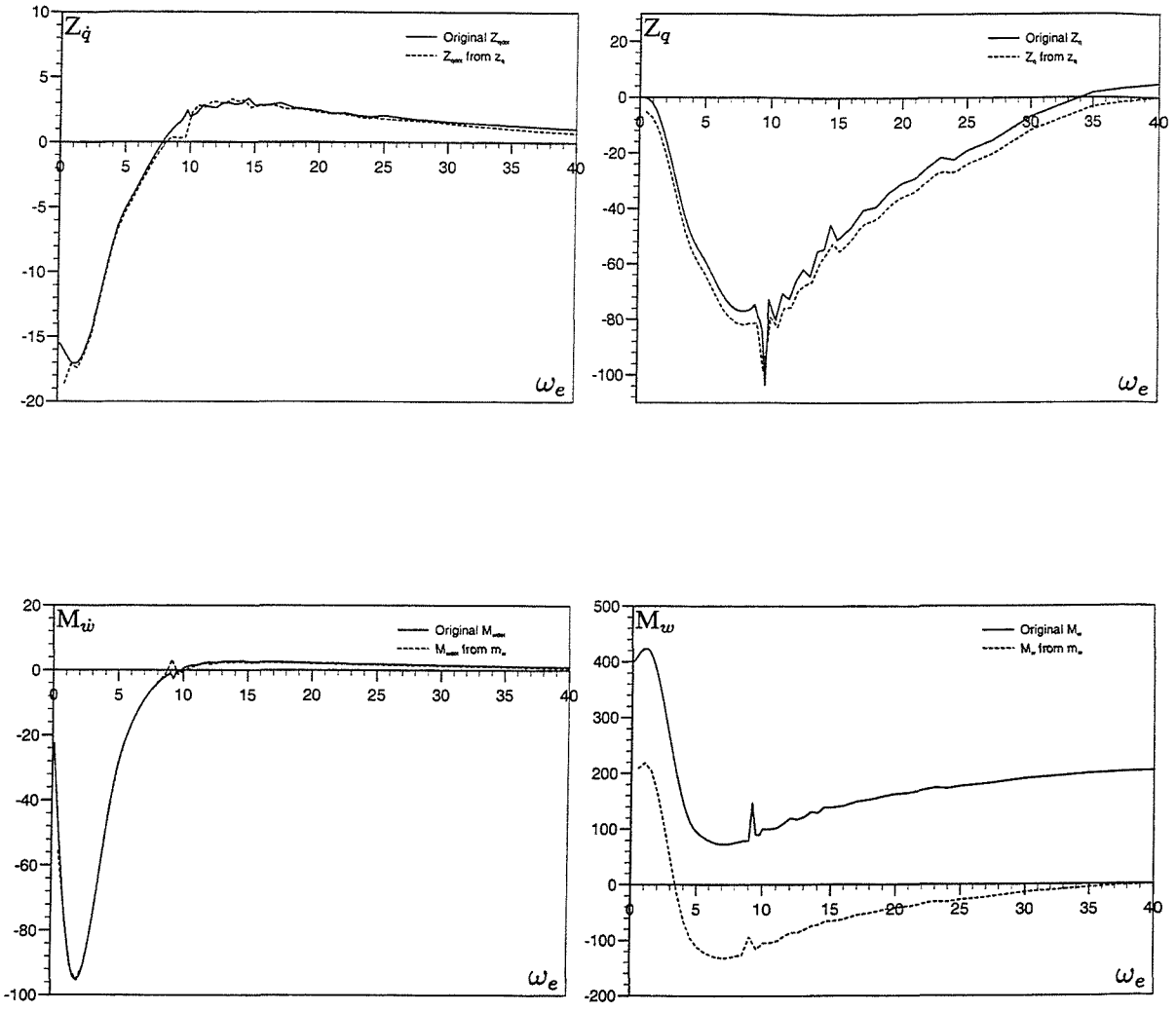

Figure 7.5: Cross coupled heave and pitch frequency domain derivatives calculated directly and by reverse transformation from impulse response functions. Series 60 mono-hull, L=3.048m, Fn=0.2.

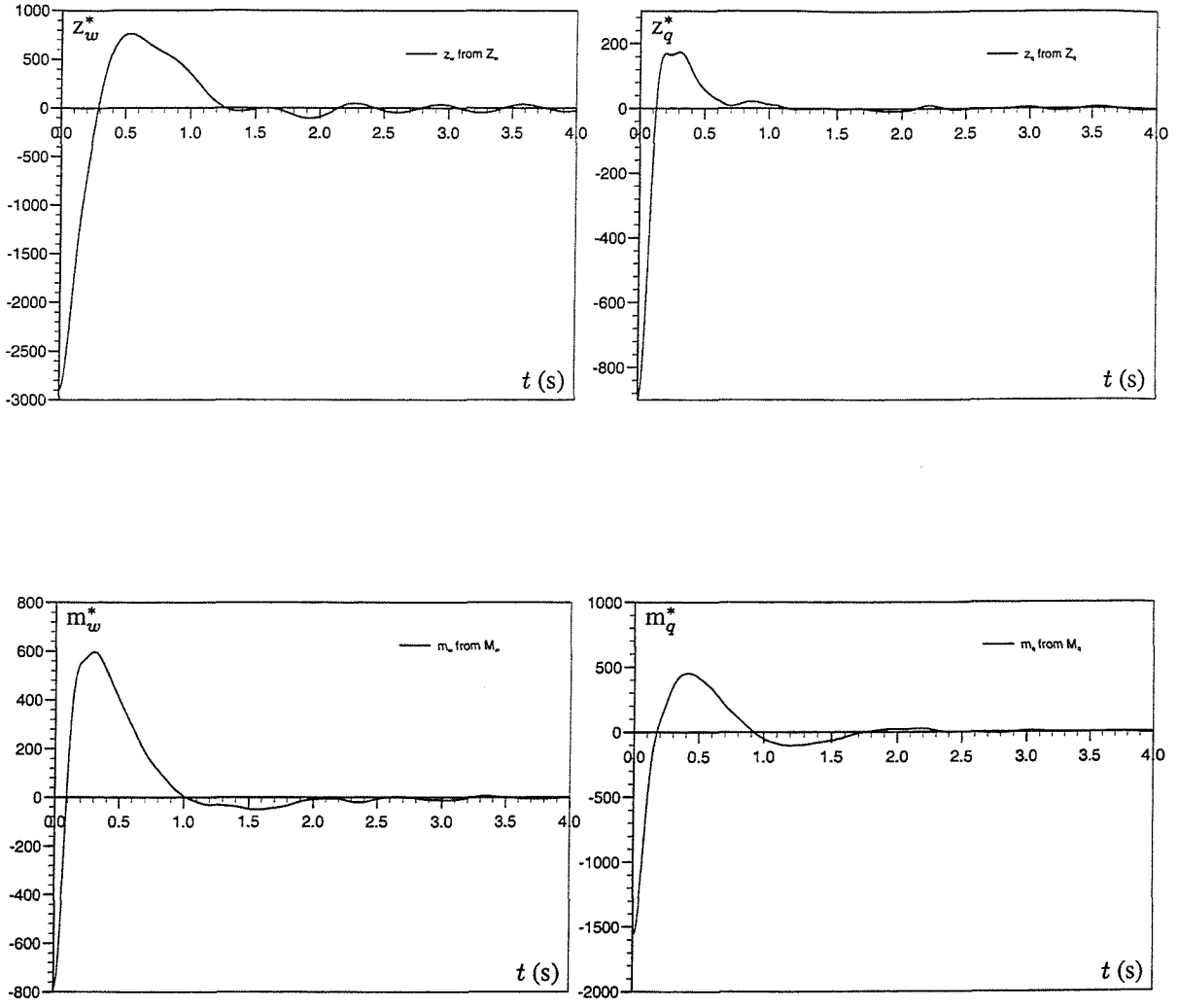

Figure 7.6: Impulse response functions calculated using frequency domain velocity derivatives. Series 60 mono-hull, L=3.048m, Fn=0.2.

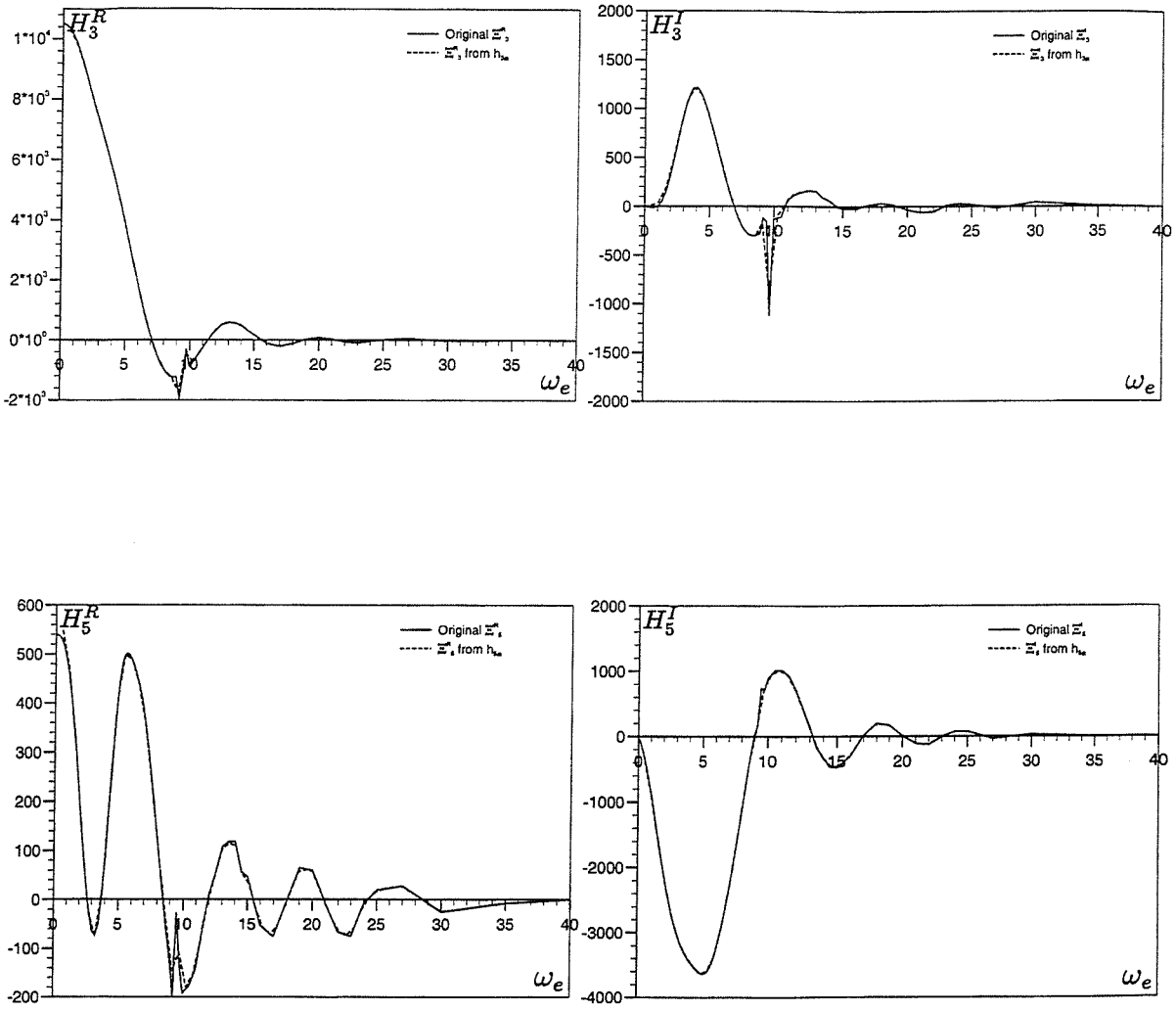

Figure 7.7: Real and imaginary parts of the heave and pitch frequency domain excitation forces, calculated directly and by reverse transformation from impulse response functions. Data referenced to an equilibrium axis system. Series 60 mono-hull, L=3.048m, Fn=0.2.

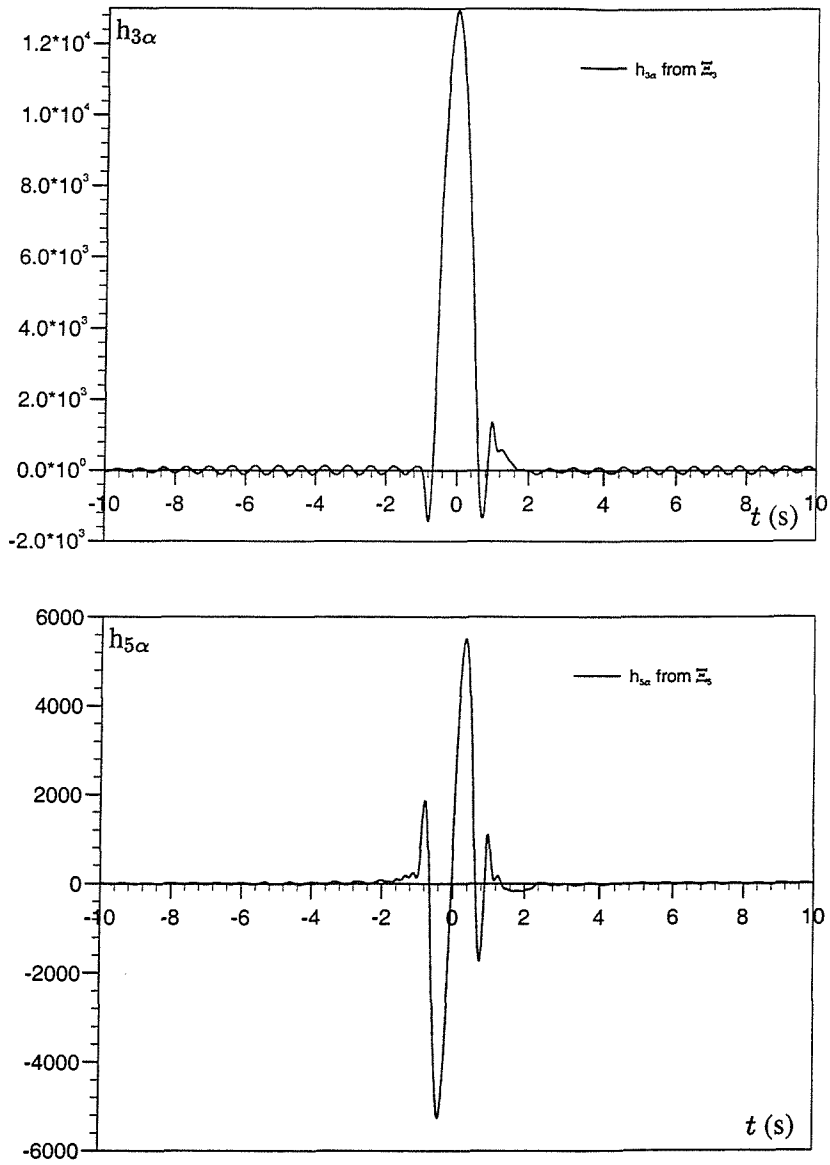

Figure 7.8: Heave and pitch excitation impulse response functions calculated using frequency domain data for a Series 60 mono-hull, referenced to an equilibrium axis system. L=3.048m, Fn=0.2.

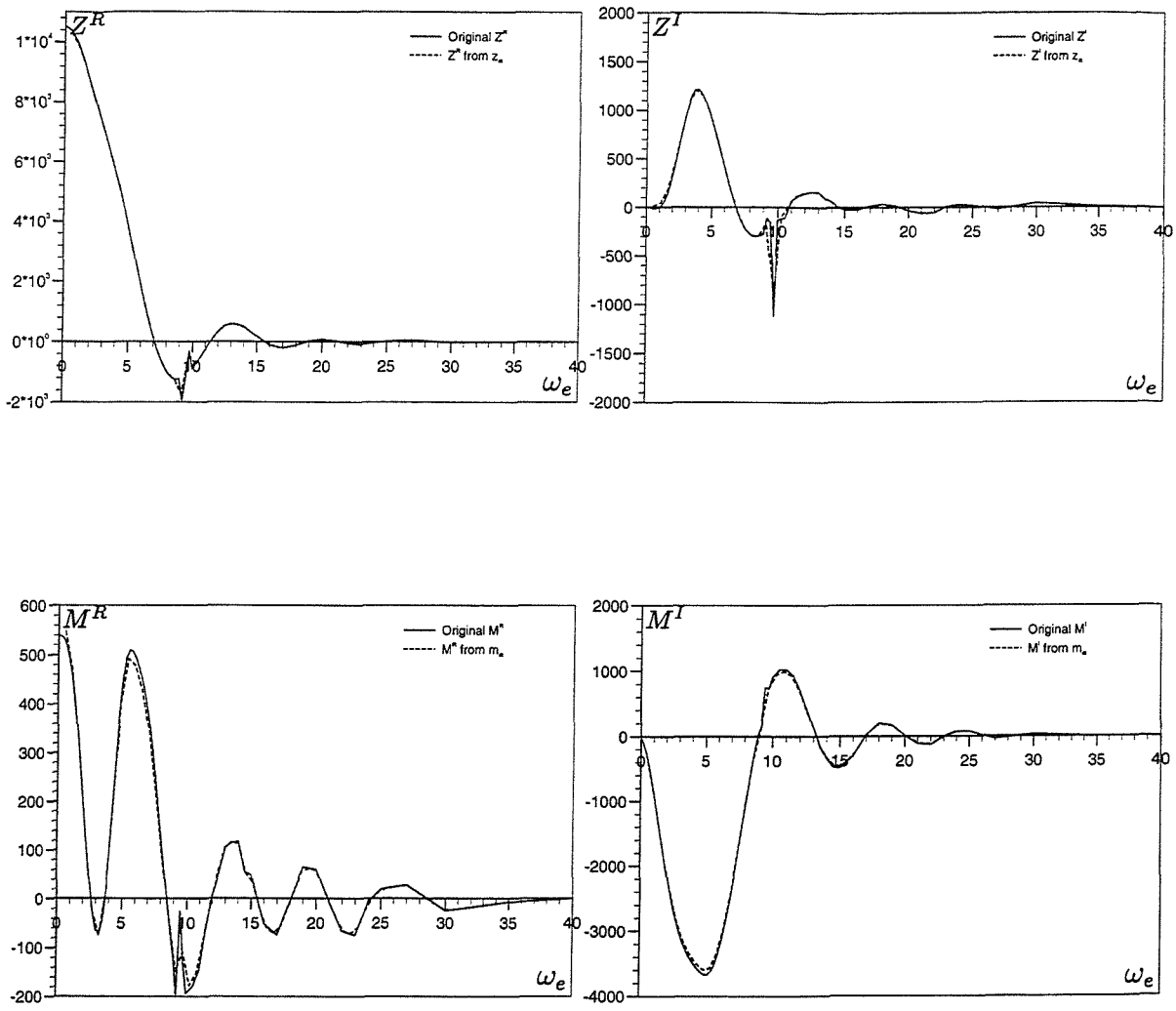

Figure 7.9: Real and imaginary parts of the heave and pitch frequency domain excitation forces, calculated directly and by reverse transformation from impulse response functions. Data referenced to a body fixed axis system. Series 60 mono-hull, L=3.048m, Fn=0.2.

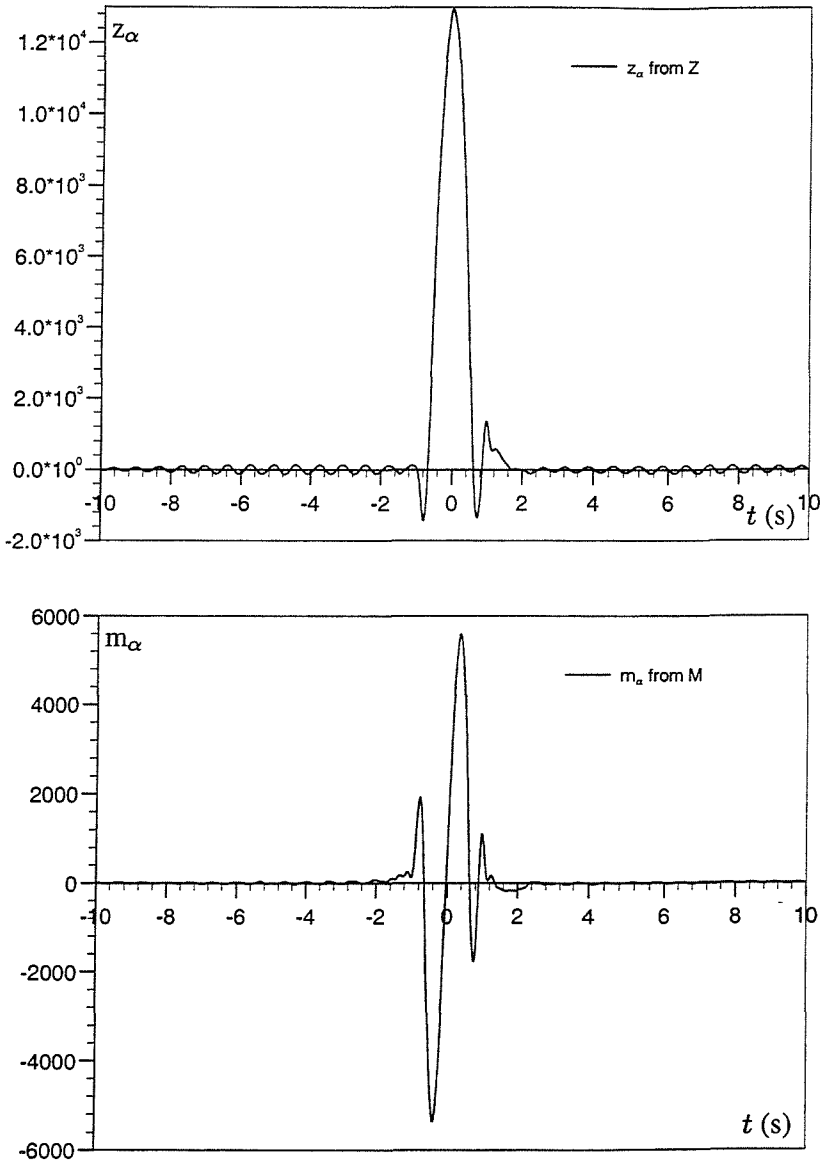

Figure 7.10: Heave and pitch excitation impulse response functions calculated using frequency domain data for a Series 60 mono-hull, referenced to a body fixed axis system. L=3.048m, Fn=0.2.

8 Time Domain Simulation Techniques

This chapter presents methods by which the theoretical techniques described in the previous chapters may be used to perform a time domain simulation of ship motions in waves. These methods incorporate hydrodynamic data in the form of impulse response functions as part of a convolution integral formulation which allows for the inclusion of memory effects. These simulation techniques are applicable for arbitrary excitation, but for the purposes of numerical verification, sinusoidal actions only are considered, allowing comparison with frequency domain results.

8.1 Equations of Motion in Time Domain

Chapter 4 presented the frequency domain equations of motions for the rigid body motions of a ship in six degrees of freedom. These equations of motion were given referenced to both an equilibrium and a body fixed axis system. These equations must be converted to a time domain representation before they may be used as part of a simulation technique. This conversion to a time domain representation involves the substitution of frequency domain coefficients and derivatives for the corresponding convolution integrals. Chapter 5 discussed the transformation of frequency domain data into impulse response functions which may be used in a convolution integral formulation. It is these relationships which are used to develop the following equations of motion.

8.1.1 Equilibrium Axis Equations of Motion

Equations 4.15 and 4.16 presented the equations of motion for the symmetric and anti-symmetric motions of a rigid body, respectively. It was shown in Chapter 5 that the frequency domain radiation data may be expressed in a form incorporating convolution integral as follows,

$$f(t) = -A(\infty)\dot{v}(t) + B(\infty)v(t) + \int_0^t h^*(\tau)v(t-\tau)\,d\tau.$$

Furthermore, the frequency domain wave excitation contribution may be represented as

$$f_\alpha(t) = \int_0^t h_\alpha(\tau)\alpha(t-\tau)\,d\tau. \tag{8.1}$$

which is again in the form of a convolution integral formulation. Hence the equations of motion referenced to an equilibrium axis system may be written as follows [4]

$$\begin{bmatrix} \ddot{\eta}_1(t) \\ \ddot{\eta}_2(t) \\ \ddot{\eta}_3(t) \\ \ddot{\eta}_4(t) \\ \ddot{\eta}_5(t) \\ \ddot{\eta}_6(t) \end{bmatrix} = \begin{bmatrix} f_1^m(\dot{\eta}_1,\dot{\eta}_2,\dot{\eta}_3,\dot{\eta}_4,\dot{\eta}_5,\dot{\eta}_6,\eta_1,\eta_2,\eta_3,\eta_4,\eta_5,\eta_6,t) \\ f_2^m(\dot{\eta}_1,\dot{\eta}_2,\dot{\eta}_3,\dot{\eta}_4,\dot{\eta}_5,\dot{\eta}_6,\eta_1,\eta_2,\eta_3,\eta_4,\eta_5,\eta_5,t) \\ f_3^m(\dot{\eta}_1,\dot{\eta}_2,\dot{\eta}_3,\dot{\eta}_4,\dot{\eta}_5,\dot{\eta}_6,\eta_1,\eta_2,\eta_3,\eta_4,\eta_5,\eta_6,t) \\ f_4^m(\dot{\eta}_1,\dot{\eta}_2,\dot{\eta}_3,\dot{\eta}_4,\dot{\eta}_5,\dot{\eta}_6,\eta_1,\eta_2,\eta_3,\eta_4,\eta_5,\eta_6,t) \\ f_5^m(\dot{\eta}_1,\dot{\eta}_2,\dot{\eta}_3,\dot{\eta}_4,\dot{\eta}_5,\dot{\eta}_6,\eta_1,\eta_2,\eta_3,\eta_4,\eta_5,\eta_6,t) \\ f_6^m(\dot{\eta}_1,\dot{\eta}_2,\dot{\eta}_3,\dot{\eta}_4,\dot{\eta}_5,\dot{\eta}_6,\eta_1,\eta_2,\eta_3,\eta_4,\eta_5,\eta_6,t) \end{bmatrix}$$

$$= \mathbf{M^{-1}} \begin{bmatrix} f_1(\dot{\eta}_1,\dot{\eta}_2,\dot{\eta}_3,\dot{\eta}_4,\dot{\eta}_5,\dot{\eta}_6,\eta_1,\eta_2,\eta_3,\eta_4,\eta_5,\eta_6,t) \\ f_2(\dot{\eta}_1,\dot{\eta}_2,\dot{\eta}_3,\dot{\eta}_4,\dot{\eta}_5,\dot{\eta}_6,\eta_1,\eta_2,\eta_3,\eta_4,\eta_5,\eta_6,t) \\ f_3(\dot{\eta}_1,\dot{\eta}_2,\dot{\eta}_3,\dot{\eta}_4,\dot{\eta}_5,\dot{\eta}_6,\eta_1,\eta_2,\eta_3,\eta_4,\eta_5,\eta_6,t) \\ f_4(\dot{\eta}_1,\dot{\eta}_2,\dot{\eta}_3,\dot{\eta}_4,\dot{\eta}_5,\dot{\eta}_6,\eta_1,\eta_2,\eta_3,\eta_4,\eta_5,\eta_6,t) \\ f_5(\dot{\eta}_1,\dot{\eta}_2,\dot{\eta}_3,\dot{\eta}_4,\dot{\eta}_5,\dot{\eta}_6,\eta_1,\eta_2,\eta_3,\eta_4,\eta_5,\eta_6,t) \\ f_6(\dot{\eta}_1,\dot{\eta}_2,\dot{\eta}_3,\dot{\eta}_4,\dot{\eta}_5,\dot{\eta}_6,\eta_1,\eta_2,\eta_3,\eta_4,\eta_5,\eta_6,t) \end{bmatrix} \tag{8.2}$$

where the mass matrix $\mathbf{M}$ is given by

$$\mathbf{M} = \begin{bmatrix} M_{11} & 0 & M_{13} & 0 & M_{15} & 0 \\ 0 & M_{22} & 0 & M_{24} & 0 & M_{26} \\ M_{31} & 0 & M_{33} & 0 & M_{35} & 0 \\ 0 & M_{42} & 0 & M_{44} & 0 & M_{46} \\ M_{51} & 0 & M_{53} & 0 & M_{55} & 0 \\ 0 & M_{62} & 0 & M_{64} & 0 & M_{66} \end{bmatrix} \tag{8.3}$$

and includes mass and inertia terms as follows

$$\begin{aligned} M_{11} &= m + A_{11}(\infty) & M_{42} &= m\bar{\zeta} + A_{42}(\infty) \\ M_{13} &= A_{13}(\infty) & M_{44} &= I_{44} + m\bar{\zeta}^2 + A_{44}(\infty) \\ M_{15} &= -m\bar{\zeta} + A_{15}(\infty) & M_{46} &= -I_{46} + A_{46}(\infty) \\ M_{22} &= m + A_{22}(\infty) & M_{51} &= -m\bar{\zeta} + A_{51}(\infty) \\ M_{24} &= m\bar{\zeta} + A_{24}(\infty) & M_{53} &= A_{53}(\infty) \\ M_{26} &= A_{26}(\infty) & M_{55} &= I_{55} + m\bar{\zeta}^2 + A_{55}(\infty) \\ M_{31} &= A_{31}(\infty) & M_{62} &= A_{62}(\infty) \\ M_{33} &= m + A_{33}(\infty) & M_{64} &= -I_{64} + A_{64}(\infty) \\ M_{35} &= A_{35}(\infty) & M_{66} &= I_{66} + A_{66}(\infty). \end{aligned} \tag{8.4}$$

The functions $f_{1,2,\ldots,6}$ in Equation 8.2 are expressed fully as

$$\begin{aligned} f_1 &= -F_{1\tau} - F_{1\alpha r} - B_{11}(\infty)\dot{\eta}_1 - B_{13}(\infty)\dot{\eta}_3 - B_{15}(\infty)\dot{\eta}_5 + \overline{H}_1(t) \\ f_2 &= -F_{2\tau} - F_{2\alpha r} - B_{22}(\infty)\dot{\eta}_2 - B_{24}(\infty)\dot{\eta}_4 - B_{26}(\infty)\dot{\eta}_6 + \overline{H}_2(t) \\ f_3 &= -F_{3\tau} - F_{3\alpha r} - B_{31}(\infty)\dot{\eta}_1 - B_{33}(\infty)\dot{\eta}_3 - B_{35}(\infty)\dot{\eta}_5 + \overline{H}_3(t) \\ f_4 &= -F_{4\tau} - F_{4\alpha r} - B_{42}(\infty)\dot{\eta}_2 - B_{44}(\infty)\dot{\eta}_4 - B_{46}(\infty)\dot{\eta}_6 + \overline{H}_4(t) \\ f_5 &= -F_{5\tau} - F_{5\alpha r} - B_{51}(\infty)\dot{\eta}_1 - B_{53}(\infty)\dot{\eta}_3 - B_{55}(\infty)\dot{\eta}_5 + \overline{H}_5(t) \\ f_6 &= -F_{6\tau} - F_{6\alpha r} - B_{62}(\infty)\dot{\eta}_2 - B_{64}(\infty)\dot{\eta}_4 - B_{66}(\infty)\dot{\eta}_6 + \overline{H}_6(t). \end{aligned} \tag{8.5}$$

The terms with the subscript τ in Equation 8.5 are the radiation forces and moments and

they may be written in terms of convolution integrals in the following way,

$$F_{1\tau} = \int_0^t h^*_{11}(\tau)\dot{\eta}_1(t-\tau)d\tau + \int_0^t h^*_{13}(\tau)\dot{\eta}_3(t-\tau)d\tau + \int_0^t h^*_{15}(\tau)\dot{\eta}_5(t-\tau)d\tau$$

$$F_{2\tau} = \int_0^t h^*_{22}(\tau)\dot{\eta}_2(t-\tau)d\tau + \int_0^t h^*_{24}(\tau)\dot{\eta}_4(t-\tau)d\tau + \int_0^t h^*_{26}(\tau)\dot{\eta}_6(t-\tau)d\tau$$

$$F_{3\tau} = \int_0^t h^*_{31}(\tau)\dot{\eta}_1(t-\tau)d\tau + \int_0^t h^*_{33}(\tau)\dot{\eta}_3(t-\tau)d\tau + \int_0^t h^*_{35}(\tau)\dot{\eta}_5(t-\tau)d\tau$$

$$F_{4\tau} = \int_0^t h^*_{42}(\tau)\dot{\eta}_2(t-\tau)d\tau + \int_0^t h^*_{44}(\tau)\dot{\eta}_4(t-\tau)d\tau + \int_0^t h^*_{46}(\tau)\dot{\eta}_6(t-\tau)d\tau$$

$$F_{5\tau} = \int_0^t h^*_{51}(\tau)\dot{\eta}_1(t-\tau)d\tau + \int_0^t h^*_{53}(\tau)\dot{\eta}_3(t-\tau)d\tau + \int_0^t h^*_{55}(\tau)\dot{\eta}_5(t-\tau)d\tau$$

$$F_{6\tau} = \int_0^t h^*_{62}(\tau)\dot{\eta}_2(t-\tau)d\tau + \int_0^t h^*_{64}(\tau)\dot{\eta}_4(t-\tau)d\tau + \int_0^t h^*_{66}(\tau)\dot{\eta}_6(t-\tau)d\tau.$$

The terms with subscript αr in Equation 8.5 refer to the wave excitation and restoring contributions. The calculation of these contributions are dependent upon the nature of the time domain method used and will be elaborated upon in Chapters 9 and 10.

It can be seen that although Equation 8.2 represents a system with six degrees of freedom, the inertia and radiation related terms result in the uncoupling of the symmetric and anti-symmetric motions for a vessel with port/starboard symmetry.

8.1.2 Body Fixed Axis Equations of Motion

Using identical arguments to those used for the equilibrium axis equations representation, the body fixed axis equations of motion, initially given in Equations 4.18 and 4.19, may be rewritten as follows for a convolution integral representation.

$$\begin{bmatrix} \dot{u}(t) \\ \dot{v}(t) \\ \dot{w}(t) \\ \dot{p}(t) \\ \dot{q}(t) \\ \dot{r}(t) \end{bmatrix} = \mathbf{M^{-1}} \begin{bmatrix} f_1(u,v,w,p,q,r,X^*,y^*,z^*,\theta,\phi,\psi,t) \\ f_2(u,v,w,p,q,r,X^*,y^*,z^*,\theta,\phi,\psi,t) \\ f_3(u,v,w,p,q,r,X^*,y^*,z^*,\theta,\phi,\psi,t) \\ f_4(u,v,w,p,q,r,X^*,y^*,z^*,\theta,\phi,\psi,t) \\ f_5(u,v,w,p,q,r,X^*,y^*,z^*,\theta,\phi,\psi,t) \\ f_6(u,v,w,p,q,r,X^*,y^*,z^*,\theta,\phi,\psi,t) \end{bmatrix} \tag{8.6}$$

The mass matrix **M** takes the same form as Equation 8.3 with the coefficients given by

$$\begin{aligned}
M_{11} &= m - X_{\dot{u}}(\infty) & M_{42} &= -K_{\dot{v}}(\infty) \\
M_{13} &= -X_{\dot{w}}(\infty) & M_{44} &= I_{44} - K_{\dot{p}}(\infty) \\
M_{15} &= -X_{\dot{q}}(\infty) & M_{46} &= -I_{46} - K_{\dot{r}}(\infty) \\
M_{22} &= m - Y_{\dot{v}}(\infty) & M_{51} &= -M_{\dot{u}}(\infty) \\
M_{24} &= -Y_{\dot{p}}(\infty) & M_{53} &= -M_{\dot{w}}(\infty) \\
M_{26} &= -Y_{\dot{r}}(\infty) & M_{55} &= I_{55} - M_{\dot{q}}(\infty) \\
M_{31} &= -Z_{\dot{u}}(\infty) & M_{62} &= -N_{\dot{v}}(\infty) \\
M_{33} &= m - Z_{\dot{w}}(\infty) & M_{64} &= -I_{64} - N_{\dot{p}}(\infty) \\
M_{35} &= -Z_{\dot{q}}(\infty) & M_{66} &= I_{66} - N_{\dot{r}}(\infty).
\end{aligned} \tag{8.7}$$

In a similar fashion to the equilibrium case, the functions $f_{1,2,\ldots,6}$ in Equation 8.6 may be expressed fully as

$$\begin{aligned}
f_1 &= X_\tau + X_{\alpha r} + X_u(\infty)u + X_w(\infty)w + X_q(\infty)q + \overline{X}(t) \\
f_2 &= Y_\tau + Y_{\alpha r} + Y_v(\infty)v + Y_p(\infty)p + Y_r(\infty)r - mr\overline{U} + \overline{Y}(t) \\
f_3 &= Z_\tau + Z_{\alpha r} + Z_u(\infty)u + Z_w(\infty)w + Z_q(\infty)q + mq\overline{U} + \overline{Z}(t) \\
f_4 &= K_\tau + K_{\alpha r} + K_v(\infty)v + K_p(\infty)p + K_r(\infty)r + \overline{K}(t) \\
f_5 &= M_\tau + M_{\alpha r} + M_u(\infty)u + M_w(\infty)w + M_q(\infty)q + \overline{M}(t) \\
f_6 &= N_\tau + N_{\alpha r} + N_v(\infty)v + N_p(\infty)p + N_r(\infty)r + \overline{N}(t).
\end{aligned} \tag{8.8}$$

Once more, the terms with the subscript τ in Equation 8.8 are the radiation forces and moments and they may be written in terms of convolution integrals in the following way,

$$\begin{aligned}
X_\tau &= \int_0^t x_u^*(\tau)u(t-\tau)d\tau + \int_0^t x_w^*(\tau)w(t-\tau)d\tau + \int_0^t x_q^*(\tau)q(t-\tau)d\tau \\
Y_\tau &= \int_0^t y_v^*(\tau)v(t-\tau)d\tau + \int_0^t y_p^*(\tau)p(t-\tau)d\tau + \int_0^t y_r^*(\tau)r(t-\tau)d\tau \\
Z_\tau &= \int_0^t z_u^*(\tau)u(t-\tau)d\tau + \int_0^t z_w^*(\tau)w(t-\tau)d\tau + \int_0^t z_q^*(\tau)q(t-\tau)d\tau
\end{aligned}$$

$$
\begin{aligned}
K_\tau &= \int_0^t k_v^*(\tau)v(t-\tau)d\tau + \int_0^t k_p^*(\tau)p(t-\tau)d\tau + \int_0^t k_r^*(\tau)r(t-\tau)d\tau \\
M_\tau &= \int_0^t m_u^*(\tau)u(t-\tau)d\tau + \int_0^t m_w^*(\tau)w(t-\tau)d\tau + \int_0^t m_q^*(\tau)q(t-\tau)d\tau \\
N_\tau &= \int_0^t n_v^*(\tau)v(t-\tau)d\tau + \int_0^t n_p^*(\tau)p(t-\tau)d\tau + \int_0^t n_r^*(\tau)r(t-\tau)d\tau.
\end{aligned}
$$

The terms in Equation 8.8 with subscript αr are the wave excitation and restoring contributions. As was the case for the equilibrium axis equations of motion, the calculation of these contributions depends upon the time domain simulation method and will be elaborated upon in Chapters 9 and 10.

Again it can be seen that although Equation 8.6 represents a system with six degrees of freedom, the inertia and radiation related terms result in the uncoupling of symmetric and anti-symmetric motions for a vessel with port/starboard symmetry. The use of the six degree of freedom equation of motion will become clearer in Chapter 10, when the use of the instantaneous wetted surface results in the coupling of symmetric and anti-symmetric motions in oblique waves.

8.2 Reduction in Order of Differential Equations

The equations of motion for the six degree of freedom motions of a rigid ship are second order differential equations. To aid the solution of these equations it is convenient to convert them into a more easily calculated set of equations. It is possible to reduce a second order differential equation into a pair of first order equations, greatly reducing the complexity of obtaining a solution.

As an example, consider the case of a simple, single degree of freedom mass-spring-damper system, the equation of motion being given by

$$M\ddot{x} + B\dot{x} + Cx = F(t),$$

where M is the mass, B is the damping coefficient and C is the restoring coefficient.

Making $\ddot{x}$ the subject, it can be shown that

$$\ddot{x} = \frac{1}{M}\left[F(t) - Bx_1 - Cx\right].$$

By introducing a new variable x_1, such that $x_1 = \dot{x}$, two first order systems can be formed:

$$\begin{aligned} \dot{x_1} &= \frac{1}{M}[F(t) - Bx_1 - Cx] \\ \dot{x} &= x_1. \end{aligned}$$

Hence the second order equation can be changed into a system of the form $\dot{\mathbf{X}}$=$\mathbf{F}$($\mathbf{X}$,t), made up of two first order equations,

$$\dot{\mathbf{X}} = \begin{pmatrix} \dot{x_1} \\ \dot{x} \end{pmatrix} \quad \text{and} \quad \mathbf{F} = \begin{pmatrix} \frac{1}{M}[F(t) - Bx_1 - Cx] \\ x_1 \end{pmatrix}. \tag{8.9}$$

For the purposes of illustration, this method is applied to the equations of motion referenced to equilibrium axes. Hence, from Equation 8.2 it is possible to obtain the following expressions for $\mathbf{X}$ and $\mathbf{F}$,

$$\mathbf{X}(t) = \begin{bmatrix} \dot{\eta_1}(t) \\ \dot{\eta_2}(t) \\ \dot{\eta_3}(t) \\ \dot{\eta_4}(t) \\ \dot{\eta_5}(t) \\ \dot{\eta_6}(t) \\ \eta_1(t) \\ \eta_2(t) \\ \eta_3(t) \\ \eta_4(t) \\ \eta_5(t) \\ \eta_6(t) \end{bmatrix} \quad \text{and} \quad \mathbf{F} = \begin{bmatrix} f_1^m(\dot{\eta_1}, \dot{\eta_2}, \dot{\eta_3}, \dot{\eta_4}, \dot{\eta_5}, \dot{\eta_6}, \eta_1, \eta_2, \eta_3, \eta_4, \eta_5, \eta_6, t) \\ f_2^m(\dot{\eta_1}, \dot{\eta_2}, \dot{\eta_3}, \dot{\eta_4}, \dot{\eta_5}, \dot{\eta_6}, \eta_1, \eta_2, \eta_3, \eta_4, \eta_5, \eta_6, t) \\ f_3^m(\dot{\eta_1}, \dot{\eta_2}, \dot{\eta_3}, \dot{\eta_4}, \dot{\eta_5}, \dot{\eta_6}, \eta_1, \eta_2, \eta_3, \eta_4, \eta_5, \eta_6, t) \\ f_4^m(\dot{\eta_1}, \dot{\eta_2}, \dot{\eta_3}, \dot{\eta_4}, \dot{\eta_5}, \dot{\eta_6}, \eta_1, \eta_2, \eta_3, \eta_4, \eta_5, \eta_6, t) \\ f_5^m(\dot{\eta_1}, \dot{\eta_2}, \dot{\eta_3}, \dot{\eta_4}, \dot{\eta_5}, \dot{\eta_6}, \eta_1, \eta_2, \eta_3, \eta_4, \eta_5, \eta_6, t) \\ f_6^m(\dot{\eta_1}, \dot{\eta_2}, \dot{\eta_3}, \dot{\eta_4}, \dot{\eta_5}, \dot{\eta_6}, \eta_1, \eta_2, \eta_3, \eta_4, \eta_5, \eta_6, t) \\ \dot{\eta_1} \\ \dot{\eta_2} \\ \dot{\eta_3} \\ \dot{\eta_4} \\ \dot{\eta_5} \\ \dot{\eta_6} \end{bmatrix}.$$

8.3 Time Stepping Scheme

Having determined first order differential equations to describe the equations of motion of the rigid ship, one requires a method for the solution of these equations. A number of methods exist for the numerical solution of initial value type differential equations, such as characterised by the ship motion problem. Such methods work by calculating the solution at a series of steps at discrete time intervals, building up a history of the solution to the equation over a period of time.

The solution to a differential equation can be considered to be of the form of a Taylor series, where for a given value $x(t)$ and time t, the solution at time $t + h$ is

$$x(t+h) = x(t) + h\frac{\partial x}{\partial t} + \left(\frac{h^2}{2}\right)\frac{\partial^2 x}{\partial t^2} + \cdots,$$

if we consider the solution to be of the form

$$\frac{\partial x}{\partial t} = f(x,t), \qquad \text{where} \qquad x(t_0) = y_0.$$

If h is a small value, it is apparent that the higher powers $h^2, h^3, \ldots$ are very small. This suggests that a crude approximation of the solution can be made by simply ignoring higher order terms. This gives the Euler method, which for the general case is given by,

$$x_{n+1} = x_n + hf(x_n, t_n) \qquad \text{for} \quad n = 0, 1, \ldots$$

Given that the higher order terms are ignored, there is a global error of the order of h ($O(h)$). This relatively high error factor is the reason why this simplistic method is not used widely. Instead methods have been developed which consider the higher order terms of the Taylor series and consequently give smaller errors [71].

Among these improved methods are those that use a predictor-corrector technique. Such methods consider higher order terms in the Taylor series, making an initial calculation of one or more auxiliary values between the current and the next step. The most basic method of this type is the Euler-Cauchy method which calculates a single auxiliary step and then uses that to provide a correction to the final estimate of the solution. The error using this

method is now reduced to $O(h^2)$. Further accuracy is obtained as more intermediate values are included. One such higher order method is the fourth order Runge-Kutta technique. In this method four auxiliary solutions are obtained, all of which are used to estimate the value of the final solution. The error of this method is $O(h^4)$.

The fourth order Runge-Kutta method is very simple to implement and offers a high level of robustness. Hence it is this method that will be used for the solution of the rigid body equations of motion. The fourth order Runge-Kutta method takes as input initial values of x and t, a constant step size h and a number of steps N.

Using the notation of Equation 8.9, for the steps $n = 0, 1, \ldots, N-1$ the following calculations are made to determine the value of the solution at the next time step,

$$\begin{aligned} k_1 &= h\mathbf{F}(\mathbf{X}_n, t) \\ k_2 &= h\mathbf{F}(\mathbf{X}_n + k_1/2, t + h/2) \\ k_3 &= h\mathbf{F}(\mathbf{X}_n + k_2/2, t + h/2) \\ k_4 &= h\mathbf{F}(\mathbf{X}_n + k_3, t + h) \\ \mathbf{X}_{n+1} &= \frac{1}{6}(k_1 + 2k_2 + 2k_3 + k_4). \end{aligned}$$

This routine has been shown to be sufficiently robust for applications of this type [7].

8.4 Numerical Convolution Techniques

The equations of motion given in Equations 8.2 and 8.6 include convolution integrals, which require solution at each step of the time domain simulation. The time domain techniques implemented herein use a trapezoidal summation technique for the evaluation of the convolution integrals at each time step.

Calculating the numerical solution of the radiation convolution integrals in a particular mode of motion involves the body velocity in that direction and the corresponding impulse

response function. These are both represented as a series of discrete points. In the general case, the numerical evaluation of the convolution integral is complicated by the fact that the time step for which the velocity trace is defined is likely to be different from the time step of the impulse response function. To account for this, the time step of the impulse response function data has been chosen for the evaluation of the convolution integral and the velocity trace is linearly interpolated, enabling it to be represented at identical time steps.

Figure 8.1 shows an example of the implementation of the numerical method for the solution of the radiation convolution integrals. In this example the convolution integral is being solved at time t. The time steps at which the velocity trace is initially defined are at the times labelled $n = 0, 1, 2, \ldots$, identified by the squares on the velocity trace. The impulse response function is defined at a series of time points $r = 0, 1, 2, \ldots$, marked by circles on the trace.

To enable to calculation of the solution, the velocity trace must be redefined at a series of points with time step equal to that of the impulse response function data. These newly defined points are marked on the diagram by crosses and occur at $r = 0, 1, 2, \ldots$.

Because the velocity data and the impulse response function data are now defined at the same intervals, it becomes possible to represent the convolution integral formulation

$$f(t) = \int_0^t h(\tau)\, v(t-\tau)\, d\tau$$

in terms of a simple trapezoidal summation. Hence, for time step Δt, the integral above may be solved using the trapezium rule as follows,

$$\begin{aligned} f(t) &= \int_0^t h(\tau)\, v(t-\tau)\, d\tau \\ &\approx \Delta t \left\{ \frac{1}{2}\Big[h(0)\, v(t)\Big] + \Big[h(\Delta t)\, v(t-\Delta t)\Big] \right. \\ &\qquad + \Big[h(2\Delta t)\, v(t-2\Delta t)\Big] + \ldots \\ &\qquad \left. + \Big[h((n-1)\Delta t)\, v(t-(n-1)\Delta t)\Big] + \frac{1}{2}\Big[h(t)\, v(0)\Big] \right\}. \end{aligned}$$

Figure 8.2 shows a similar diagram for the numerical method for the solution of the wave excitation convolution integrals. In this example. the convolution integral now includes a negative time component as follows,

$$f(t) = \int_{-T}^{t} h_\alpha(\tau)\, \alpha(t-\tau)\, d\tau.$$

In the diagram it can be seen that it is again assumed that the time steps at which the wave elevation trace is defined may not necessarily be the same as those at which the impulse response function is defined. The original points at which the wave elevation trace is defined are shown on the diagram by a square symbol. It should be noted that these are defined only up to time t, point $n = 5$ in the diagram. When the wave elevation trace is linearly interpolated to obtain values at time step Δt, corresponding to that of the impulse response function, the wave trace is defined for an additional length of time, equal to the negative time component of the impulse response function. This prediction of the future wave height employs the definition of the wave spectrum and accounts for the vessel heading.

Hence, using the trapezoid summation technique, the wave excitation convolution integral at time t is given by

$$\begin{aligned} f(t) &= \int_{-T}^{t} h_\alpha(\tau)\, \alpha(t-\tau)\, d\tau \\ &\approx \Delta t \Big\{ \frac{1}{2}\Big[h_\alpha(-T)\, \alpha(t+T)\Big] + \Big[h_\alpha(\Delta t - T)\, \alpha(t-\Delta t+T)\Big] \\ &\quad + \Big[h_\alpha(2\Delta t - T)\, \alpha(t-2\Delta t+T)\Big] + \ldots \\ &\quad + \Big[h_\alpha((n-1)\Delta t - T)\, \alpha(t-(n-1)\Delta t+T)\Big] + \frac{1}{2}\Big[h_\alpha(t)\, \alpha(0)\Big] \Big\}. \end{aligned}$$

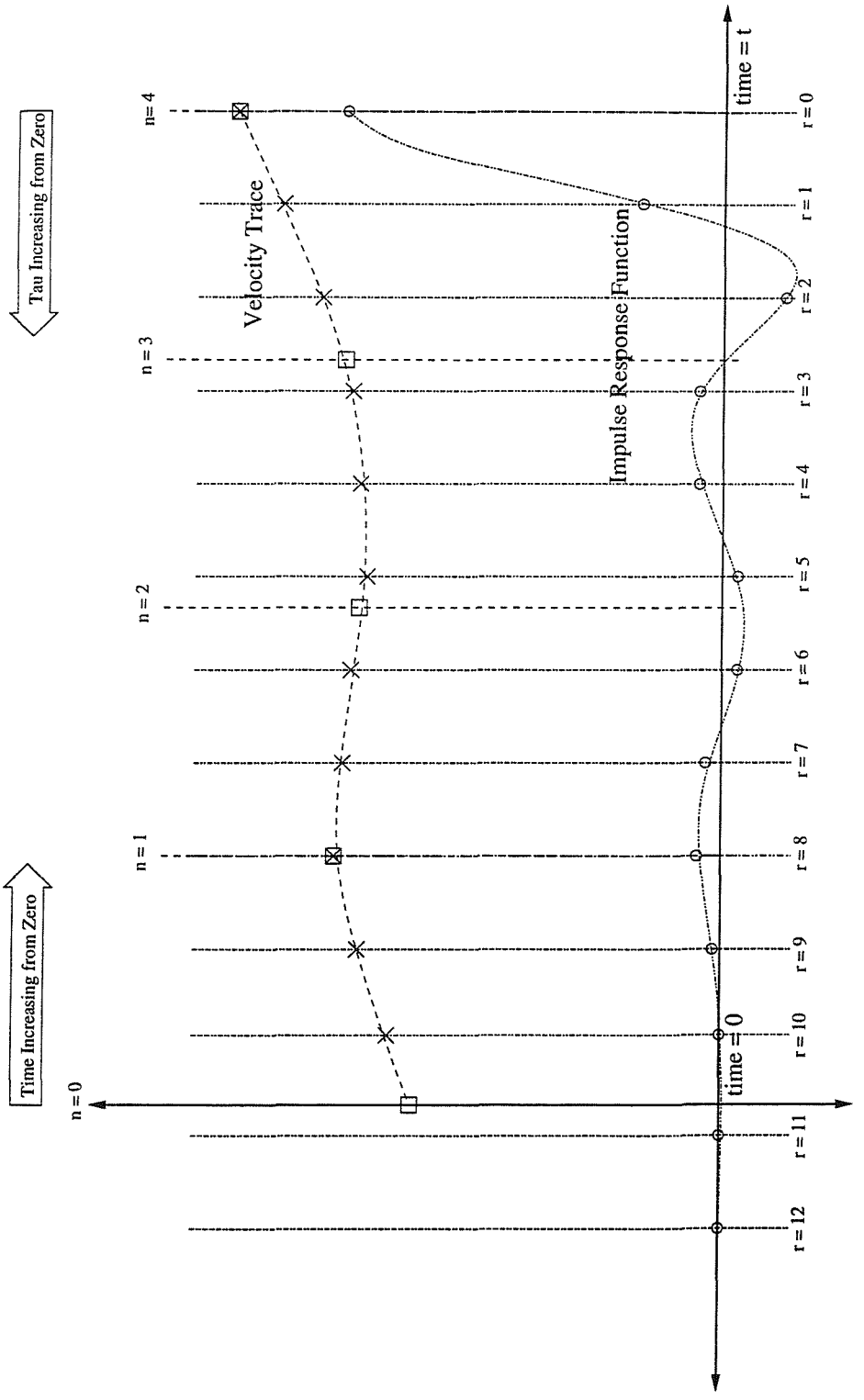

Figure 8.1: Schematic diagram of numerical integration of radiation convolution integral.

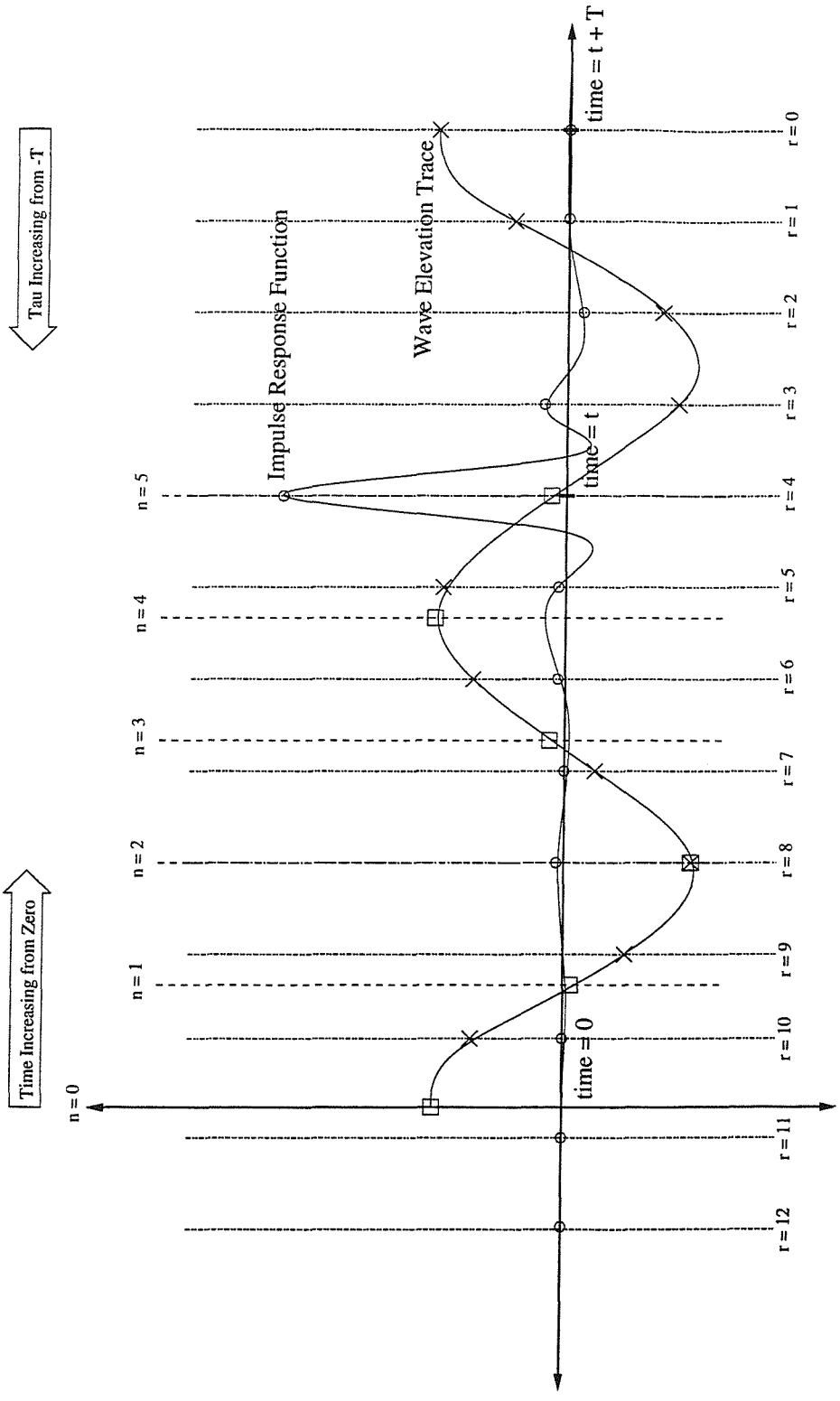

Figure 8.2: Schematic diagram of numerical integration of wave excitation convolution integral.

9 Linear Time Domain Simulation

Previous chapters have examined the development and implementation of methods required for the successful application of a time domain simulation technique. This has included routines for the determination of impulse response functions from frequency domain data and the formulation of equations of motion in six degrees of freedom referenced to both equilibrium and body fixed axis systems. These equations of motion include convolution integrals and are solved using a fourth order Runge-Kutta time stepping scheme.

This chapter will focus on the validation of the numerical simulation techniques, initially using both equilibrium and body fixed axis data. The accuracy of the solutions obtained using data referenced to either axis system will be examined by comparing the results of time domain simulations to frequency domain predictions. To allow such a comparison to be performed, the incident waves will be sinusoidal in form. The methods used for the calculation of the amplitude of steady state response will be discussed and a *Series 60* monohull will be used to compare the results of the equilibrium and body fixed axis time domain methods.

Having determined the most appropriate axis system to reference hydrodynamic data to, the resultant linear time domain method will be further tested on two hull forms at a range of headings and speeds. The first hull form will be the *Series 60*, followed by an *NPL5b* type hull. Initially the *NPL5b* will be in mono-hull form, followed by two catamaran arrangements with different hull separations. Comparison will be made between the simulated responses for these arrangements and frequency domain predictions.

9.1 Equations of Motion for Linear Time Domain Method

The equations of motion for the time domain simulation technique are given in Equations 8.2 and 8.6 for equilibrium and body fixed axis representations respectively. It was noted in Sections 8.1.1 and 8.1.2 that the calculation of the wave excitation and restoring contributions is dependent upon the time domain method being used. The linear time domain method uses a convolution integral formulation to describe the combined incident wave and diffraction wave excitation contributions obtained from frequency domain data referenced to the vessel's mean wetted surface. The restoring forces and moments are described using constant value coefficients, determined for the vessel in its calm water position.

9.1.1 Equilibrium Axes

The terms in Equation 8.5 denoted by subscript αr are the wave excitation and restoring contributions. They can be considered to be made up of separate contributions such that

$$F_{i\alpha r} = F_{i\alpha} + F_{ir} \qquad \text{for} \quad i = 1, 2, \ldots, 6$$

where the α and r are the wave excitation and restoring components respectively.

The wave excitation contributions are calculated using impulse response functions determined from frequency domain data using Equation 5.24. Hence, the excitation contributions may be expressed in a convolution integral formulation as follows,

$$F_{1\alpha} = \int_{-T}^{t} h_{1\alpha}(\tau)\alpha(t-\tau)d\tau \qquad F_{4\alpha} = \int_{-T}^{t} h_{4\alpha}(\tau)\alpha(t-\tau)d\tau$$

$$F_{2\alpha} = \int_{-T}^{t} h_{2\alpha}(\tau)\alpha(t-\tau)d\tau \qquad F_{5\alpha} = \int_{-T}^{t} h_{5\alpha}(\tau)\alpha(t-\tau)d\tau$$

$$F_{3\alpha} = \int_{-T}^{t} h_{3\alpha}(\tau)\alpha(t-\tau)d\tau \qquad F_{6\alpha} = \int_{-T}^{t} h_{6\alpha}(\tau)\alpha(t-\tau)d\tau.$$

The restoring force contributions, denoted by subscript r, are calculated as follows,

$$F_{3r} = -C_{33}\eta_3 - C_{35}\eta_3$$

$$F_{4r} = -C_{44}\eta_4$$

$$F_{5r} = -C_{53}\eta_3 - C_{55}\eta_5$$

where C_{33}, C_{35}, C_{44} etc. are constant value coefficients. It should be noted that $F_{1r} = 0 = F_{2r} = F_{6r}$.

9.1.2 Body Fixed Axes

Similarly, the terms in Equation 8.6 with subscript αr also denote wave excitation and restoring contributions which may be considered as separate components, for example,

$$X_{\alpha r} = X_\alpha + X_r$$

$$Z_{\alpha r} = Z_\alpha + Z_r \quad \text{etc.}$$

Hence the wave excitation contributions, also incorporating impulse response functions in a convolution integral formulation, are given by

$$X_\alpha = \int_{-T}^{t} x_\alpha(\tau)\alpha(t-\tau)d\tau \qquad K_\alpha = \int_{-T}^{t} k_\alpha(\tau)\alpha(t-\tau)d\tau$$

$$Y_\alpha = \int_{-T}^{t} y_\alpha(\tau)\alpha(t-\tau)d\tau \qquad M_\alpha = \int_{-T}^{t} m_\alpha(\tau)\alpha(t-\tau)d\tau$$

$$Z_\alpha = \int_{-T}^{t} z_\alpha(\tau)\alpha(t-\tau)d\tau \qquad N_\alpha = \int_{-T}^{t} n_\alpha(\tau)\alpha(t-\tau)d\tau.$$

and the restoring force contributions are calculated using,

$$Z_r = Z_{z^*}z^* + Z_\theta\theta$$

$$K_r = K_\phi\phi$$

$$M_r = M_{z^*}z^* + M_\theta\theta,$$

where the restoring coefficients are again constant values, i.e.

$$Z_{z^*} = C_{33}$$

$$K_\phi = C_{44} \quad \text{etc.}$$

Once again, it should be noted that $X_r = 0 = Y_r = N_r$.

9.2 Comparison of Simulations Using Equilibrium and Body Fixed Axis System Data

The development of novel numerical techniques requires a process of verification to be carried out. Such a process will establish the accuracy of the methods, allowing errors to be identified and different numerical procedures to be compared.

The verification of the linear time domain simulation techniques was carried out using, initially, a *Series 60* hull form. Two versions of the linear motion simulation methods were used. The first of these employed equations of motion and hydrodynamic data referenced to an equilibrium axis system. The second method was identical in all respects except that the equations of motion and the hydrodynamic data were referenced to body fixed axes.

The simulation of linear heave and pitch motions for the *Series 60* model was carried out using hydrodynamic data calculated using methods described in Chapter 7. In particular, the impulse response functions referenced to equilibrium axes are those shown in Figures 7.3 and 7.8 whilst those referenced to body fixed axes may be found in Figures 7.6 and 7.10.

Each simulation was carried out for a total of 1000 time steps. The increment of each time step was 0.05 seconds, giving a total simulation time of 50 seconds. This length of simulation was considered to be sufficiently long to allow the motions to settle to a steady state sinusoidal response of constant amplitude. The simulations were performed for the vessel travelling at $F_n = 0.2$ in regular head waves of constant frequency and amplitude. The amplitude of the waves was chosen as 0.01m, sufficiently small with respect to the model dimensions to be considered reasonable for a linear method. The starting position for each of the simulations was zero displacement in each of the six degrees of freedom.

9.2.1 Calculation of Response Amplitudes

Each time domain simulation produces an output file containing the displacement and velocity traces for each of the six degrees of freedom. It is possible to specify that only certain motions be calculated, in which case the displacement and velocity of the unspecified motions is zero for all time steps. In the case being used here, only heave and pitch motions are considered, surge being neglected. This is because for a linear theory there is considered to be no coupling between symmetric and anti-symmetric motions and in head waves anti-symmetric excitation contributions for a ship which is symmetric about its centreline are assumed to be negligible.

The amplitude of the motion responses was calculated by fitting a Fourier series to the sinusoidal displacement traces once they had settled to a steady state response. Having determined the amplitude of the response from the motion trace, response amplitude operators (RAOs) were calculated by dividing the amplitude of the response by the amplitude of the exciting waves.

Figures 9.1 and 9.2 show examples of the heave and pitch motion traces calculated by the time domain simulation technique using equilibrium axis data. It can be seen that the linear responses are sinusoidal in form, allowing the Fourier fit sinusoidal traces to exactly match the motions. Figures 9.3 and 9.4 show similar results for the linear time domain method when using body fixed axis data. It is clear that irrespective of the data type used, the time domain methods produce stable solutions for which the amplitude may be calculated accurately using a Fourier fit method.

9.2.2 Predictions in Head Waves

Given that there is confidence in the stability of the solutions obtained using the two time domain methods, simulations may be carried out at a range of frequencies using both methods. The predicted heave and pitch responses for a *Series 60* model travelling at $F_n = 0.2$ in head waves are shown in Figure 9.5. The solid line in each of the graphs is the response

predicted by the linear frequency domain pulsating source method. The individual points are frequencies at which simulations have been carried out using the linear time domain methods described in Chapter 8. The responses have been calculated using hydrodynamic data (pulsating source method) and equations of motion referenced to both equilibrium axis and body fixed axis systems.

It can be seen that the heave responses calculated using the equilibrium axis referenced data do not match the frequency domain predictions well, especially in the region of resonance. On the other hand, the responses predicted by simulations using body fixed axis data show excellent agreement with the frequency domain predictions over the entire frequency range. Similar results can be seen for the predicted pitch motions, with the simulations using body fixed axis impulse response functions producing far better agreement with the frequency domain data.

In order to establish the precise reason for the lack of agreement between the time domain equilibrium axis predictions and those of the frequency domain methods, a process of elimination was undertaken. Initially, to check whether the problem was a result of the calculation of the radiation actions, these were assumed to be a constant value corresponding to the frequency domain value of the added mass and damping at the encounter frequency of the regular waves considered. The wave excitation remained represented using convolution integrals. The results of these simulations may be seen in Figure 9.6, where they are referred to as Combination 1.

Next, to establish the role of the wave excitation contribution in the errors, the wave excitation was assumed to have a constant value corresponding to the frequency domain values for the respective encounter frequencies of the regular waves, whilst the hydrodynamic added mass and damping contributions were calculated using a convolution integral formulation. These results may also be seen in Figure 9.6, where they are referred to as Combination 2.

It is clear that the results denoted as Combination 1, which has constant frequency domain data describing the radiation actions and convolution integrals describing the wave actions,

show much better agreement with the frequency domain predictions than the results Combination 2. This suggests that the cause of the problems lies in the convolution integral representation of the hydrodynamic actions. To further test this hypothesis it was decided to examine the effect of using a convolution integral formulation for the wave excitation actions and all radiation contributions except A_{55} and B_{55}, for which constant frequency domain values at the respective encounter frequencies were used. The pitch-pitch coefficients were chosen because of the inaccuracies that had been noted in the verification of the methods for the calculation of the impulse response functions, carried out in Section 7.2. This data has been referred to as Combination 3 and is also shown in Figure 9.6. It can be seen that Combination 3 predictions very closely match Combination 1 as well as the frequency domain predictions. This suggests that the problem has been isolated to the pitch-pitch contributions in the radiation convolution integral formulation used in the equilibrium axes referenced equations of motion.

It is thought that the differences between time domain predictions using a convolution integral representation of equilibrium axis data and frequency domain predictions can be attributed to the inability to accurately determine pitch-pitch added mass contributions from the h_{55} impulse response function. This problem is not thought to be a result of the numerical methods used, rather, it is thought to result from the nature of the frequency domain pitch-pitch data. In particular, it is thought that the characteristic of the $A_{55}(\omega_e)$ coefficient to tend to an infinitely high value at low frequency cannot be represented using the numerical methods employed in this study (see Section 7.2.1). Consider, by way of example, the forward speed corrections applied to A_{55} and B_{55} (see Section 4.3.1) when using the pulsating source method,

$$A_{55}(\omega_e) = A^0_{55}(\omega_e) + \left(\frac{\overline{U}}{\omega_e}\right)^2 A^0_{33}(\omega_e)$$

$$B_{55}(\omega_e) = B^0_{55}(\omega_e) + \left(\frac{\overline{U}}{\omega_e}\right)^2 B^0_{33}(\omega_e)$$

where, as previously, the superscript 0 denotes the zero speed coefficient. Given that

$$H(i\omega_e) = B_{55}(\omega_e) + i\omega_e(A_{55}(\omega_e)) = \int_{-\infty}^{\infty} h_{55}(\tau)e^{-i\omega_e\tau}\,d\tau,$$

then it may be shown that

$$\left\{B^0_{55}(\omega_e) + \left(\frac{\overline{U}}{\omega_e}\right)^2 B^0_{33}(\omega_e)\right\}$$

$$-i\omega_e\left[A^0_{55}(\omega_e) + \left(\frac{\overline{U}}{\omega_e}\right)^2 A^0_{33}(\omega_e)\right] = \int_{-\infty}^{\infty} h_{55}(\tau)e^{-i\omega_e\tau}\,d\tau$$

$$= \int_{-\infty}^{\infty} h^0_{55}(\tau)e^{-i\omega_e\tau}\,d\tau + \int_{-\infty}^{\infty} h^0_{33}{}'(\tau)e^{-i\omega_e\tau}\,d\tau$$

where

$$\left(\frac{\overline{U}}{\omega_e}\right)^2 B^0_{33}(\omega_e) + i\omega_e\left(\frac{\overline{U}}{\omega_e}\right)^2 A^0_{33}(\omega_e) = \int_{-\infty}^{\infty} h^0_{33}{}'(\tau)e^{-i\omega_e\tau}\,d\tau.$$

However, because A^0_{33} and B^0_{33} are uniquely related by h^0_{33} as follows,

$$B^0_{33}(\omega_e) + i\omega_e(A^0_{33}(\omega_e)) = \int_{-\infty}^{\infty} h^0_{33}(\tau)e^{-i\omega_e\tau}\,d\tau,$$

then it would have to be the case that,

$$h^0_{33}{}'(\tau) = \left(\frac{\overline{U}}{\omega_e}\right)^2 h^0_{33}(\tau).$$

This final relationship is non-unique. Hence, for such situations it is not possible to determine the added mass contribution from an impulse response function calculated using damping data and *vice versa.*

It should be noted that the trends observed in the A_{55} added mass coefficient (which will be similar for A_{66}) with forward speed, as the frequency tends to zero, are similar whether the influence of forward speed is accounted for using an appropriate singularity distribution (i.e. translating, pulsating source) or correction [47, 49]. The analysis above merely illustrates the consequences of the forward speed effects. This suggests that some speed dependent hydrodynamic coefficients referenced to equilibrium axes do not allow Fourier transformation. This will apply to all hull forms and speeds as the nature of the problem is the same, irrespective of the particular case that is being examined.

To confirm that this is the case, an *NPL5b* monohull model with Froude Number 0.53 was also modelled in head waves. The particulars of this model are given in Appendix B.2. The mean wetted surface was modelled using a total of 500 panels, the panel distribution

having being created using the Fixed Method , with 6 panels per section and an aspect ratio of 2.

A comparison of the steady state predictions from the time domain simulations at this higher speed ($F_n = 0.53$) using both equilibrium and body fixed axis systems with frequency predictions can be seen in Figure 9.7. It is clear that once again the body fixed axis representation provides the most accurate prediction of the amplitude of response at each frequency. To confirm that the discrepancy is due not only to the forward speed correction used in the pulsating source method, frequency domain data was also calculated using the translating, pulsating source method. Impulse response functions for the hydrodynamic actions and wave excitation were calculated from this data referenced to both equilibrium and body fixed axis systems. The results of the linear time domain simulations can be seen in Figure 9.8. It can be clearly seen that the simulation using body fixed axis data provides the most accurate prediction of the response at each of the frequencies tested. It can also be seen that at this higher forward speed the differences arising from the equilibrium axis referenced time domain predictions are larger.

The results presented in Figures 9.5, 9.6, 9.7 and 9.8 clearly show that time domain simulations using body fixed axis data produce results which are in very close agreement with frequency domain predictions at the same wave excitation frequencies. Using equilibrium axis data did not provide us with sufficiently accurate results, due to the fact that certain frequency domain data referenced to equilibrium axis does permit accurate Fourier transformation when the forward speed is not zero. Hence, all further time domain simulations will use data referenced to a body fixed axis system. Because frequency domain hydrodynamic coefficients referenced to this axis system all have finite values at low frequency, the problem of inaccurate calculation of impulse response functions may be avoided.

9.3 Simulation of Monohull Motions

9.3.1 Symmetric Motions

The previous sections of this chapter have established the accuracy and stability of the numerical simulation method and the techniques for determining the response amplitude. In doing so, motions of two hulls forms in head waves were used to illustrate the processes, the first being a *Series 60*, the second a *NPL5b* monohull. As noted earlier, linear equations of motion consider symmetric and anti-symmetric motions to be uncoupled. Hence, the simulation of the symmetric linear motions of heave and pitch (ignoring surge) is carried out whilst ignoring the anti-symmetric motions of sway, roll and yaw.

Having shown that the simulation methods work for the symmetric motions of two hull forms in head waves, other headings must also be examined to further confirm the accuracy of the methods. In particular, the cases are considered of oblique and beam waves where the angle between the direction of the waves and the heading of the ship is 135° and 90° respectively. Once again the model used is the *Series 60* type ship.

Results for heave and pitch motions of a *Series 60* model in oblique waves may be seen in Figure 9.9. It can be seen that there is excellent agreement between the time domain simulations and frequency domain predictions at the same frequency. Similarly, for a beam waves the agreement between frequency and time domain methods is again good, as may be seen in Figure 9.10.

The results presented for time domain simulations of the symmetric motions of monohull ships, present a strong case confirming the accuracy of the linear time domain simulation methods. They have been shown to accurately produce results in regular waves which are very close to predictions using frequency domain data, as would be expected.

9.3.2 Anti-Symmetric Motions

The modelling of anti-symmetric motions in the time domain is problematic for a number of reasons. Firstly, there are no restoring actions for the sway and yaw motions. This means that perturbations in these modes will result in the ship being deviated from its initial course if there is no method to correct the heading, such as the application of a rudder moment. Such changes in heading will have the effect of rendering the wave excitation impulse response functions incorrect, as they are specific to the original heading of the vessel, χ_0.

In addition, the anti-symmetric motions of sway and yaw are significantly affected by viscous contributions, which cannot be accounted for by the potential flow methods used to obtain the theoretical hydrodynamic data. Without viscous effects, low frequency anti-symmetric motions such as yaw are lightly damped, resulting in large amplitude perturbations which do not correspond to realistic ship motions.

Roll motions are excluded due the lack of experimental data by which viscous contributions could be estimated. Given that the radiation damping predicted by potential flow theory is only a small part of the total roll damping [65], it is important that the inclusion of roll is accompanied by a realistic estimation of the total damping. As such data is not available, it is thought sensible to neglect roll contributions, though their importance should not, in general, be underestimated. Needless to say, the time domain simulation is capable of including such motions, suggesting that future studies might wish to concentrate on this area.

It has been suggested by Bailey et al [2] that viscous effects may be accounted for by creating hybrid frequency domain data sets, in which the high frequency data is determined using potential flow methods whilst the low frequency data, in which viscous effects are most evident, is determined experimentally. Bailey et al [6] suggest the use of a "viscous ramp". This ramp function has an initial value equal to the zero frequency damping found experimentally and decays linearly to zero at a defined upper frequency. This ramp function is added to the frequency domain data determined using the potential flow methods to obtain the hybrid data set.

Figure 9.11 shows pure and cross coupled sway and yaw velocity derivatives predicted theoretically using the pulsating source method and as measured experimentally by Van Leeuwen [95]. The theoretical data was calculated using the same panelled hull model as the symmetric data for the *Series 60* presented in Chapter 7. Using the zero frequency value of the experimental data as the initial magnitude of the viscous contribution, a ramp function was added to the theoretical data, the upper frequency of the ramp function being 35 rad/s. It can be seen that the addition of the ramp function means that all of the velocity derivative functions now have non-zero low frequency values. This contrasts with the unmodified theoretical data, in which three of the four sets of velocity derivative data tended to zero at low frequency. It can be seen that the addition of the viscous ramp does not necessarily make the theoretical data match the experimental data exactly, but for the most part it appears to offer an improvement. The corresponding impulse response functions, determined using the hybrid frequency domain data, are shown in Figure 9.12.

Time domain simulations were performed with impulse response functions determined using both the unmodified velocity derivative data and that with the addition of viscous ramps. The time domain simulations were performed with the vessel being free in sway and yaw, but unable to roll. Symmetric motions were excluded, which does not change the predicted results as the anti-symmetric motions are uncoupled from these motions. Simulations of the predicted course of the vessel from a given initial heading were performed for two wave amplitudes. The first wave amplitude chosen was very small, $\alpha = 0.0001$m, so as to ensure that any departure from the initial heading due to sway and yaw perturbations was as small as possible. The second was 0.1m, to examine the effects of larger waves on the predicted deviation from the initial course.

Figure 9.13 shows the predicted course for a *Series 60* model in head waves with encounter frequency equal to 2 rad/s. The vessel's starting point is at the point (0,0) on the axes. When the smaller wave amplitude is used it can be seen that the simulation using the hybrid velocity derivatives predicts the vessel maintaining a constant heading. Where the theoretical velocity derivative data without viscous ramp is used, it can be seen that the ships course begins to alter. The rate of yaw begins to increase and because the yaw velocity derivative

(damping equivalent) is lightly damped, the time domain solution predicts the vessel performing an extremely tight circle manoeuvre. Increasing the wave amplitude to 0.1m sees the simulation using the hybrid data set again predicting a straight line motion. However, when the hydrodynamic data without viscous contributions is used in the simulation, the vessel is again predicted to begin to perform a yawing manoeuvre. In this case the yaw velocity increases to such a high value that the solution becomes unstable, as can be seen when the trace of the course leaves the bounds of the graph.

Figure 9.14 shows the vessel's simulated course in oblique waves ($\chi = 135°$). When the hybrid hydrodynamic data is used to simulate the motions for the smaller wave amplitude it can be seen that a straight line motion is predicted, with virtually no deviation from the original course. Increasing the wave amplitude sees a similar course predicted using the hybrid data, this time with slight sway about a straight line course. The simulations using the potential flow data predicted the ship performing ever fast circle manoeuvres before the solution becomes unstable. This occurred for both wave amplitudes, the yawing motion causing instability in the solution at an earlier time for the large wave amplitude.

Similar results can be seen in Figure 9.15 where the vessel is now in beam waves ($\chi = 90°$). In this case the simulations using the hybrid data predict a straight line course for the smaller wave amplitude, whilst the larger wave amplitude simulation predicts a drift into the waves. Once again, when the potential flow method data is used the solution becomes unstable at both wave amplitudes.

It is clear from these results that in order for reasonable predictions to be made of the anti-symmetric motions of ships to be made, account must be taken of viscous effects. It has been shown that one possible method for incorporating such viscous effects is to introduce a viscous ramp function to the theoretical data calculated using potential flow methods. The use of the viscous ramp is dependent upon the availability of data, most likely experimental, which gives an accurate indication of the viscous effects. Without the incorporation of viscous effects, the accurate modelling of anti-symmetric ship motions is not possible in most cases.

9.4 Simulation of Catamaran Motions

Further verification of the linear time domain simulation techniques were carried using an *NPL5b* type hull form in catamaran configuration. The *NPL5b* is part of a family of symmetrical, round bilge, transom stern hull forms that have been the subject of experimental studies at the University of Southampton [69, 101]. A body plan of the vessel and its particulars may be found in B.2.

The two catamaran configurations used are defined by the ratio of the hull separation to the hull length (S/L ratio) and are made up of a pair of identical *NPL5b* demi-hulls. Frequency domain hydrodynamic data was calculated using a panel representation of the hull made up of two mirror image demi-hulls. A single demi-hull was panelled using the Fixed Method panelling technique, with 6 panels per section and an aspect ratio of 2 (see Figure B.5). This gave a total of 500 panels for the demi-hull. By creating a mirror image of this hull at a defined spacing, the catamaran panel model was created, having a total of 1000 panels.

The two separations that are considered are S/L = 0.2 and 0.4, which for a 4.5m model gives distances between the centrelines of the demi-hulls of 0.9m and 1.8m respectively.

The simulations of the catamaran motions were carried out at Froude number 0.53. Because of the comparatively high speed, theoretical hydrodynamic data was calculated using both pulsating source and translating, pulsating source methods. Because the translating, pulsating source method implicitly accounts for forward speed effects, it is considered that this method is likely to offer a better estimation of the hydrodynamic effects that are present for catamaran vessels. Of particular interest in the modelling of catamaran motions are the effects of interaction between the two hulls. This interaction has been the subject of a number of studies, including those of Wang and Wahab [99], Lee et al [61], Kim [51], Ohkusu and Faltinsen [83], Hudson et al [43], Van't Veer and Siregar [96] and Centeno et al [23].

Van't Veer and Siregar [96] showed that for very low speeds the wave excitation could be considered to be two-dimensional and was well predicted using methods such as strip theory. However, as the speed increased there was a change in the interaction effects. In

particular, if the speed was high enough it was possible that there might be no interaction at all.

The two theoretical methods available for the calculation of theoretical hydrodynamic data are likely to give different predictions of interaction effects. The pulsating source method solves the zero speed solution, to which a forward speed correction is applied. This solution of the zero speed problem is likely to result in an over prediction of the interaction effects in cases where the forward speed is non-zero. The translating, pulsating source method on the other hand accounts for forward speed effects implicitly and is more likely to give an accurate prediction of the interaction effects for cases with moderate forward speed.

Centeno et al [23] showed that it is possible to perform a simple kinematic analysis to calculate whether interaction is likely to occur between the two hulls of a catamaran. For a vessel of length L, spacing between the inner sides of the hulls of H and speed U, the frequency of encounter ω_e above which there should be no wave interaction is given by

$$\omega_e > \frac{L}{H} \cdot \frac{g}{U} \tag{9.1}$$

For the *NPL5b* catamarans with hull separation of $S/L = 0.2$ and 0.4, and Froude Number 0.53, the encounter frequencies at which wave interaction should cease are 25.53 and 9.01 rad/s respectively.

Wang and Wahab [99] showed that for the zero speed case, the theoretical steady wave formation resonance frequencies between the two hulls would occur at frequencies defined by

$$\omega_{n3} = \sqrt{\frac{2\pi g n}{H}} \qquad \text{for} \quad n = 1, 2, 3, \ldots \tag{9.2}$$

where, again, H is the inner distance between the hulls. For the *NPL5b* catamarans considered, the predicted heave resonance frequencies using Equation 9.2 are given in Table 9.1.

As was seen in Figures 9.13 to 9.15, without low frequency non-zero velocity derivatives time domain simulations of anti-symmetric motions are unstable. In the absence of suitable experimental results for low frequency anti-symmetric velocity derivatives, only the

Harmonic	Interaction Frequencies (rad/s)	
	S/L = 0.2	S/L = 0.4
1	11.26	6.67
2	15.85	9.41
3	19.41	11.53
4	22.41	13.31

Table 9.1: Predicted heave resonance frequencies for *NPL5b* catamarans.

symmetric motions of heave and pitch, which are stable without viscous contributions, will be considered for linear time domain simulation.

9.4.1 S/L=0.2

Heave and pitch velocity derivatives for an *NPL5b* catamaran, S/L = 0.2, are shown in Figure 9.16. Data is compared from both pulsating source and translating, pulsating source methods. It can be seen that the pulsating source data suffers from large spikes in the vicinity of the frequencies associated with interactions between the two hulls. In particular, the predicted interactions at around 5 rad/s are very large and result in spikes in the data that are far in excess of the other predicted interactions. This first spike is at a lower frequency than interactions predicted by Equation 9.2 and can be related physically to the resonance of the water column trapped between the two hulls. By comparison, the data from the translating, pulsating source method is well behaved throughout the frequency range. Such a trend would be expected, given that forward speed effects are correctly accounted for.

As noted in Section 7.2.1, when discussing irregular frequencies, the presence of large spikes in the frequency domain data has an unfavourable effect of the subsequent calculation of the impulse response functions. This can be seen in Figure 9.17 which shows the impulse response functions corresponding to the frequency domain data in Figure 9.16. It can be seen that the impulse response functions calculated using the pulsating source data

show large amplitude oscillations, with period corresponding to the frequencies where the spikes are observed, which are slow to die out. On the other hand, the impulse response functions calculated using the translating, pulsating source data do not display such oscillations, the response decaying quickly to zero.

In spite of the large oscillations in the radiation impulse response functions predicted using pulsating source frequency domain data, it can be seen in Figure 9.18 that the predicted responses for the heave and pitch motions are in very close agreement with the frequency domain predictions. This suggests that the numerical methods are able to cope with the large oscillations observed in the impulse response functions calculated from pulsating source data.

9.4.2 S/L=0.4

Frequency domain velocity derivatives for the *NPL5b* catamaran with $S/L = 0.4$ are shown in Figure 9.19. It can be seen that once again the pulsating source method predicts very large interaction effects between the two hulls. Whereas the frequency domain velocity derivatives for the narrower separation only showed a particularly large spike at the lowest interaction frequency, the data for the $S/L = 0.4$ model exhibits very large spikes at a number of frequencies, namely 3.5, 6.7, 9.4, 11.5, ... which, except for the first, correspond to the frequencies shown in Table 9.1. The translating, pulsating source method again shows a very smooth response by comparison, predicting only a relatively small spike at around 1 rad/s. The differences in the frequency domain data are very clearly reflected in the corresponding impulse response functions, see in Figure 9.20. In particular, the impulse response functions calculated using the pulsating source data show large, irregular sinusoidal responses which are very slow to die out. This is due to multiple spikes at predicted interaction frequencies which cause a series of sinusoidal responses which, when combined, give the irregularity seen in the impulse response functions. By contrast, the impulse response functions calculated using translating, pulsating source frequency domain data show very little oscillation and decay to zero comparatively quickly.

The heave and pitch responses predicted using the impulse response functions in Figure 9.20 can be seen in Figure 9.21. Both the heave and pitch responses calculated using the impulse response functions found using pulsating source data show a trough in the response at around $\omega_e' = 4.6$ rad/s which corresponds to $\omega_e = 6.8$ rad/s, which is very close to the value predicted for the first interaction in Table 9.1. It can be seen that the agreement with the frequency domain predictions is not always good and it is thought that this could be the result of the multiple interaction effects that are predicted and their effect on the impulse response functions. Responses using translating, pulsating source data on the other hand show excellent agreement with the frequency domain predictions.

The comparison of catamaran hydrodynamic data calculated using the pulsating source and translating, pulsating source methods has shown that the pulsating source method appears to greatly over predict the interaction effects between the two hulls. These effects appear as spikes in the frequency domain data and have an adverse effect of the subsequent impulse response functions and, in principle, the predicted time domain steady state RAOs, depending on the severity of the spikes. On the other hand, the translating, pulsating source method predicts less interaction effects, giving smoother frequency domain data which translates into impulse response functions which show better characteristics. It is thought that the translating, pulsating source method offers an improved method for the determination of hydrodynamic data for use in a linear time domain simulation of catamaran motions. It should be noted that this improvement in the frequency domain data comes at the price of a considerable increase in the computational time required to obtain the frequency domain data. However, for a catamaran vessel with forward speed, such lengthy calculation is necessary to account for important interaction effects between the hulls of the vessel.

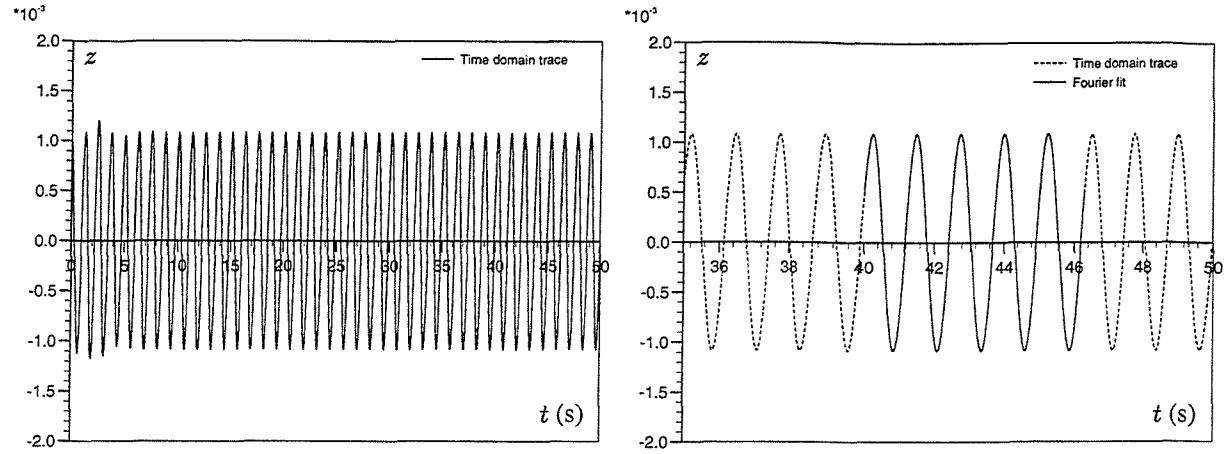

(a) Wave encounter frequency, ω_e = 5 rad/s, ω_e' = 2.79 rad/s

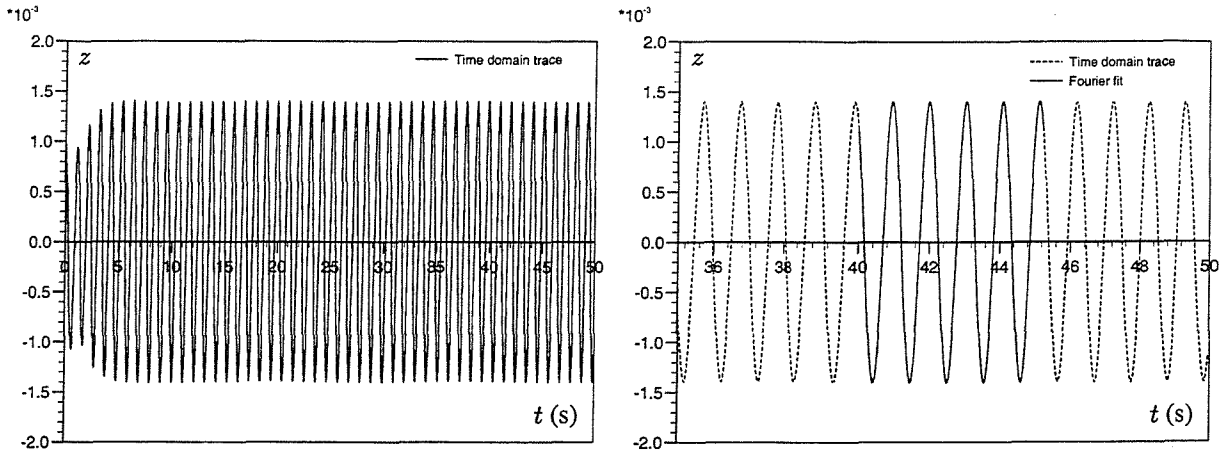

(b) Wave encounter frequency, ω_e = 6 rad/s, ω_e' = 3.34 rad/s

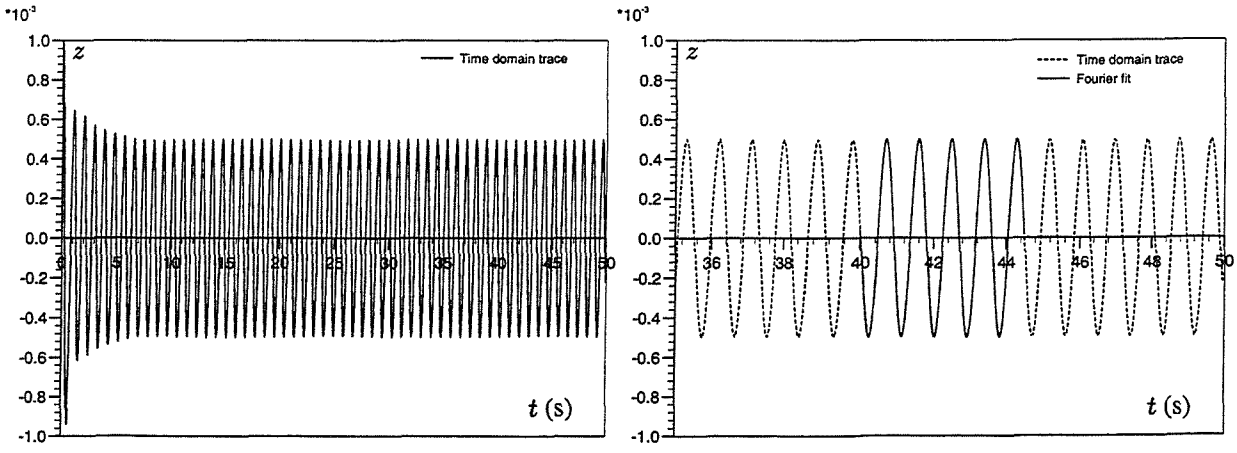

(c) Wave encounter frequency, ω_e = 7 rad/s, ω_e' = 3.90 rad/s

Figure 9.1: Heave traces for simulated motions of a *Series 60* model in head waves using equilibrium axis data, complete trace on left and trace in region of Fourier fit on right. L=3.048m, Fn=0.2 , α=0.01m, time step = 0.05s.

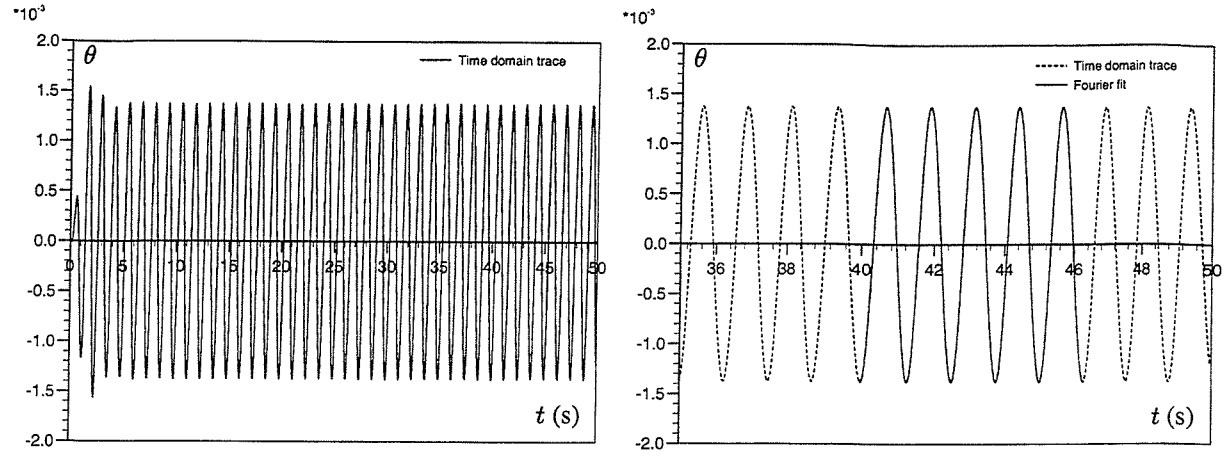

(a) Wave encounter frequency, ω_e = 5 rad/s, ω_e' = 2.79 rad/s

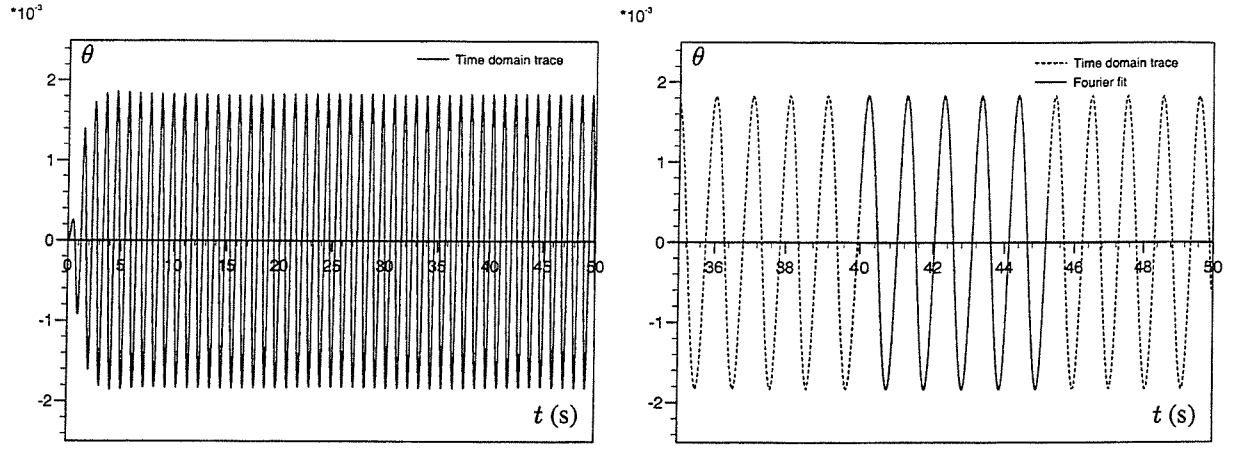

(b) Wave encounter frequency, ω_e = 6 rad/s, ω_e' = 3.34 rad/s

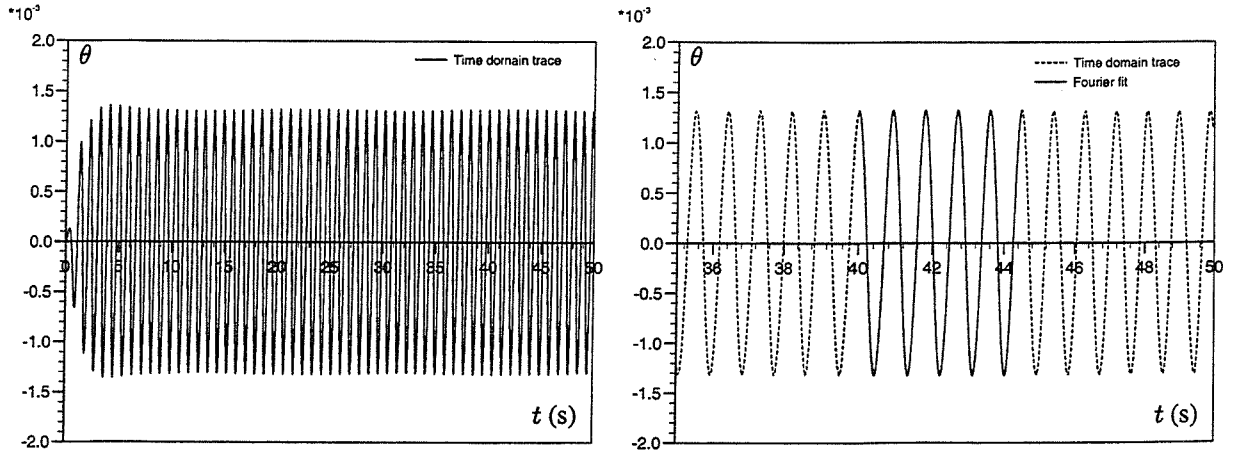

(c) Wave encounter frequency, ω_e = 7 rad/s, ω_e' = 3.90 rad/s

Figure 9.2: Pitch traces for simulated motions of a *Series 60* model in head waves using equilibrium axis data, complete trace on left and trace in region of Fourier fit on right. L=3.048m, Fn=0.2 , α=0.01m, time step = 0.05s.

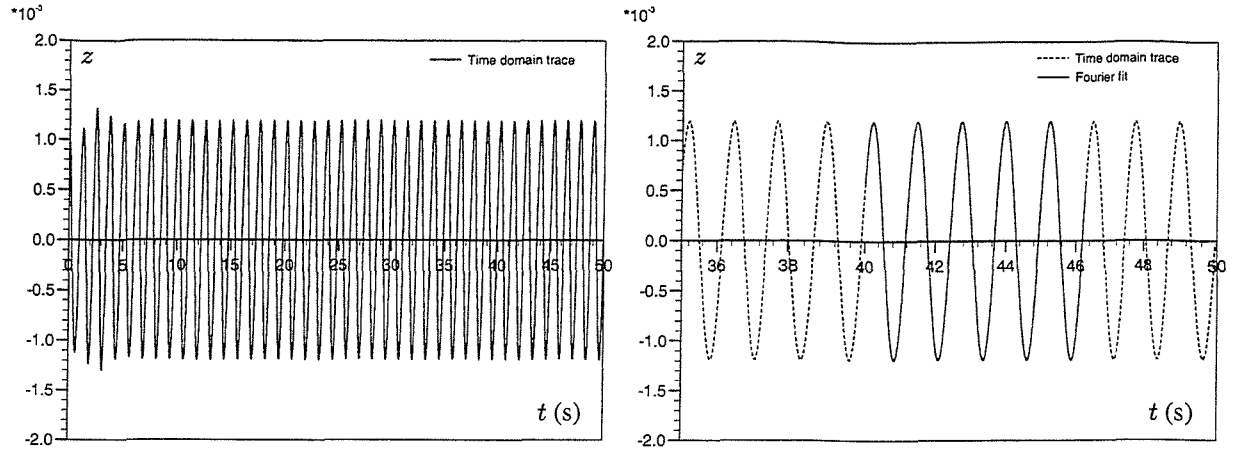

(a) Wave encounter frequency, ω_e = 5 rad/s, ω_e' = 2.79 rad/s

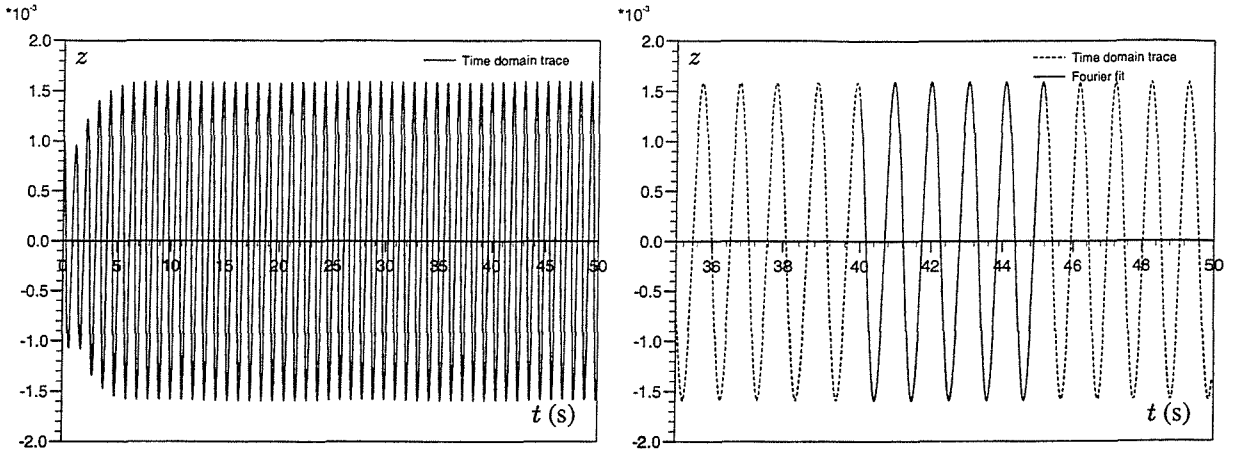

(b) Wave encounter frequency, ω_e = 6 rad/s, ω_e' = 3.34 rad/s

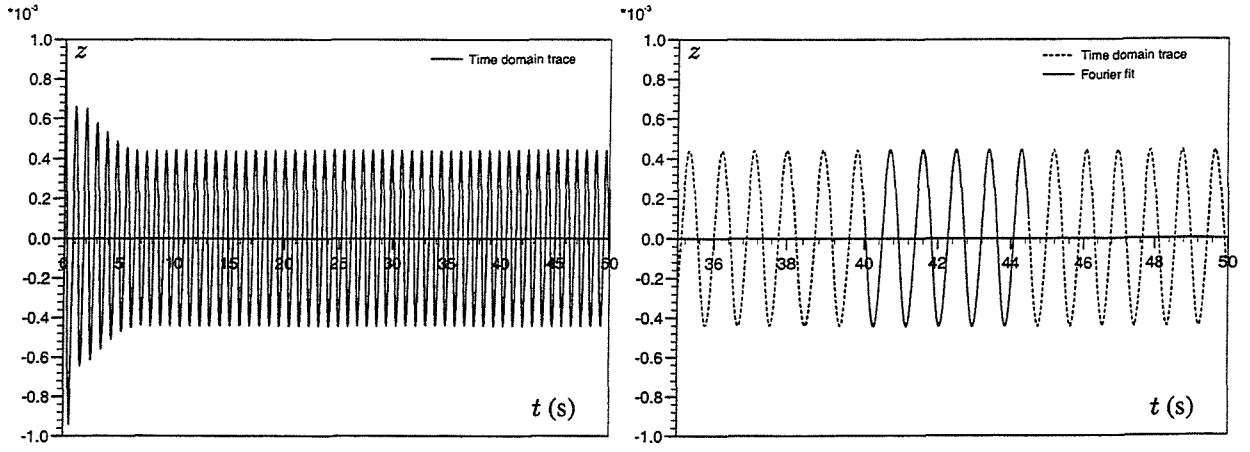

(c) Wave encounter frequency, ω_e = 7 rad/s, ω_e' = 3.90 rad/s

Figure 9.3: Heave traces for simulated motions of a *Series 60* model in head waves using body fixed axis data, complete trace on left and trace in region of Fourier fit on right. L=3.048m, Fn=0.2 , α=0.01m, time step = 0.05s.

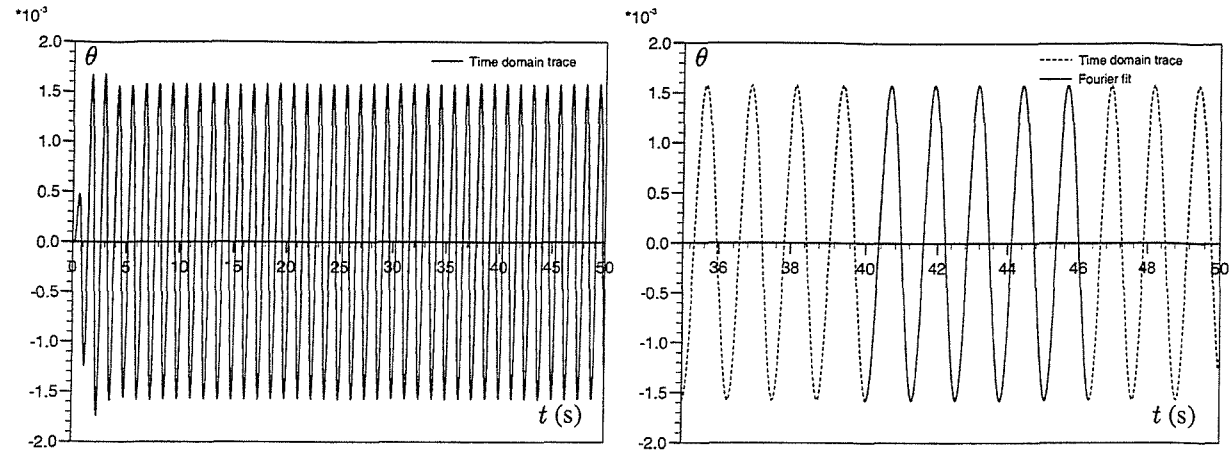

(a) Wave encounter frequency, ω_e = 5 rad/s, ω_e' = 2.79 rad/s

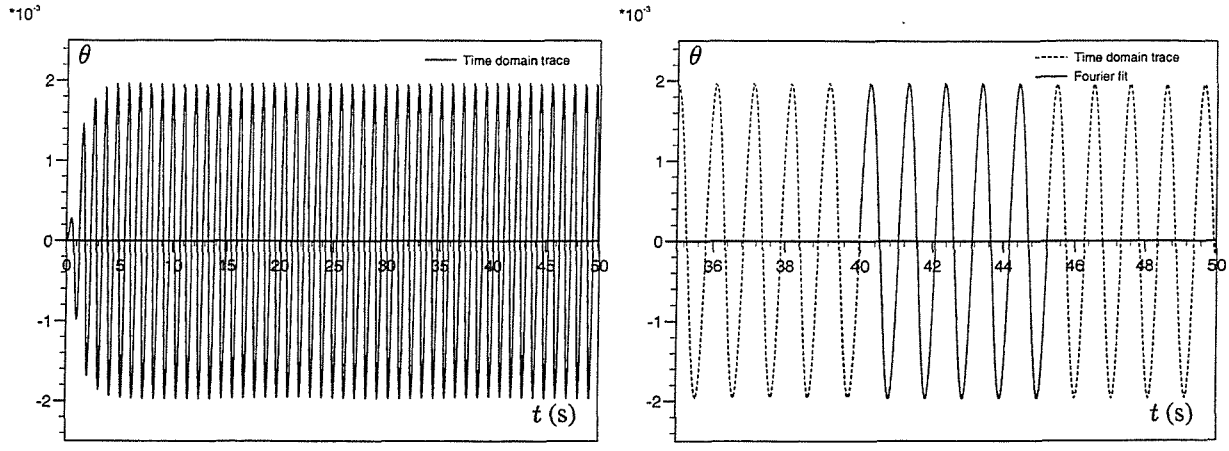

(b) Wave encounter frequency, ω_e = 6 rad/s, ω_e' = 3.34 rad/s

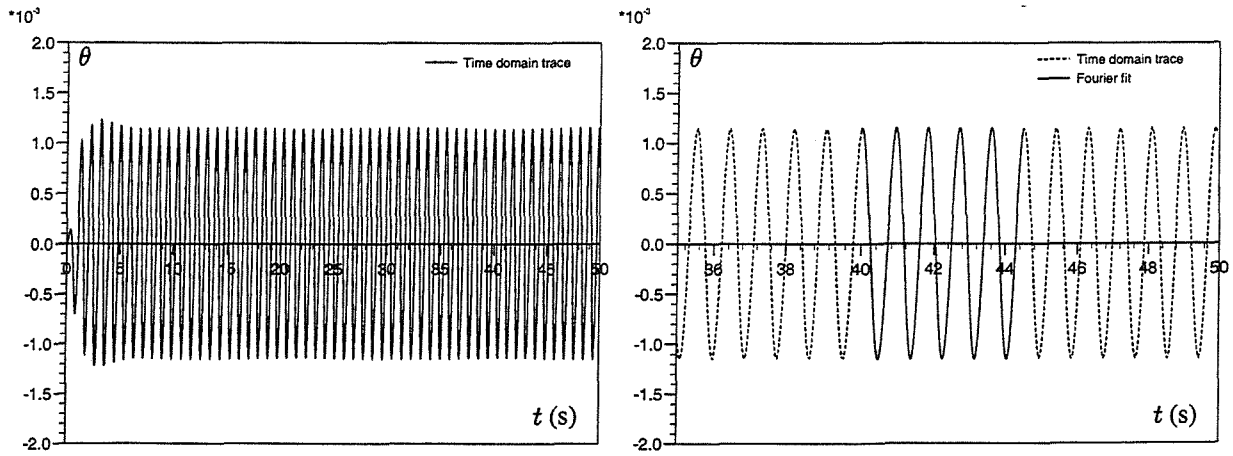

(c) Wave encounter frequency, ω_e = 7 rad/s, ω_e' = 3.90 rad/s

Figure 9.4: Pitch traces for simulated motions of a *Series 60* model in head waves using body fixed axis data, complete trace on left and trace in region of Fourier fit on right. L=3.048m, Fn=0.2 , α=0.01m, time step = 0.05s.

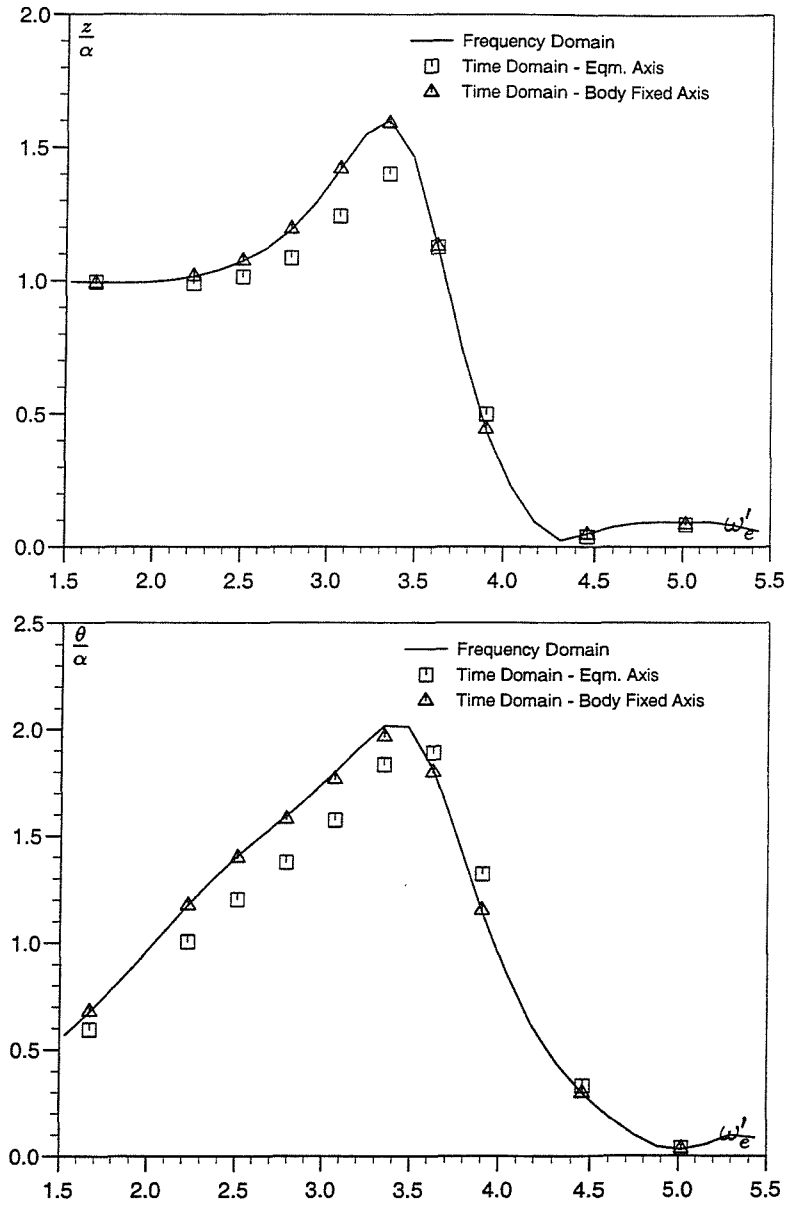

Figure 9.5: Heave and pitch response amplitude operators for Series 60 mono-hull in head waves, L=3.048m, Fn=0.2, $\chi = 180°$.

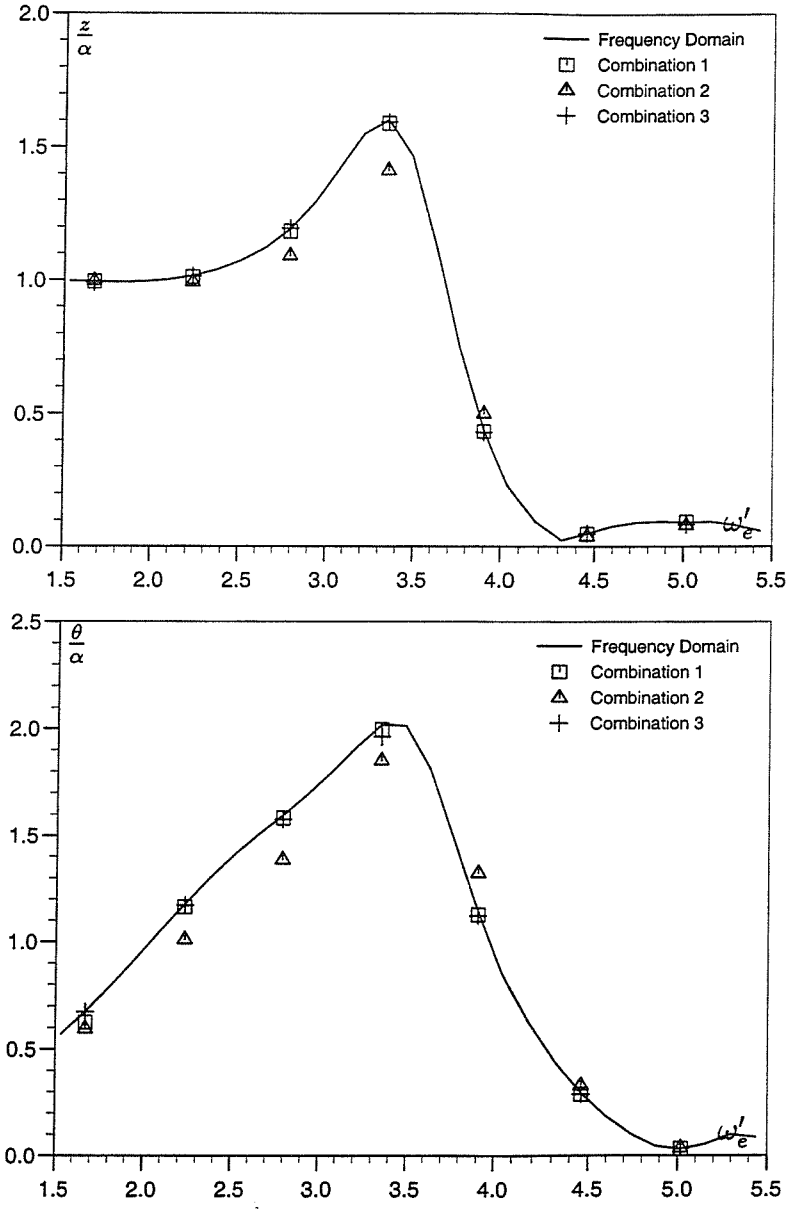

Figure 9.6: Heave and pitch response amplitude operators for Series 60 mono-hull in head waves, calculated using different combinations of data, L=3.048m, Fn=0.2, $\chi = 180°$.

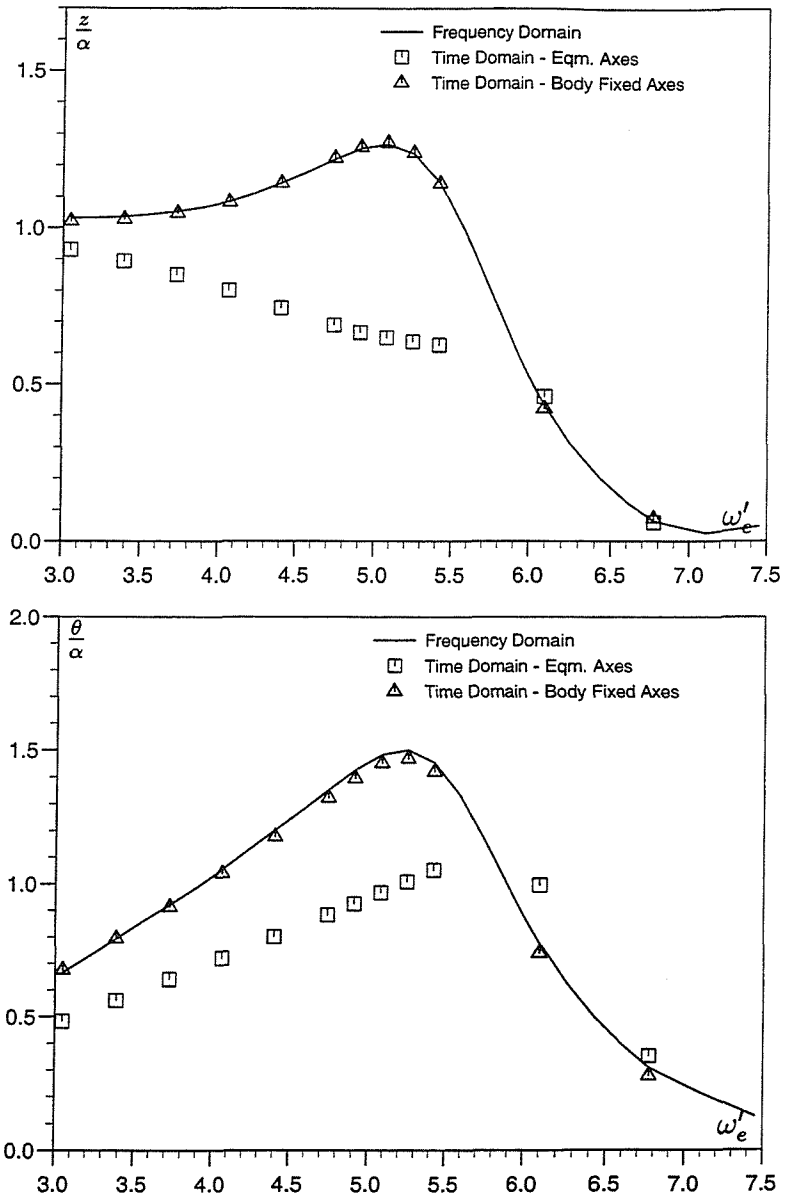

Figure 9.7: Heave and pitch response amplitude operators for *NPL5b* monohull in head waves, using pulsating source data, L=4.5m, Fn=0.53, $\chi = 180°$.

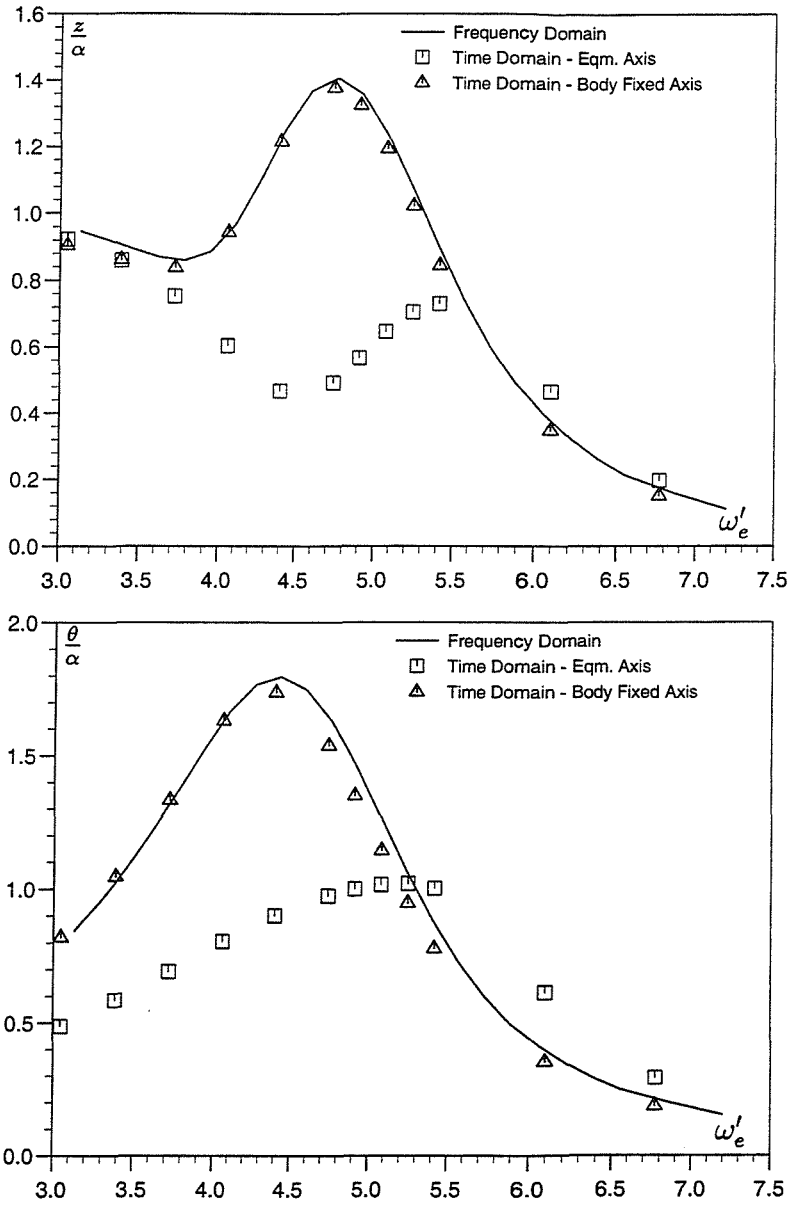

Figure 9.8: Heave and pitch response amplitude operators for *NPL5b* monohull in head waves, using translating, pulsating source data, L=4.5m, Fn=0.53, $\chi = 180°$.

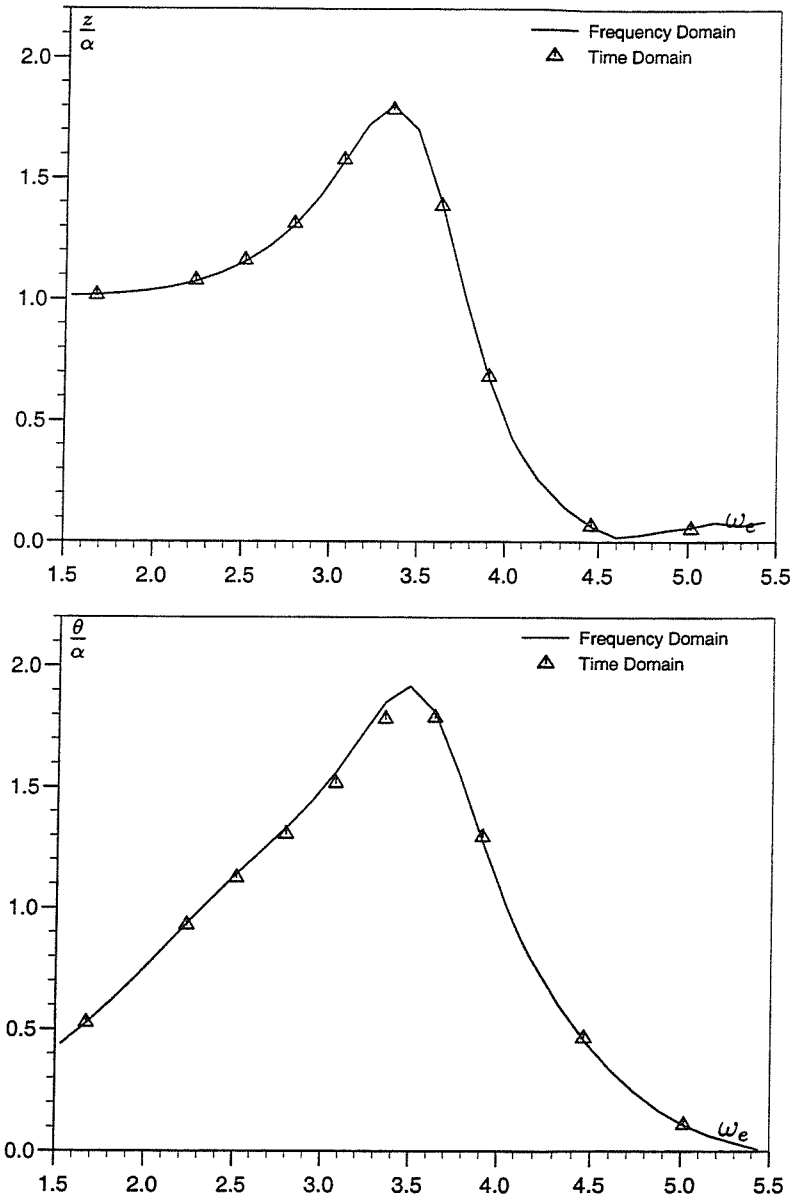

Figure 9.9: Heave and pitch response amplitude operators for Series 60 mono-hull in oblique waves, L=3.048m, Fn=0.2, $\chi = 135°$.

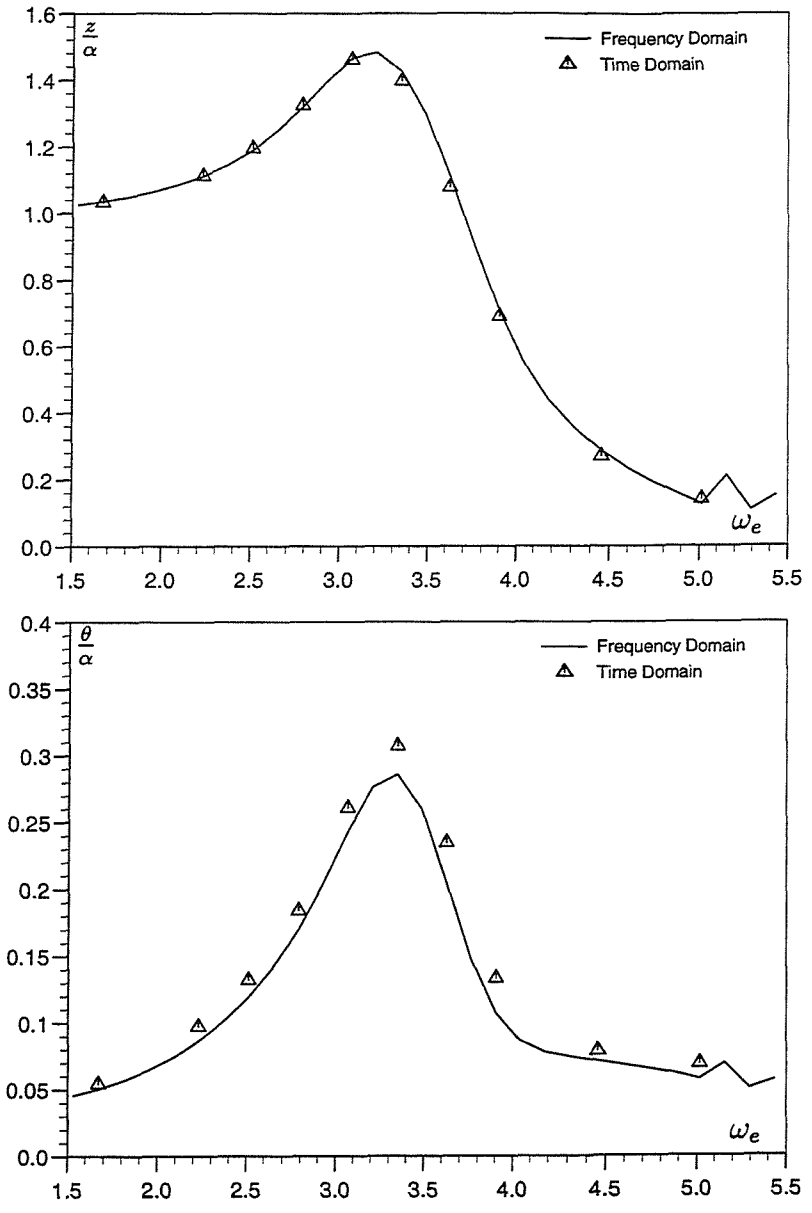

Figure 9.10: Heave and pitch response amplitude operators for Series 60 mono-hull in oblique waves, L=3.048m, Fn=0.2, $\chi = 90°$.

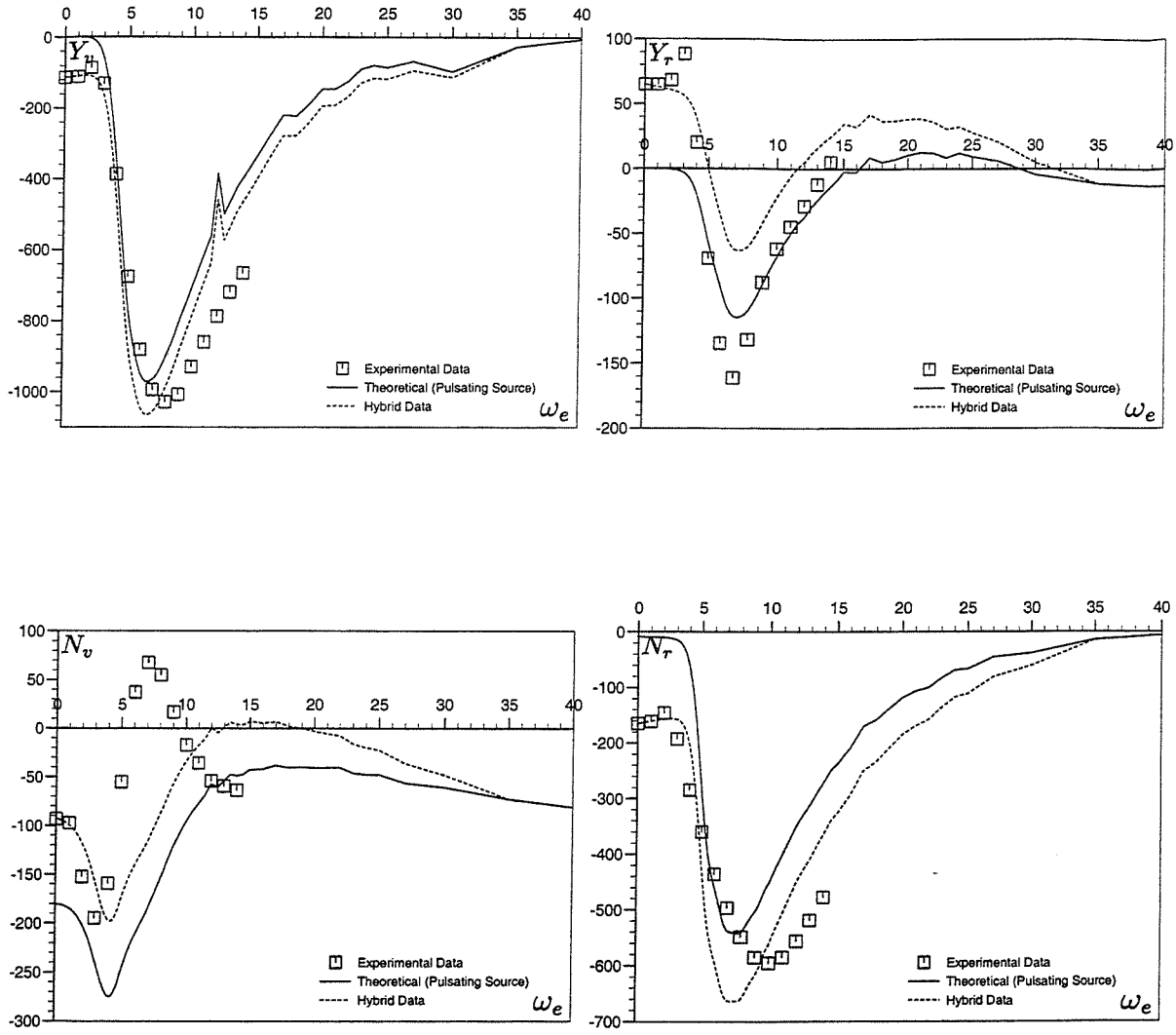

Figure 9.11: Sway and yaw velocity derivatives found using experimental and theoretical methods. Series 60 mono-hull, L=3.048m, Fn=0.2.

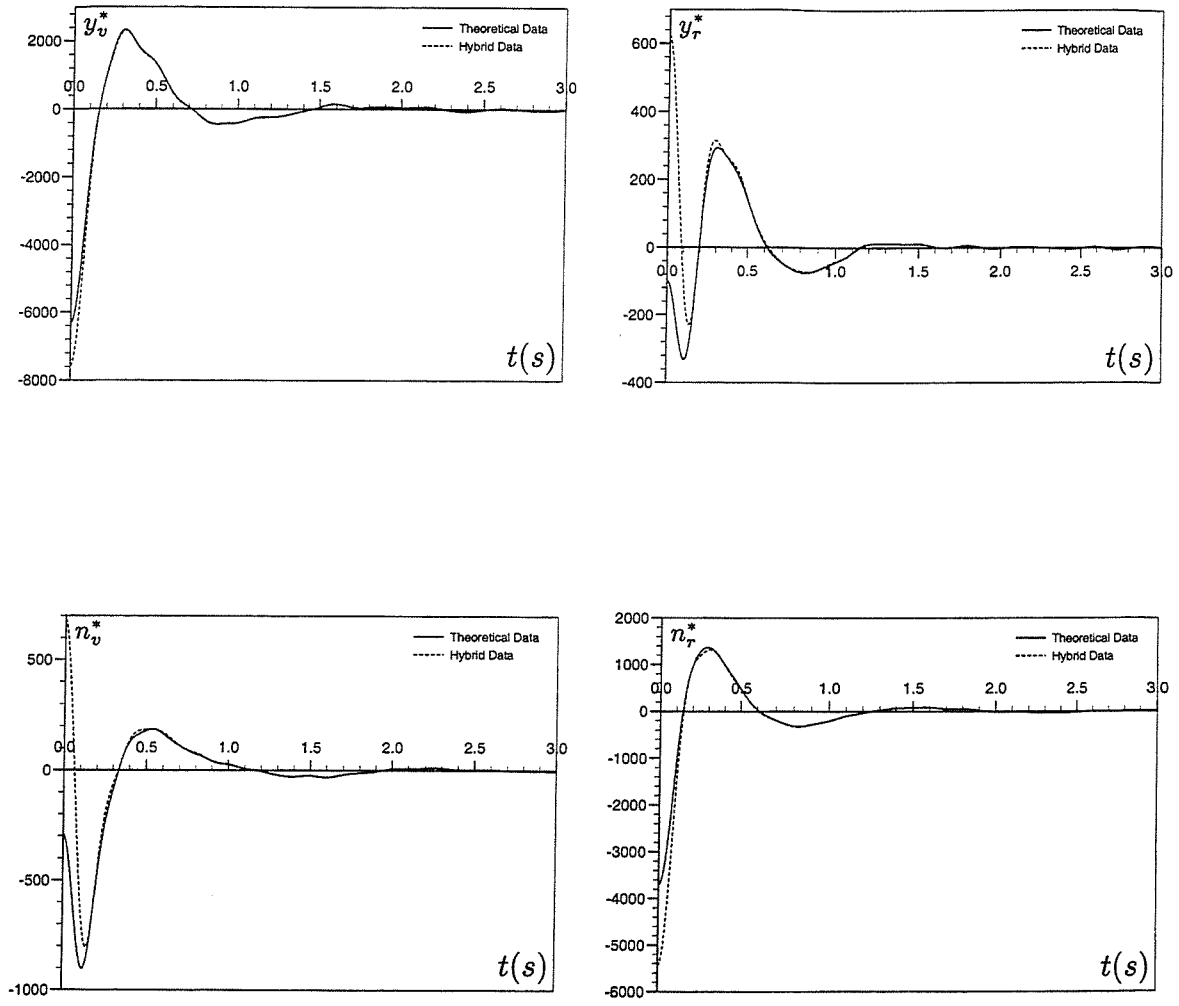

Figure 9.12: Sway and yaw radiation impulse response functions found using theoretical and hybrid methods. Series 60 mono-hull, L=3.048m, Fn=0.2.

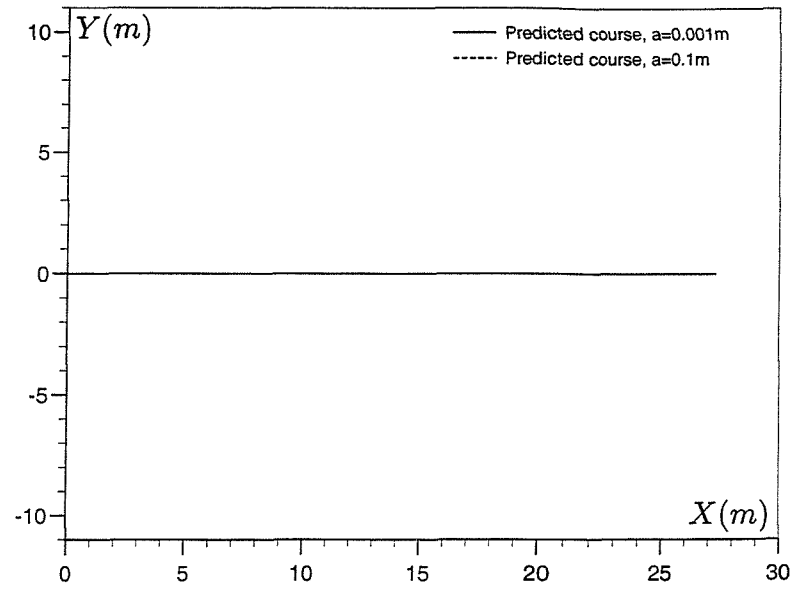

(a) With viscous contributions

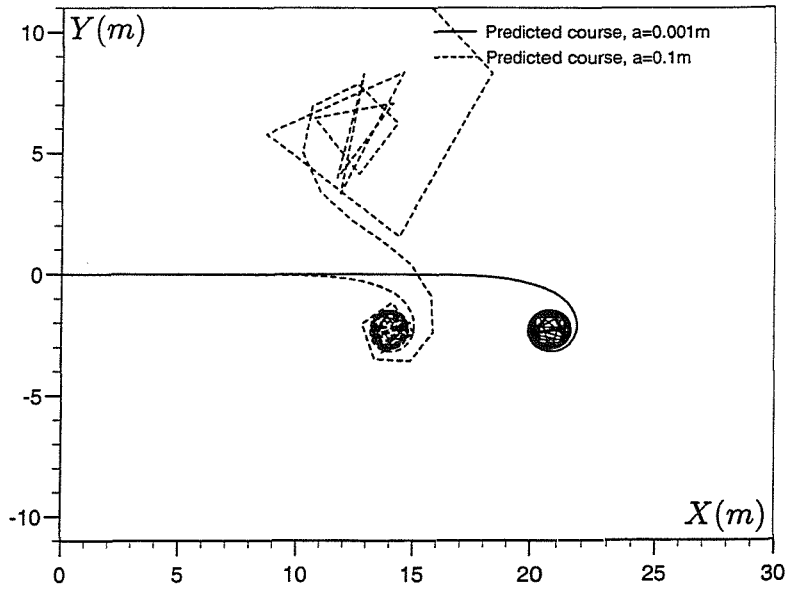

(b) Without viscous contributions

Figure 9.13: Predicted course of *Series 60* models, using data with (a) and without (b) viscous contributions, ω_e = 2 rad/s, L=3.048m, Fn=0.2, initial χ = 180°. Waves travelling in negative x-direction.

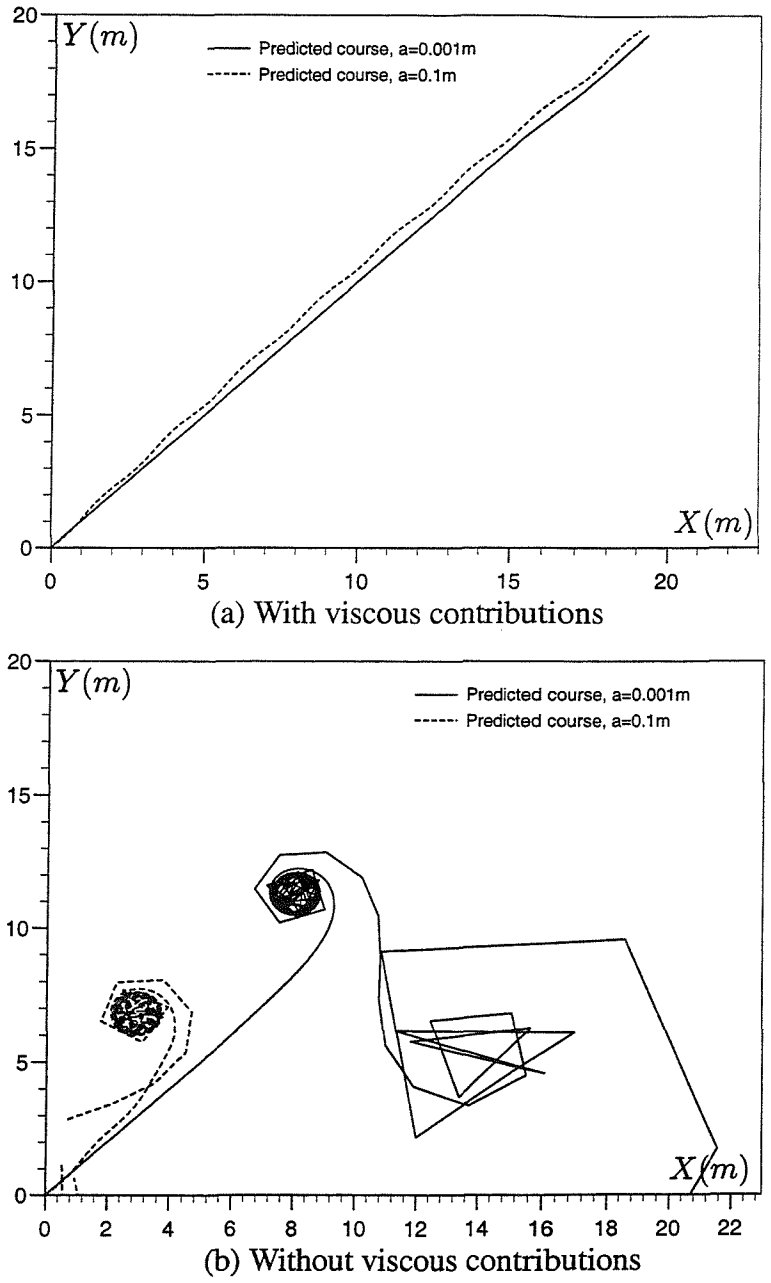

Figure 9.14: Predicted course of *Series 60* models, using data with (a) and without (b) viscous contributions, ω_e = 2 rad/s, L=3.048m, Fn=0.2, initial χ = 135°. Waves travelling in negative x-direction.

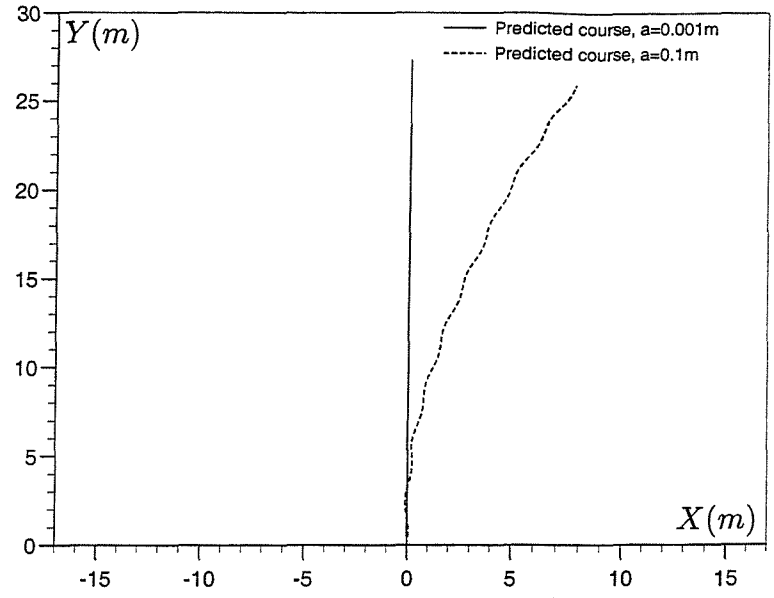

(a) With viscous contributions

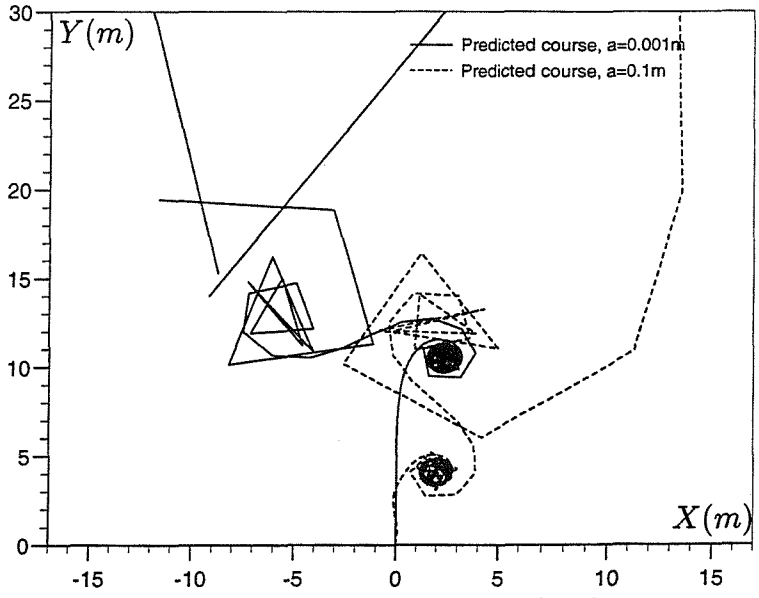

(b) Without viscous contributions

Figure 9.15: Predicted course of *Series 60* models, using data with (a) and without (b) viscous contributions, ω_e = 2 rad/s, L=3.048m, Fn=0.2, initial $\chi = 90°$. Waves travelling in negative x-direction.

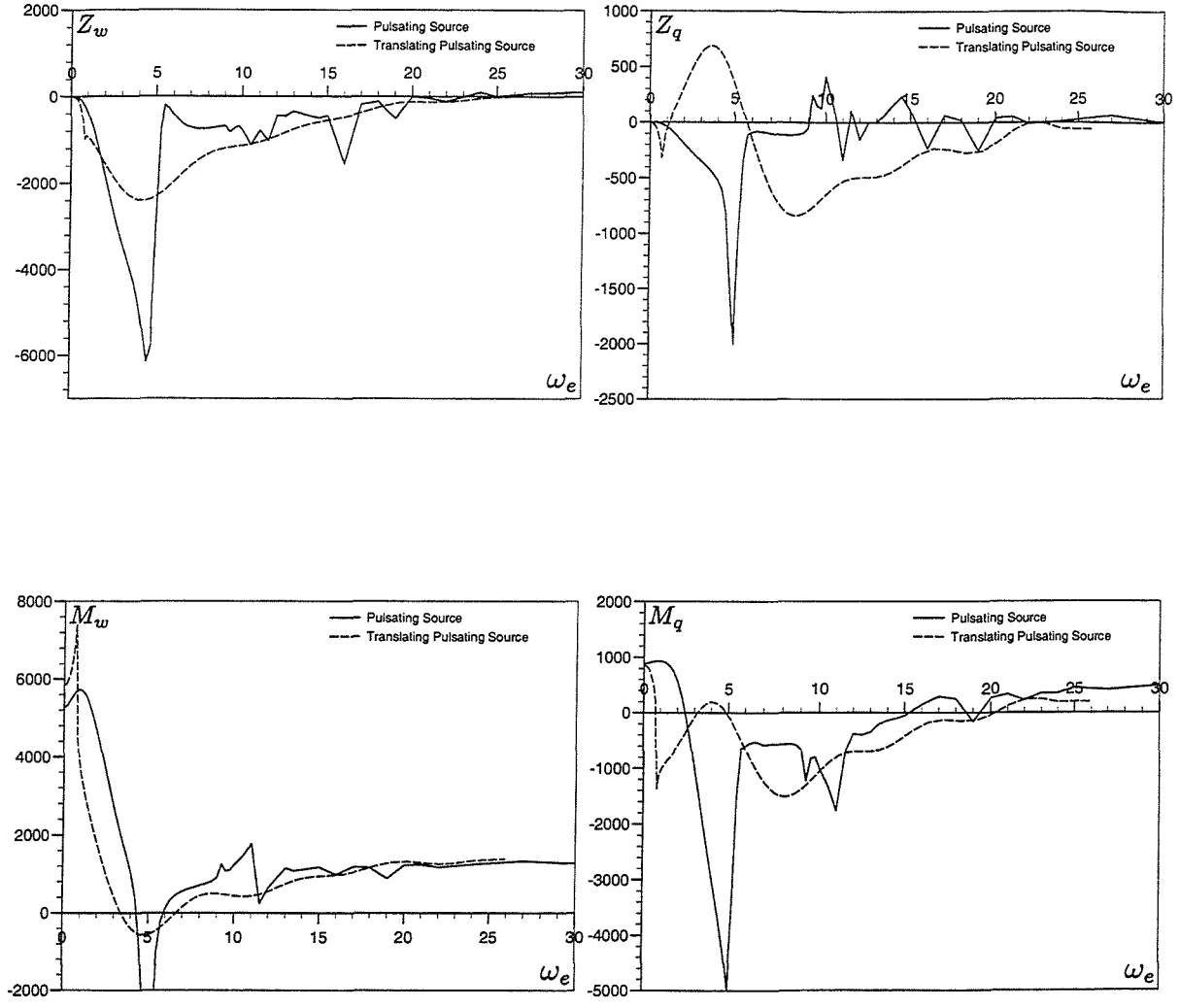

Figure 9.16: Frequency domain velocity derivatives calculated using pulsating and translating, pulsating source methods. *NPL5b* catamaran, S/L=0.2, L=4.5m, Fn=0.53.

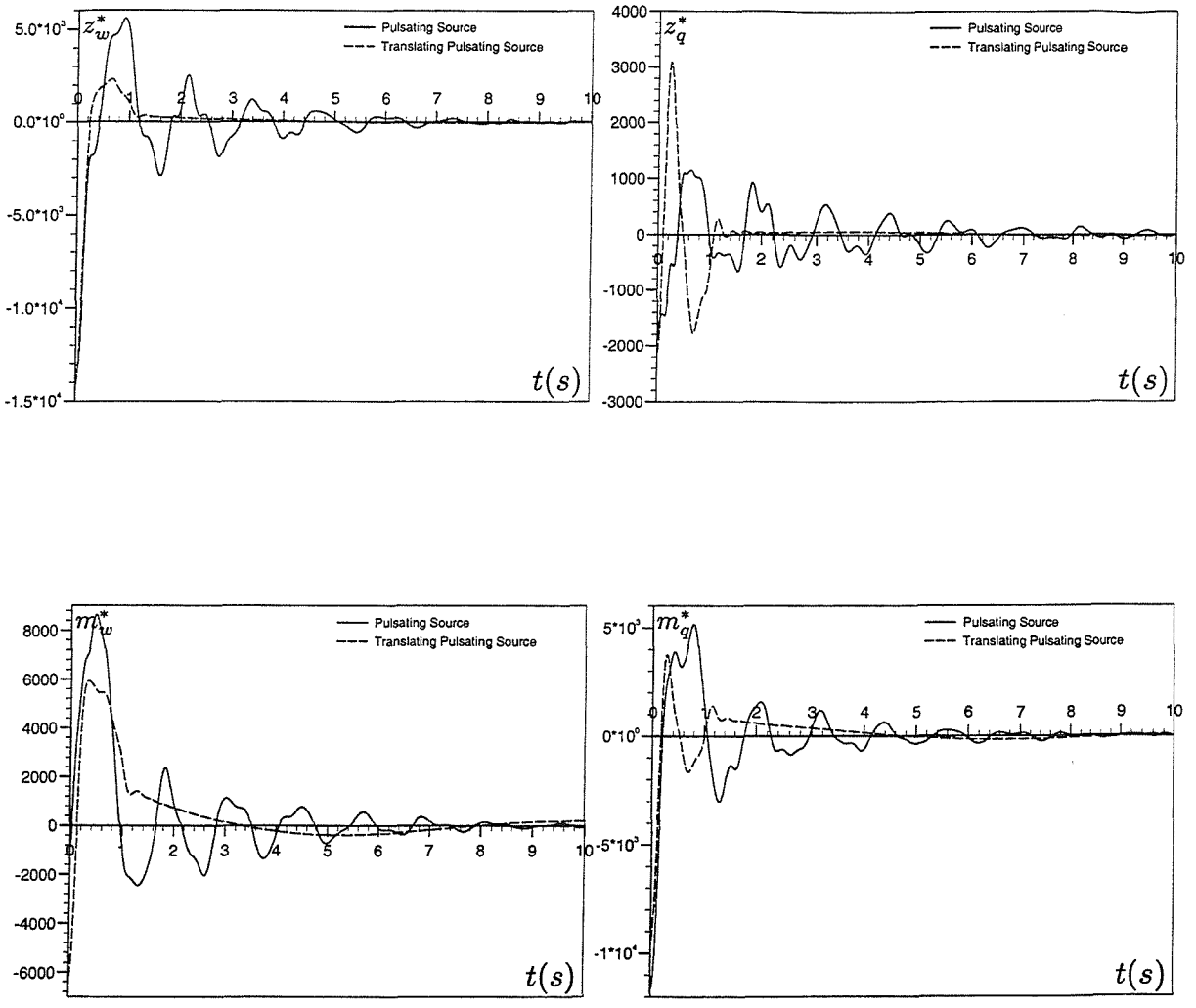

Figure 9.17: Radiation impulse response functions calculated from frequency domain velocity derivatives. *NPL5b* catamaran, S/L=0.2, L=4.5m, Fn=0.53.

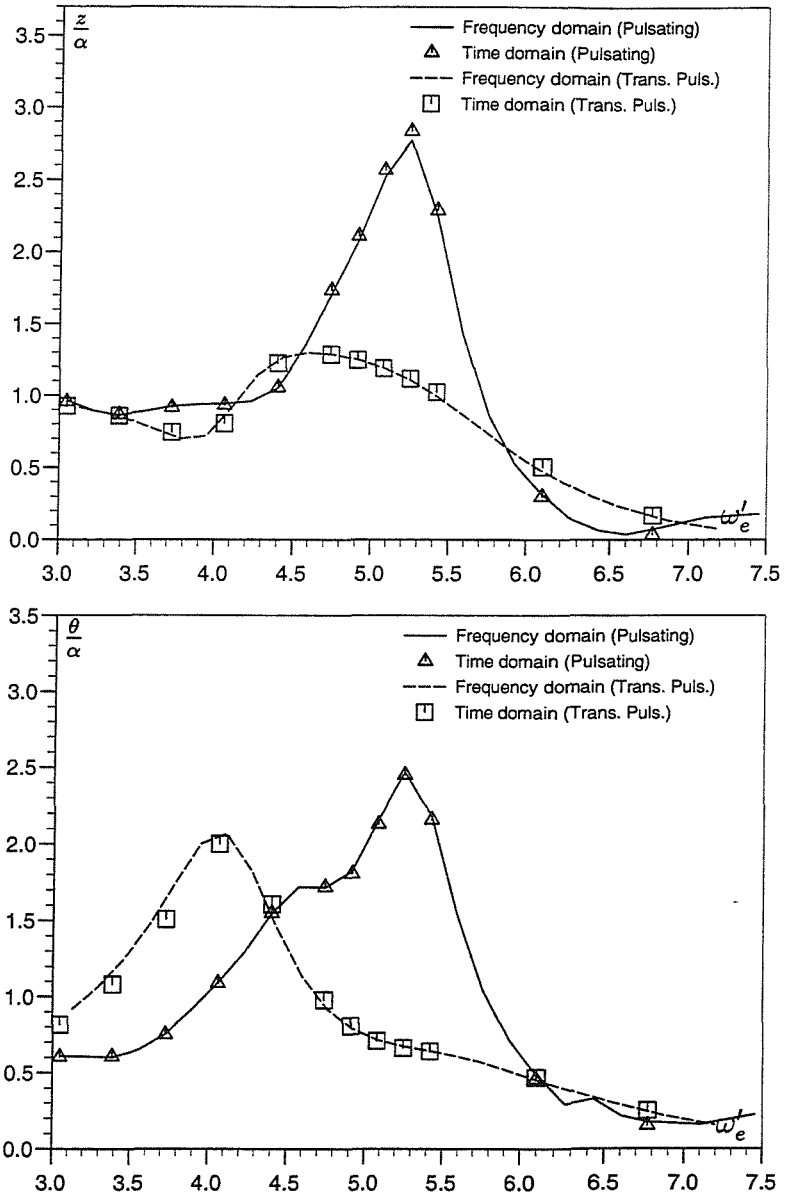

Figure 9.18: Heave and pitch response amplitude operators for *NPL5b* catamaran in head waves, using pulsating source data, L=4.5m, S/L = 0.2, Fn = 0.53, $\chi = 180°$.

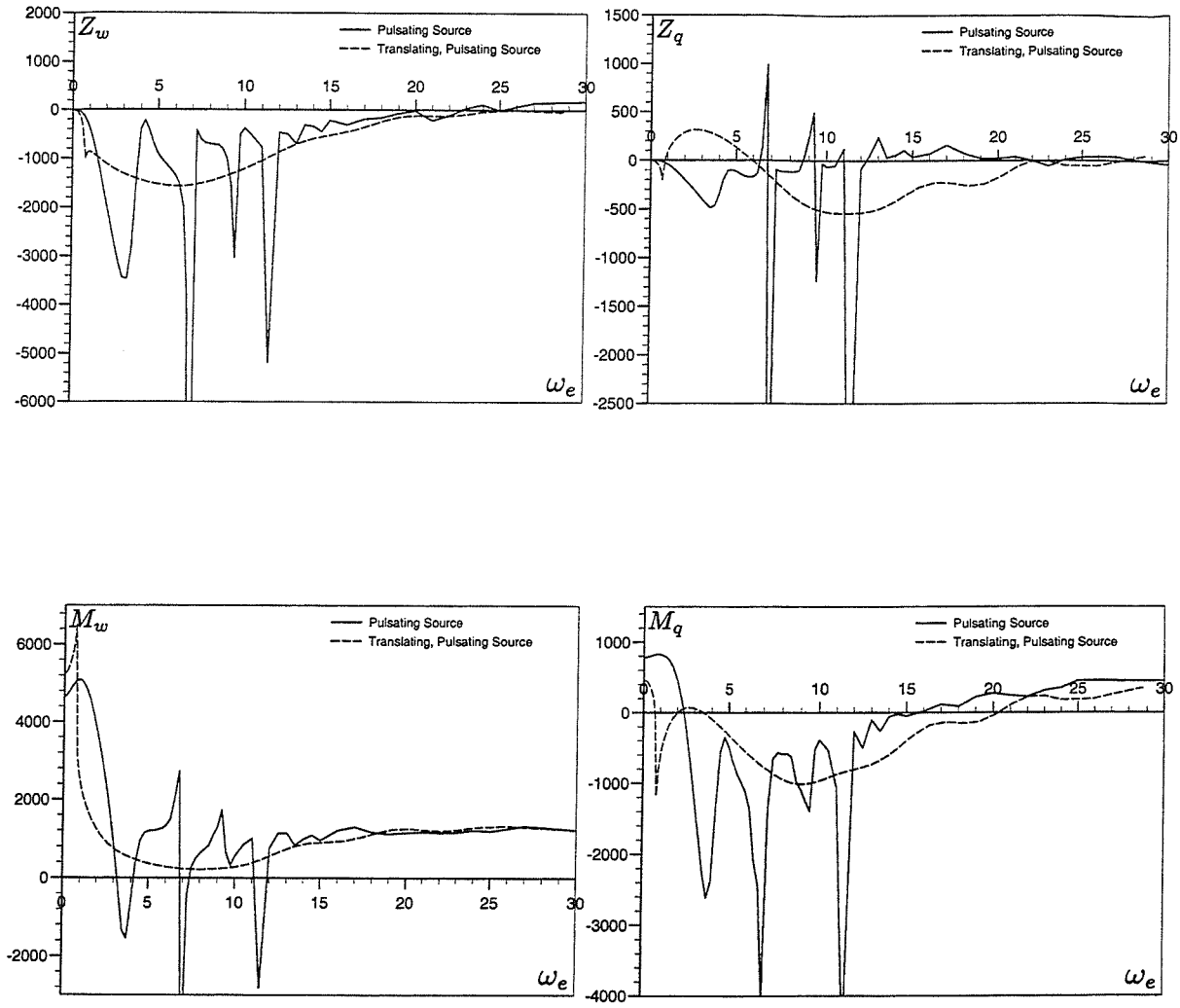

Figure 9.19: Frequency domain velocity derivatives calculated using pulsating and translating, pulsating source methods. *NPL5b* catamaran, S/L=0.4, L=4.5m, Fn=0.53.

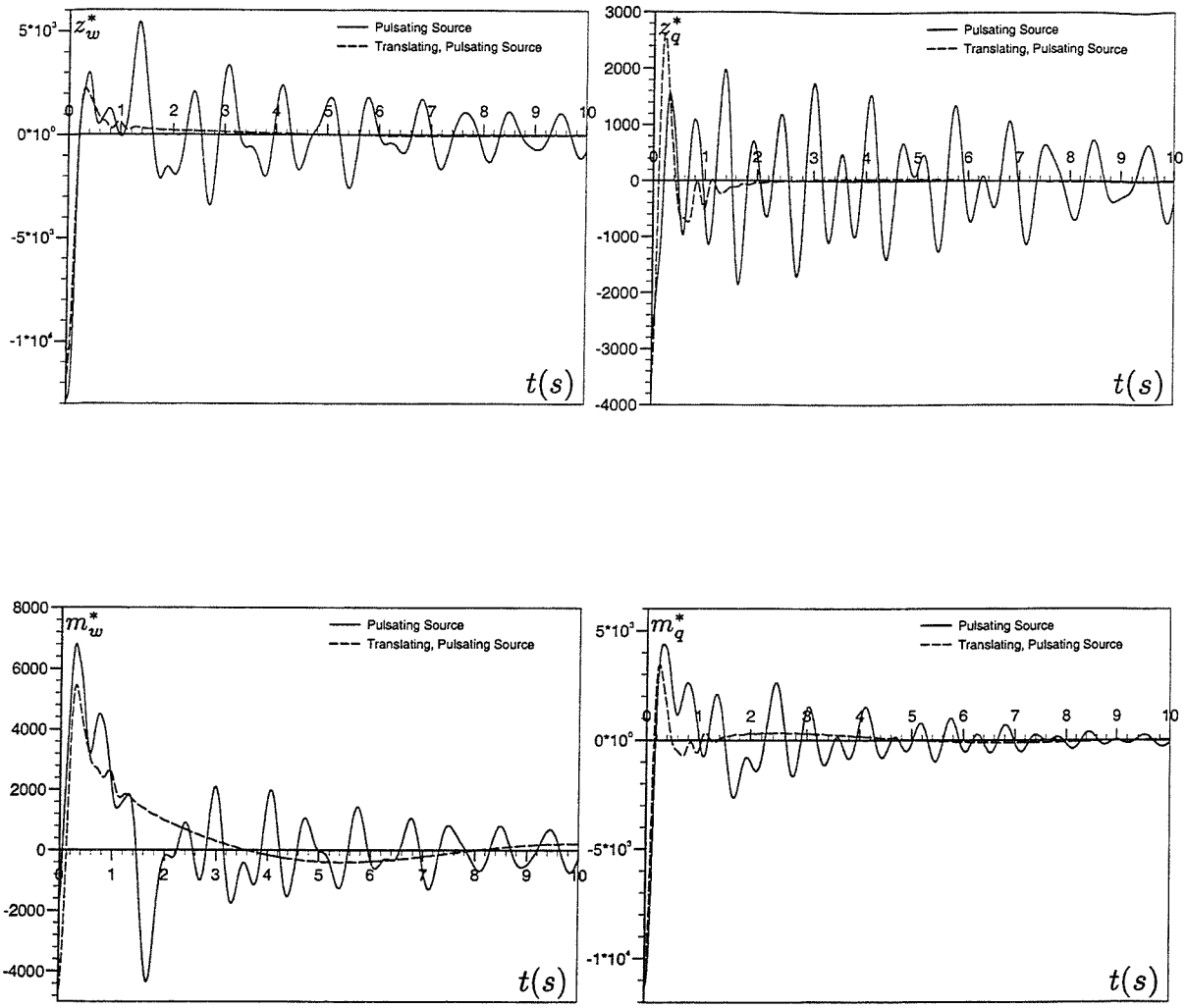

Figure 9.20: Radiation impulse response functions calculated from frequency domain velocity derivatives. *NPL5b* catamaran, S/L=0.4, L=4.5m, Fn=0.53.

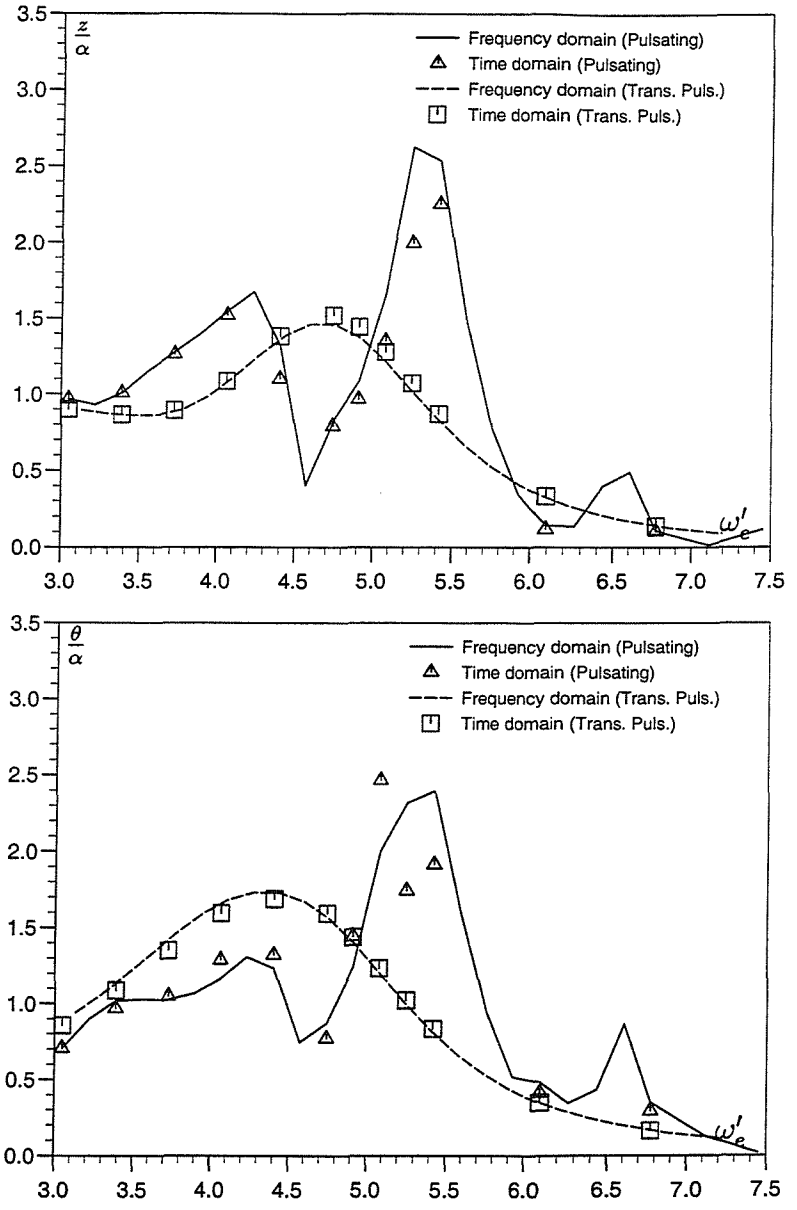

Figure 9.21: Heave and pitch response amplitude operators for *NPL5b* catamaran in head waves, using pulsating source data, L=4.5m, S/L = 0.4, Fn = 0.53, $\chi = 180°$.

10 Partly Non-Linear Time Domain Simulation

The time domain method adopted for the simulation of ship motions provides the opportunity to incorporate non-linear effects into an otherwise linear formulation through the excitation terms. Experimental measurements indicate differences between transfer functions obtained using varying wave amplitudes [67, 79], most likely due to non-linear effects. Given that the realistic motions of ships in waves of even modest amplitude show non-linear effects, it is important to assess the influence of certain non-linear contributions on predicted motions.

It is believed by many researchers in the seakeeping field that the observed differences between theoretical motion predictions and experimental results can be attributed, to some extent, to the nature of the excitation [13, 34, 42, 57, 56]. This is particularly the case for ships where there are rapid changes in the shape of the hull above the mean waterline, such as bow flare and overhanging sterns. It is believed that accounting for non-linearities associated with the incident wave and hydrostatic restoring contributions can be thought of as a first step towards a fully non-linear method [33].

The inclusion of such non-linear effects, in an otherwise linear method, gives the opportunity to assess the significance of these contributions for ships and operational conditions where the instantaneous underwater surface of the ship differs from the mean wetted surface used in linear theories. Cases where such contributions are likely to be of importance include ships with large flare, large wave amplitudes, coupling between roll and heave/pitch in oblique waves, etc. Figure 10.1 illustrates how the mean wetted surface differs from the

actual wetted surface of the hull when the vessel is undergoing vertical motions in waves of moderate amplitude. This gives an idea of how large amplitude motions are likely to result in considerable changes in the underwater portion of the hull over time. Any method which attempts to determine motions of all but the smallest amplitude, cannot ignore such changes.

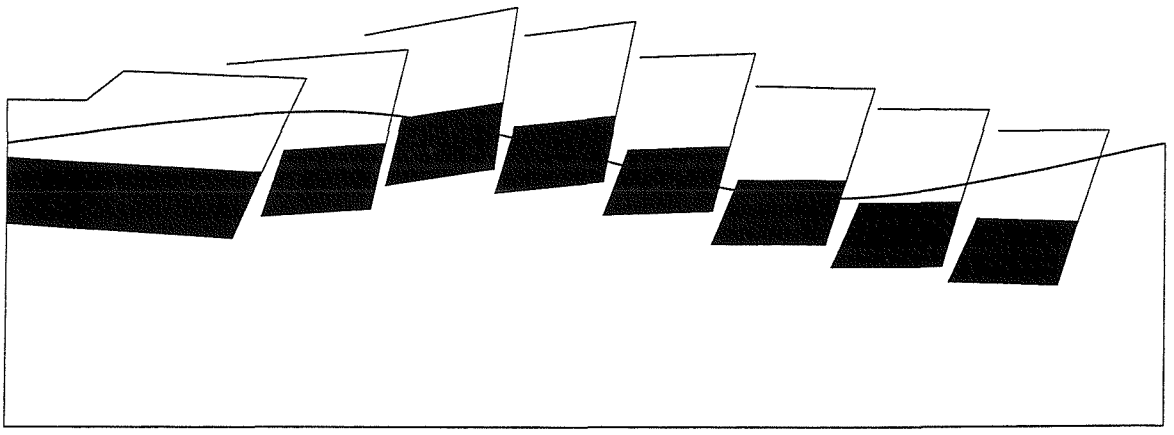

Figure 10.1: Simplified example of the discrepancies between the mean wetted surface and the actual wetted surface for the bow of a vessel in moderately large waves.

Other researchers have attempted to incorporate effects due to the changing underwater hull shape in otherwise linear methods. Lin et al. [63] presented results from the Large Amplitude Motions Program LAMP-2, which used a partly non-linear method to determine ship motions. In this method the radiation and diffraction contributions were calculated using a time domain Green's Function method whilst the incident wave and restoring forces/moments were calculated using the instantaneous underwater portion of the hull. The instantaneous underwater surface was repanelled at each time step. It was said that this partly non-linear method offered a far more computationally acceptable method for the solution of large amplitude motions than a fully non-linear method.

Fonseca and Guedes Soares [34] developed a partly non-linear method whereby the frequency domain radiation actions were calculated using a strip theory method. The Froude-Krylov and restoring forces/moments were calculated using a strip method over the in-

stantaneous wetted surface. Because of the use of frequency domain radiation actions this method was applicable for regular sinusoidal waves only.

Bailey et al. [4] assessed the manoeuvring and seakeeping characteristics of vessels in waves using a partly non-linear time domain technique. In this method, radiation contributions were described using impulse response functions, while the wave excitation and restoring contributions were evaluated by accounting for the instantaneous underwater portion of the hull. The wave excitation accounted for incident wave forces only, diffraction contributions being ignored. The neglecting of diffraction effects meant that the comparison of the predicted seakeeping motions in regular waves was limited to frequency domain data which also ignored diffraction contributions.

The partly non-linear time domain simulation technique developed in this study is identical to the linear version in most respects. The difference lies in the calculation of the wave excitation and restoring contributions. The diffraction contributions continue to be calculated using convolution integrals which employ impulse response functions. These impulse response functions are calculated using frequency domain diffraction data. The Froude-Krylov and restoring forces/moments are now calculated using a method which accounts for the changing underwater surface of the hull with time. By accounting for non-linear incident wave and restoring actions, an approximation may be made of non-linear ship motions which is far less computationally expensive than a fully non-linear method. It is believed that this reduction in the time taken to simulate particular scenarios makes this method more suitable for practical application than a fully non-linear method.

10.1 Equations of Motion for Partly Non-Linear Method

As noted earlier, the basis of the partly non-linear method is very similar to the linear time domain simulation method developed previously. Convolution integrals are used to describe the radiation actions, the required impulse response functions having been determined from frequency domain methods in an identical manner to the linear method.

The difference between the two methods lies in the calculation of the wave excitation and restoring forces. Whereas the linear method used convolution integrals to describe the total wave excitation contribution and constant coefficients for the determination of the restoring actions, the partly non-linear method uses convolution integrals to describe only the diffraction component of the wave excitation. The wave excitation due to the incident wave (Froude-Krylov forces) and the restoring forces due to the displacement of the vessel are calculated using the methods described in Section 10.2.

Hence the wave excitation and restoring contributions in Equation 8.8 may be rewritten as,

$$\begin{aligned} X_{\alpha r} &= X_{I\alpha r} + X_{D\alpha} & K_{\alpha r} &= K_{I\alpha r} + K_{D\alpha} \\ Y_{\alpha r} &= Y_{I\alpha r} + Y_{D\alpha} & M_{\alpha r} &= M_{I\alpha r} + M_{D\alpha} \\ Z_{\alpha r} &= Z_{I\alpha r} + Z_{D\alpha} & N_{\alpha r} &= N_{I\alpha r} + N_{D\alpha}. \end{aligned}$$

where the subscript $I\alpha r$ refers to the instantaneous Froude-Krylov and restoring forces/moments and the subscript $D\alpha$ refers the diffraction contributions. These diffraction contributions are defined in terms of convolution integrals in the following way

$$\begin{aligned} X_{D\alpha} &= \int_{-T}^{t} x_{D\alpha}(\tau)\alpha(t-\tau)d\tau & K_{D\alpha} &= \int_{-T}^{t} k_{D\alpha}(\tau)\alpha(t-\tau)d\tau \\ Y_{D\alpha} &= \int_{-T}^{t} y_{D\alpha}(\tau)\alpha(t-\tau)d\tau & M_{D\alpha} &= \int_{-T}^{t} m_{D\alpha}(\tau)\alpha(t-\tau)d\tau \\ Z_{D\alpha} &= \int_{-T}^{t} z_{D\alpha}(\tau)\alpha(t-\tau)d\tau & N_{D\alpha} &= \int_{-T}^{t} n_{D\alpha}(\tau)\alpha(t-\tau)d\tau. \end{aligned}$$

with the diffraction impulse response functions $x_{D\alpha}, y_{D\alpha}, \ldots$ being calculated from the real and imaginary parts of the frequency domain diffraction data using Equation 5.24.

10.2 Calculation of Non-Linear Incident Wave and Restoring Contributions

The calculation of non-linear incident wave and restoring forces requires a means by which the instantaneous underwater surface of the hull may be described. Such a description of the underwater surface will allow the forces acting on the hull due to the water pressure

to be determined. Practically, this involves discretising this underwater surface, so that the total forces/moments may be regarded as the sum of the contributions of the individual elements.

The methods described in Chapter 4 for the discretisation of the mean wetted surface provide an ideal basis for the calculation of the instantaneous underwater portion of the hull. Instead of only panelling the mean wetted surface, it is a basic step to simply continue this panelling process right up to the deck line or other appropriate height. The processes involved in the panelling are identical and, in a similar manner to the mean wetted surface case, the Fixed Method of panelling will be used. This means that the required number of panels per section will be chosen, along with an ideal aspect ratio for the panels.

The panels describing the entire surface of the hull are initially defined with reference to a body fixed axis system with its origin on the keel at midships. The process of determining the instantaneous underwater portion of the hull at each time step begins with the placing of the panelled hull in its perturbed position, based on the calculated displacements from the previous time step. The panels that define the hull are placed in this position by first rotating them about the centre of mass and then translating them by the required amount.

Having placed the panelled representation of the entire hull surface in its perturbed position, the next step is to determine the underwater portion of the hull at this instant. This is done by examining the relationship of each of the panels in turn with the instantaneous free surface elevation. Each of the four corners of the particular panel are examined. If all four panel corners are above the free surface, this indicates that the panel is clear of the water and is hence disregarded. Similarly, if all four panels are found to be below the free surface, then this panel is retained, as it is clearly part of the instantaneous underwater surface.

Provided the panels were small enough, it would theoretically be possible to limit the process to simply defining whether panels were above or below the water and ignore those panels that were not completely submerged. However, this is likely to result in step changes in the forces calculated for successive time steps [7]. To avoid having to use a very large

number of panels, special measures are taken for panels which cross the instantaneous free surface. Panels either have certain corners moved in order to form smaller panels, or are replaced by two new panels using some identical corner points [7].

Figure 10.2 shows a visualisation of the instantaneous underwater hull determined at a particular instant for an *NPL5b* catamaran. In this figure the amplitude of the wave is beyond the scope of this investigation, having been used for clarity. In this figure the light coloured panels are the ones that are above the waterline and have been excluded from the calculation of the instantaneous Froude-Krylov and restoring forces. The dark panels are those which are under the instantaneous free surface. Figure 10.3 gives a close up view of the region around the free surface. The outlines of the original panels crossed by the waterline are still clear, but it can be seen how using at least one of the original corners the new underwater panels (dark colour) have been formed by shifting the corners that were above the instantaneous waterline so that they lie on it.

Having created a quadrilateral panel description of the instantaneous underwater portion of the hull, the centre of each panel is determined by averaging the coordinates of the panel corners. The pressure P acting on each panel is assumed uniform and equal to the pressure acting on the center of the panel. The contribution of the pressure on each panel to the overall forces and moments is found using the normal of each panel. Consider, for example, a panel of area A_n, unit normal $n_n = (n_{Xn}, n_{Yn}, n_{Zn})$ and with the coordinates of the centre being $r_n = (X_n, Y_n, Z_n)$ in the earth fixed system. The total force and moment are found by summing the contributions for the N panels which define the underwater surface, as follows,

$$
\begin{aligned}
X_{I\alpha r} &= \sum_{n=1}^{N} A_n P(X_n, Y_n, Z_n) n_{Xn} + (-mg \sin\theta) \\
Y_{I\alpha r} &= \sum_{n=1}^{N} A_n P(X_n, Y_n, Z_n) n_{Yn} + (-mg \cos\theta \sin\phi) \\
Z_{I\alpha r} &= \sum_{n=1}^{N} A_n P(X_n, Y_n, Z_n) n_{Zn} + (-mg \cos\theta \cos\phi) \\
K_{I\alpha r} &= \sum_{n=1}^{N} Y_n A_n P(X_n, Y_n, Z_n) n_{Zn} - \sum_{n=1}^{N} Z_n A_n P(X_n, Y_n, Z_n) n_{Yn}
\end{aligned}
$$

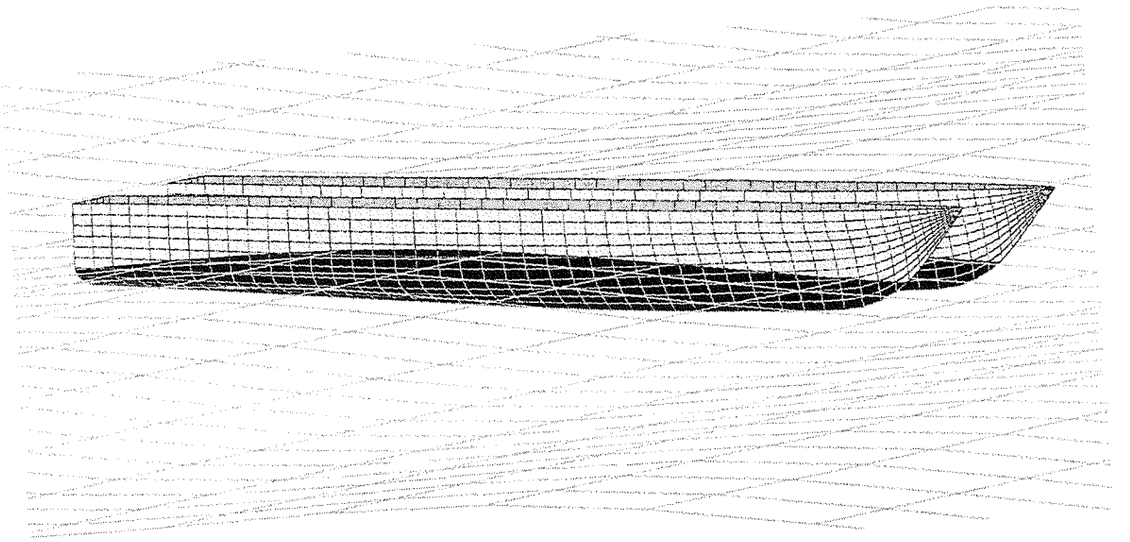

Figure 10.2: Portions of the mesh above and below the instantaneous waterline on an NPL5b catamaran, L = 4.5m, λ = 6.9312m, wave amplitude = 0.1m.

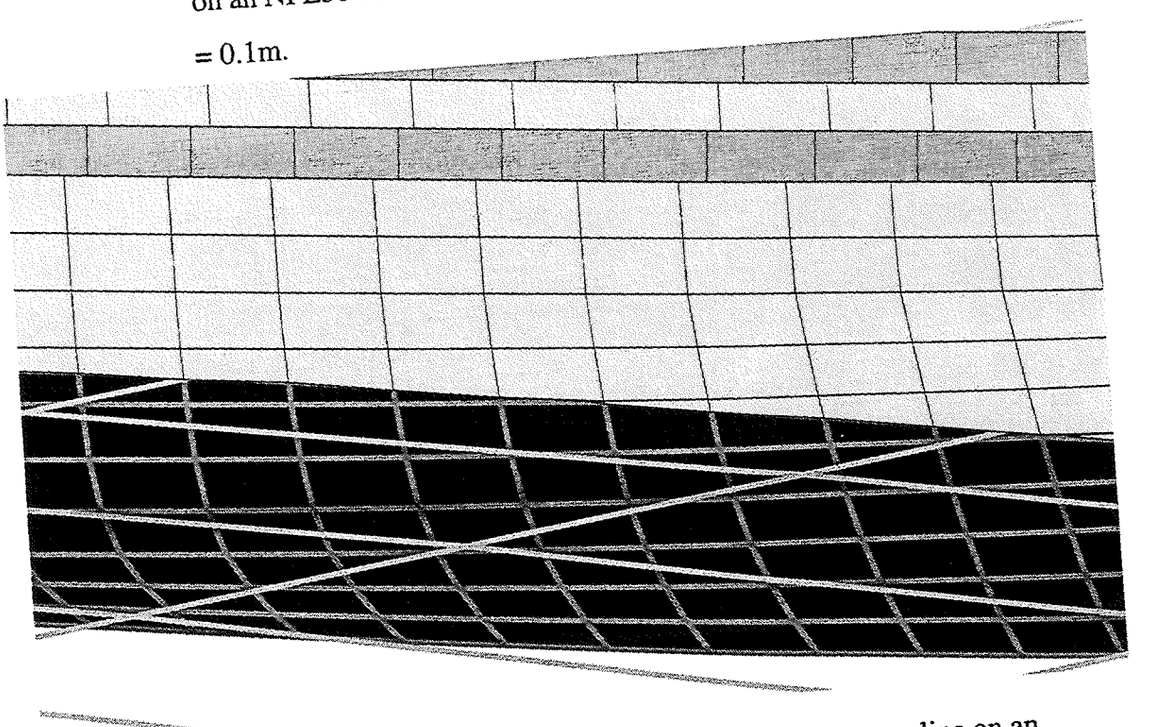

Figure 10.3: Close-up view of panels around the instantaneous waterline on an NPL5b catamaran. Panels above the waterline are light coloured, panels below the waterline are dark.

$$M_{I\alpha r} = -\sum_{n=1}^{N} X_n A_n P(X_n, Y_n, Z_n) n_{Zn} + \sum_{n=1}^{N} Z_n A_n P(X_n, Y_n, Z_n) n_{Xn}$$

$$N_{I\alpha r} = \sum_{n=1}^{N} X_n A_n P(X_n, Y_n, Z_n) n_{Yn} - \sum_{n=1}^{N} Y_n A_n P(X_n, Y_n, Z_n) n_{Xn},$$

where the $I\alpha r$ subscript refers to the instantaneous part of the excitation contribution which includes the non-linear Froude-Krylov and restoring contributions. The pressure P is calculated using the sum of the hydrostatic and undisturbed incident wave pressures. The hydrostatic pressure is linearly related to the wave depth while the dynamic incident wave pressure is related to the wave amplitude, wave number and the depth. The combined pressure distribution may be calculated as follows [30],

$$\begin{cases} P(X_O, Y_O, Z_O) = 0 & Z_O > \alpha \\ P(X_O, Y_O, Z_O) = -\rho g Z_O + \rho g \alpha(X_O, Y_O) & 0 \leq Z_O \leq \alpha \\ P(X_O, Y_O, Z_O) = -\rho g Z_O + \rho g \alpha(X_O, Y_O) e^{kZ_O} & Z_O < 0 \end{cases}$$

where the location (X_O, Y_O, Z_O) at which the pressure is defined is referenced to space fixed axes as described in Chapter 3 and α is the wave amplitude.

It should be noted that using the pressure at the panel centre as the average for calculating the total pressure acting on each panel is not entirely correct. In reality the average pressure will be acting at a point somewhere between half and two-thirds of the way from the top to the bottom of the panel. However, provided that a sufficiently large number of panels is used the error due to this assumption is negligible.

Time domain simulations using this partly non-linear method commence with the ship being placed in its calm water equilibrium position using an iterative method developed by Bailey [7]. This is designed to ensure that the subsequent motions do not settle about a value too dissimilar from the starting value.

10.3 Series 60 Monohull

The linear motions of a *Series 60* monohull model were examined in Chapter 9. The *Series 60* hull form is particularly appropriate for analysis with a linear method due to the shape

of its hull. It is fairly wall-sided, meaning that for motions of moderate amplitude there are no major changes in the shape of the underwater portion of the hull. Given that one might reasonably expect the non-linear effects present in the motions of the *Series 60* to be relatively small, this makes it an ideal initial test case for a partly non-linear method.

In addition, there are a large number of experimental studies that have been carried out using the *Series 60* hull form including those of Gerritsma and Beukelman [38, 39], Van Leeuwen [95], Vossers [97] and Vugts [98]. This allows the comparison of linear and partly non-linear methods to experiments, giving an indication of any improvements in the accuracy of the motion predictions which might result from the inclusion of non-linear effects.

The mean wetted surface of the hull was idealised using the same panelled representation that was used for the linear time domain technique (see Figure B.2). The idealisation of the entire hull up to the deckline was created using the Fixed Method , with 15 panels per section and an aspect ratio of 2, giving a total of 1830 panels (see Figure B.3).

10.3.1 Symmetric Motions

As previously noted, given the wall sided shape of the hull form of the *Series 60*, one would expect it show relatively small non-linear effects for waves of moderate amplitude. To confirm the accuracy of the partly non-linear method, time domain simulations were initially performed for a range of encounter frequencies using a very small wave amplitude, a=0.001m. At such small amplitudes one might reasonably expect the responses to be linear.

Response amplitude operators for the frequencies at which the simulations were performed, for the hull travelling in regular head waves at $F_n = 0.2$, may be seen in Figure 10.4. It can be seen that the heave responses calculated for the very low wave amplitude show excellent agreement with frequency domain predictions. The agreement is less good for the pitch responses at the low amplitude, but nevertheless is still close to the frequency domain

predictions. The differences between the time domain and frequency domain predictions is thought to be a result of differences between the constant restoring coefficients used for the calculation of the frequency domain RAOs and the instantaneous restoring forces that are used in the partly non-linear method. The fact that the ship is allowed to settle to its equilibrium position before the time domain simulation begins means that it is difficult to quantify whether the value of the constant restoring coefficients are equivalent.

Traces of the heave and pitch motions around resonance are shown in Figures 10.5 and 10.6 for various wave amplitudes. Figure 10.5 shows heave trace at frequency close to resonance as well as the corresponding Fourier fits used to calculate the amplitude of the responses. The wave amplitude increases from the smallest (0.001m) to the largest (0.1m) case. Figure 10.6 gives similar results for the pitch motions. It can be seen that for the wall sided *Series 60* hull form the responses remain roughly sinusoidal even as the amplitude of the waves increases.

The predicted heave and pitch motions were also compared to experimental results. The results of a number of experimental studies were compared by Nakamura [70]. The spread of these results was quite large and hence Figure 10.4 show the upper and lower limits of the range of results presented.

It can be seen that the frequency domain results over predict the heave response compared with the experimental results. Increasing the wave amplitude results in little change in the responses predicted using the partly non-linear time domain method. Such results would be expected, considering the wall sided shape of the *Series 60* model.

Pitch responses predicted using the frequency domain method give somewhat better agreement with the experiments than was seen for heave. Increasing the wave amplitude to moderate (with respect to the draft of the model) levels has little effect on the predicted responses using the time domain simulation. However, when it is increased to 0.1m there is a considerable reduction in the predicted response. This is believed to be due to the submergence of the overhanging stern of the vessel.

10.3.2 Anti-Symmetric Motions

It was noted in Section 9.3.2 that viscous contributions play an important role in anti-symmetric ship motions. It was found that if a linear time domain simulation was performed using data that did not account for viscous effects the predicted course of the vessel was unrealistic. However, if viscous contributions were accounted for by the addition of a "viscous ramp", then time domain simulations of the vessel's course at a range of headings were more realistic.

A similar comparison has been performed using hydrodynamic data with and without viscous contributions using the partly non-linear time domain simulation method. Again, two wave amplitudes have been used and the predicted course of a *Series 60* vessel is compared when using both hybrid and potential flow hydrodynamic data. Unlike the simulations using the linear time domain method, those made using the partly non-linear method include motions in sway, heave, pitch and yaw. The vessel was free to move in these four degrees of freedom. The method for the calculation of the incident wave and restoring contributions means that there is now coupling between the symmetric motions of heave and pitch and the anti-symmetric motions of sway and yaw. The fact that roll motions have not been included is only a reflection of the fact that suitable data was not available to determine an appropriate viscous contribution. Nevertheless, had such data been available, the simulation of roll motions would have been possible. It should be noted that Bailey [7] found that the addition of roll motions to the simulation of a vessel's course in waves made little difference to the results obtained when excluding roll.

Figure 10.7 shows four courses predicted by the partly non-linear time domain simulation method. Part (a) shows the simulated courses for wave amplitudes 0.001m and 0.1m using hybrid hydrodynamic data sets. It can be seen that for both wave amplitudes the predicted course does not alter from the initial heading. However, the courses predicted using hydrodynamic data without viscous contributions, seen in part (b) of the figure, both predict the vessel deviating from its initial heading. In the case of the large wave amplitude the yaw velocity becomes so large that it causes the solution to become unstable.

Figure 10.8 shows similar results for an initial heading of 135 degrees. When using hybrid hydrodynamic data the predicted course for the smaller wave amplitude is a straight line. Increasing the wave amplitude causes the vessel to depart from its initial heading and drift in the direction the waves are travelling in. This compares to the essentially straight line course predicted by the linear method (see Figure 9.14). The courses predicted using the hydrodynamic data without viscous contributions once again suggest an ever increasing yaw velocity which eventually causes the solution to become unstable.

The courses predicted by the partly non-linear simulation for initial heading of 90 degrees are shown in Figure 10.9. When using the viscous data the course predicted for the smallest wave amplitude shows a slight drift in the direction of the waves. This drift is more pronounced when the wave amplitude is increased. Contrasting this against the results of the linear time domain simulation (Figure 9.15) where the ship drifted into the direction of the waves, suggests that the partly non-linear method gives a more realistic prediction of the motions in such conditions. Again, the courses predicted using the unaltered potential flow hydrodynamic data do not provide good results, becoming unstable.

It is believed that the addition of a viscous contribution to data calculated using a potential flow method provides an opportunity to more realistically simulate the anti-symmetric motions of ships in waves. It has been shown that the use of potential flow hydrodynamic data results in simulations that are unstable, this instability being attributed to the under damping of the yaw and sway motions. When viscous contributions are added to the hydrodynamic data from potential flow methods, the predicted courses appear to be more realistic. It is particularly encouraging to see that when the partly non-linear method is used and symmetric and anti-symmetric motions become coupled that the predicted courses appear to offer more realistic predictions than the linear method (drift is now with the waves rather than into them). It is difficult to know how these predicted courses would compare to experiments, such data being unavailable. It is also important to realise that the diffraction contributions remain specific to the initial heading of the vessel, hence as the heading changes these will no longer necessarily be correct.

10.4 S175 Containership

Having shown that the partly non-linear time domain simulation method produces acceptable results for the *Series 60* type hull form, it is an obvious step to test the method on a hull form which is more likely to show non-linear effects. The hull form that has been chosen is the *S175* container ship, whose linesplan and particulars are given in Appendix B.3. This hull form has considerable bow flare as well as a moderately overhanging stern. It has also been the subject of experimental investigations on non-linear effects in symmetric motions [67, 79]. In addition, theoretical methods have been tested on this hull form, giving another source of information to compare predicted responses against. Time domain simulations were performed in regular head waves at two forward speeds, F_n = 0.2 and 0.275, corresponding to the experimental results available.

The linear radiation and diffraction contributions were calculated using the frequency domain pulsating source method. The idealisation of the mean wetted surface of the hull was created using the Fixed Method, with 10 panels per section, aspect ratio 2, giving a total of 884 panels, shown in Figure B.8. The entire hull, to a depth of 20m was idealised for the determination of the instantaneous wave excitation and restoring forces/moments. This idealisation used 15 panels per section, aspect ratio 2, giving a total of 1676 panels (see Figure B.9).

10.4.1 Fn = 0.2

Results for the simulations of heave and pitch motions in head waves at F_n = 0.2 for a range of wave amplitudes (0.1, 1, 2, 3 and 4m) can be seen in Figure 10.10. The time domain simulations were initially performed using a very low incident wave amplitude in order to compare the responses to linear, frequency domain predictions. It can be seen that the agreement for the heave motions is very good. As the wave amplitude is increased the heave RAOs decrease around the region of resonance.

Pitch motions calculated using the smallest wave amplitude also show good agreement

with the frequency domain predictions. Once again, increasing the wave amplitude results in the amplitude of the RAOs decreasing. However, the amount by which the pitch RAOs decrease is less than was seen for the heave RAOs.

Experiments were carried out on an *S175* model at $F_n = 0.2$ by O'Dea et al. [79]. They compared the changes in the heave and pitch responses with increasing wave amplitude for three different wavelengths. The wavelengths tested were $1.4 \times L_{pp}$, $1.2 \times L_{pp}$ and $1.0 \times L_{pp}$. To enable comparison of the results of the partly non-linear time domain method to the experiments, simulations were carried out for a range of wave amplitudes at these three wave lengths. The results of these simulations are shown in Figure 10.11. In each of the graphs there are the experimentally measured amplitudes, responses predicted using the partly non-linear time domain method and a line representing the amplitude predicted using a linear pulsating source frequency domain method. It can be seen that in each case the responses predicted using the time domain simulation method for the smallest wave amplitude are in agreement with the frequency domain predictions, as would be expected. These frequency domain predictions are not always that close to the experimental predictions at low amplitude. As a result the time domain predictions start with an offset from the experimental values, yet in general they appear to show similar trends to the experimental results.

In particular, the heave predictions show a decrease in amplitude with increasing wave slope which is very similar to that shown in experiments. The experimental pitch motions show less of a tendency to decrease as the wave slope is increased, a trend which is reflected reasonably well in the results of the time domain method.

10.4.2 Fn = 0.275

Further experimental results were presented by O'Dea et al. [79] for $F_n = 0.275$. Time domain simulations were performed for a range of wave amplitudes (0.1, 1, 2, 3 and 4m) at this speed and the predicted responses are shown in Figure 10.12. Once again it can be seen that as the amplitude of the incident waves increases there is a decrease in the amplitude of

the responses, especially in the region of resonance.

It is interesting to compare the response traces of the heave and pitch motions with the Fourier fits that have been applied in order to determine the amplitude of the responses. It can be seen in Figure 10.13 and 10.14 that for the smaller wave amplitudes the responses for both heave and pitch motions remain roughly sinusoidal. However, when the wave amplitude is increased to 4m it can be seen that the pitch motions are no longer sinusoidal and this brings into question the validity of using the Fourier fit method to measure the responses. The fact that the responses are no longer sinusoidal also suggests that the amplitude of the motions must be quite large in terms of the size of the ship. Hence, it is interesting to attempt to visualise what the changing underwater surface of the hull is actually like, to see whether this is realistic.

Visualisations of the underwater portion of the hull for wave amplitude 1m are shown in Figure 10.16. It can be seen that the height of the waterline on the bow changes considerably, while the overhanging stern can be seen to emerge and then submerge as the ship pitches. It appears that the underwater portion of the hull does not differ too significantly from the mean wetted surface, which is logical given that the predicted motions at this wave amplitude are quite similar to those predicted by the linear frequency domain method.

When the wave amplitude is increased to 4m, the motions of the ship (see Figure 10.17) are now much more extreme. It can be seen that the bow submerges as the ship pitches forward before emerging again to reveal the entire forefoot of the bow. Such extreme motions are likely to be out of the range of what a partly non-linear method can ever hope to accurately simulate. However, it is encouraging to note that despite the large amplitude of the motions and the submergence of the bow, the predicted heave and pitch traces remain stable and a not too unrealistic solution is able to be obtained.

Experimental results at F_n = 0.275 presented by O'Dea et al. [79] were also for three wave lengths with a range of wave amplitudes tested for each. A comparison of these experimental results with time domain predictions can be seen in Figure 10.15. Once again, the experimental measurements are compared against time domain predictions as well as

the predicted linear frequency domain response. As was noted for the $F_n = 0.2$ results, the amplitude of the responses predicted by the time domain tend towards the linear prediction as the wave amplitude decreases. As was noted in the lower Froude number results, there is generally some difference between the experimental results at low amplitude and the linear frequency domain predictions. However, given the fact that the basis of the partly non-linear time domain method (linear frequency domain data) differs from experiment, the time domain method still appears to show similar trends to the experimental results in most cases. This would appear to suggest that the use of instantaneous Froude-Krylov and restoring contributions offers an improved method by which non-linear ship motions may be approximated, compared the linear techniques. Comparison is also made between the results of the partly non-linear method and those of the *LAMP2* and *LAMP4* methods of Lin et al. [64, 63] (see Section 2.2), where, in general, encouraging agreement is found. The formulation of the *LAMP2* method is the most similar to the partly non-linear method presented here and this is reflected in the comparison of the results.

10.5 Yacht Hullform

Having achieved encouraging results for the *S175* containership, it was decided to test the accuracy of the partly non-linear method on a more challenging hull form. An MSc research project undertaken at the University of Southampton [105] during 2000 sought to determine the effects of bow shape on the motions of a yacht. As part of this research project a number of seakeeping tests were performed using models in the towing tank at the Southampton Institute. A single hull form was examined using the partly non-linear time domain method, the results of the time domain simulations being compared to the experimental results for $\alpha = 0.24m$. A comparison of these results may be seen in Figure 10.18 for regular head waves at $F_n = 0.25$.

The mean wetted surface was idealised using the Fixed Method , with 10 panels per section and aspect ratio 2, giving a total of 876 panels and is shown in Figure B.11. The complete hull up to the deckline was idealised using the Fixed Method, with 15 panels per section

and aspect ratio 2, giving a total of 1504 panels (see Figure B.12).

It can be seen that for both heave and pitch, amplitude of the responses determined using the time domain simulation technique for low wave amplitudes agree well with the linear frequency domain predictions. With the wave amplitude increased to the same at which the experiments were carried out at, it can be seen that there is a change in simulated heave and pitch motions. In both cases it appear that the responses predicted using the partly non-linear time domain method are in closer agreement with the experimental results, especially for the pitch responses.

These results suggest that incorporating non-linear incident wave and restoring contributions in a time domain simulations technique offers improvements to the predictions of motions of hulls forms which have highly flared hull sections, such as yachts.

10.6 NPL5b Catamarans

The responses of an *NPL5b* catamaran in waves were simulated in the previous chapter using hydrodynamic data calculated using two methods. The first of these was a pulsating source method, the second a translating, pulsating source method. It was shown that the pulsating source method over predicted the interaction effects between the two hulls, which had a negative effect on the subsequent prediction of the response amplitudes.

The hull form of the *NPL5b* has a moderately flared bow (see Appendix B.2), making use of the partly non-linear method appropriate for all but the smallest incident wave amplitudes. The linear radiation and diffraction contributions were calculated using the same method and mean wetted surface idealisations used previously for the linear time domain method. For the partly non-linear time domain method an additional panelled hull representation was required for the entire hull up to deck line. This was created using the Fixed Method, having a total of 906 panels per demi-hull, giving a total of 1812 (see Figure B.6).

10.6.1 S/L = 0.2

Figure 10.19 shows heave and pitch response amplitude operators for an *NPL5b* catamaran with Separation to Length ratio 0.2. These were calculated using hydrodynamic data determined using the pulsating source frequency domain technique. Initially the partly non-linear method was used to calculate the responses of the vessel in incident waves of very small amplitude, allowing comparison to frequency domain predictions. Subsequently the wave amplitude was increased to match that of experiments by Molland et al. [69]. The responses for the low and high wave amplitudes are plotted along with the frequency domain predictions and experimental results. It can be seen that the responses predicted by the linear frequency domain method show little resemblance to the experimental measurements other than at low frequency. When the amplitude of the excitation is increased to match that at which the experiments were performed, the agreement between time domain simulations and experiment is mixed. The heave responses are somewhat higher than the experiments, yet the resonance peak is in quite good agreement. Pitch results are less good, with the simulated responses having a much higher amplitude, although it appears to be an improvement over the frequency domain predictions.

Figure 10.20 present similar results for the S/L=0.2 catamaran, this time using translating, pulsating source data. Again, the low amplitude responses predicted using the partly non-linear time domain method closely match the frequency domain predictions. It can be seen that the frequency domain and low amplitude time domain predictions closely match the heave experimental values. Agreement of the frequency domain and low amplitude time domain pitch predictions with the experiments is not as good. Increasing the incident wave amplitude to match that of the experiments has little effect on the predicted heave responses. The predicted pitch responses tend to reduce in value for the larger wave amplitude.

10.6.2 S/L = 0.4

Results for the wider hull separation (S/L=0.4) using pulsating source data are shown in Figure 10.21. Partly non-linear time domain simulations at low amplitude show a similar level of agreement with frequency domain predictions as was found using the linear time domain method (see Figure 9.21). Comparison of pulsating source method frequency domain predictions to experiments shows that there is little agreement, except at low and high frequencies. This is due to the over-prediction of interaction effects between the hulls. Increasing the incident wave amplitude appears to have little effect on the predicted heave responses and does not improve agreement with the experiments. The pitch responses appear to reduce slightly in amplitude, marginally improving their agreement with the experiments.

Predicted responses for the S/L=0.4 catamaran using translating, pulsating source data are compared to experimental data in Figure 10.22. By comparison to the predictions using pulsating source data in the previous Figure, the agreement of the frequency domain and low incident wave amplitude time domain predictions with the experiments is much improved. Heave responses are slightly over-predicting the amplitude compared to the experiments, whilst the pitch responses are rather more over-predicted. In both heave and pitch the frequency of resonance is well predicted. Increasing the incident wave amplitude results in the heave responses predicted by the time domain method increasing and the predicted frequency of resonance decreasing. This reduces the level of agreement with the experiments. The pitch responses predicted for the larger wave amplitude also show a shift in the predicted resonance frequency. The amplitude of the peak reduces compared to the low amplitude simulations and more closely matches that of the experiments.

Figures 10.19 and 10.21 have shown that the RAOs predicted using pulsating source data do not agree well with experimental measurements, except at very low and very high frequencies. This is a result of the overestimation of the interactions between the hulls and their consequent effect on the relevant hydrodynamic data.

At the Froude number investigated, the catamaran RAOs predicted using hydrodynamic

data determined by the translating, pulsating source method show reasonable agreement for the heave RAO and, in general, poor agreement for the pitch RAO. Increasing the wave amplitude results reasonable prediction of the pitch amplitude, whilst heave predictions become somewhat poorer, especially for S/L = 0.4. Nevertheless, this method is a superior method, compared to the pulsating source method, as it accounts more accurately for the interactions between the hulls of the catamaran.

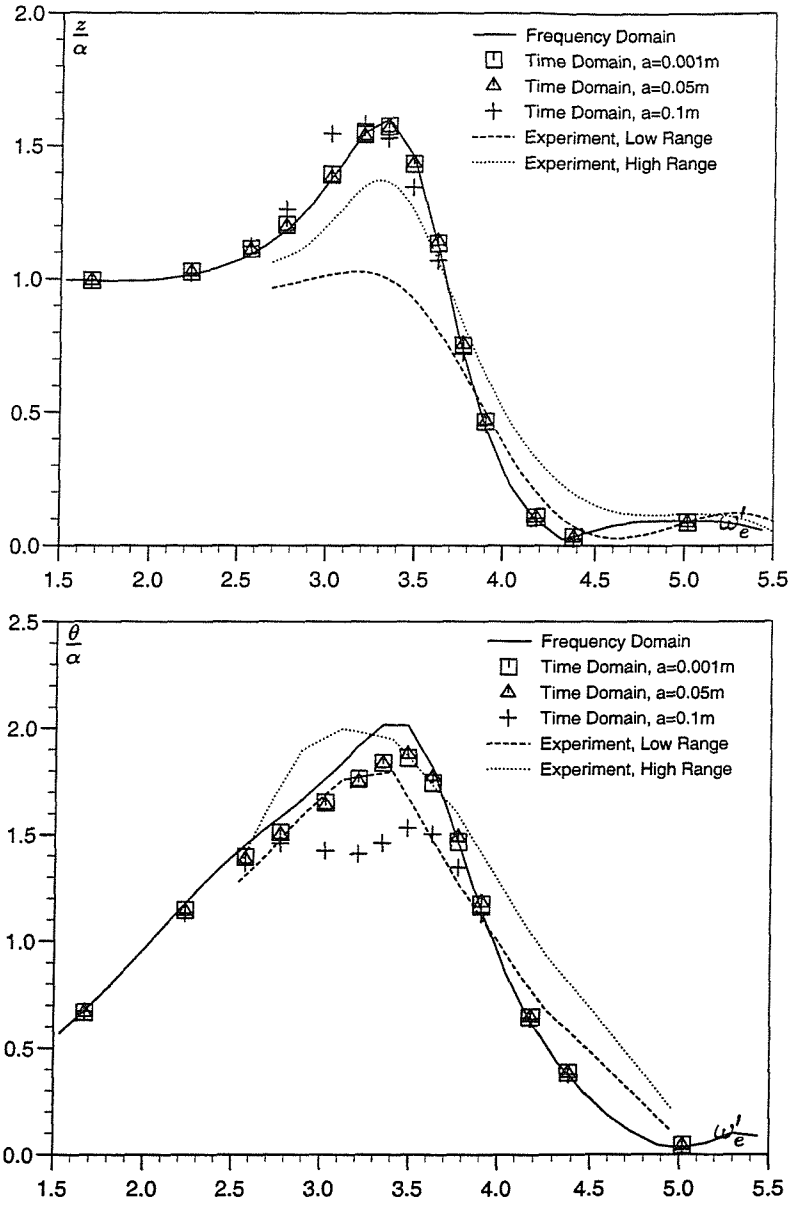

Figure 10.4: Heave and pitch response amplitude operators for *Series 60* mono-hull in head waves, L=3.048m, Fn=0.2, $\chi = 180°$.

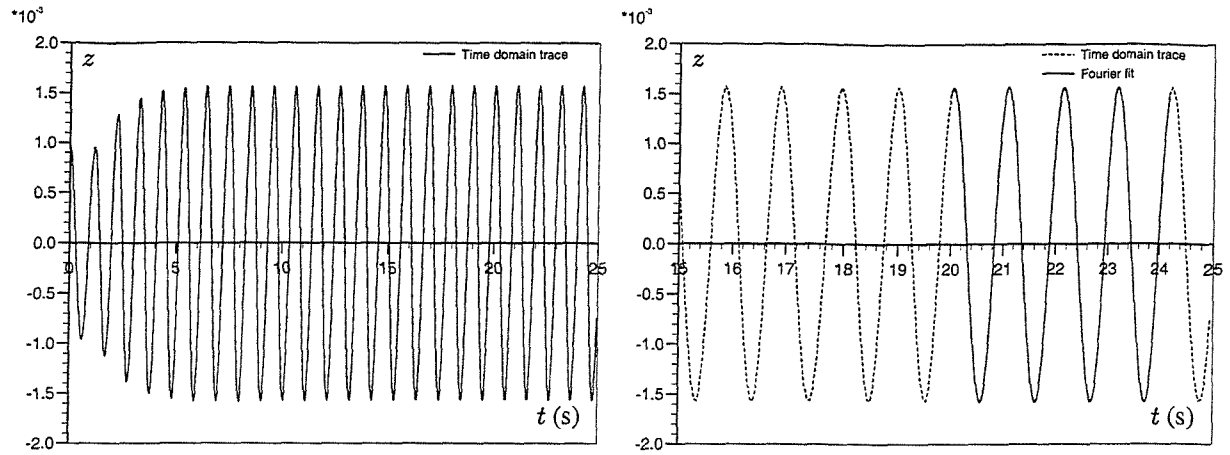

(a) Wave amplitude = 0.001m

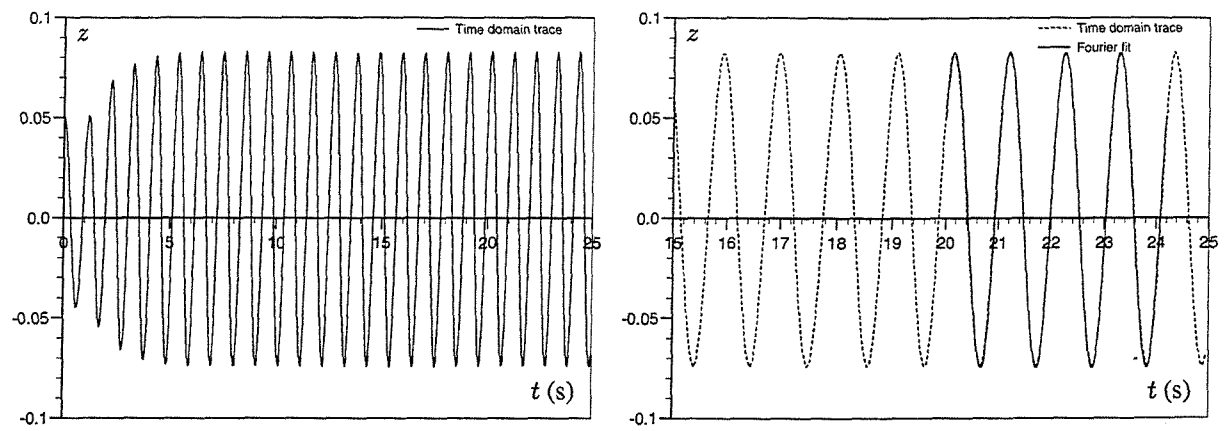

(b) Wave amplitude = 0.05m

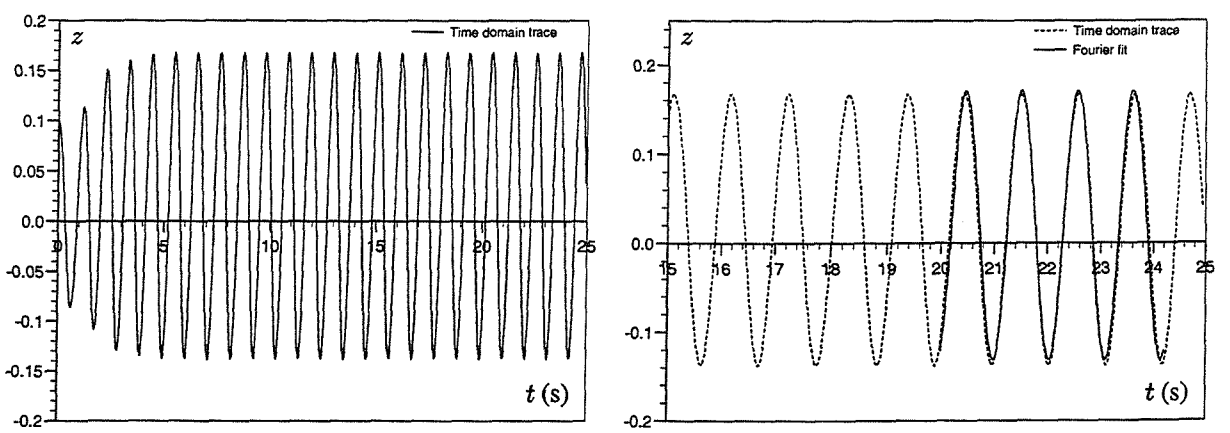

(c) Wave amplitude = 0.1m

Figure 10.5: Heave traces for simulated motions of a *Series 60* model in head waves using partly non-linear method, complete trace on left and trace in region of Fourier fit on right. L=3.048m, Fn=0.2 , ω_e = 6 rad/s, time step = 0.05s.

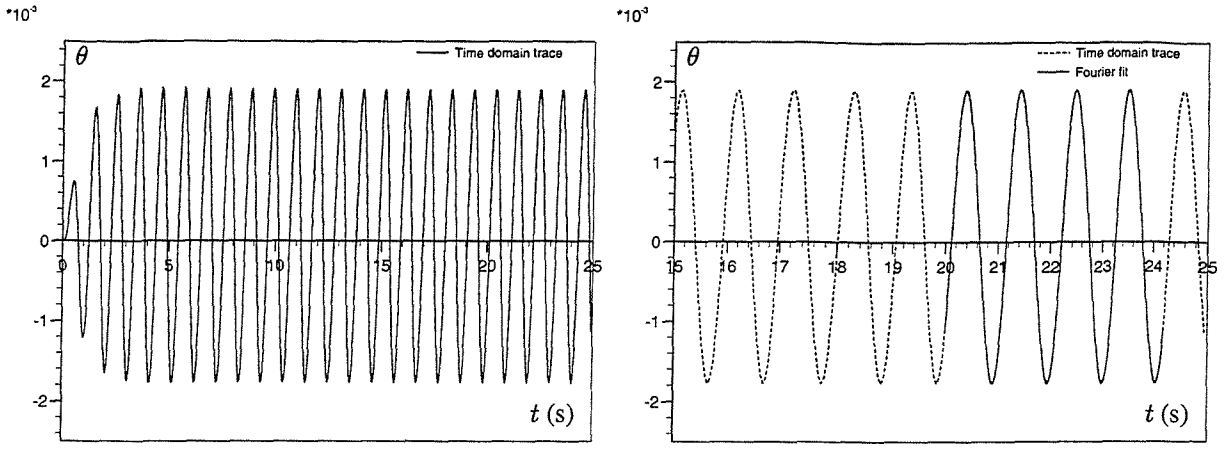

(a) Wave amplitude = 0.001m

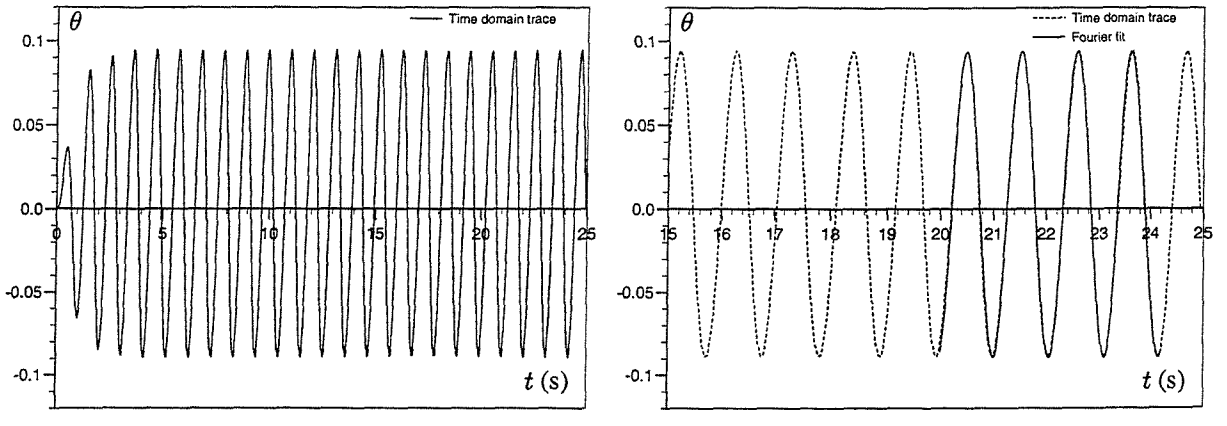

(b) Wave amplitude = 0.05m

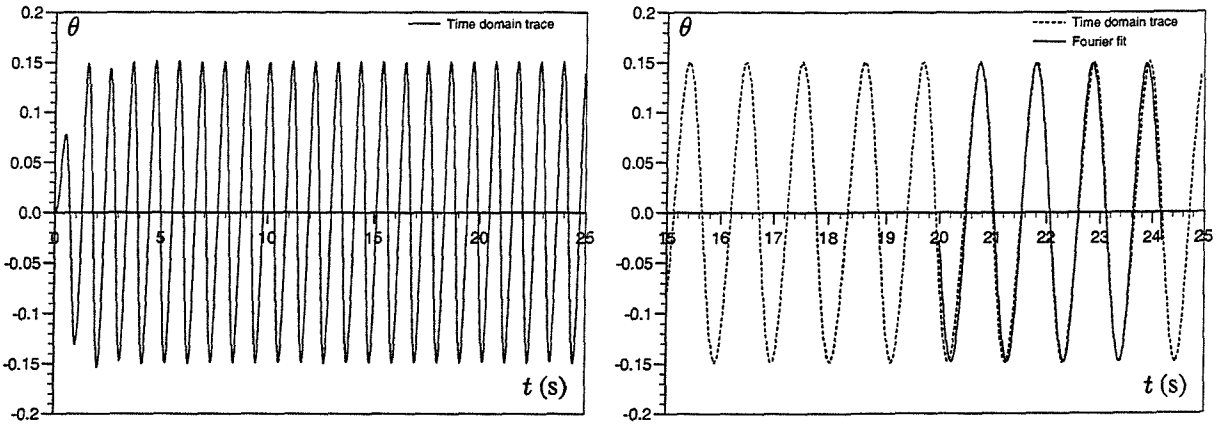

(c) Wave amplitude = 0.1m

Figure 10.6: Pitch traces for simulated motions of a *Series 60* model in head waves using partly non-linear method, complete trace on left and trace in region of Fourier fit on right. L=3.048m, Fn=0.2 , $\omega_e = 6$ rad/s, time step = 0.05s.

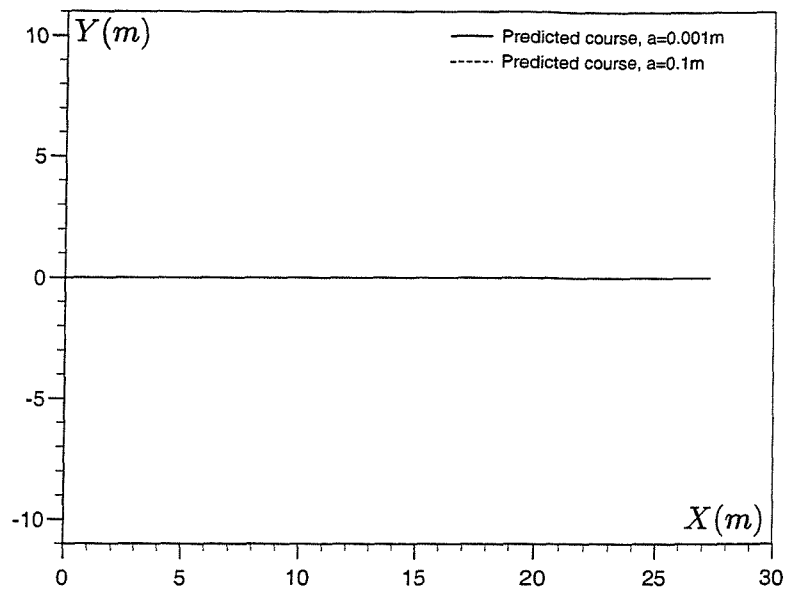

(a) With viscous contributions

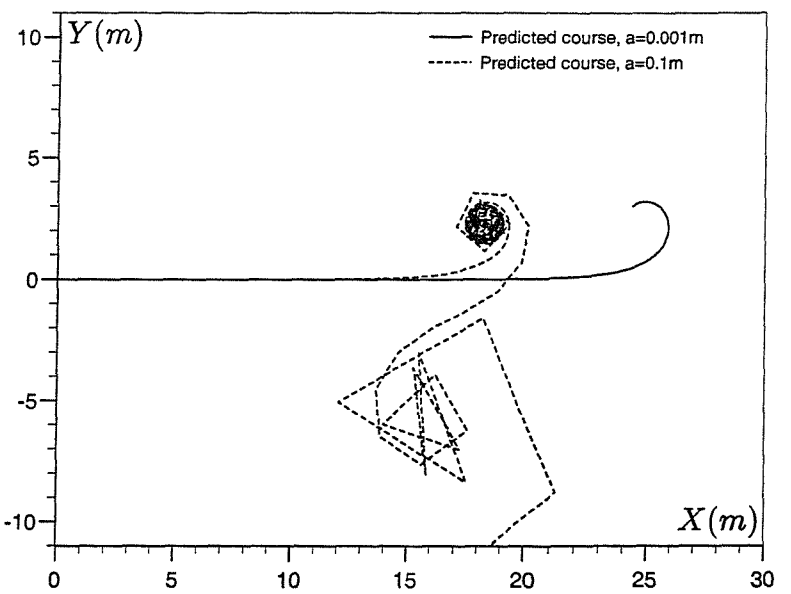

(b) Without viscous contributions

Figure 10.7: Predicted course of *Series 60* models, using data with (a) and without (b) viscous contributions, calculated using partly non-linear time domain method. ω_e = 2 rad/s, L=3.048m, Fn=0.2, initial $\chi_0 = 180°$. Waves travelling in negative X-direction.

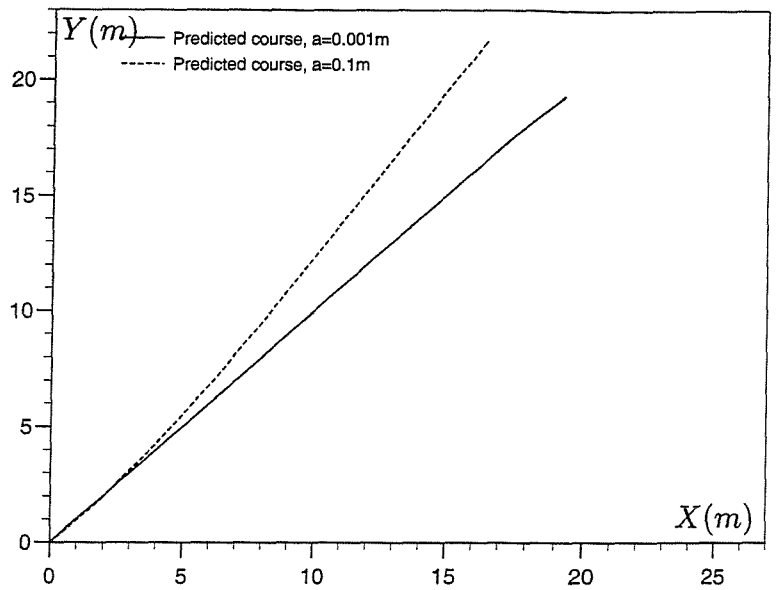

(a) With viscous contributions

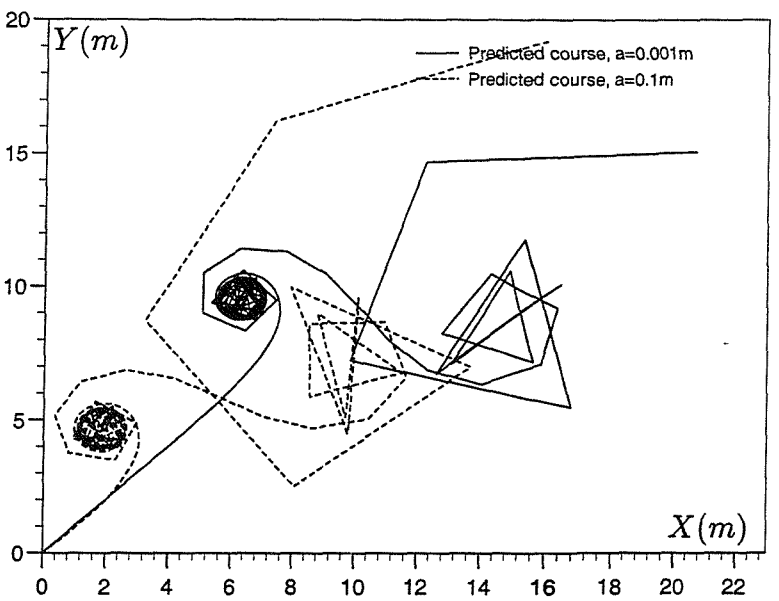

(b) Without viscous contributions

Figure 10.8: Predicted course of *Series 60* models, using data with (a) and without (b) viscous contributions, calculated using partly non-linear time domain method. ω_e = 2 rad/s, L=3.048m, Fn=0.2, initial $\chi_0 = 135°$. Waves travelling in negative X-direction.

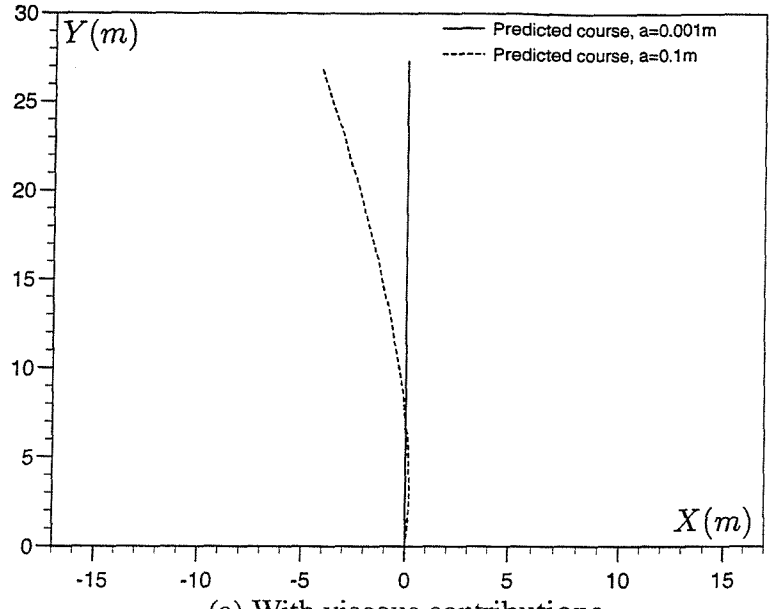

(a) With viscous contributions

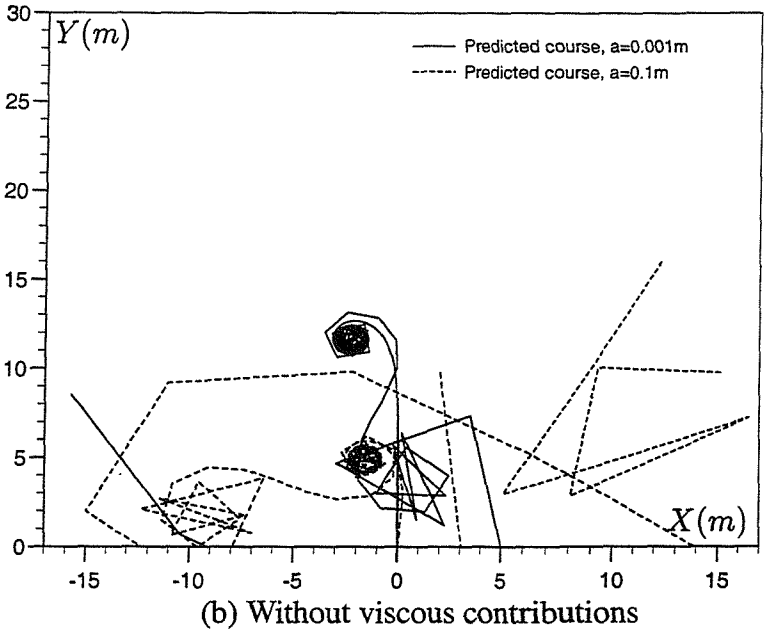

(b) Without viscous contributions

Figure 10.9: Predicted course of *Series 60* models, using data with (a) and without (b) viscous contributions, calculated using partly non-linear time domain method. ω_e = 2 rad/s, L=3.048m, Fn=0.2, initial $\chi_0 = 90°$. Waves travelling in negative X-direction.

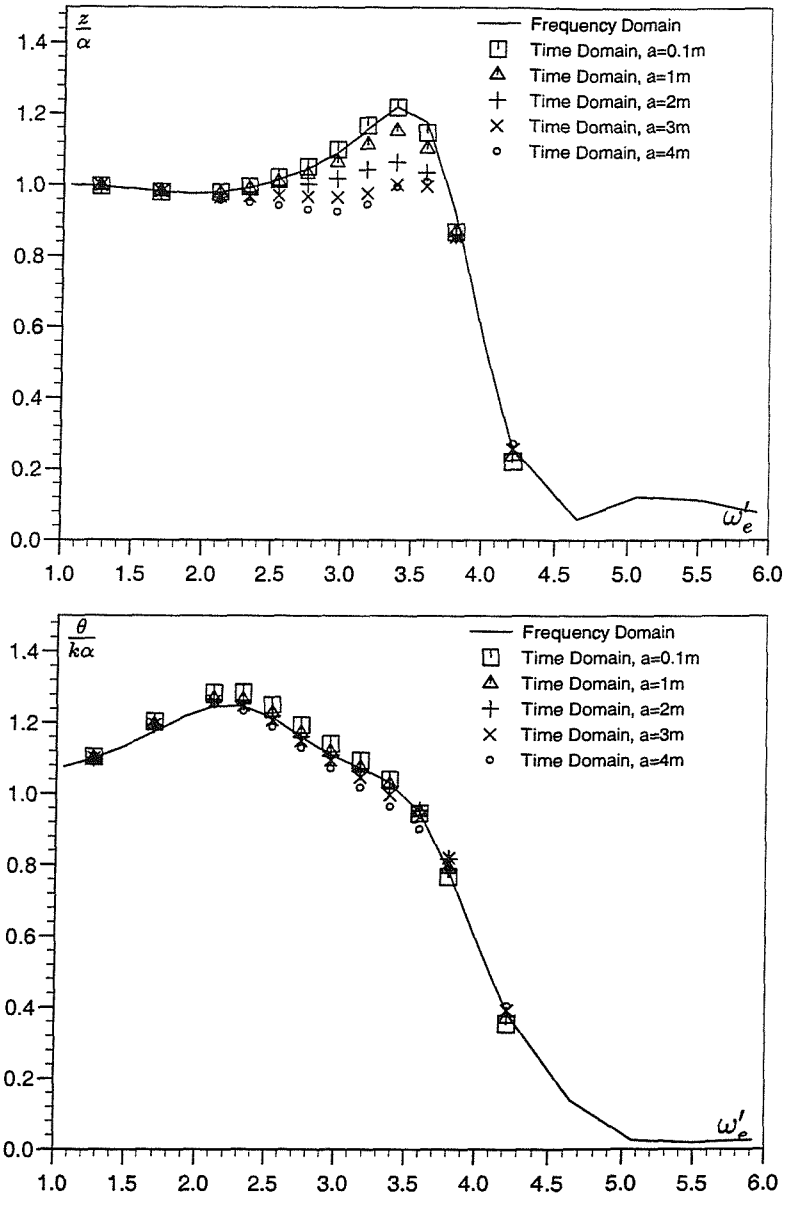

Figure 10.10: Heave and pitch response amplitude operators for *S175* containership in head waves, L=175m, Fn=0.2, $\chi_0 = 180°$.

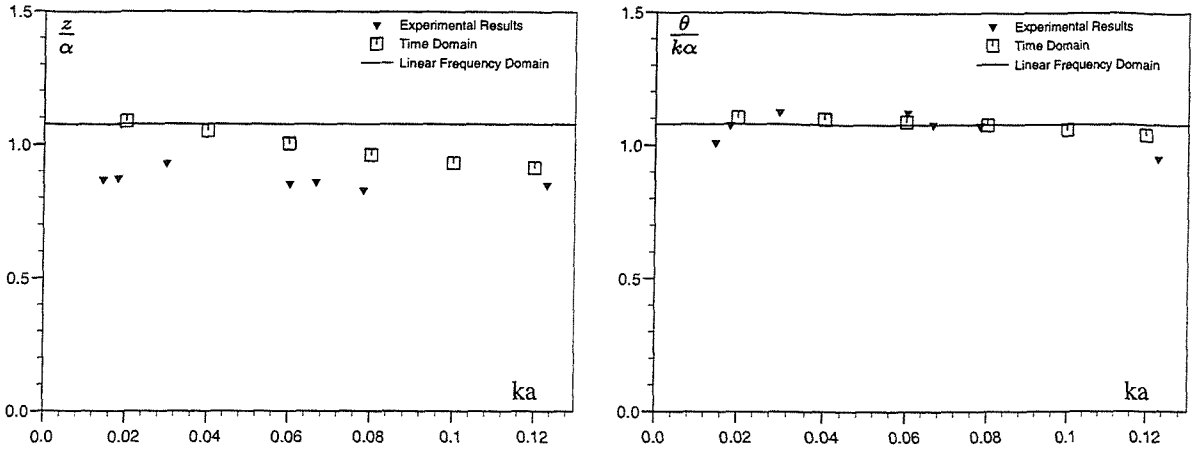

(a) Wave length = 245m

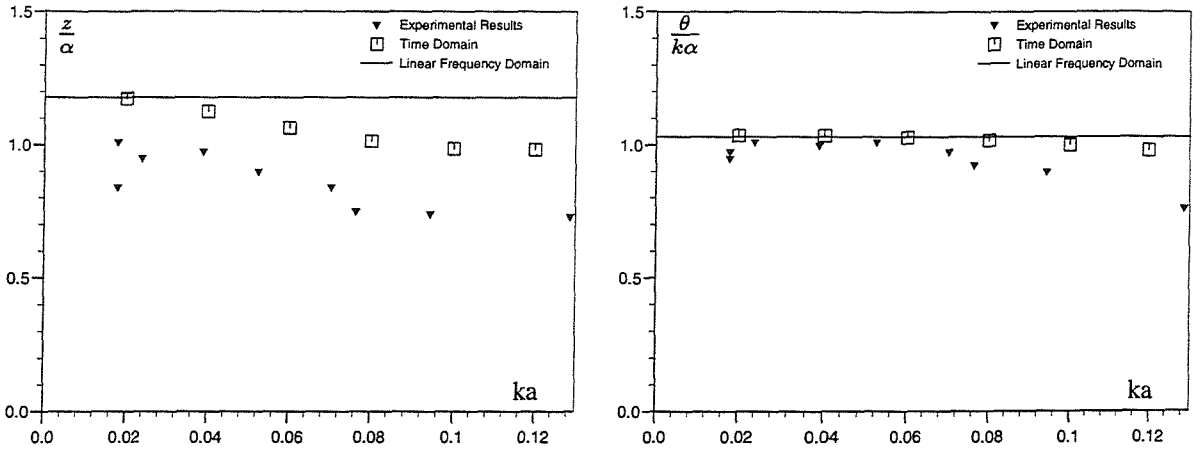

(b) Wave length = 210m

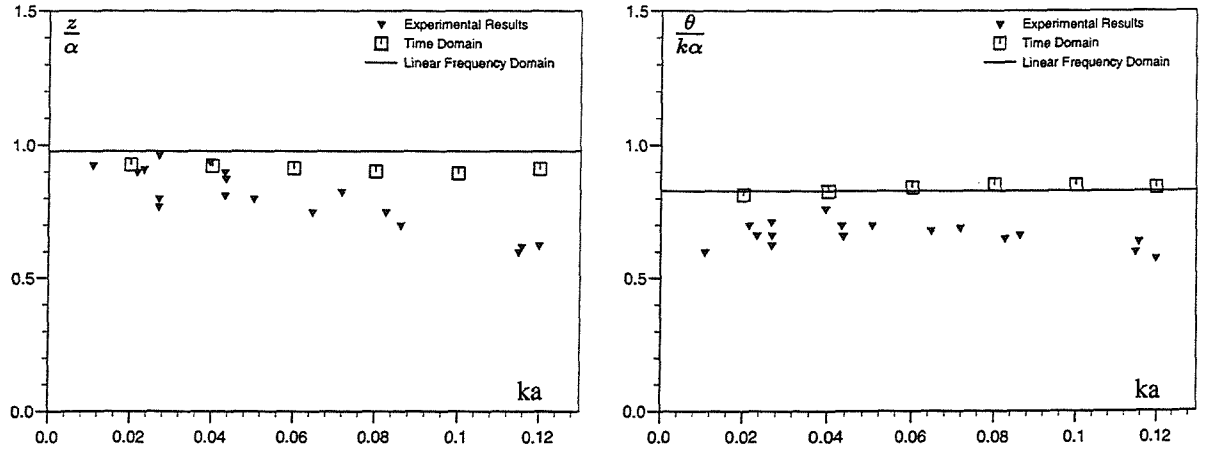

(c) Wave length = 175m

Figure 10.11: Heave and pitch response amplitude operators for *S175* containership in waves of variable amplitude. L=175m, Fn=0.2, χ_0 = 180°.

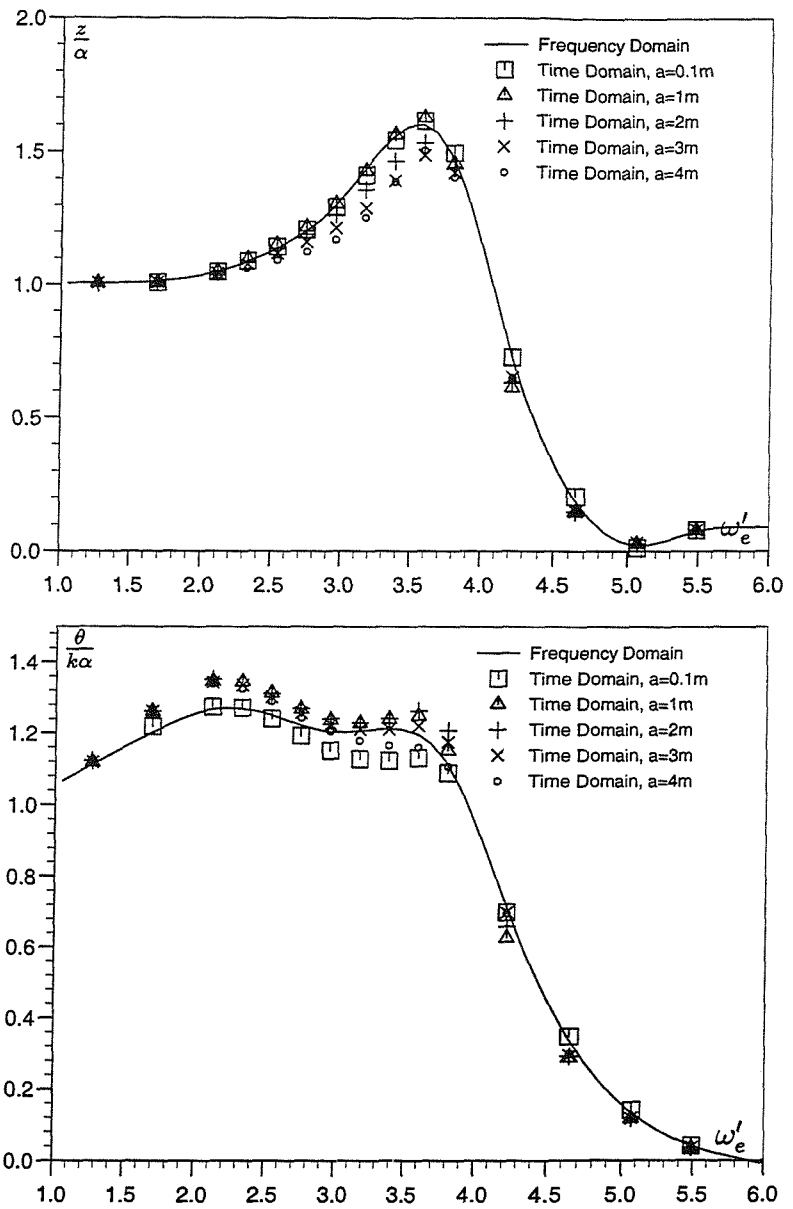

Figure 10.12: Heave and pitch response amplitude operators for *S175* containership in head waves, L=175m, Fn=0.275, $\chi_0 = 180°$.

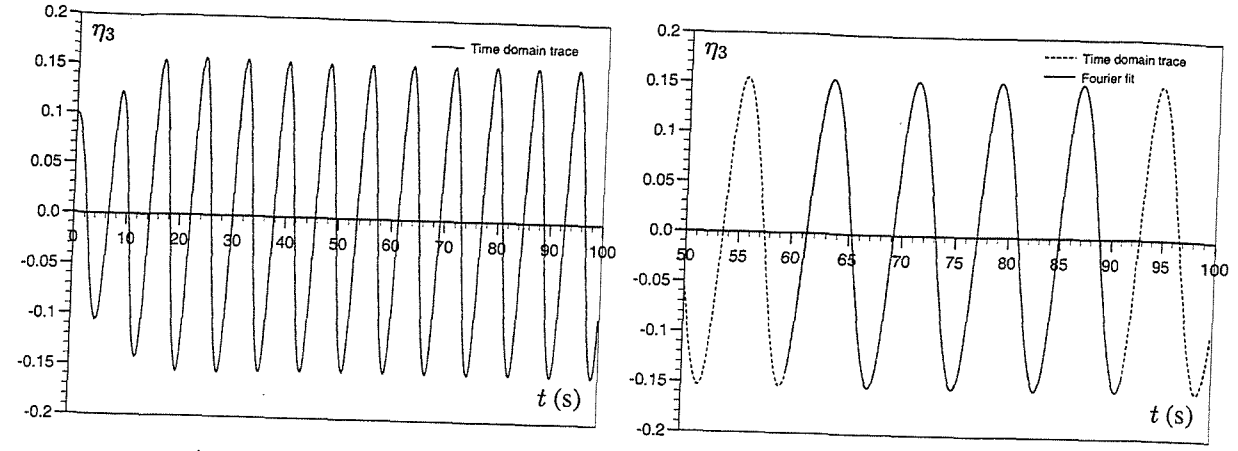

(a) Wave amplitude = 0.1m

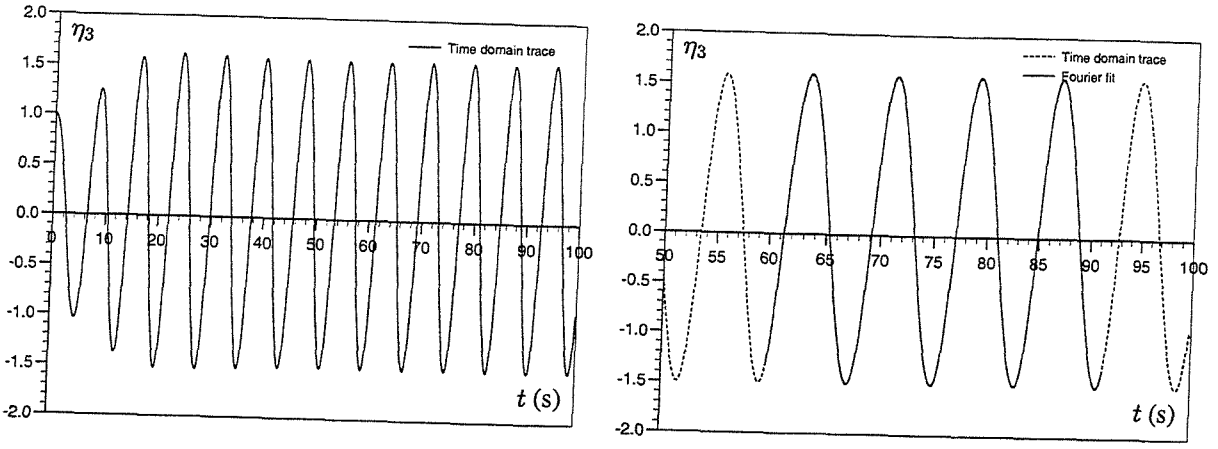

(b) Wave amplitude = 1m

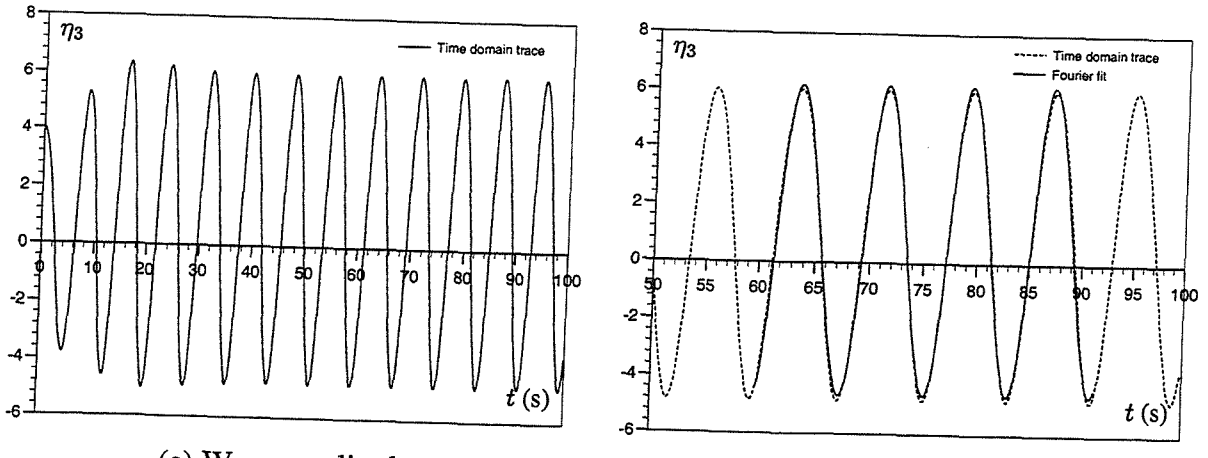

(c) Wave amplitude = 4m

Figure 10.13: Heave traces for simulated motions of a *S175* containership in head waves using partly non-linear method, complete trace on left and trace in region of Fourier fit on right. L=175m, Fn=0.275 , ω_e = 0.8 rad/s, time step = 0.05s.

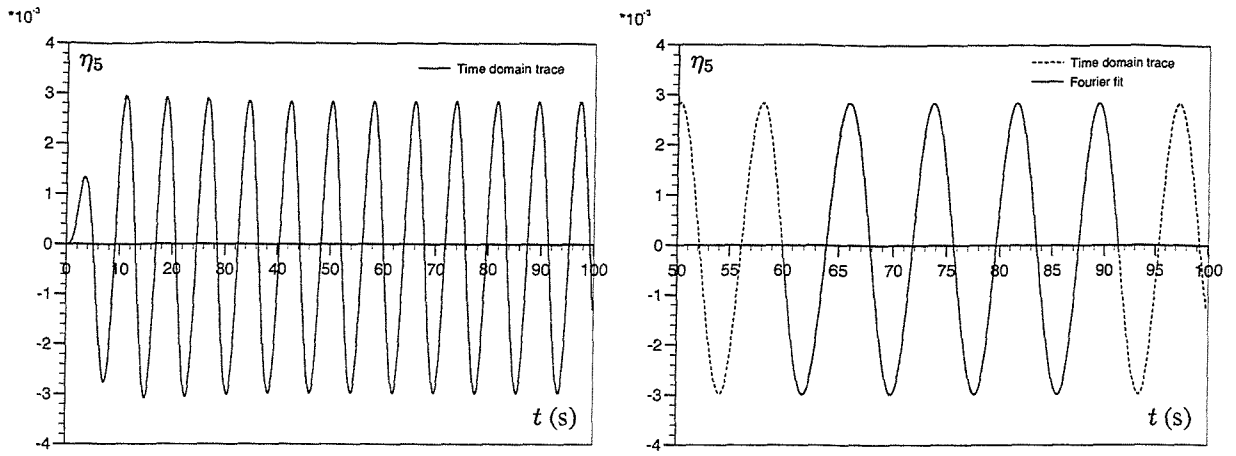

(a) Wave amplitude = 0.1m

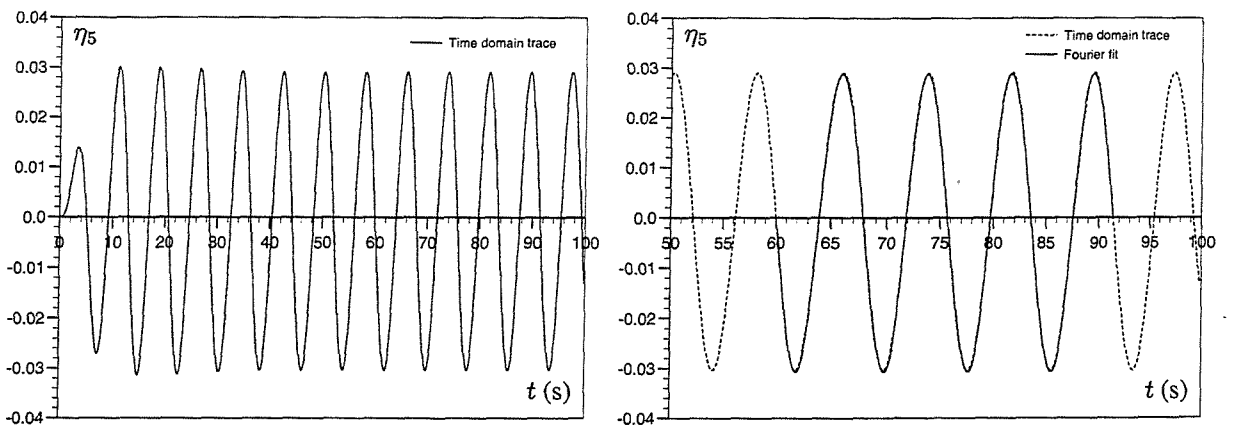

(b) Wave amplitude = 1m

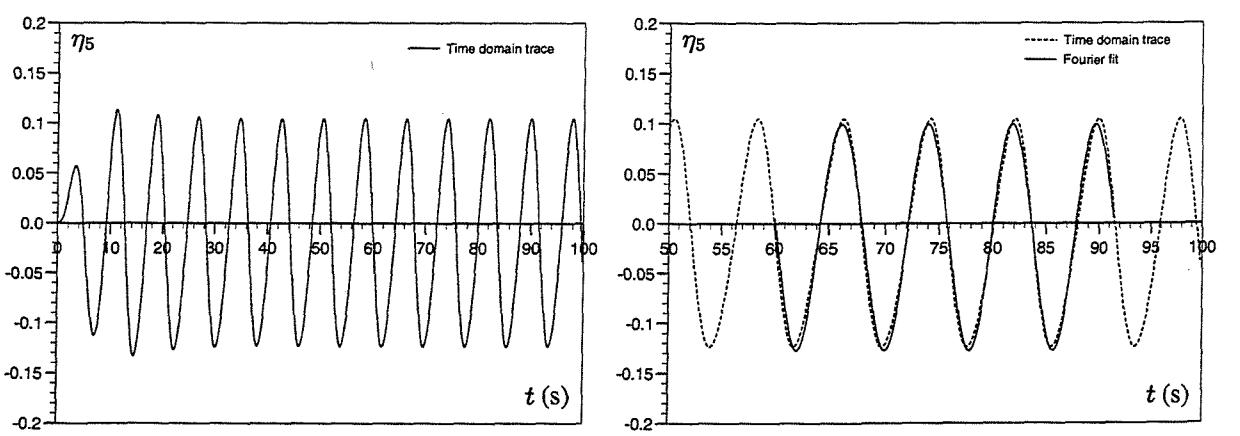

(c) Wave amplitude = 4m

Figure 10.14: Pitch traces for simulated motions of a *S175* containership in head waves using partly non-linear method, complete trace on left and trace in region of Fourier fit on right. L=175m, Fn=0.2 , $\omega_e = 0.8$ rad/s, time step = 0.05s.

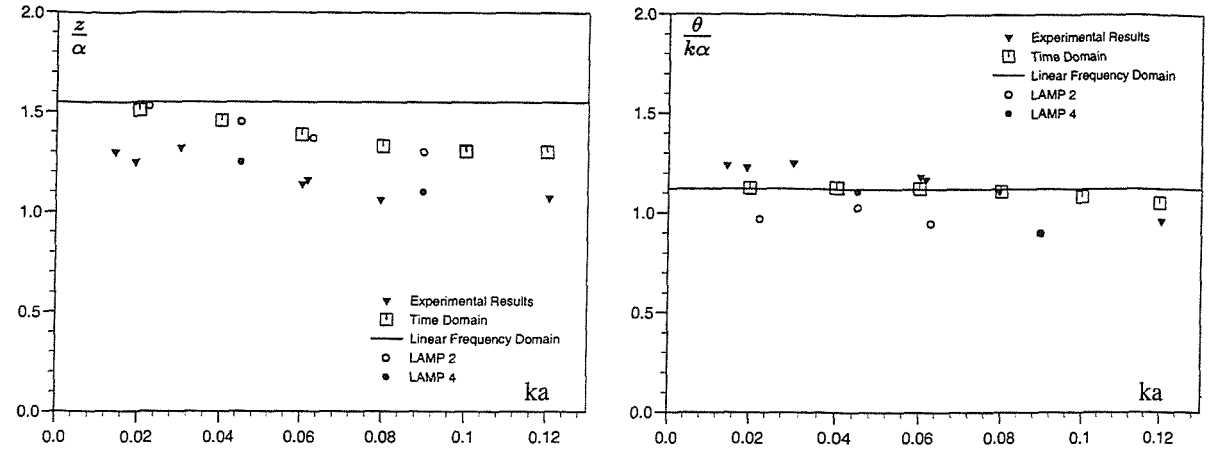

(a) Wave length = 245m

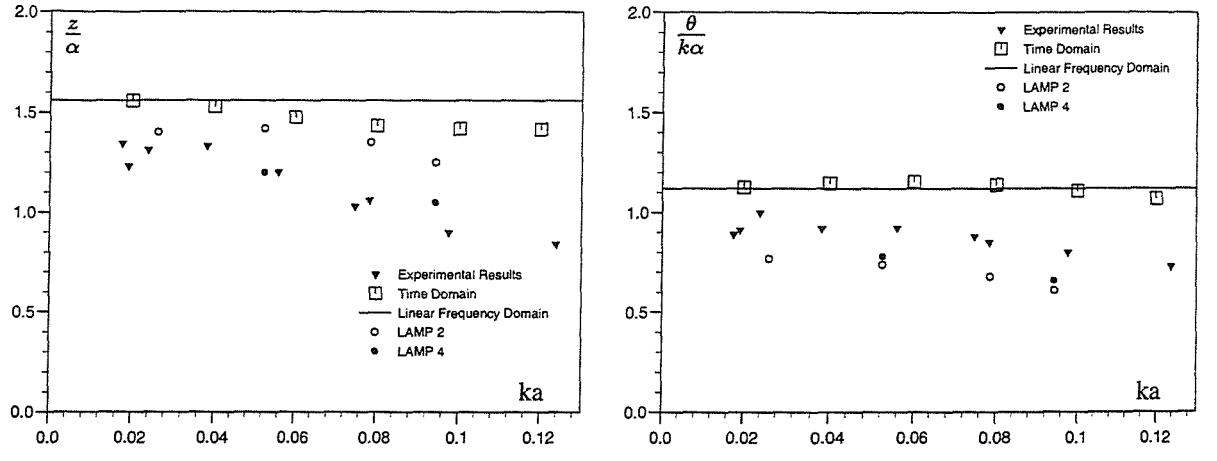

(b) Wave length = 210m

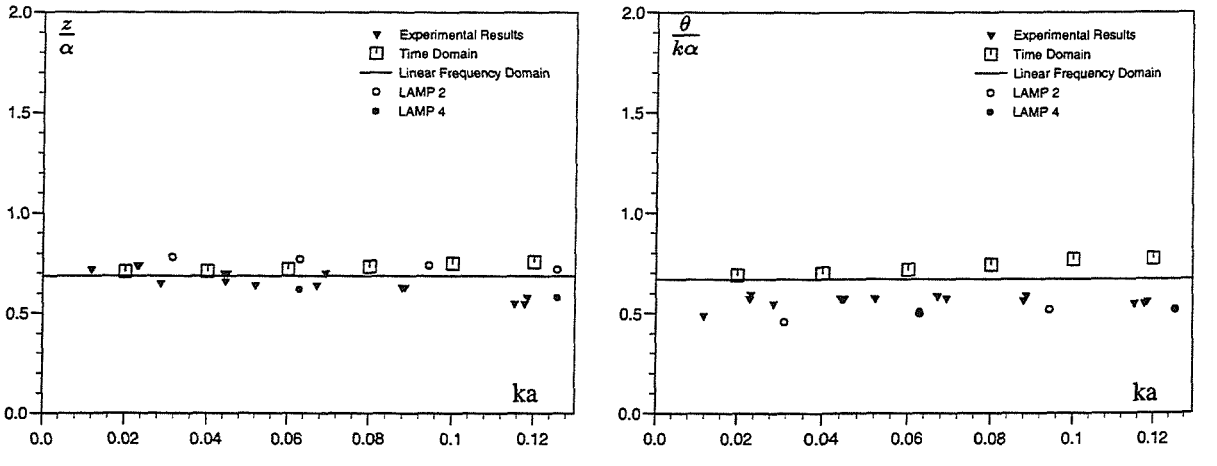

(c) Wave length = 175m

Figure 10.15: Heave and pitch response amplitude operators for *S175* container-ship in head waves of variable amplitude. L = 175m, Fn = 0.275, $\chi = 180°$.

Time = 20 seconds
Heave = -1.485 m
Pitch = 0.021 rad

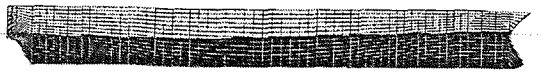

Time = 20.8 seconds
Heave = -1.359 m
Pitch = 0.0005 rad

Time = 21.6 seconds
Heave = -0.656 m
Pitch = -0.020 rad

Time = 22.4 seconds
Heave = 0.332 m
Pitch = -0.032 rad

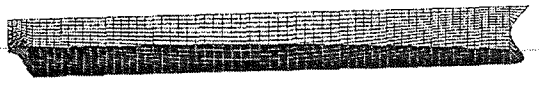

Time = 23.2 seconds
Heave = 1.209 m
Pitch = -0.032 rad

Time = 24 seconds
Heave = 1.627 m
Pitch = -0.0197 rad

Time = 24.8 seconds
Heave = 1.422 m
Pitch = -0.0005 rad

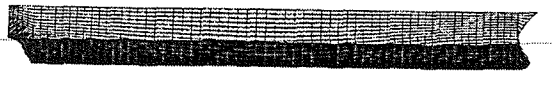

Time = 25.6 seconds
Heave = 0.669 m
Pitch = 0.019 rad

Figure 10.16: Visualisations of the instantaneous underwater portion of the hull of a *S175* containership in head waves, as calculated using partly non-linear method, wave amplitude = 1m. $F_n = 0.275$, $\lambda = 210$m.

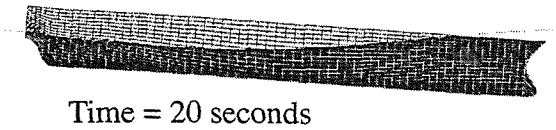

Time = 20 seconds
Heave = -5.001 m
Pitch = 0.061 rad

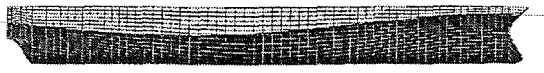

Time = 20.8 seconds
Heave = -4.126 m
Pitch = -0.031 rad

Time = 21.6 seconds
Heave = -1.287 m
Pitch = -0.108 rad

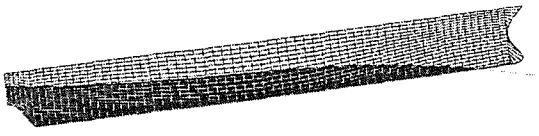

Time = 22.4 seconds
Heave = 2.269 m
Pitch = -0.139 rad

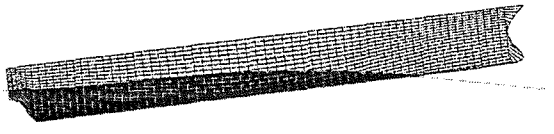

Time = 23.2 seconds
Heave = 5.180 m
Pitch = -0.121 rad

Time = 24 seconds
Heave = 6.439 m
Pitch = -0.072 rad

Time = 24.8 seconds
Heave = 5.629 m
Pitch = -0.009 rad

Time = 25.6 seconds
Heave = 2.943 m
Pitch = 0.057 rad

Figure 10.17: Visualisations of the instantaneous underwater portion of the hull of a *S175* containership in head waves, as calculated using partly non-linear method, wave amplitude = 4m. $F_n = 0.275$, $\lambda = 210$m.

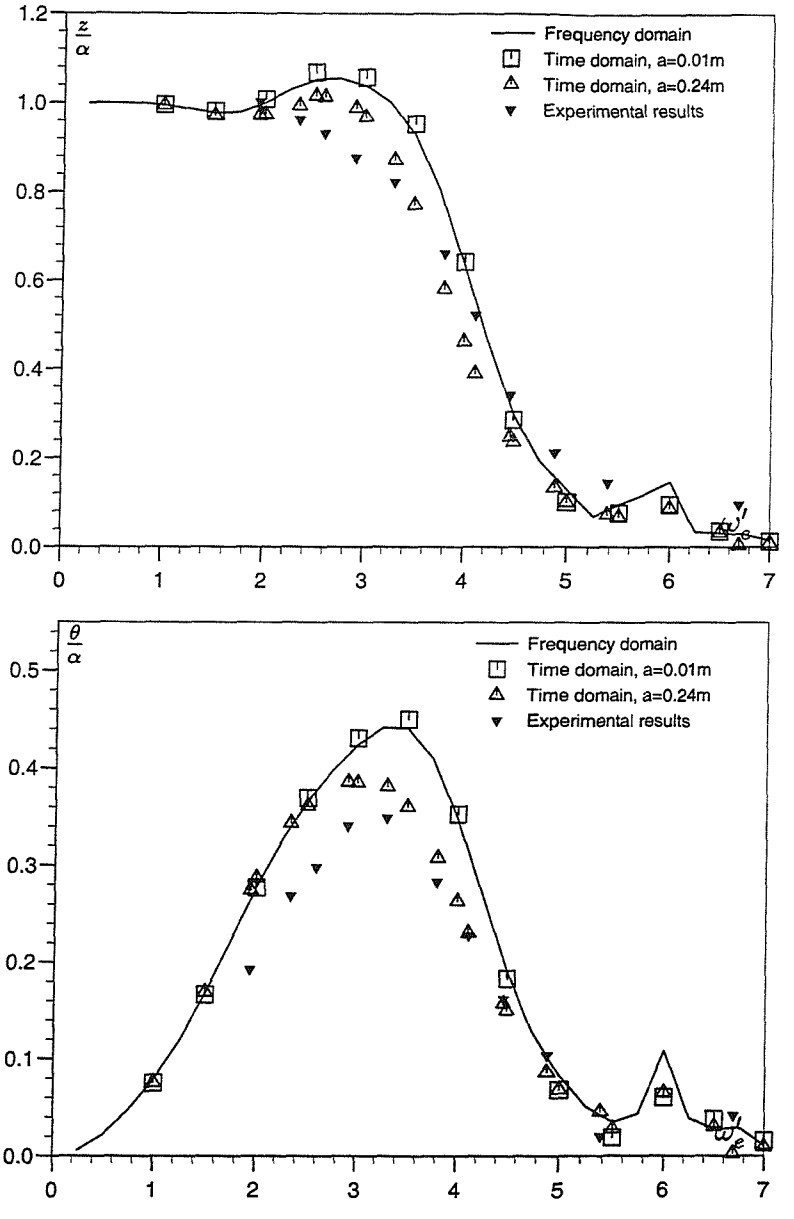

Figure 10.18: Heave and pitch response amplitude operators for yacht hull form in head waves, L=9.367m, Fn=0.25, $\chi_0 = 180°$.

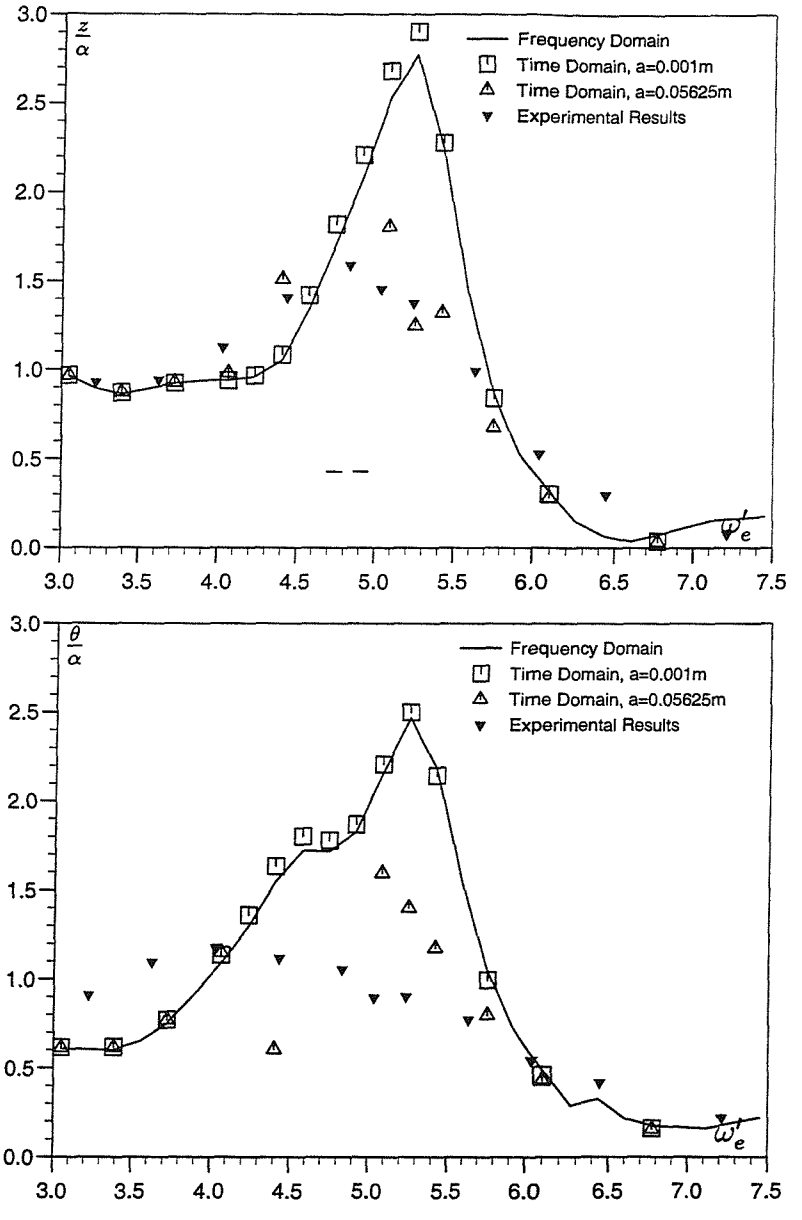

Figure 10.19: Heave and pitch response amplitude operators for *NPL5b* catamaran in head waves, using pulsating source data L=4.5m, S/L = 0.2, Fn=0.53, $\chi_0 = 180°$.

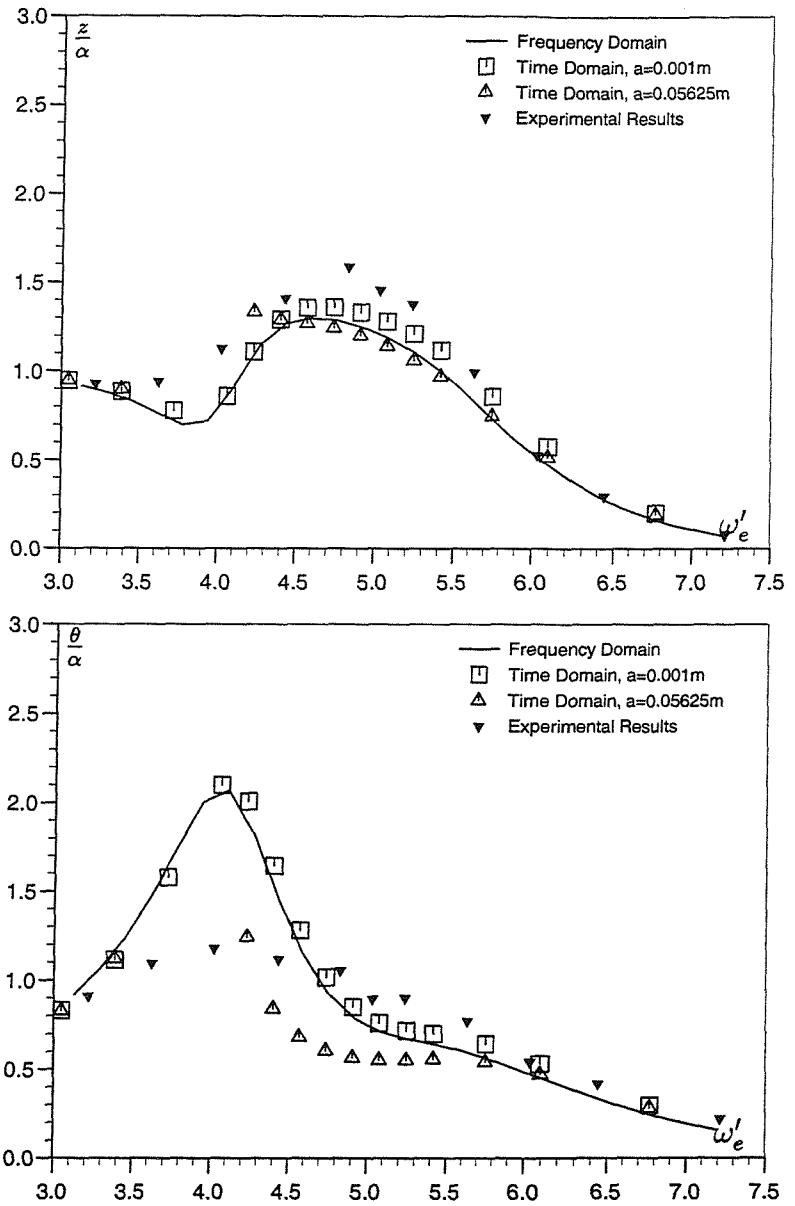

Figure 10.20: Heave and pitch response amplitude operators for *NPL5b* catamaran in head waves, using translating, pulsating source data. L=4.5m, S/L = 0.2, Fn=0.53, $\chi_0 = 180°$.

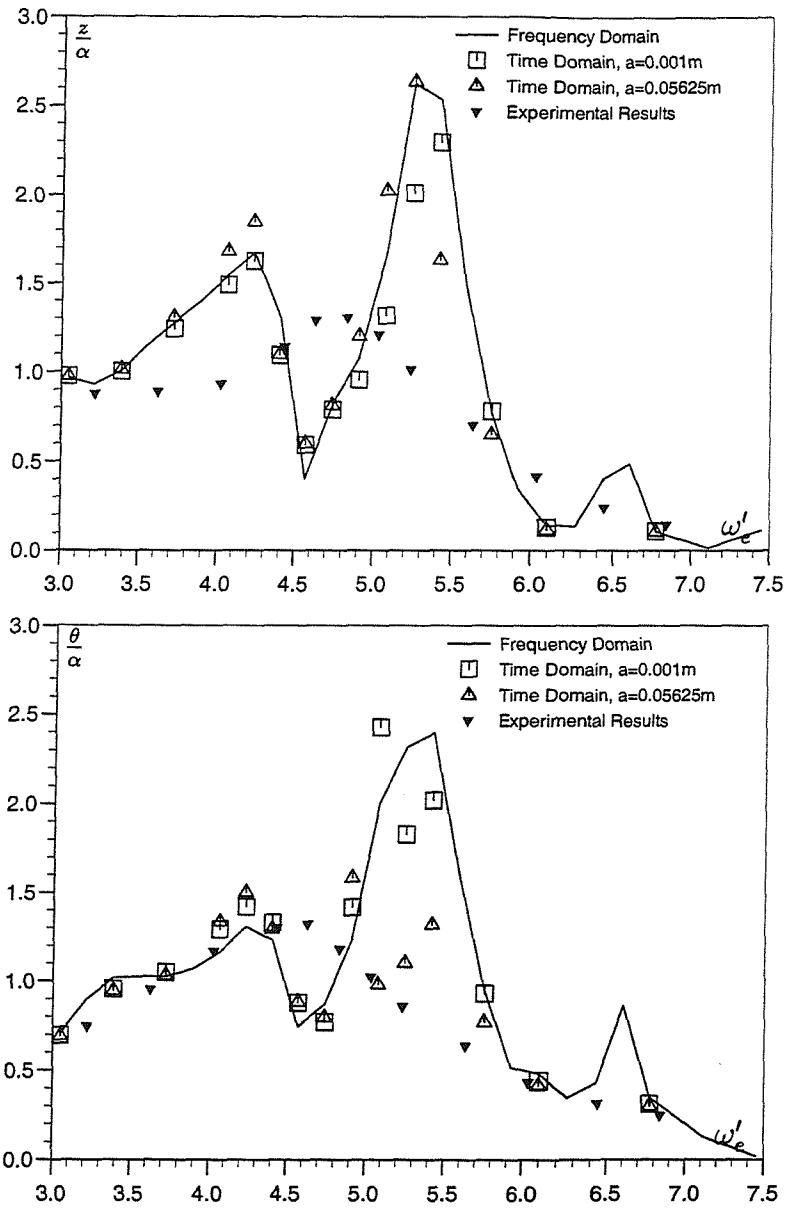

Figure 10.21: Heave and pitch response amplitude operators for *NPL5b* catamaran in head waves, using pulsating source data. L=4.5m, S/L = 0.4, Fn=0.53, $\chi_0 = 180°$.

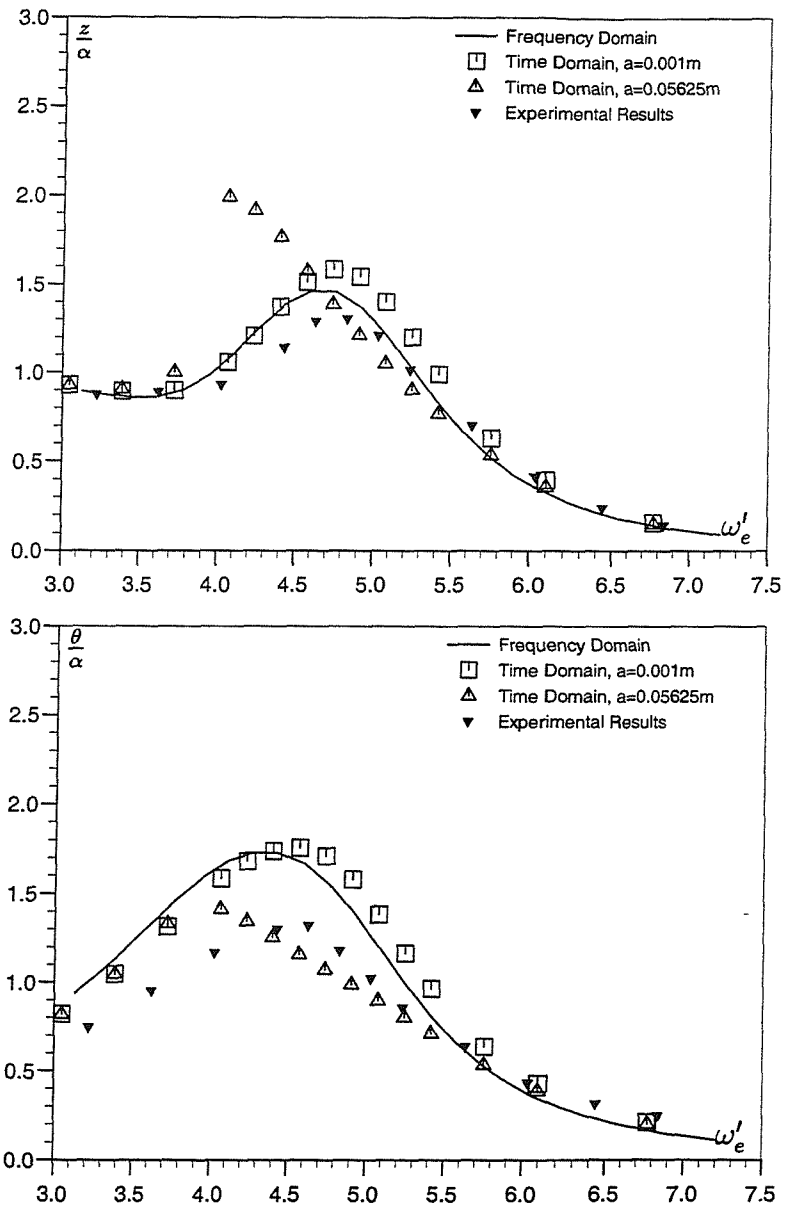

Figure 10.22: Heave and pitch response amplitude operators for *NPL5b* catamaran in head waves, using translating, pulsating source data. L=4.5m, S/L = 0.4, Fn=0.53, $\chi_0 = 180°$.

11 Conclusions and Recommendations

This thesis has demonstrated methods for the simulation of ship motions in waves. These simulation techniques incorporate convolution integrals, thus accounting for fluid memory effects. In addition, such methods are applicable for simulating the responses of vessels to arbitrary excitation. Two time domain simulation techniques have been developed. The first uses linear impulse response functions to describe the hydrodynamic actions (including wave excitation) and constant value restoring coefficients. The second method calculates the incident wave and restoring forces and moments using the instantaneous underwater portion of the hull at each time step.

A number of steps are required to obtain the necessary hydrodynamic data to perform these time domain simulations. The processes required to produce this data have made up a large part of this study and are an important part of the time domain simulation technique. Frequency domain data has been obtained from both theoretical and experimental sources, referenced to both equilibrium and body fixed axis systems. This data has been transformed to obtain the corresponding time domain impulse response functions, referenced to equilibrium and body fixed axes.

Equations have been presented for the rigid body motions of a vessel in waves, demonstrating that they can be referenced to either an equilibrium or a body fixed axis system. Whereas traditionally the choice of axis system has depended on the nature of the ship motion problem, transformations presented in Chapter 3 relate the equilibrium and body fixed axis systems, making it possible to use either axis system to describe a particular motion.

This is an advantage if the available hydrodynamic data is not referenced to the axis system preferred for the equations of motion. Relationships between kinematic actions referenced to both axis system have also been presented, allowing for the development of complete relationships between motions referenced to either axis system.

The ability to use data referenced to either axis system when performing time domain simulations in a particular axis system is useful. In this study the methods available for calculating theoretical frequency domain hydrodynamic data have referenced this data to equilibrium axes. Using the transformations discussed in Chapter 4 and Appendix A, it is possible to convert this data to a body fixed axis representation as required. Another benefit of being able to transform hydrodynamic data between axis systems is the ability to incorporate experimental data, regardless of the axis system to which it is referenced. Hence one may use data from such sources as planar motion experiments and seakeeping tests.

The conclusions of this study may be divided up into a number of parts:

Determination of Impulse Response Functions

Chapter 5 discussed the development of relationships between the frequency domain and time domain representations of hydrodynamic data. Impulse response functions describing radiation actions may be determined using either the real or imaginary parts of the frequency domain transfer function. In practice, the use of the real part is favoured as this results in faster convergence of the solution. The determination of the wave excitation impulse response functions presents an additional problem. One requires a means to account for the effect of a particular wave before it reaches the reference point at the centre of mass of the ship. Given that it is considered undesirable to move the reference point, the solution developed has been to represent these contributions using impulse response functions which include a negative time component. In doing so the relationship between the frequency domain and time domain data has had to be reconsidered. The impulse response functions are now calculated using both the real and imaginary parts of the frequency domain transfer function.

The effects of the hull idealisation used for the determination of the frequency domain hydrodynamic data were examined in Chapter 6. The determination of frequency domain data for the purpose of calculating impulse response functions from it introduces requirements not normally associated with frequency domain analysis. In particular, the need to calculate frequency domain data to high frequencies requires care to be taken in the distribution of singularities over the mean wetted surface. Given that the computational time required to determine the hydrodynamic data at each frequency is proportional to the square of the number of singularities, it is important to establish the best compromise between speed of solution and accuracy. Two different techniques for the generation of a panelled representation of the mean wetted surface of the hull have been compared. It has been found that the preferred method is one which will create a mesh representation which consists of a constant number of panels around sections of the ship, all having identical aspect ratio. In using this method it is possible to maintain sufficient resolution in the placement of the singularities to ensure that high frequency effects associated with very short wavelength (for both incident and radiated waves) are correctly represented.

Having established methods for the determination of frequency domain data, Chapter 7 examined the numerical evaluation of the impulse response functions. Numerical methods for the transformation of frequency domain data to the corresponding time domain representation have been presented. In addition, reverse transformations methods have been noted and used to determine the accuracy of the numerical transformation routines. It has been found that, in general, the numerical methods used are very accurate. For example, irregular frequency effects in the frequency domain data, typified by large spikes in the data at certain frequencies, are reflected in the corresponding impulse response functions as oscillations which are slow to die out. Inverse transformation sees these effects accurately recreated at the same frequencies as in the original data, giving confidence in the accuracy of the techniques. The exception to this statement occurs in cases where the frequency domain data tends to very high values at low frequency. Examples of such behaviour include pure pitch and yaw added mass coefficients referenced to equilibrium axes. For these particular data sets the numerical transformation methods do not produce accurate results. The proposed solution to this problem is to convert the frequency domain data to a body

fixed axis representation, for which none of the frequency domain data displays undesirable characteristics at low frequency.

Linear Time Domain Simulation

A linear time domain simulation technique has been presented in Chapter 9 in which the radiation and total wave excitation contributions are represented using a convolution integral formulation. Restoring force and moment contributions are determined using constant value restoring coefficients. Verification of the accuracy of the methods has been carried out by comparing the amplitude of time domain simulations in regular waves to frequency domain predictions. Using a *Series 60* model in head waves, it has been shown that the use of equilibrium axis equations of motion does not result in agreement with frequency domain predictions. By contrast, when using a body fixed axis formulation, the agreement with frequency domain predictions is very good. Using a process of elimination, it has been shown that the inaccuracies in the predictions using equilibrium axis data may be attributed to the pure pitch contributions. As noted earlier, the tendency of pure pitch and yaw added mass coefficients to reach very high values at low frequency prevents accurate calculation of the corresponding impulse response functions. It is these inaccuracies that cause the incorrect time domain predictions. It has been shown that these inaccuracies will be present regardless of the forward speed value or whether the forward speed effects are accounted for by mathematical correction (using the pulsating source method) or explicitly (using the translating, pulsating source method). This final conclusion is confirmed by comparing simulations using pulsating source and translating, pulsating source data for an *NPL5b* monohull at a higher speed, $F_n = 0.53$, where similar results are obtained. Hence, it is concluded that a body fixed axis formulation is the best method to use for a time domain simulation technique.

Subsequently, the body fixed axis time domain method has been used to simulate the motions of a *Series 60* model at a range of headings. Predictions of symmetric motions for constant heading in head, oblique and beam wave have all shown good agreement with frequency domain predictions.

It has been shown that when time domain simulations are performed for the anti-symmetric motions of sway and yaw, viscous effects must be accounted for. These effects have been incorporated using a so-called "viscous ramp". Comparison of simulations using hydrodynamic data both with and without viscous contributions suggests that neglecting viscous effects results in a lightly damped condition, giving unstable solutions. Simulations of anti-symmetric motions must be carried out in the knowledge that the wave excitation impulse response functions are specific to the initial heading. Large changes in heading during the simulation will result in the wave excitation contributions no longer being strictly correct, although a solution will continue to be calculated, requiring care when interpreting the predictions.

In addition to the *Series 60* model, the motions of an *NPL5b* catamaran with varying demi-hull separation have been modelled. Frequency domain hydrodynamic data was calculated using both pulsating source and translating, pulsating source methods. It was found that the pulsating source method over predicts the interaction effects between the catamaran hulls. The frequencies at which these exaggerated effects occur are characterised by large spikes in the frequency domain data. These spikes have an adverse effect on the subsequent calculation of the corresponding impulse response functions, along the same lines as the irregular frequency effects noted earlier, but more severe. The overprediction of the interaction between the hulls is worst for the wider hull separation, which results in the impulse response functions exhibiting oscillations which are very slow to die out. These oscillations result in time domain motion predictions which do not match frequency domain predictions well. By comparison, frequency domain data determined using the translating, pulsating source method did not contain these overpredicted interaction effects. Consequently the corresponding impulse response functions did not show the oscillations seen previously and time domain simulations using these impulse response functions gave good agreement with frequency domain predictions.

Partly Non-Linear Time Domain Simulation

Having established the stability and accuracy of the linear time domain methods referenced to body fixed axes, the formulation has been altered in incorporate non-linear incident wave

and restoring force/moment contributions. Whilst radiation and diffraction contributions continue to be described using linear convolution integrals, the incident wave and restoring contributions are calculated using the instantaneous underwater portion of the hull at each time step. This allows for predictions of motions where non-linear body geometry effects, such as flare and overhangs, may be influential. In addition, simulations may be carried at wave amplitudes similar to experiments, enabling comparison.

This partly non-linear method has initially been used to simulate the symmetric motions of a *Series 60* model in head waves. Using waves with very small amplitude, commensurate with the assumptions of linearity, good agreement has been found with linear predictions. Increasing the wave amplitude to match that of experimental results has resulted in only small changes in the predicted amplitude, as would be expected for an essentially wall sided ship.

Simulations of the coupled sway, heave, pitch and yaw motions were carried out using hydrodynamic data both with and without viscous contributions included. The partly non-linear method introduces a coupling between the symmetric and anti-symmetric motions not present in the linear method. Simulations of the coupled sway, heave, pitch and yaw motions at identical headings to those tested using the linear time domain method appeared to have offered some improvement. In particular, the predicted direction of drift, with the waves, appears to be more realistic.

The motions of an *S175* containership, with flared bow and moderate stern overhang, have also been simulated. There has been found to be generally good agreement between the trends of the simulated motions and both experiments and similar theoretical methods as the amplitude of the incident waves is increased, with differences mostly in the pitch motions. It is thought that these differences may be attributed to the fact that non-linear hydrodynamic effects, such as damping, are not accounted for in this method.

In addition to the two merchant ship hull forms, the partly non-linear method has also been used to simulate the motions of a yacht hull form. The yacht hull form displays considerable flare above the calm waterline and would be expected to show non-linear effects.

Time domain predictions using the partly non-linear method have shown an improvement in the predicted heave and pitch responses in head waves of identical amplitude to the experiments when compared to linear predictions.

The motions of an *NPL5b* catamaran with varying hull separation have also been predicted, using both pulsating source and translating, pulsating source hydrodynamic data. Responses predicted using pulsating source method data do not agree with experimental results, except at low frequencies. This is a result of the overestimation of the interactions between the hulls and the consequent effects on the relevant impulse response functions. Increasing the wave amplitude appears to only affect the responses at relatively high frequencies. Responses predicted using translating, pulsating source method data have been found to show reasonable agreement with experimental results for the prediction of heave responses, though poorer agreement for pitch responses. Increasing the wave amplitude results, in general, in mixed agreement with experimental results in the vicinity of resonance. In certain cases the agreement is poor, while in others, such as the predicted pitch responses for S/L = 0.4, there is reasonably good agreement with experiments. Overall it is considered that the use of translating, pulsating source data represents the best method for predicting multi-hull motions, as it accounts more accurately for the interactions between the component hulls.

Recommendations for Future Research

It is an inevitable, and desirable, consequence of any study that a number of questions are posed which, due to restrictions on the time available, may not be fully answered. In mentioning some of these, it is hoped that they may provide the basis for further advancement of the work presented in this thesis.

One aspect of incorporating a convolution integral formulation in a time domain simulation technique is the possibility of using arbitrary wave excitation. This study has only examined regular waves, in doing so attempting the verify the accuracy of the numerical methods by enabling comparison with frequency domain methods. The introduction of arbitrary wave excitation could provide useful insights. Time simulations over long periods

could be conducted and the results subjected to statistical analysis. Such analysis could, for example, be used to determine the operational reliability of a vessel based on a variety of motion related criterion, i. e. seasickness, systems operation.

A technique using arbitrary wave excitation would most likely benefit from the introduction of a more accurate method of solution to the time domain equations of motion. Whilst the fourth order Runge-Kutta method is sufficiently robust for most seakeeping applications, the Runge-Kutta-Fehlberg method, which has an order of five, is worth noting. This method involves the solution of the problem using two different Runge-Kutta methods, of order four and five. The solution of the two methods requires the calculation of only six auxiliary solutions per step and allows the determination of an error estimate using the difference between the two methods. This ability to estimate the error means that this method can be used as an adaptive time stepping scheme. This means that, based on the calculated error at a particular step, the value of the step may be altered to maintain the error within predefined bounds. Thus, it is possible to have a method of solution which automatically selects the most appropriate time step, using smaller steps when needed and larger ones where the solution is more easily estimated. This could be of considerable importance should arbitrary motions be considered, given that there may be sudden large changes in the solution at certain points within the calculated time range. Further investigations which incorporate arbitrary excitation would most likely benefit from the implementation of such a technique.

The use of the instantaneous underwater surface in the partly non-linear time domain method introduces a coupling between symmetric and anti-symmetric motions not accounted for by linear methods. This makes possible the investigation of coupled heave, roll and pitch motions of catamarans in oblique waves. It is known that the "corkscrewing" motions of such vessels can be extremely uncomfortable for passengers. Investigations could be made on the relationship between the sea state, vessel heading/speed and the thresholds for passenger discomfort.

The partly non-linear method requires a quadrilateral panel representation of the entire hull surface for the calculation of the instantaneous incident wave and restoring forces. It has

been shown in Chapter 6 that the hull representation can have a considerable effect on the calculation of the frequency domain hydrodynamic data. It would be worthwhile to ascertain the effects of increasing the refinement of the mesh representation on the calculation of the instantaneous forces and moments.

Time domain simulation of the manoeuvring of vessels in waves using the methods presented in this thesis presents a problem at present, due to the fact that the diffraction impulse response functions are correct for the initial heading of the vessel only. It would be interesting to investigate the possibility of accounting for the changing nature of the diffraction contributions as the heading of the vessel changes, thus allowing for accurate simulation of manoeuvring in waves.

Last, but by no means least, is the calculation of radiation and diffraction contributions which account for the instantaneous underwater portion of the hull at each time step, thus allowing fully non-linear time domain simulation. Such methods have been the subject of much study and represent the ultimate in ship motions prediction. It is hoped that the results of this thesis inspire work in this area by, firstly, suggesting that improvements over linear thoery are possible and, secondly, revealing the limitations of a method that only partly accounts for non-linear effects.

Appendices

A Equilibrium and Body Fixed Axis Relationships

A.1 Kinematic Relationships

From Equations 3.21, 3.22 and Equations 3.3, 3.4, the body fixed axis motion variables may be expressed in terms of the equilibrium axis equivalents as follows [1]

$$\begin{aligned} \overline{U} + u_X &= \overline{U} + u = \overline{U} + \dot{\eta}_1 - \overline{\zeta}\dot{\eta}_5 & \omega_X &= p = \dot{\phi} = \dot{\eta}_4 \\ u_Y &= v + \bar{U}\psi = \dot{\eta}_2 + \overline{\zeta}\dot{\eta}_4 & \omega_Y &= q = \dot{\theta} = \dot{\eta}_5 \\ u_Z &= w - \bar{U}\theta = \dot{\eta}_3 & \omega_Z &= r = \dot{\psi} = \dot{\eta}_6 \end{aligned} \tag{A.1}$$

$$\begin{aligned} \dot{u}_X &= \dot{u} = \ddot{\eta}_1 - \overline{\zeta}\ddot{\eta}_5 & \Omega_X &= \dot{p} = \ddot{\phi} = \ddot{\eta}_4 \\ \dot{u}_Y &= \dot{v} + \bar{U}r = \ddot{\eta}_2 + \overline{\zeta}\ddot{\eta}_4 & \Omega_Y &= \dot{q} = \ddot{\theta} = \ddot{\eta}_5 \\ \dot{u}_Z &= \dot{w} + \bar{U}q = \ddot{\eta}_3 & \Omega_Z &= \dot{r} = \ddot{\psi} = \ddot{\eta}_6 \end{aligned} \tag{A.2}$$

$$\begin{aligned} x^* &= \int_0^t u\,dt = \int_0^t \left\{\dot{\eta}_1 - \overline{U}\dot{\eta}_5\right\} dt = \eta_1 - \overline{\zeta}\eta_5 \\ y^* &= \int_0^t \{v + \psi\}\, dt = \int_0^t \left\{\dot{\eta}_2 + \overline{\zeta}\dot{\eta}_4\right\} dt = \eta_2 + \overline{\zeta}\eta_4 \\ z^* &= \int_0^t \left\{w - \overline{U}\theta\right\} dt = \int_0^t \{\dot{\eta}_3\}\, dt = \eta_3 \end{aligned} \tag{A.3}$$

Similarly, it may be shown that the equilibrium axis motion variables may be represented in terms of their body fixed equivalents as follows, for symmetric motions

$$\begin{aligned} \ddot{\eta}_1 &= \dot{u} + \overline{\zeta}\dot{q} & \dot{\eta}_1 &= u + \overline{\zeta}q \\ \ddot{\eta}_3 &= \dot{w} - \dot{q}\overline{U} & \dot{\eta}_3 &= w + \dot{q}(\overline{U}/\omega_e^2) \\ \ddot{\eta}_5 &= \dot{q} & \dot{\eta}_5 &= q \end{aligned} \tag{A.4}$$

[1] These relationships ignore the products of small quantities and assume that the origin of the equilibrium axis system is on the centre line directly above (or below) the centre of mass

$$\begin{aligned}\eta_1 &= \int_0^t \left\{u + \overline{\zeta} q\right\}\, dt \equiv x^* \\ \eta_3 &= \int_0^t \left\{w + \dot{q}(\overline{U}/\omega_e^2)\right\}\, dt \equiv z^* \\ \eta_5 &= \int_0^t \{q\}\, dt = \theta\end{aligned} \tag{A.5}$$

and for anti-symmetric motions

$$\begin{aligned}\ddot{\eta}_2 &= \dot{v} - \overline{\zeta}\dot{p} + \overline{U} r & \dot{\eta}_2 &= v - \overline{\zeta} p - \dot{r}(\overline{U}/\omega_e^2) \\ \ddot{\eta}_4 &= \dot{p} & \dot{\eta}_4 &= p \\ \ddot{\eta}_6 &= \dot{r} & \dot{\eta}_6 &= r\end{aligned} \tag{A.6}$$

$$\begin{aligned}\eta_2 &= \int_0^t \left\{v - \overline{\zeta} p - \dot{r}(\overline{U}/\omega_e^2)\right\}\, dt \equiv y^* \\ \eta_4 &= \phi \\ \eta_6 &= \psi\end{aligned} \tag{A.7}$$

A.2 Hydrodynamic Relationships

Surge Relations

Oscillatory Derivatives referenced to body fixed axis	Oscillatory Derivatives in terms of hydrodynamic coefficients referenced to equilibrium axes.
Acceleration Derivatives	
$\tilde{X}_{\dot{u}}(\omega_e)$	$-A_{11}(\omega_e)$
$\tilde{X}_{\dot{w}}(\omega_e)$	$-A_{13}(\omega_e)$
$\tilde{X}_{\dot{q}}(\omega_e)$	$-A_{15}(\omega_e) - \overline{\zeta} A_{11}(\omega_e) - (\overline{U}/\omega_e^2) B_{13}(\omega_e)$
Velocity Derivatives	
$\tilde{X}_u(\omega_e)$	$-B_{11}(\omega_e)$
$\tilde{X}_w(\omega_e)$	$-B_{13}(\omega_e)$
$\tilde{X}_q(\omega_e)$	$-B_{15}(\omega_e) - \overline{\zeta} B_{11}(\omega_e) + \overline{U} A_{13}(\omega_e)$
External Actions	
$X(t)$	$H_1(t)$

Sway Relations

Oscillatory Derivatives referenced to body fixed axis	Oscillatory Derivatives in terms of hydrodynamic coefficients referenced to equilibrium axes.
Acceleration Derivatives	
$\tilde{Y}_{\dot{v}}(\omega_e)$	$-A_{22}(\omega_e)$
$\tilde{Y}_{\dot{p}}(\omega_e)$	$\overline{\zeta}A_{22}(\omega_e) - A_{24}(\omega_e)$
$\tilde{Y}_{\dot{r}}(\omega_e)$	$(\overline{U}/\omega_e^2)B_{22}(\omega_e) - A_{26}(\omega_e)(\omega_e)$
Velocity Derivatives	
$\tilde{Y}_{v}(\omega_e)$	$-B_{22}(\omega_e)$
$\tilde{Y}_{p}(\omega_e)$	$\overline{\zeta}B_{22}(\omega_e) - B_{24}(\omega_e)$
$\tilde{Y}_{r}(\omega_e)$	$-\overline{U}A_{22}(\omega_e) - B_{26}(\omega_e)$
External Actions	
$Y(t)$	$H_2(t)$

Heave Relations

Oscillatory Derivatives referenced to body fixed axis	Oscillatory Derivatives in terms of hydrodynamic coefficients referenced to equilibrium axes.
Acceleration Derivatives	
$\tilde{Z}_{\dot{u}}(\omega_e)$	$-A_{31}(\omega_e)$
$\tilde{Z}_{\dot{w}}(\omega_e)$	$-A_{33}(\omega_e)$
$\tilde{Z}_{\dot{q}}(\omega_e)$	$-A_{35}(\omega_e) - \overline{\zeta}A_{31}(\omega_e) - (\overline{U}/\omega_e^2)B_{33}(\omega_e)$
Velocity Derivatives	
$\tilde{Z}_{u}(\omega_e)$	$-B_{31}(\omega_e)$
$\tilde{Z}_{w}(\omega_e)$	$-B_{33}(\omega_e)$
$\tilde{Z}_{q}(\omega_e)$	$-B_{35}(\omega_e) - \overline{\zeta}B_{31}(\omega_e) - (\overline{U}/\omega_e^2)B_{33}(\omega_e)$
Restoring Coefficients	
Z_{z^*}	$-C_{33}$
Z_{θ}	$-C_{35}$
External Actions	
$Z(t)$	$H_3(t)$

Roll Relations

Oscillatory Derivatives referenced to body fixed axis	Oscillatory Derivatives in terms of hydrodynamic coefficients referenced to equilibrium axes.
Acceleration Derivatives	
$\tilde{K}_{\dot{v}}(\omega_e)$	$\overline{\zeta}A_{22}(\omega_e) - A_{42}(\omega_e)$
$\tilde{K}_{\dot{p}}(\omega_e)$	$\overline{\zeta}\{A_{42}(\omega_e) + A_{24}(\omega_e)\} - \{\overline{\zeta}^2 A_{22}(\omega_e) + A_{44}(\omega_e)\}$
$\tilde{K}_{\dot{r}}(\omega_e)$	$\overline{\zeta}A_{26}(\omega_e) - A_{46}(\omega_e) + (\overline{U}/\omega_e^2)\{B_{42}(\omega_e) - \overline{\zeta}B_{22}(\omega_e)\}$
Velocity Derivatives	
$\tilde{K}_v(\omega_e)$	$\overline{\zeta}B_{22}(\omega_e) - B_{42}(\omega_e)$
$\tilde{K}_p(\omega_e)$	$\overline{\zeta}\{B_{42}(\omega_e) + B_{24}(\omega_e)\} - \{\overline{\zeta}^2 B_{22}(\omega_e) + B_{44}(\omega_e)\}$
$\tilde{K}_r(\omega_e)$	$\overline{\zeta}B_{26}(\omega_e) - B_{46}(\omega_e) - \overline{U}\{A_{42}(\omega_e) - \overline{\zeta}A_{22}(\omega_e)\}$
Restoring Coefficients	
K_ϕ	C_{44}
External Actions	
$K(t)$	$H_4(t)$

Pitch Relations

Oscillatory Derivatives referenced to body fixed axis	Oscillatory Derivatives in terms of hydrodynamic coefficients referenced to equilibrium axes.
Acceleration Derivatives	
$\tilde{Z}_{\dot{u}}(\omega_e)$	$-A_{51}(\omega_e) - \overline{\zeta}A_{11}(\omega_e)$
$\tilde{Z}_{\dot{w}}(\omega_e)$	$-A_{53}(\omega_e) - \overline{\zeta}A_{13}(\omega_e)$
$\tilde{Z}_{\dot{q}}(\omega_e)$	$-A_{55}(\omega_e) - \overline{\zeta}\{A_{51}(\omega_e) + A_{15}(\omega_e)\}$ $-\overline{\zeta}^2 A_{11}(\omega_e) - (\overline{U}/\omega_e^2)\{B_{53}(\omega_e) + \overline{\zeta}B_{13}(\omega_e)$
Velocity Derivatives	
$\tilde{Z}_u(\omega_e)$	$-B_{51}(\omega_e) - \overline{\zeta}B_{11}(\omega_e)$
$\tilde{Z}_w(\omega_e)$	$-B_{53}(\omega_e) - \overline{\zeta}B_{13}(\omega_e)$
$\tilde{Z}_q(\omega_e)$	$-B_{55}(\omega_e) - \overline{\zeta}\{B_{51}(\omega_e) + B_{15}(\omega_e)\}$ $-\overline{\zeta}^2 B_{11}(\omega_e) + \overline{U}\{B_{53}(\omega_e) + \overline{\zeta}B_{13}(\omega_e)$
Restoring Coefficients	
$M_{z^\bullet}$	$-C_{53}$
M_θ	$-C_{55}$
External Actions	
$M(t)$	$H_5(t) + \overline{\zeta}H_1(t)$

Yaw Relations

Oscillatory Derivatives referenced to body fixed axis	Oscillatory Derivatives in terms of hydrodynamic coefficients referenced to equilibrium axes.
Acceleration Derivatives	
$\tilde{N}_{\dot{v}}(\omega_e)$	$-A_{62}(\omega_e)$
$\tilde{N}_{\dot{p}}(\omega_e)$	$\overline{\zeta}A_{62}(\omega_e) - A_{64}(\omega_e)$
$\tilde{N}_{\dot{r}}(\omega_e)$	$(\overline{U}/\omega_e^2)B_{62}(\omega_e) - A_{66}(\omega_e)(\omega_e)$
Velocity Derivatives	
$\tilde{N}_v(\omega_e)$	$-B_{62}(\omega_e)$
$\tilde{N}_p(\omega_e)$	$\overline{\zeta}B_{62}(\omega_e) - B_{64}(\omega_e)$
$\tilde{N}_r(\omega_e)$	$-\overline{U}A_{62}(\omega_e) - B_{66}(\omega_e)$
External Actions	
$N(t)$	$H_6(t)$

B Hull Forms

B.1 *Series 60*

Quantity	Symbol	Value
Length (between perpendiculars)	L_{BP}	3.048 m
Beam	B	0.435 m
Draft	T	0.174 m
Displacement	∇	0.1616 m^2
Block Coefficient	C_B	0.70
Longitudinal Centre of Buoyancy (fwd. of midships)	LCB	0.015 m
Longitudinal Centre of Gravity (fwd. of midships)	LCG	0.015 m
Vertical Centre of Gravity (below waterline)	VCG	0.028 m
Roll Inertia (about centre of gravity)	I_{44}	3.265 kg m^2
Pitch Inertia (about centre of gravity)	I_{55}	93.83 kg m^2
Yaw Inertia (about centre of gravity)	I_{66}	93.83 kg m^2
Coupled Roll-Yaw Inertia (about centre of gravity)	I_{46}	0.40 kg m^2

Table B.1: Particulars of *Series 60* hullform.

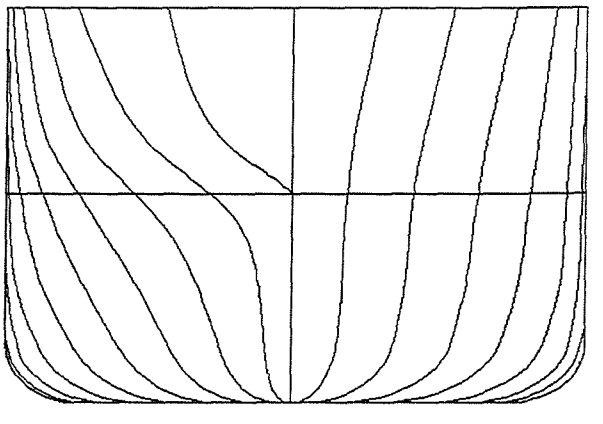

Figure B.1: Lines plan for Todd *Series 60* model.

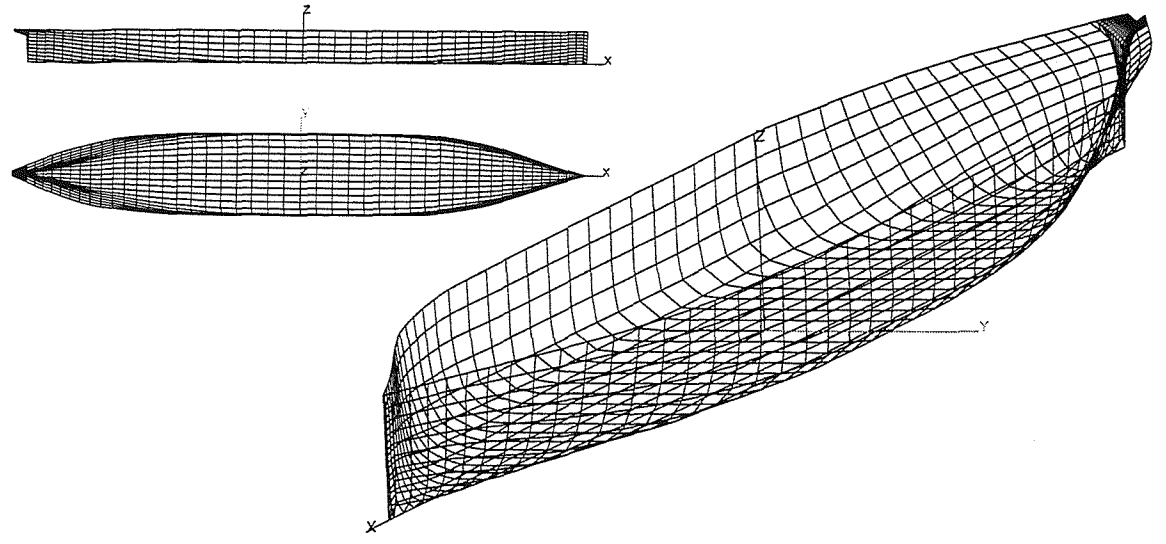

Figure B.2: Discretisation of underwater surface of *Series 60* monohull, using a fixed number of panels per section. 10 panels per section, aspect ratio=2.0, total number of panels 1040

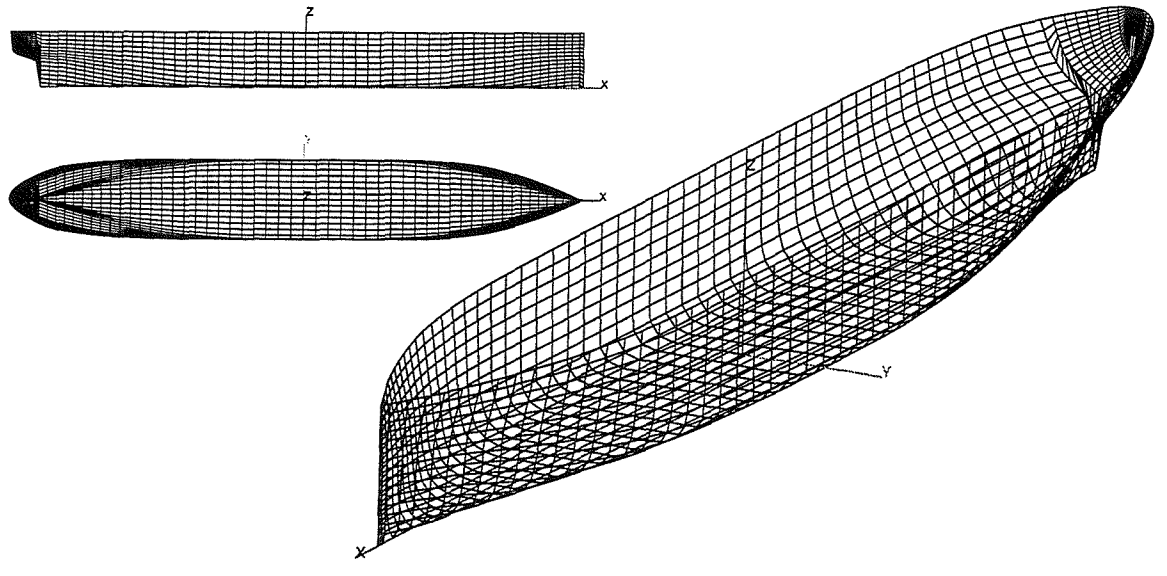

Figure B.3: Discretisation of entire surface of *Series 60* monohull, using a variable number of panels per section. 15 panels per section, aspect ratio=2.0, total number of panels 1830

B.2 *NPL5b*

Quantity	Monohull	Catamaran	
		S/L = 0.2	S/L = 0/4
L_{BP}	4.5 m	4.5 m	4.5 m
B	0.409 m	0.9 m *	1.8 m *
T	0.205 m	0.205 m	0.205 m
∇	0.14838 m^2	0.29676 m^2	0.29676 m^2
C_B	0.40	0.40	0.40
LCB	-0.288 m	-0.288 m	-0.288 m
LCG	-0.288 m	-0.288 m	-0.288 m
VCG	-0.102 m	-0.102 m	-0.102 m
K_{44}	—	$0.112L_{BP}$	$0.204L_{BP}$
K_{55}	$0.26L_{BP}$	$0.26L_{BP}$	$0.255L_{BP}$
K_{66}	—	$0.279L_{BP}$	$0.323L_{BP}$
* Separation between centrelines of demihulls.			

Table B.2: Particulars of *NPL5b* hullform in monohull and catamaran configurations.

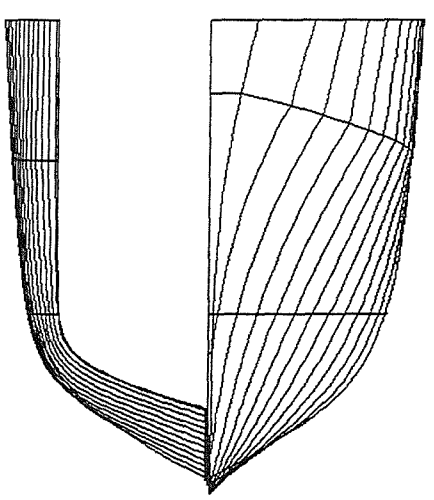

Figure B.4: Lines plan for *NPL5b* demi-hull.

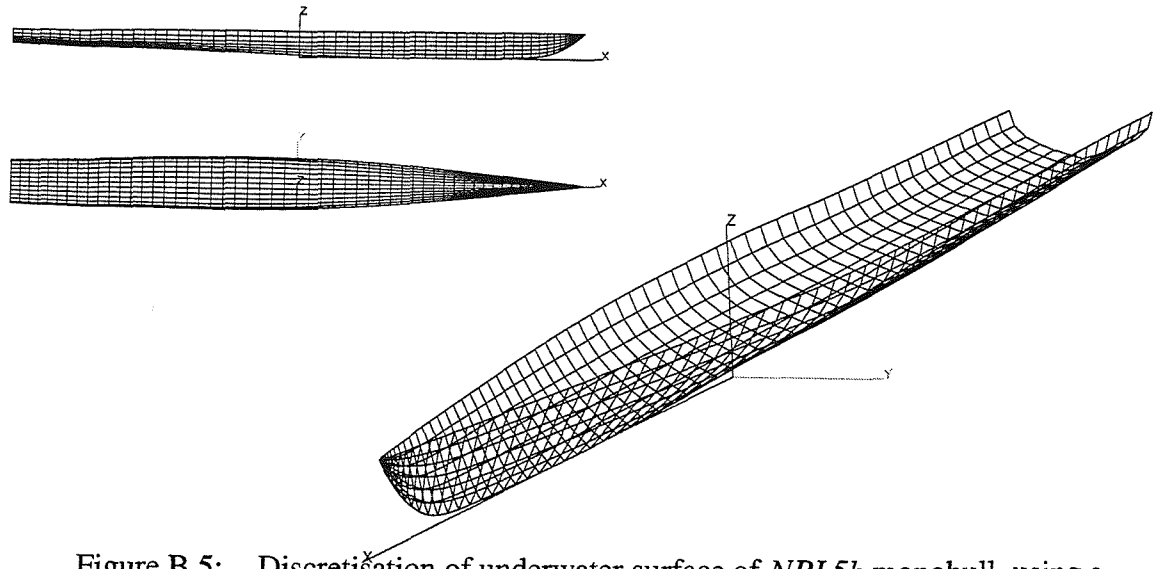

Figure B.5: Discretisation of underwater surface of *NPL5b* monohull, using a fixed number of panels per section. 6 panels per section, aspect ratio=2.0, total number of panels 500

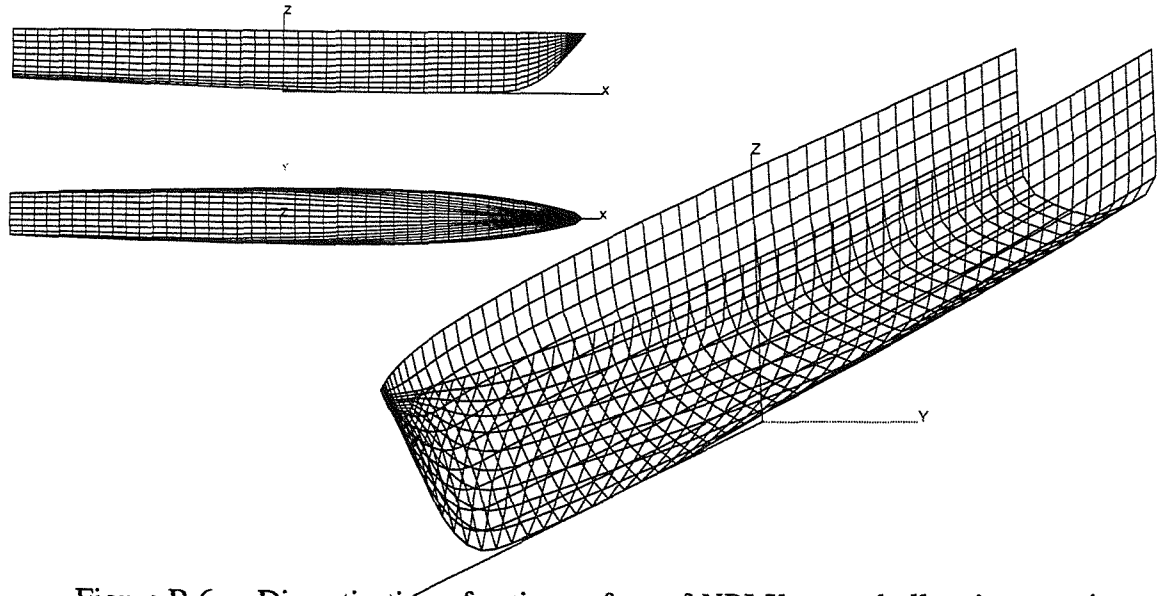

Figure B.6: Discretisation of entire surface of *NPL5b* monohull, using a variable number of panels per section. 10 panels per section, aspect ratio=2.0, total number of panels 906

B.3 *S175* Containership

Quantity	Value
L_{BP}	175 m
B	25.4 m
T	9.5 m
∇	24138 m^2
LCG	-2.5 m
VCG	2.844 m
K_{55}	$0.236L_{BP}$

Table B.3: Particulars of S175 containership hullform.

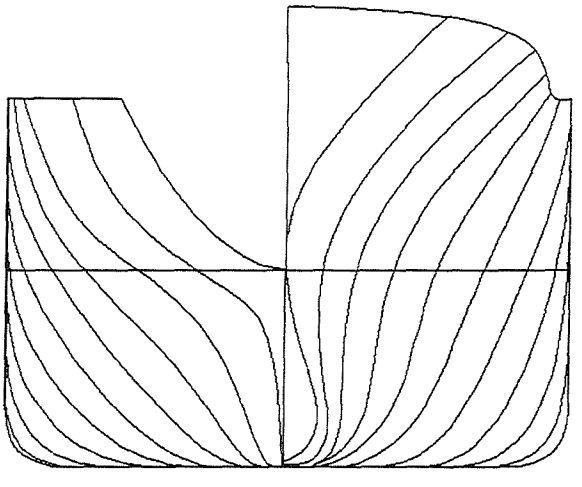

Figure B.7: Lines plan for S175 containership.

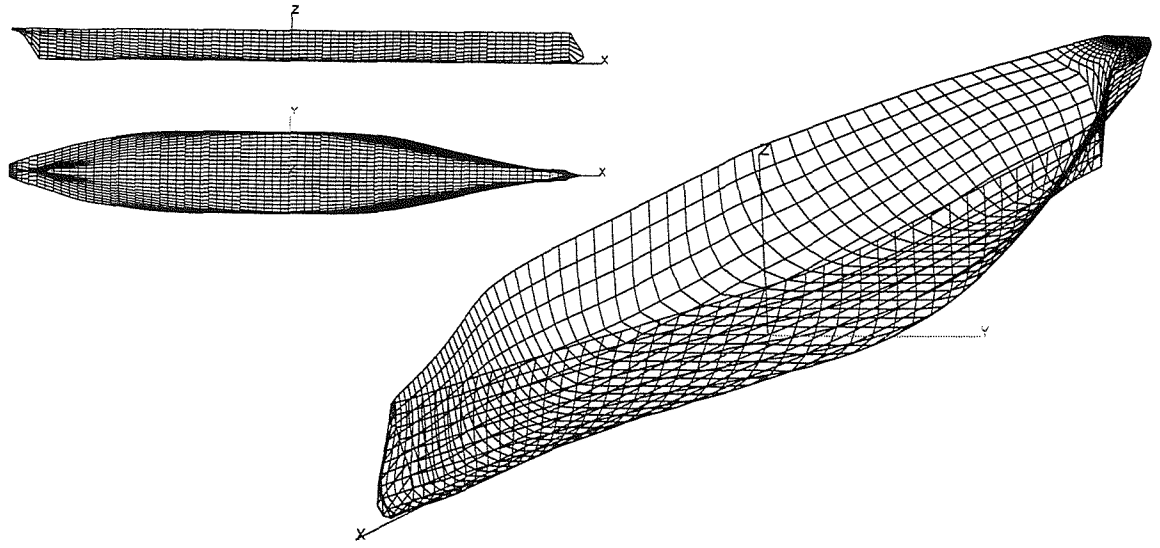

Figure B.8: Discretisation of underwater surface of *S175* containership, using a fixed number of panels per section. 10 panels per section, aspect ratio=2.0, total number of panels 884

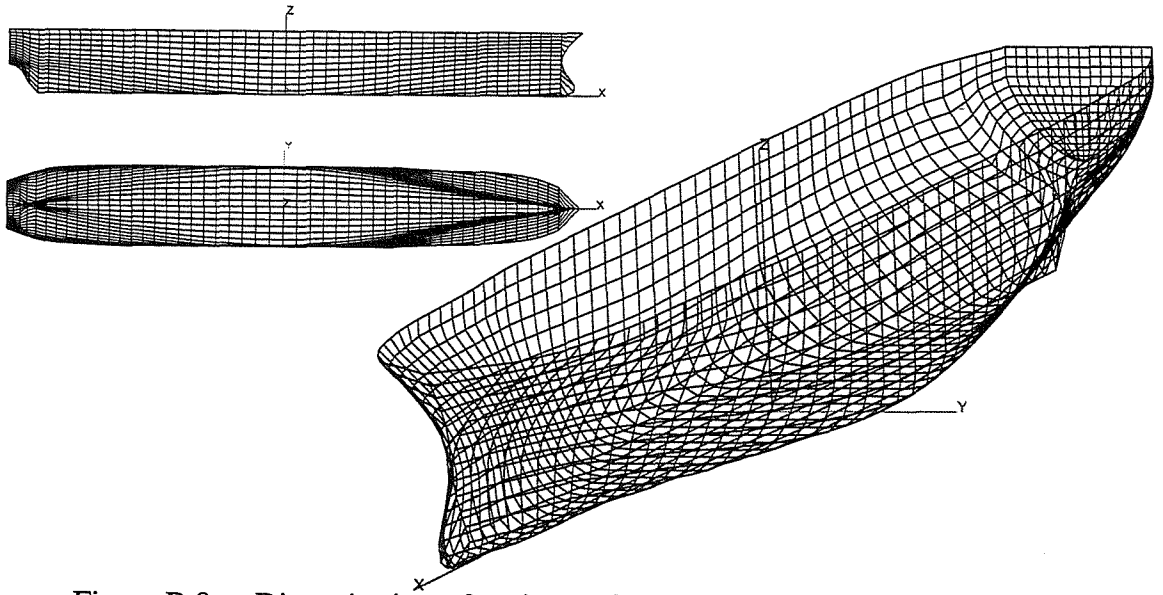

Figure B.9: Discretisation of entire surface of *S175* monohull, using a variable number of panels per section. 15 panels per section, aspect ratio=2.0, total number of panels 1676

B.4 Yacht Hull Form

Quantity	Value
L_{BP}	9.367 m
B	3.32 m
T	0.423 m
∇	4.2862 m^2
LCG	-0.25 m
VCG	0.158 m
K_{55}	$0.25L_{BP}$

Table B.4: Particulars of yacht hull form.

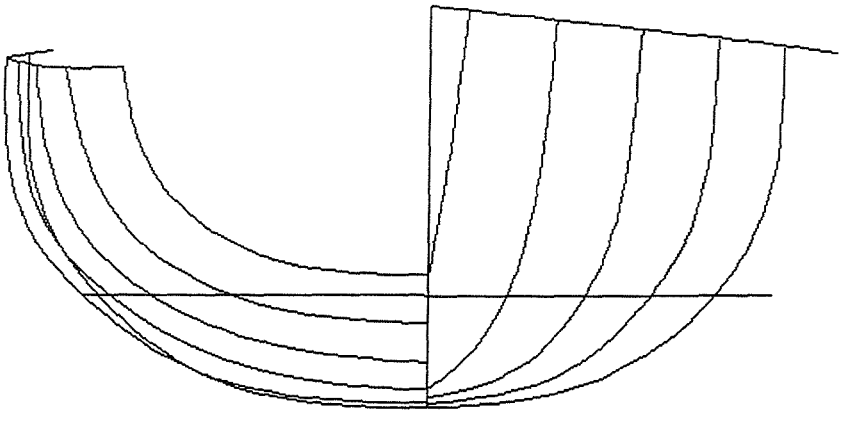

Figure B.10: Lines plan for yacht hull form.

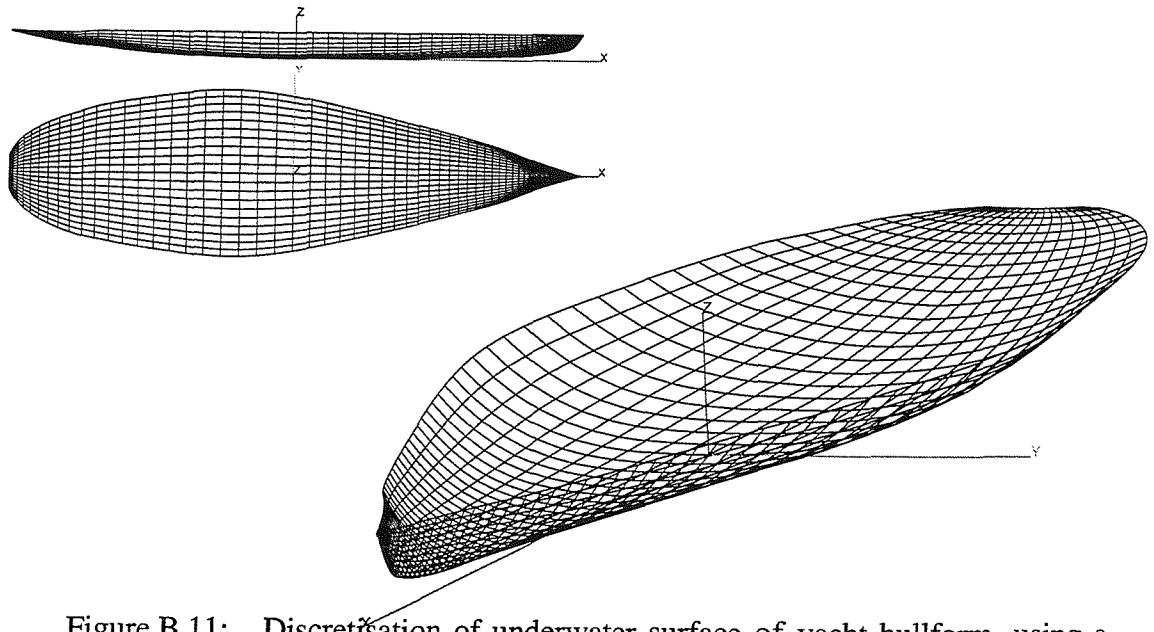

Figure B.11: Discretisation of underwater surface of yacht hullform, using a fixed number of panels per section. 10 panels per section, aspect ratio=2.0, total number of panels 876

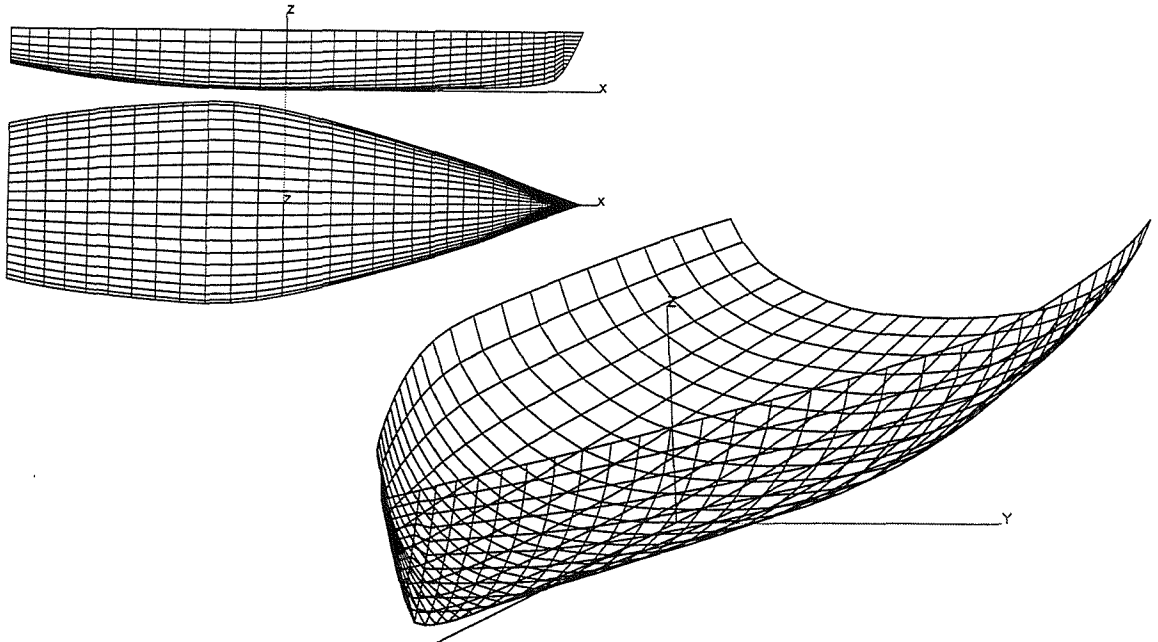

Figure B.12: Discretisation of entire surface of yacht hullform, using a variable number of panels per section. 15 panels per section, aspect ratio=2.0, total number of panels 1504

C Time Domain Analysis of Vessels in Waves Accounting for Fluid Memory Effects

Published in :

Proceedings of NAV 2000, International Conference on Ship and Shipping Research, Volume II, Paper No. 9.4.,Sept. 2000,Venice, Italy.

TIME DOMAIN ANALYSIS OF VESSELS IN WAVES ACCOUNTING FOR FLUID MEMORY EFFECTS

P.A. Bailey, E.J. Ballard, D.A. Hudson and P. Temarel.

School of Engineering Sciences, Ship Science
University of Southampton
Southampton SO17 1BJ
United Kingdom

ABSTRACT

A time domain mathematical model of ship motions allows for the incorporation of arbitrary and/or transient excitation, such as the influence of control surfaces and random waves. The dynamic behaviour of rigid vessels in waves is investigated using a time domain analysis, fully accounting for fluid memory effects. To this end radiation and wave excitation contributions are described through a convolution integral formulation. The impulse response functions in these convolution integrals are obtained from the frequency domain hydrodynamic damping and wave excitation respectively. The impulse response functions for the latter include values in the negative time to account for the influence of a particular wave before it reaches the reference point.

Results are presented for heave and pitch motions in regular waves. A Series 60 mono-hull is used to demonstrate the applicability of the method. Time domain simulation results in sinusoidal waves are discussed with reference to frequency domain predictions.

1. INTRODUCTION

Traditionally, seakeeping analyses simplify the representation of motion dependent hydrodynamic actions (i.e. radiation problem) by assuming that the motions are either sinusoidal or slow. In these limiting cases the memory effects are not apparent. However, for the general case it has been shown that fluid actions on a ship are dependent upon the previous motions of the vessel [1]. The cause of this memory effect can be linked to the motion of the fluid induced by the vessel (e.g. surface waves).

The use of a convolution integral formulation allows for memory effects to be included in the modelling of ship responses to arbitrary wave excitation. This enables more realistic modelling of ship motions in seaways. The investigation herein uses a frequency domain rigid body motion prediction method to determine the frequency dependent hydrodynamic coefficients (radiation terms) and wave excitation forces of a ship travelling in a sinusoidal seaway [2,3]. Using Fourier transforms these frequency domain characteristics are transformed into time domain impulse response functions. These are then used as part of a convolution integral formulation of the equations of motion to allow the time domain simulation of the vessel's response.

The time domain simulation is carried out using a fourth order Runge-Kutta time stepping technique to solve the equations of motion. These methods are validated by comparing the simulated heave and pitch responses with the corresponding frequency domain predictions. The comparisons are made for sinusoidal waves, and demonstrate the validity of the numerical methodologies used.

2. AXIS SYSTEM AND EQUATIONS OF MOTION

Seakeeping theory has traditionally referenced the rigid body motions of a vessel to equilibrium axes. This axis system moves with the ship, but remains unaffected by the vessel's parasitic motions.

The equilibrium axis system used here is a right handed axis system *Cxyz* such that the origin *C* is at the centre of gravity. The *z*-axis is positive upwards and the *x* and *y* axes lie in a plane parallel to the undisturbed free surface. This equilibrium axis system translates with velocity U in the positive *x*-direction.

The equations of motion for coupled heave and pitch, considered in this paper, are as follows:

$$\begin{bmatrix} m & 0 \\ 0 & I_{55} \end{bmatrix} \begin{bmatrix} \ddot{\eta}_3 \\ \ddot{\eta}_5 \end{bmatrix} = -\begin{bmatrix} A_{33} & A_{35} \\ A_{53} & A_{55} \end{bmatrix} \begin{bmatrix} \ddot{\eta}_3 \\ \ddot{\eta}_5 \end{bmatrix} - \begin{bmatrix} B_{33} & B_{35} \\ B_{53} & B_{55} \end{bmatrix} \begin{bmatrix} \dot{\eta}_3 \\ \dot{\eta}_5 \end{bmatrix} - \begin{bmatrix} C_{33} & C_{35} \\ C_{53} & C_{55} \end{bmatrix} \begin{bmatrix} \eta_3 \\ \eta_5 \end{bmatrix} + \begin{bmatrix} \Xi_3(t) \\ \Xi_5(t) \end{bmatrix}, \qquad (1)$$

where $\eta_3(t)$ and $\eta_5(t)$ represent heave and pitch motions respectively. In this equation A_{ij} and B_{ij} (i=3,5=j) represent frequency domain hydrodynamic coefficients of added mass and damping, C_{ij} the restoring coefficients and $\Xi_j(t)$ represents sinusoidal external actions such as wave excitation.

Alternatively, these equations of motion can be written using a convolution integral formulation in the following way [4]:

$$\begin{bmatrix}\ddot{\eta}_3\\ \ddot{\eta}_5\end{bmatrix} = M^{-1}\begin{bmatrix}f_3(\dot{\eta}_3,\dot{\eta}_5,\eta_3,\eta_5)\\ f_5(\dot{\eta}_3,\dot{\eta}_5,\eta_3,\eta_5)\end{bmatrix}, \tag{2}$$

where
$$f_3 = -B_{3\tau} - B_{33}(\infty)\dot{\eta}_3 - B_{35}(\infty)\dot{\eta}_5 - C_{33}\eta_3 - C_{35}\eta_5 + \int_{-\infty}^{t} h_{3\alpha}(\tau)\alpha(t-\tau)d\tau$$
$$f_5 = -B_{5\tau} - B_{53}(\infty)\dot{\eta}_3 - B_{55}(\infty)\dot{\eta}_5 - C_{53}\eta_3 - C_{55}\eta_5 + \int_{-\infty}^{t} h_{5\alpha}(\tau)\alpha(t-\tau)d\tau .$$

The terms with the subscript τ are the radiation forces and moments expressed using the corresponding impulse response functions $h_{ij}(t)$

$$B_{3\tau} = \int_0^t h^*_{33}(\tau)\dot{\eta}_3(t-\tau)d\tau + \int_0^t h^*_{35}(\tau)\dot{\eta}_5(t-\tau)d\tau$$
$$B_{5\tau} = \int_0^t h^*_{53}(\tau)\dot{\eta}_3(t-\tau)d\tau + \int_0^t h^*_{55}(\tau)\dot{\eta}_5(t-\tau)d\tau ,$$

and the mass matrix is given by

$$M = \begin{bmatrix} m + A_{33}(\infty) & A_{35}(\infty) \\ A_{53}(\infty) & I_{55} + A_{55}(\infty)\end{bmatrix}$$

$\alpha(t)$ denotes the wave disturbance and $h_{3\alpha}$ and $h_{5\alpha}$ are the wave excitation (incident and diffracted) impulse response functions for heave and pitch respectively. To calculate hydrodynamic actions theoretically, the fluid motion can be represented by a velocity potential satisfying Laplace's equation throughout the fluid domain. The velocity potential is found by applying appropriate boundary conditions and using Green's Second Theorem, whereby the problem of modelling the fluid domain is reduced to the modelling of its boundaries. To further simplify the solution of the velocity potential problem an appropriate singularity is used.

The method used for this investigation uses a stationary pulsating source that satisfies a linearised free surface condition as well as the radiation condition at infinity. Unlike a translating pulsating source method [5,6] which implicitly accounts for forward speed effects, the pulsating source method accounts for forward speed in a limited fashion, using corrections to the zero speed solution. These corrections are much the same as used for strip theory [7]. However, it has been shown that for moderate forward speeds, such as examined in this investigation, the results of the two methods are similar [3,8].

3. CONVOLUTION INTEGRAL FORMULATION

Convolution integrals and impulse response functions are widely used to model the responses of a linear system to arbitrary or random input [9]. In its most general form, for an input $v(t)$, output $f(t)$ and impulse response function $h(t)$, the convolution integral takes the form

$$f(t) = \int_{-\infty}^{\infty} h(\tau)v(t-\tau)d\tau \tag{3}$$

To calculate the impulse response functions, Fourier transforms are used to express them in terms of frequency domain coefficients. The Fourier transform of the integral in equation 3 is the product of the transforms of the convoluted variables. That is to say

$$F(i\omega_e) = \int_{-\infty}^{\infty} f(\tau) e^{-i\omega_e \tau} d\tau = H(i\omega_e) V(i\omega_e)$$

where $$H(i\omega_e) = \int_{-\infty}^{\infty} h(\tau) e^{-i\omega_e \tau} d\tau$$

and $$V(i\omega_e) = \int_{-\infty}^{\infty} v(\tau) e^{-i\omega_e \tau} d\tau .$$

Taking the inverse Fourier transform of the frequency domain transfer function $H(i\omega_e)$, the impulse response function can be obtained as

$$h(\tau) = \frac{1}{2\pi} \int_{-\infty}^{\infty} H(i\omega_e) e^{i\omega_e \tau} d\omega_e$$

This can be expanded to give

$$h(\tau) = \frac{1}{2\pi} \int_{-\infty}^{\infty} \{H^R(\omega_e)\cos(\omega_e \tau) - H^I(\omega_e)\sin(\omega_e \tau)\} d\omega_e +$$
$$\frac{i}{2\pi} \int_{-\infty}^{\infty} \{H^I(\omega_e)\cos(\omega_e \tau) + H^R(\omega_e)\sin(\omega_e \tau)\} d\omega_e ,$$

where the superscripts I and R denote real and imaginary parts of the frequency domain transfer function respectively.

It can be argued that if the impulse response function is real then the second integral is zero [10]. Also, the symmetry of the integrand of the first integral suggests that the impulse response function may be written as

$$h(\tau) = \frac{1}{\pi} \int_{0}^{\infty} \{H^R(\omega_e)\cos(\omega_e \tau) - H^I(\omega_e)\sin(\omega_e \tau)\} d\omega_e \text{ for } \textbf{all } \tau. \qquad (4)$$

3.1 Radiation Force and Moment Impulse Response Functions

By applying the condition of realisability to equation 4, i.e. $h(\tau)=0$ for $\tau<0$, whereby there can be no response prior to input and substituting $\tau=-\tau$, it is possible to show that the impulse response function can be obtained from either the real or imaginary part of the frequency domain transfer function. For an input of sinusoidal velocity the conventional seakeeping concepts of added mass and damping can be related to the real and imaginary parts of the transfer function. The following expressions may then be obtained [11]

$$h(\tau) = \frac{2}{\pi} \int_{0}^{\infty} B(\omega_e)\cos(\omega_e \tau) d\omega_e \qquad (5)$$

$$\text{or} \quad h(\tau) = -\frac{2}{\pi}\int_0^\infty A(\omega_e)\omega_e \sin(\omega_e\tau)d\omega_e \,. \tag{6}$$

Because in many cases the frequency dependent added mass and damping tend to non-zero values at high frequency, the evaluation of equations 5 and 6 can be difficult. To avoid this problem Bishop et al. [1] expressed the frequency dependent terms in the following way

$$A(\omega_e) = A^*(\omega_e) + A(\infty)$$
$$B(\omega_e) = B^*(\omega_e) + B(\infty),$$

where $A(\infty)$ and $B(\infty)$ are the asymptotic values of added mass and damping respectively. $A^*(\omega_e)$ and $B^*(\omega_e)$ tend to zero as ω_e tends to infinity. Hence it can be shown that the convolution integral representing the radiation hydrodynamic component can be written in the following way

$$f(t) = \int_0^t h(\tau)v(t-\tau)d\tau = A(\infty)\dot{v}(t) + B(\infty)v(t) + \int_0^t h^*(\tau)v(t-\tau)d\tau \,, \tag{7}$$

where $h^*(t)$ can be obtained as per equation 5 or 6, using $B^*(\omega_e)$ or $A^*(\omega_e)$.

3.2 Wave Excitation Impulse Response Functions

Unlike the case of the radiation components, where it was assumed that the impulse response function was zero for $\tau < 0$, the incident wave and diffraction impulse response functions are in fact non-zero for $\tau < 0$. This is because the influence of a particular wave is apparent before it reaches the reference point (at t=0), and hence the impulse response functions must include a negative time component to account for this [12].

Consequently, the condition of physical realisability cannot be applied and the impulse response function is written in the general form of equation 4, i.e.

$$h_\alpha(\tau) = \frac{1}{\pi}\int_0^\infty \{\Xi^R(\omega_e)\cos(\omega_e\tau) - \Xi^I(\omega_e)\sin(\omega_e\tau)\}d\omega_e \text{ for } \textbf{all } \tau,$$

where $\Xi(i\omega_e)$ is the frequency domain complex wave excitation (incident wave and diffraction) for unit wave amplitude. Unlike the radiation components, the real or imaginary part of the wave excitation alone cannot be used to obtain an impulse response function.

4. NUMERICAL IMPLEMENTATION

4.1 Evaluation of the Impulse Response Functions

The impulse response functions for both the hydrodynamic coefficients and the wave excitation are evaluated using a modified trapezoidal method [4], originally

developed by Burcher. This numerical approximation to the integral equation is both efficient and relatively simple to implement.

The radiation coefficient impulse response functions were evaluated using the damping coefficients, since the Fourier transform is numerically simpler, as can be seen in equation 5. Also, at high frequencies $B*(\omega_e)$ tends to zero at a lower frequency, thus ensuring convergence from a smaller frequency range. The wave excitation impulse response functions were calculated using both the real and imaginary parts, both of which tend to zero at high frequencies.

4.2 Time Domain Simulation Techniques

The time domain simulation of the vessel's motions is undertaken using a fourth order Runge-Kutta method of solution [4] in which the vessel's velocity and displacement are calculated for a series of time steps of fixed increment.

At each step, the convolution integrals are calculated using a numerical convolution method, whereby the velocity and impulse response functions are represented using a series of discrete points. These convolution integrals are evaluated using trapezoidal summation. To account for the fact that time steps of the velocity and impulse response functions may be different, the time steps of the impulse response function are used in this evaluation and the velocity trace is linearly interpolated.

5. RESULTS FOR SERIES 60

The presented results are for a model size (L=3.048m) Series 60 hull form. This form was chosen because there is a large amount of validated data available to make comparisons against [6].

5.1 Validation of Fourier Transform Methods

Impulse response functions h^*_{ij} were calculated from B^*_{ij}. Using the Inverse Fourier Transform A^*_{ij} and B^*_{ij} are recalculated from h^*_{ij} and compared against the original traces from the frequency domain method. The graphs in Figure 1 show the added mass and damping coefficients A_{55} and B_{55} for Froude number 0.2, as well as corresponding h^*_{55} trace.

The values of B^*_{55} calculated from h^*_{55} are virtually identical to the original values. It can be seen that the newly calculated values of the A^*_{55} are offset vertically by a constant value from the original frequency domain method values. This is consistent with there being an infinite frequency value $A_{55}(\infty)$. However, for low frequencies there is some discrepancy between the values in addition to that of the vertical shift. This shows a weakness of the method, in that it is not able to create an impulse response function that reflects accurately all hydrodynamic properties when corrections for forward speed, based on the equations of motion with reference to the equilibrium axes system, are incorporated. This matter is further discussed in the following section. Nevertheless, it should noted that the frequency to time domain (and vice versa) transformation for all other radiation terms used in this paper is very satisfactory.

Figure 2 shows the real and imaginary parts of the frequency domain pitch excitation moment and the corresponding impulse response function. No problems were experienced with transformation from time domain back to frequency domain.

5.2 Motions in Head Seas

The time domain simulation, as outlined in equation 2, was used to calculate the ship motions in terms of Response Amplitude Operators (RAOs). For both heave and pitch these are given by the amplitude of motion per wave amplitude, *a*. A typical time record is shown in figure 2, in which a steady motion state is observed. The motion amplitudes were obtained using a Fourier fit of the steady state part of the time traces.

Heave and pitch RAOs for a Series 60 model in regular head and beam waves are shown in figures 3 and 4, and figure 5 respectively. These figures compare the RAOs obtained from the frequency domain method to those obtained using different forms of the time domain simulation program.

The data combinations tested in the time domain method were

(a) Convolution Integrals describing both radiation and wave excitation components. (i.e. equations of motion of the form of equation 2).

(b) Frequency domain hydrodynamic coefficients of added mass and damping at the appropriate frequency and convolution integrals for wave excitation.

(c) Convolution integrals for all radiation components except for pure pitch, for which A_{55} and B_{55} at the required frequency are used, convolution integrals for wave excitation.

These combinations of data were chosen in light of the fact that it had been noted that it was not possible to obtain an accurate representation of A_{55} from h_{55}, as seen in figure 1. As can be seen in figures 3,4 and 5, the time domain predictions calculated using convolution integrals to fully describe the hydrodynamic characteristics and wave forces (data combination (a)) do not show satisfactory agreement with the corresponding frequency domain predictions. Data combination (b) was used to confirm that there were no problems directly related to the representation of the wave excitation by convolution integral. It can be seen in figures 3,4 and 5 that the results for data combination (b) show good agreement with the corresponding frequency domain predictions. As the results using the data combination (c) show, when all the radiation actions except A_{55} and B_{55} are calculated using impulse response functions the agreement with the frequency domain results is very good. Calculations for other headings (e.g. 135 degrees) indicate the same level of agreement.

The inability to determine accurate values of A_{55} from h_{55} is not believed to be a result of the numerical methods used to determine the impulse response functions. Rather, it is thought to be a result of the formulation used in the adopted frequency domain method to correct for forward speed. The forward speed corrections for A_{55} and B_{55} are as follows

$$A_{55}(\omega_e) = A^0{}_{55}(\omega_e) + (\overline{U}/\omega_e)^2 A^0{}_{33}$$
$$B_{55}(\omega_e) = B^0{}_{55}(\omega_e) + (\overline{U}/\omega_e)^2 B^0{}_{33},$$

where the superscript 0 denotes the zero speed coefficient. The Fourier transform of these is

$$B^0{}_{55}(\omega_e)+(\overline{U}/\omega_e)^2 B^0{}_{33}-i\omega_e\left[A^0{}_{55}(\omega_e)+(\overline{U}/\omega_e)^2 A^0{}_{33}\right]=\int_0^\infty h_{55}(\tau)e^{-i\omega_e\tau}d\tau$$
$$=\int_0^\infty h^0{}_{55}(\tau)e^{-i\omega_e\tau}d\tau+\overline{U}^2\int_0^\infty h^0{}_{33}{}'(\tau)e^{-i\omega_e\tau}d\tau.$$

Given that $A^0{}_{33}$ and $B^0{}_{33}$ are uniquely defined by $h^0{}_{33}$, then it would have to be the case that

$$\int_0^\infty h^0{}_{33}{}'(\tau)e^{-i\omega_e\tau}d\tau=\int_0^\infty \frac{h^0{}_{33}(\tau)}{\omega_e{}^2}(\tau)e^{-i\omega_e\tau}d\tau.$$

The integral on the right hand side is not unique. It should be noted that the trends observed in A_{55} (as well as A_{66}) with forward speed, as the frequency tends to zero, are similar whether its influence is accounted for using an appropriate singularity distribution or correction [2,3]. The above analysis merely illustrates the consequences of the forward speed effects. This suggests some speed dependent radiation components do not allow for Fourier transformation. A possible solution to this problem could be the use of a body fixed axis system. Due to the co-ordinate transformation involved, the body fixed axis formulation produces frequency domain coefficients (oscillatory derivatives) that do not have the same trend as the frequency tends towards zero [4,12].

6. CONCLUSIONS

A time domain analysis of ship motions has been carried out, employing a convolution integral formulation that allows for memory effects. Both radiation and wave excitation contributions have been described using impulse response functions calculated from a frequency domain analysis.

It has been shown that it is usually possible to use Fourier transforms to convert frequency domain vessel characteristics into their corresponding equivalents in the time domain. In the case of radiation actions this involves the calculation of an impulse response function h^*_{ij} from the real part B^*_{ij} which uniquely relates A_{ij} and B_{ij}. For the wave excitation, the impulse response function $h_{\alpha j}$ is determined from both the real and imaginary parts of the excitation. The wave excitation impulse response function contains values in the negative time domain, thus accounting for the influence of waves prior to their reaching the reference point.

The time domain simulation technique developed was used, to begin with, to model the motions of a Series 60 model in sinusoidal waves. The accuracy of the impulse response functions used as part of the convolution integrals was found to be very important, especially when calculating the motions around the frequencies of resonance. Problems were experienced with obtaining the pitch impulse response function, suggesting that further work is required to determine the best method by which to avoid this problem. It is thought that using body fixed axes may provide a solution, with the additional advantage of being more convenient when going on to tackle the coupled antisymmetric motions of sway, roll and yaw.

Having validated the numerical techniques used, the time domain simulation method, based on impulse response functions, can now be extended, for example to model viscous effects using the ramp function described by Bailey et al [13] and arbitrary excitation such as non-sinusoidal excitation and random seas.

REFERENCES

[1] Bishop, R.E.D., Burcher, R.K. and Price, W.G.: The fifth annual Fairey Lecture: On the linear representation of fluid forces and moments in unsteady flow, Journal of Ship Research, 29(1): 113-128, (1973).

[2] Inglis, R.B., and Price, W.G.: The influence of speed dependent boundary conditions in three dimensional ship motion problems, *International Shipbuilding Progress*, 28(318): 22-29, (1981).

[3] Inglis, R.B., and Price, W.G.: A three dimensional ship motion theory: Comparison between theoretical predictions and experimental data of the hydrodynamic coefficients with forward speed, *Trans. RINA*, 124:141-157, (1982).

[4] Bailey, P.A.: Manoeuvring of a ship in a seaway, *PhD. Thesis*, University of Southampton, (1999).

[5] Du, X.S., Hudson, D.A., Price, W.G. and Temarel, P.: Comparison of numerical evaluation techniques for the hydrodynamic analysis of a ship travelling in waves, *Trans. RINA*, 141, (1999).

[6] Du, X.S., Hudson, D.A., Price, W.G. and Temarel, P.: A validation study on mathematical models of speed and frequency dependence in seakeeping, *J. Mech. Eng. Sci.*, Part C Millennium Edition, 214, 181-202, (2000).

[7] Beck, R.F., Cummins, W.E., Dalzell, J.F., Mandel, P. and Webster, W.C.: Principles of Naval Architecture, Volume 3, Chapter 8, *Trans. SNAME* (1989).

[8] Bailey, P.A., Hudson, D.A., Price, W.G. and Temarel, P.: Theoretical and Experimental Validation of the Seakeeping Characteristics of High Speed Mono- and Multi-hulled Vessels, *FAST '99: Fifth International Conference on Fast Sea Transportation,* Seattle, 429-441, (September 1999).

[9] Meirovitch, L.: Elements of Vibration Analysis, McGraw Hill (1986).

[10] Solodovnikov, V.V.: Statistical Dynamics of Linear Automatic Control Systems, D. Van Nostrand Co. Ltd, London (1965).

[11] Bailey, P.A., Price, W.G. and Temarel, P.: A unified mathematical model describing the manoeuvring of a ship travelling in a seaway, *Trans. RINA*, 140, 131-149 (1998).

[12] King, B.K., Beck, R.F. and Magee, A.R.: Seakeeping calculations with forward speed using time domain analysis. In 17th Symposium on Naval Hydrodynamics, pages 557-596, The Hague, Netherlands, (1988).

[13] Bailey, P.A., Hudson, D.A., Price, W.G. and Temarel, P.: Theoretical and experimental techniques for predicting seakeeping and manoeuvring ship characteristics, *RINA Int. Conf. on Ship Motions and Manoeuvrability,* London, (February 1998), Paper 5.

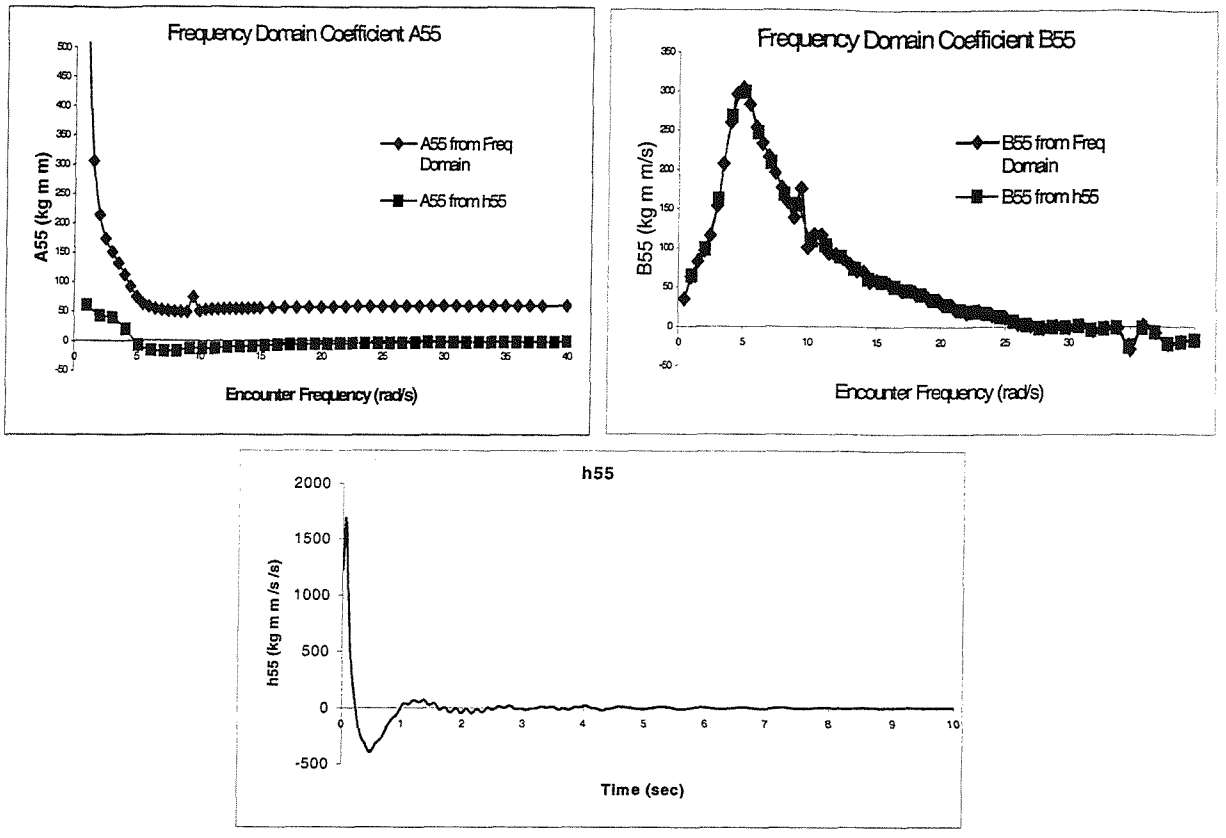

Figure 1: Hydrodynamic Coefficients A_{55} and B_{55} and h_{55} calculated from B_{55}, Fn = 0.2.

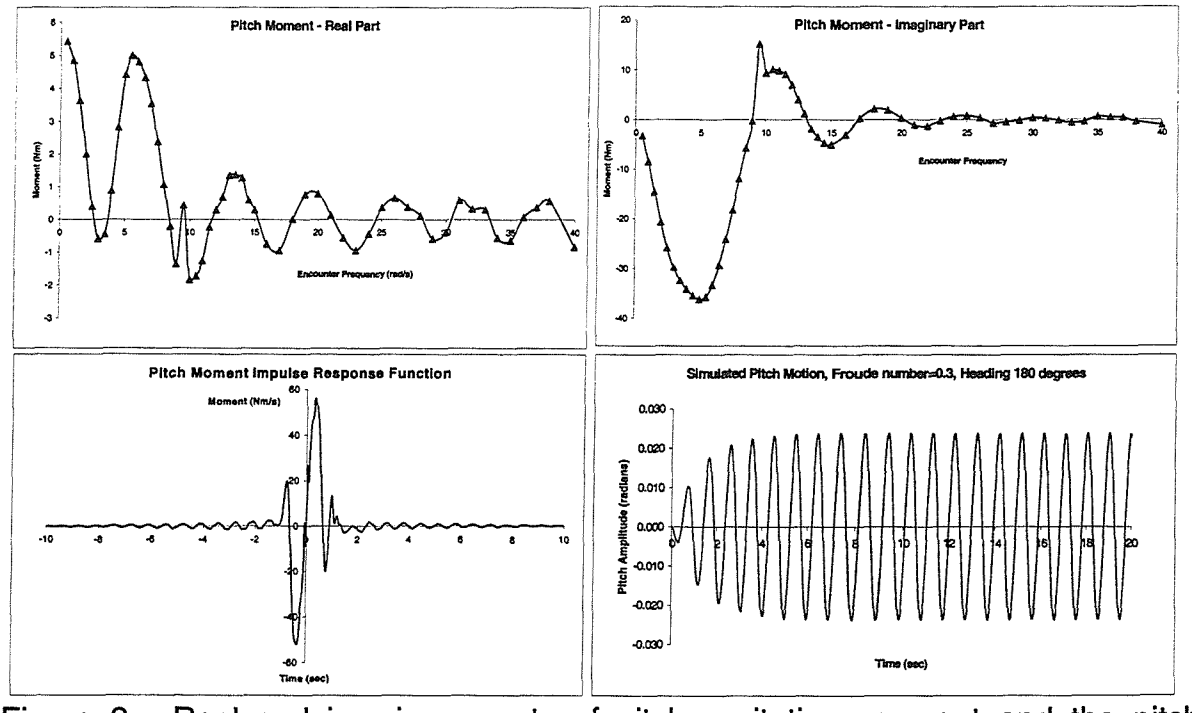

Figure 2: Real and imaginary parts of pitch excitation moment and the pitch moment impulse response function and the pitch amplitude for the vessel travelling at Fn=0.3 in regular head waves of amplitude 0.01m.

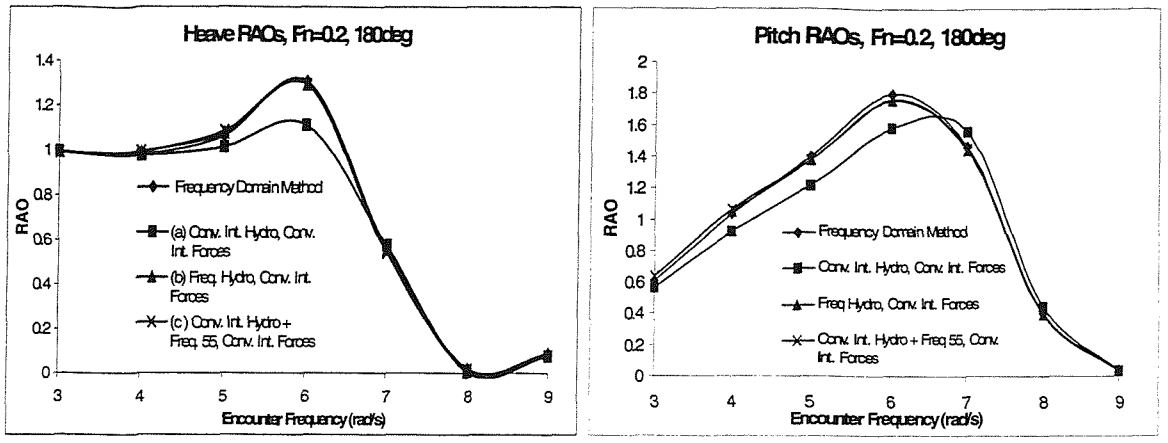

Figure 3: Heave and Pitch RAOs for Series 60 model, Froude number=0.2, Heading 180 degrees.

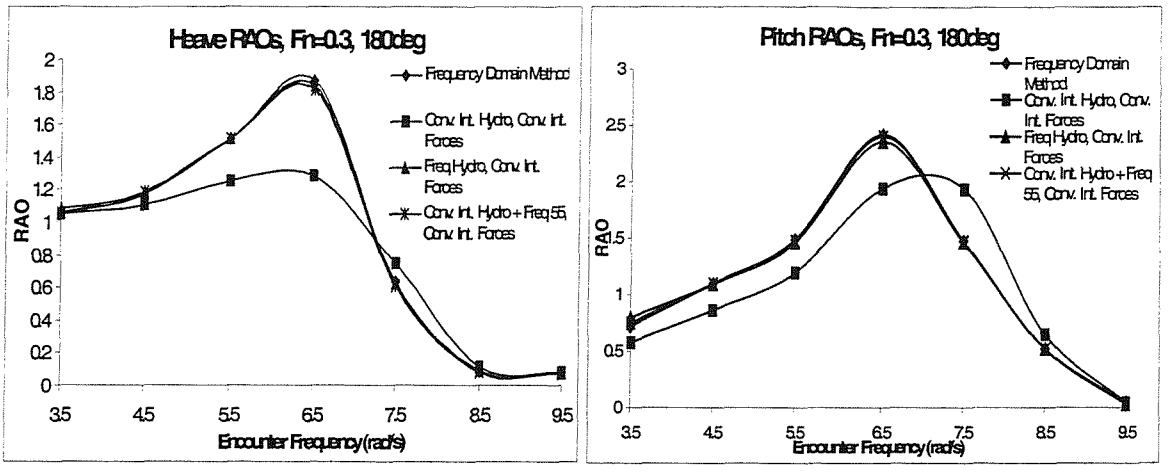

Figure 4: Heave and Pitch RAOs for Series 60 model, Froude number=0.3, Heading 180 degrees.

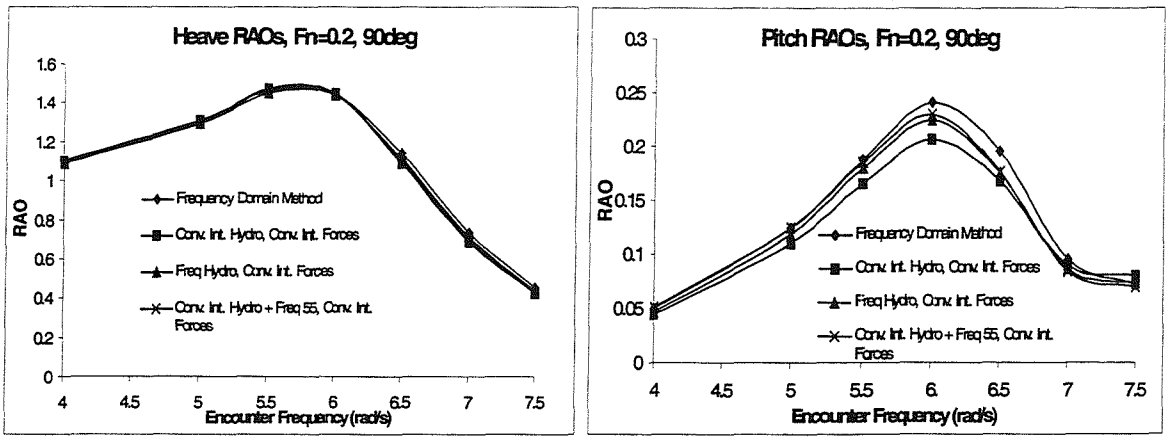

Figure 5: Heave and Pitch RAOs for Series 60 model, Froude number=0.2, Heading 90 degrees.

D Dynamic Behaviour of Rigid Mono- and Multi-Hulled Vessels in Waves, Incorporating Non-Linear Excitation

Published in :

Proceedings of 8th International Symposium on Practical Design of Ships and Other Floating Structures, PRADS 2001, Sept. 2001, Shanghai, China.

DYNAMIC BEHAVIOUR OF RIGID MONO- AND MULTI-HULLED VESSELS IN WAVES, INCORPORATING NON-LINEAR EXCITATION

P. A. Bailey, E. J. Ballard and P. Temarel

School of Engineering Sciences, Ship Science, University of Southampton,
Southampton, SO17 1BJ, UK

ABSTRACT

A time domain model for the prediction of ship motions in waves is presented in this paper. Fluid forces and moments acting on the ship are represented by convolution integral expressions thus accounting for fluid memory effects. The required impulse response functions are obtained from transforms of frequency domain data evaluated using a three-dimensional potential flow analysis based on a source distribution over the mean wetted surface of the vessel. Convolution integrals are used to describe both the radiation and diffraction contributions to the ship motion problem. Non-linear restoring and Froude-Krylov excitation forces are determined at each time step using the instantaneous underwater portion of the hull. Results are presented in head and oblique regular waves for a fast hull form, namely an NPL round bilge series, in both mono-hull and catamaran configurations. Initially the wave amplitude conforms to the concept of linearity, allowing for the validation of the numerical procedures. Subsequently the effects of non-linear excitation are investigated by increasing the amplitude of the regular waves.

KEYWORDS

Rigid body motions, seakeeping, non-linear, wave excitation, multi-hulled vessels.

INTRODUCTION

Modelling of ship motions in the time domain allows for the evaluation of responses to arbitrary and/or transient excitation. Such a method enables, for example, the influence of control surfaces and excitation by random waves to be accounted for in a way that is not possible using conventional frequency domain approaches. The fluid memory effect, exemplified by the generation of motion induced surface waves, introduces a dependence of the forces and moments on past motion/excitation. The use of impulse response functions and a convolution integral formulation for the fluid actions allows for the generation of a time domain model that is capable of incorporating the aforementioned influences and excitations. Bailey et al (1998a) presented a mathematical model for the manoeuvring of a ship in a seaway that is also capable of simulating the conventional seakeeping behaviour and

manoeuvring in calm water, as illustrated for a Mariner ship by Bailey et al (2001a). These investigations were further extended to include the influence of diffracted waves and applied to a Series 60 hullform, Bailey et al (2000a). The fundamental building blocks of these investigations are the use of frequency domain hydrodynamic data to generate the requisite impulse response functions and transforms between the equilibrium axes and the body fixed axes of conventional seakeeping and manoeuvring theories, respectively, as shown by Bailey et al (1998a, 2001a). The determination of the frequency domain data relies on a suitable singularity distribution over the mean wetted surface of the ship, Inglis and Price (1982), Bailey et al (1999, 2000b),

Although the mathematical model developed is capable of simulating the dynamic behaviour of a ship travelling in waves in all six degrees of freedom, results presented in this paper are focused on the symmetric motions of heave and pitch. A fast hull form from the extended NPL round bilge series, namely model 5b, is used to illustrate the applicability of the methodology. The motions of this hull form a re predicted when travelling at various speeds and headings in mono-hull and catamaran (demi-hull separation = 0.2L) configurations. Comparisons are made with available experimental measurements, Bailey et al (1999), Molland et al (2000).

AXIS SYSTEMS AND EQUATIONS OF MOTION

Seakeeping theory has traditionally referenced the rigid body motions of a vessel to equilibrium axes. However, it has been shown by Bailey et al (2000a) that the behaviour of the frequency domain added mass and damping calculated with respect to these axes results in problematic evaluation of the corresponding impulse response functions. However, Bailey (2001a) demonstrated that frequency domain data transformed to a body fixed set of axes is more amenable to the calculation of impulse response functions.

For a ship travelling with forward speed $\overline{U}$ in regular waves encountered at arbitrary heading, the heave and pitch (denoted by displacements z^* and θ) equations of motion referenced to a right handed body fixed axis *Cxyz* can be written as

$$\begin{bmatrix} m & 0 \\ 0 & I_{yy} \end{bmatrix}\begin{bmatrix} \dot{w} \\ \dot{q} \end{bmatrix}+\begin{bmatrix} 0 & -m\overline{U} \\ 0 & 0 \end{bmatrix}\begin{bmatrix} w \\ q \end{bmatrix}=\begin{bmatrix} Z_{\dot{w}} & Z_{\dot{q}} \\ M_{\dot{w}} & M_{\dot{q}} \end{bmatrix}\begin{bmatrix} \dot{w} \\ \dot{q} \end{bmatrix}+\begin{bmatrix} Z_w & Z_q \\ M_w & M_q \end{bmatrix}\begin{bmatrix} w \\ q \end{bmatrix}+\begin{bmatrix} Z_{z^*} & Z_\theta \\ M_{z^*} & M_\theta \end{bmatrix}\begin{bmatrix} z^* \\ \theta \end{bmatrix}+\begin{bmatrix} Z(t) \\ M(t) \end{bmatrix}, \quad (1)$$

where w and q are the heave and pitch velocities, respectively, terms such as $Z_{\dot{w}}, M_q$ are the oscillatory coefficients and $Z(t)$ and $M(t)$ represent the excitation. Alternatively, Bailey et al (2001a) have shown that these equations of motion can be written using a convolution integral formulation in the following way:

$$\begin{bmatrix} \dot{w}(t) \\ \dot{q}(t) \end{bmatrix} = M^{-1}\begin{bmatrix} f_3(w,q,z^*,\theta,t) \\ f_5(w,q,z^*,\theta,t) \end{bmatrix}, \quad (2)$$

where

$$\begin{aligned} f_3 &= Z_\tau + Z_\alpha + \tilde{Z}_w(\infty)w + \tilde{Z}_q(\infty)q + mq\overline{U} \\ f_5 &= M_\tau + M_\alpha + \tilde{M}_w(\infty)w + \tilde{M}_q(\infty)q. \end{aligned} \quad (3)$$

In these equations the contributions of weight, buoyancy and incident wave excitation are denoted by the terms with subscript α. The detail of these terms will be elaborated upon in later sections. The mass matrix is given by

$$M = \begin{bmatrix} m - \tilde{Z}_{\dot{w}}(\infty) & -\tilde{Z}_{\dot{q}}(\infty) \\ -\tilde{M}_{\dot{w}}(\infty) & I_{yy} - \tilde{M}_{\dot{q}}(\infty) \end{bmatrix},$$

where terms such as $\tilde{Z}_{\dot{w}}(\infty)$ and $\tilde{M}_{\dot{w}}(\infty)$ are the infinite frequency values of the acceleration oscillatory coefficients. The terms with subscript τ are the radiation forces and moments and are expressed as follows

$$\begin{aligned} Z_\tau &= \int_0^t z_w(\tau) w(t-\tau) d\tau + \int_0^t z_q(\tau) q(t-\tau) d\tau \\ M_\tau &= \int_0^t m_w(\tau) w(t-\tau) d\tau + \int_0^t m_q(\tau) q(t-\tau) d\tau. \end{aligned} \tag{4}$$

The impulse response functions used in the convolution integrals in the previous equations can be calculated using either the velocity or acceleration frequency domain data. The transformation of the frequency domain data from an equilibrium to a body axis representation enables the calculation of terms such as $\tilde{M}_w(\omega_e)$ and $\tilde{M}_{\dot{w}}(\omega_e)$, the frequency dependent velocity and acceleration oscillatory coefficients, respectively, Bailey et al (1998a, 1998b, 2000a). For example

$$z_w(\tau) = \frac{2}{\pi}\int_0^\infty \tilde{Z}_w(\omega_e)\cos(\omega_e\tau)d\omega_e = -\frac{2}{\pi}\int_0^\infty \omega_e \tilde{Z}_{\dot{w}}(\omega_e)\sin(\omega_e\tau)d\omega_e .$$

Numerical experiments have shown that the impulse response function calculated using the velocity derivative data converges faster than its equivalent determined using the acceleration data, hence the velocity data is used in preference.

The relevant frequency domain data is obtained using a three-dimensional potential flow analysis, based on the conventional equilibrium axis system, with a singularity distribution over the mean wetted surface. In this investigation two types of singularity are used, a pulsating source and translating pulsating source. Both of these source types satisfy a linearised free surface condition as well as the radiation condition at infinity. The pulsating source method accounts for forward speed in a limited fashion, using corrections to the zero speed solution much the same as are used for strip theory, Beck et al (1989). The translating, pulsating source on the other hand fully accounts for forward speed effects, but does so at considerable computational expense. It has been shown that for monohulls at moderate forward speeds the results of the two methods are quite similar, Inglis & Price (1982), Bailey et al (1999), hence results for the monohull use the simpler and faster method. However, for a catamaran model the translating pulsating source is required to fully account for interaction between the hulls.

WAVE EXCITATION

It can be argued that observed differences between theoretical linear motion predictions and experimental results can be attributed, to some extent, to the nature of the excitation, particularly for ships with large flare. To this end, it is possible to introduce a non-linear component of excitation into an otherwise linear system, the integration of the Froude-Krylov wave excitation pressure over the instantaneous wetted surface yielding such a contribution. The wave excitation and restoring terms, denoted with subscript α, in Eqn. 3 can be represented as

$$Z_\alpha = Z_\alpha{}^D + Z_\alpha{}^F + Z_z.z^* + Z_\theta\theta$$
$$M_\alpha = M_\alpha{}^D + M_\alpha{}^F + M_z.z^* + M_\theta\theta, \quad (5)$$

where the superscripts D and F refer to the linear diffraction and the non-linear Froude-Krylov components respectively. The non-linear restoring forces and moments are denoted by the subscripts z^* and θ respectively.

It has been shown by Bailey et al (2000a) that linear diffraction excitation actions can be represented using a convolution type formulation. Calculation of these wave excitation impulse response functions is more difficult than the calculation of the radiation impulse response functions, since the influence of a wave prior to its reaching the reference point must be accounted for. This means that the diffraction excitation impulse response functions are non-zero for $\tau < 0$, Bailey et al (2000a), King et al (1988), and unlike the radiation impulse response functions their calculation requires both the real and imaginary parts. For example,

$$Z_\alpha{}^D = \int_{-\infty}^{\infty} z^D(\tau)\alpha(t-\tau)d\tau$$

where
$$z^D = \frac{1}{\pi}\int_0^\infty \{\Xi_z{}^R(\omega_e)\cos(\omega_e\tau) - \Xi_z{}^I(\omega_e)\sin(\omega_e\tau)\}d\omega_e \quad \text{for } \textbf{all } \tau,$$

$\alpha(t)$ denotes the wave elevation and Ξ_z is the frequency domain diffraction term, transformed to the body fixed axis system.

The non-linear portion of the wave excitation terms in Eqn. 5 are made up of two components. These are the non-linear Froude-Krylov and restoring forces and moments. They are determined up to the intersection of the incident wave surface and the ship in its perturbed state at each time step.

The entire surface of the ships hull, including the portion above the waterline, is discretised using a mesh of quadrilateral panels. This allows a single mesh to be used to represent a range of ship loading conditions. At each time step the instantaneous underwater portion of the hull is extracted. Special consideration must be given to panels that cross the incident free surface. Panels that are entirely above the surface are ignored and those that cross the surface are either split or replaced with two smaller panels. The static and Froude-Krylov pressures are then calculated at the centre of each panel. The contribution of the force on each panel to the overall forces and moments is determined using the area of the panel and its normal. The total Froude-Krylov and buoyancy forces are then calculated by summing the contributions from all the panels. Care has been taken to ensure that the splitting, adding or destroying panels does not introduce step changes in the resulting forces and moments, Bailey (2001b).

TIME DOMAIN SIMULATION TECHNIQUES

The time domain simulation of the vessel's motions is undertaken using a fourth order Runge-Kutta method of solution, Bailey et al (2001a), in which the vessels velocity and displacement are calculated for a series of time steps of fixed increment. At each step, the convolution integrals are evaluated using a numerical convolution method, whereby the velocity and impulse response functions are represented using a series of discrete points. These convolution integrals are evaluated using trapezoidal summation. To account for the fact that the time steps of the velocity and impulse response functions may be different, the time steps of the impulse response function are used in this evaluation and the velocity trace is linearly interpolated.

DISCUSSION OF RESULTS

The length of the vessel used in the calculations is 4.5m in both mono-hull and catamaran configurations. The mean wetted surface, to a draught of 0.2m, was idealised using 554 four-cornered panels for the NPL mono-hull. 640 panels were used to idealise the entire surface of the mono-hull, to a depth of 0.35m. The first idealisation is used to evaluate frequency domain hydrodynamic/oscillatory coefficients and diffracted wave excitation, whilst the second is employed when generating the instantaneous underwater surface to evaluate the non-linear incident wave excitation and restoring forces and moments. In the same way, the mean wetted surface of the catamaran is idealised using 390 panels per demi-hull for the frequency domain analysis, whilst the entire surface to a depth of 0.4m is idealised using 415 panels per demi-hull for the evaluation of the non-linear components. The idealisations used provide a reasonably good panel aspect ratio, approximately 2, which is particularly important in ensuring a good convergence in the frequency domain data calculated using the translating, pulsating source distribution, Bailey et al (2000b).

The pitch-pitch radiation impulse response function is illustrated in Figure 1(a) for both mono-hull and catamaran configurations, albeit at different speeds. The trends of the impulse response function for the catamaran configuration requires further investigation as demi-hull separation increases. The variation of the predicted heave displacement with time is also shown in Figure 1(b). The simulation shown corresponds to the mono-hull travelling in head regular waves at Fn = 0.53, encountered at $\omega_e' = \omega_e\sqrt{L/g} = 5.42$ and amplitude $\alpha =$ 0.05625m. The simulated heave displacement quickly converges to a steady state sinusoidal variation with time that has a non-zero mean value, zero representing the still water equilibrium position, due to the relatively large wave amplitude used (approximately a quarter of the draught). The motion amplitudes are obtained from a Fourier fit of the steady state part of the time records, e.g. as shown in Figure 1(a) starting from 42 seconds.

The predicted heave and pitch transfer functions for the mono-hull in regular head waves are shown in Figures 2 and 3. These are for slow and moderate speeds corresponding to Fn = 0.2 and Fn = 0.53, respectively. The transfer functions (or RAOs) are defined as heave or pitch amplitude per wave amplitude α. The time domain predictions (two wave amplitudes α=0.001m and α=0.05625m), are compared with the frequency domain predictions, both using a pulsating source distribution, and experimental measurements carried out with a 1.6m model, Bailey et al (1999). For the lowest speed used, i.e. Fn = 0.2, frequency and time domain predictions are all in close agreement. Nevertheless, small differences are observed for the highest wave amplitude, especially for the pitch RAO around resonance, resulting in closer agreement between the time domain prediction (α=0.05625m) and experiments carried out using the same wave amplitude. For the moderate speed, Fn = 0.53, there is once again very close agreement between the time domain predictions with the smallest wave amplitude and frequency domain results. The differences using the larger wave amplitude are now more clearly seen, especially for the pitch RAO. The time domain predictions are closer to the experimental measurements using the same amplitude. It is worthwhile noting that the time domain method results in accurate predictions of the pitch RAO magnitude at resonance, although the frequency of resonance is still overestimated.

For the NPL catamaran configuration frequency and time domain predictions for heave and pitch RAOs are compared for a moderately high speed, Fn = 0.65, whilst the vessel is travelling in oblique regular waves (heading of 150 degrees), as shown in Figure 4. Experimental measurements carried out with a model of 4.5m are also shown, Molland et al (2000). When the wave amplitude is low (α=0.001m), there is good agreement between time and frequency domain RAOs, both evaluated using a translating, pulsating source distribution. Increasing the wave amplitude to α=0.01m appears to result in small differences in the predicted RAOs, unlike the trend observed in the mono-hull for Fn = 0.53, albeit with a larger wave amplitude. Consequently the differences observed between

theoretical predictions (either frequency or time domain) persist, especially in pitch RAOs. At this speed it is known that the transom runs dry, which may have an effect on the pitch damping values and corresponding impulse response functions. Furthermore, the omission of roll when determining the perturbed attitude of the ship relative to the regular incident wave at any time instant may also have an influence on the result of the time domain simulation.

CONCLUSIONS

The applicability of a time domain method, formulated using body fixed axes, impulse response functions for radiation and diffraction influences and non-linear incident wave and restoring actions, in predicting motions for mono- and multi-hulled vessels travelling in regular waves has been illustrated for various speeds and headings.

The validity of the numerical procedures involved, such as the evaluation of impulse response functions, the time stepping scheme and the generation of the instantaneous free surface, have been demonstrated by comparison with frequency domain predictions of heave and pitch RAOs.

For the NPL round bilge hull form, in mono-hull configuration, it was shown that the influence of the non-linearities in the incident wave excitation and restoring actions is very small at low speeds. However, these influences become more significant at moderate speeds. The predictions provided are in closer agreement with experimental measurements, by comparison to frequency domain and small amplitude time domain predictions.

For the same fast hull form in catamaran configuration and moderately high speeds, the requisite frequency domain data were obtained using a translating, pulsating source distribution over the mean wetted surface to better idealise the interactions between the two hulls. The applications of the partly non-linear time domain method in oblique regular waves has, so far, shown that the non-linearities in the incident wave excitation and restoring actions do not appear to have a significant influence on predicted heave and pitch RAOs. The effects of pitch damping, and consequent influences on relevant impulse response functions, are thought to be likely causes. These may arise from the transom running dry at this speed.

Further work is required, especially in the catamaran configurations, to assess the influence of:

(i) the nature of the idealisation of the mean and instantaneous wetted surfaces (i.e. panel aspect ratio) on the predicted impulse response functions and time domain simulations,
(ii) inclusion of antisymmetric motions, such as roll, and
(iii) larger wave amplitudes, similar to those used in the experimental measurements.

REFERENCES

Bailey, P.A., Price, W.G. and Temarel, P. (1998a). A Unified Mathematical Model Describing the Manoeuvring of a Ship Travelling in a Seaway. *Trans. RINA* **140**, 131-149.

Bailey, P.A., Hudson, D.A., Price, W.G. and Temarel, P. (1998b). The Measurement and Prediction of Fluid Actions Experienced by a Manoeuvring Vessel. In Proc. *Intl. Symposium and Workshop on Forces Acting on a Manoeuvring Vessel, MAN'98*, 117-123, Val de Reuil, France.

Bailey, P.A., Hudson, D.A., Price, W.G. and Temarel, P. (1999). Theoretical and Experimental Validation of the Seakeeping Characteristics of High Speed Mono and Multi-Hulled Vessels. *FAST'99: Fifth International Conference on Fast Sea Transportation*, Seattle, 429-441.

Bailey, P.A., Ballard, E.J., Hudson, D.A. and Temarel, P. (2000a). Time Domain Analysis of Vessels in Waves Accounting for Fluid Memory Effects. In Proc. *NAV2000*, 9.4.1-9.4.11.

Bailey, P.A., Hudson, D.A., Price, W.G. and Temarel, P. (2000b). Comparisons Between Theory and Experiment in a Seakeeping Validation Study, *Trans. RINA*, paper 261, 2000.

Bailey, P.A., Hudson, D.A., Price, W.G. and Temarel, P. (2001a). Time Simulation of Manoeuvring and Seakeeping Assessments Using a Unified Mathematical Model. *Trans. RINA*, Accepted for publication 2001.

Bailey, P.A., Hudson, D.A., Price, W.G. and Temarel, P. (2001b). A Simple yet Rational Approach to the Panelling of a Hull Surface. *Trans. RINA*, Accepted for publication 2001.

Beck, R.F., Cummins, W.E., Dalzell, J.F., Mandel, P. and Webster, W.C. (1989). *Principles of Naval Architecture*, Volume 3, Chapter 8, SNAME.

Fonseca, N. and Guedes Soares, C. (1994). *Marine, Offshore and Ice Technology*, chapter: Time Domain Analysis of vertical Ship Motions, pages 225-242, Computational Mechanics Publication.

Inglis, R.B. and Price, W.G. (1982). A Three Dimensional Ship Motion Theory: Comparison Between Theoretical Predictions and Experimental Data of the Hydrodynamic Coefficients with Forward Speed, *Trans. RINA* **124**, 141-157.

King, B.K., Beck, R.F. and Magee, A.R. (1988). Seakeeping Calculations with Forward Speed Using Time Domain Analysis. In *17th Symposium on Naval Hydrodynamics*, pages 557-596, The Hague, Netherlands.

Molland, A.F., Wellicome, J.F., Temarel, P., Cic, J. and Taunton, D.J. (2000). Experimental Investigation of the Seakeeping Characteristics of Fast Displacement Catamarans in Head and Oblique Seas, *Trans. RINA*, paper 261.

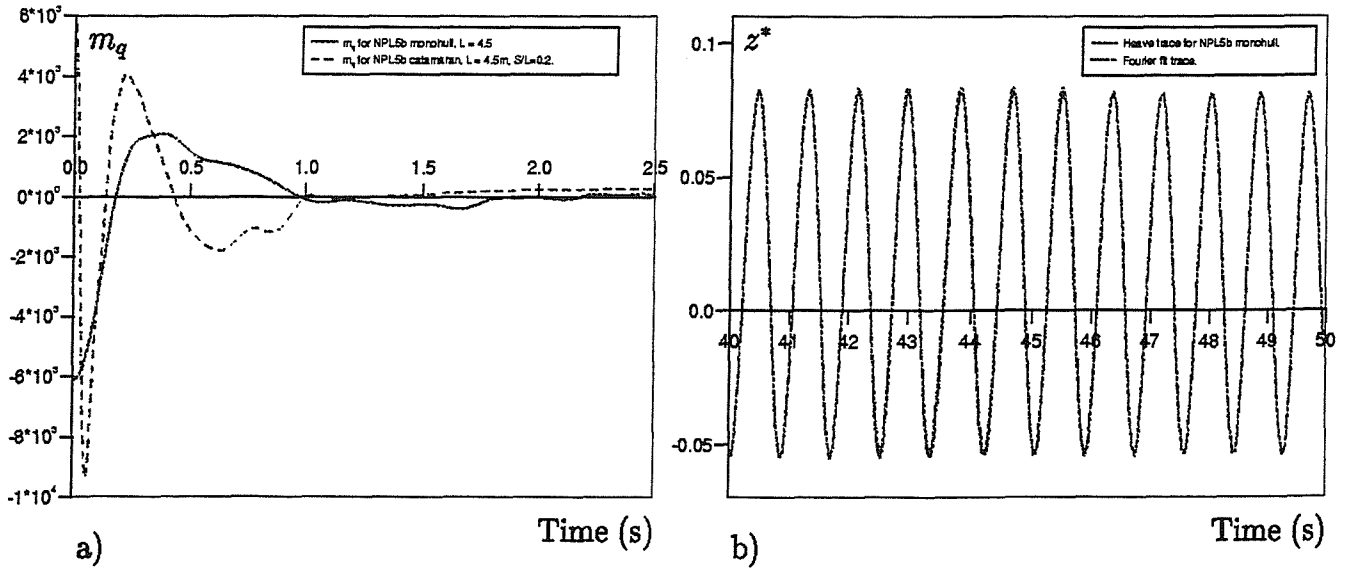

Figure 1: (a) Pitch-pitch (m_q) impulse response functions for mono-hull and catamaran configurations and (b) heave response trace for mono-hull, Fn = 0.53, Heading = 180deg, α = 0.05625m, ω_e'= 5.42

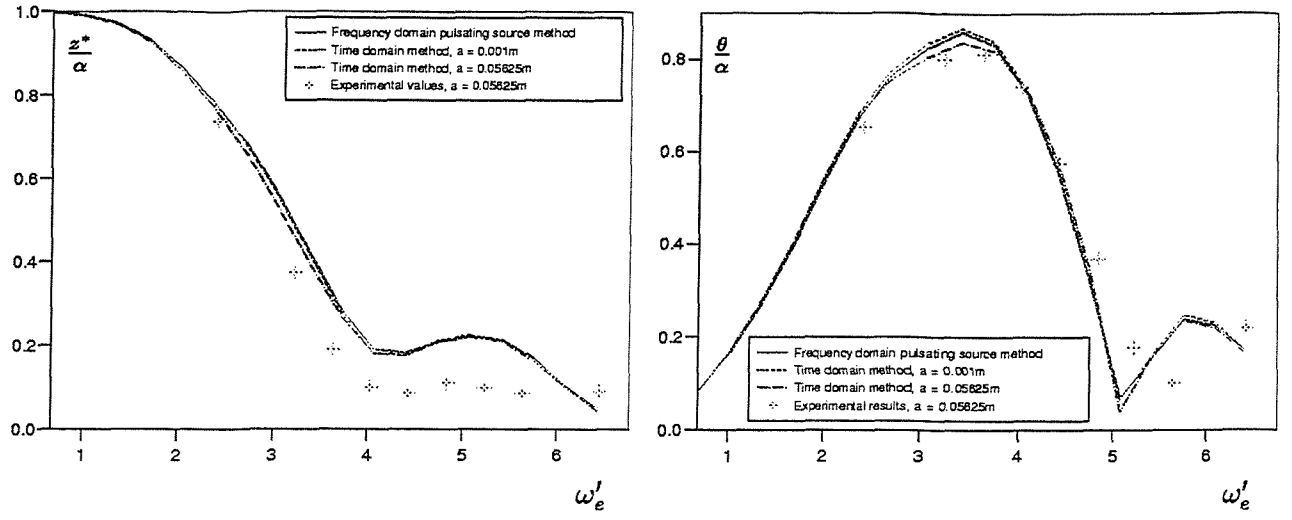

Figure 2: Heave and Pitch RAOs for a NPL5b mono-hull in regular head waves of variable amplitude. L=4.5m, Fn=0.2.

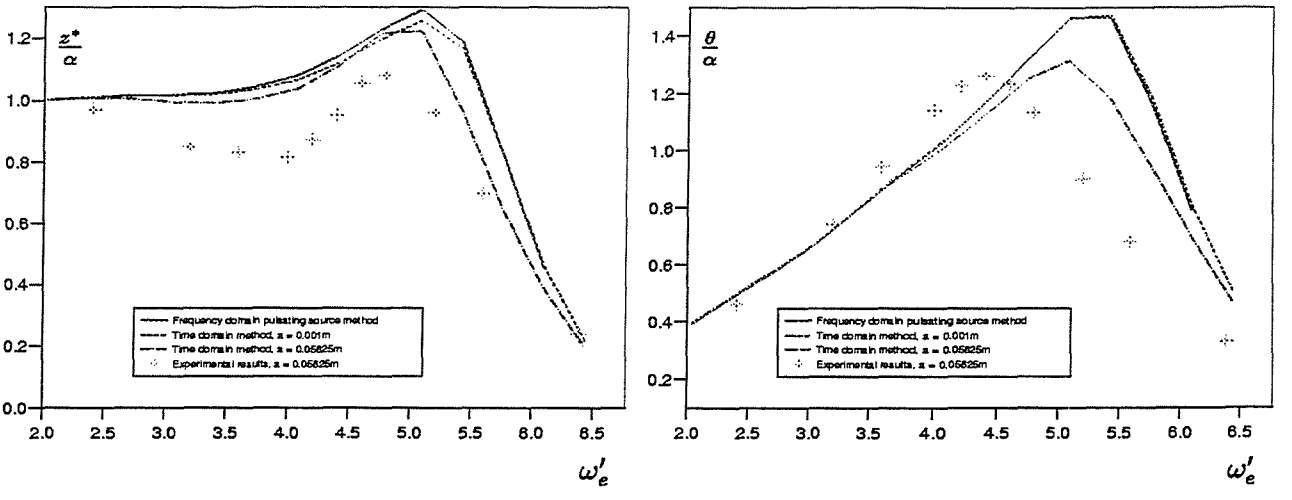

Figure 3: Heave and Pitch RAOs for a NPL5b mono-hull in regular head waves of variable amplitude. L=4.5m, Fn=0.53.

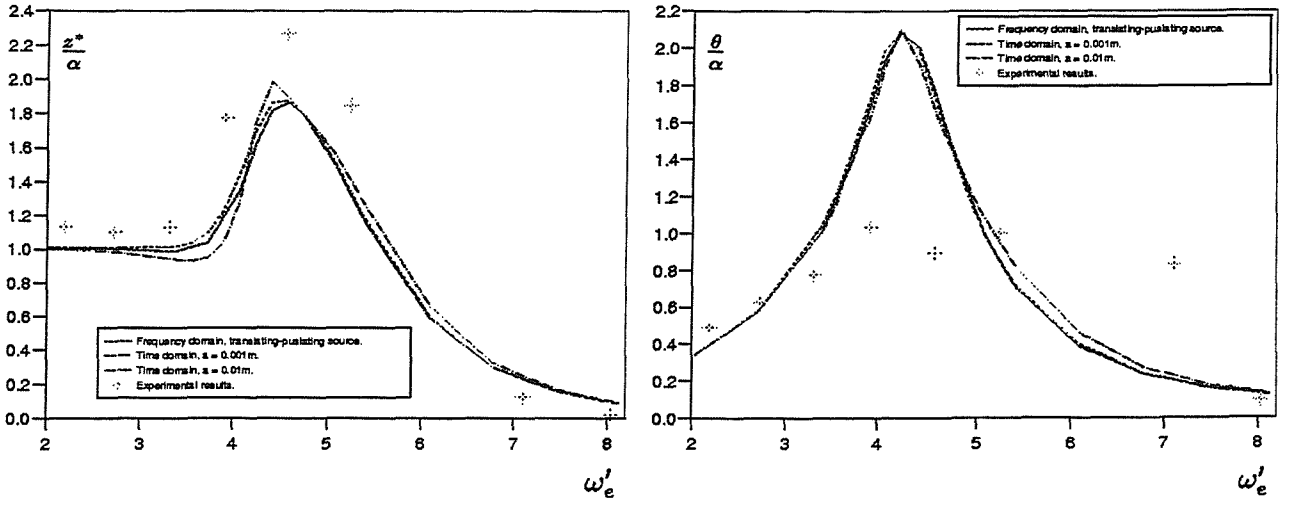

Figure 4: Heave and Pitch RAOs for a NPL5b catamaran in oblique regular waves (150 degree heading), L=4.5m, S/L=0.2, Fn=0.65

E Motions of Mono- and Multi-Hulled Vessels in Regular Waves Using a Partly Non-Linear Time Domain Method

Published in :

Proceedings of FAST 2001, 6th International Conference on Fast Sea Transportation, Sept. 2001, Southampton, UK.

Motions of Mono- and Multi-hulled Vessels in Regular Waves Using a Partly Non-Linear Time Domain Method

Edward Ballard, University of Southampton, UK.
Shuang Xing Du, University of Southampton, UK; C.S.S.R.C, Wuxi, China.
Dominic Hudson, University of Southampton, UK.
Pandeli Temarel, University of Southampton, UK.

SUMMARY

The use of a time domain simulation technique for modelling ship motions allows for the evaluation of responses to arbitrary and/or transient excitation. Such a method also accounts for fluid memory effects, exemplified by the generation of motion induced surface waves, introducing a dependence of the forces and moments on the past motion/excitation. The method used in this paper uses convolution integrals to describe both the radiation and diffraction contributions. The evaluation of the non-linear incident wave (Froude-Krylov) excitation is carried out at each step of the simulation by integrating the corresponding pressure over the instantaneous wetted surface. The corresponding, instantaneous hydrostatic restoring forces and moments are also accounted for by considering weight contributions at the instantaneous attitude of the hull.

The effects of forward speed on a fast hull form (NPL5b) travelling at Froude number 0.5 in regular head waves are investigated. Both monohull and catamaran configurations are examined, the latter with two hull separations, allowing for interaction effects to be studied. Hydrodynamic data is calculated using frequency domain singularity distribution methods. Two frequency domain methods are used, one employing a pulsating source distribution with forward speed correction, the other using a translating, pulsating source distribution. The data from the frequency domain methods, referenced to a body fixed axis system, is transformed into impulse response functions using Fourier transformations. The impulse response functions are used as part of a convolution integral formulation to perform time domain simulations of motions in head waves. Initially calculations are carried out in regular waves commensurate with the concept of linearity. Subsequently the effects of non-linearities are investigated by increasing the wave amplitude.

AUTHORS BIOGRAPHIES

Edward Ballard is a research student studying for a PhD. Fellow in the Fluid Structure Interactions Research Group within the School of Engineering Sciences at the University of Southampton. He has a Bachelor of Engineering with First Class Honours in Mechanical Engineering from the University of Canterbury, Christchurch, New Zealand. His area of research is the time domain simulation of ship motions.

Shuang Xing Du is a Research Fellow in the Fluid Structure Interactions Research Group within the School of Engineering Sciences at the University of Southampton. He is on leave of absence from the China Ship Scientific Research Centre where he holds to position of Professor. His research interests include numerical and experimental studies of hydrodynamics, seakeeping and hydroelasticity theory.

Dominic Hudson is a Research Fellow in the Fluid Structure Interactions Research Group within the School of Engineering Sciences at the University of Southampton. He received his PhD. from the University of Southampton in 1999. He contributes to the Ship Science degree programme and his research interests include hydrodynamics, seakeeping and manoeuvring, especially of high-speed craft.

Pandeli Temarel is Professor of Hydroelasticity in the Fluid Structure Interactions Research Group, School of Engineering Sciences, University of Southampton. He is Course Coordinator for Ship Science Degree Programmes. Research interests include analytical and numerical investigations of hydrodynamics, seakeeping, manoeuvring, stability and hydroelasticity theory.

NOMENCLATURE

Fn	Froude number.
$h(\tau)$	Impulse response function.
I_{yy}	Pitch Inertia (kgm^2).
L	Length between perpendiculars (m)
m	Mass of ship (kg).
m_i	Pitch impulse response function, where i is w or q for radiation actions and α for diffraction.
$\tilde{M}_i(\omega_e)$	Pitch oscillatory derivative, where i is a velocity or acceleration, referenced to body fixed axis system.
$\tilde{M}_i(\infty)$	Infinite frequency value of pitch oscillatory derivative.
$M(t)$	External pitch moment acting on ship (Nm).

$q, \dot{q}$ Pitch angular velocity and acceleration of ship, referenced to body fixed axis system (rad/s).
S Separation between hulls of catamaran (m).
t Time (s).
$\overline{U}$ Forward speed of ship (m/s).
$w, \dot{w}$ Heave velocity and acceleration of ship, referenced to body fixed axis system (m/s).
z_i Heave impulse response function, where i is w or q for radiation actions and α for diffraction.
$\tilde{Z}_i(\omega_e)$ Heave oscillatory derivative, where i is a velocity or acceleration, referenced to body fixed axis system.
$\tilde{Z}_i(\infty)$ Infinite frequency value of heave oscillatory derivative.
$Z(t)$ External heave force acting on ship (N).
z^* Heave displacement (m).
$\alpha(t)$ Wave elevation (m)
θ Pitch displacement (radians).
Θ Euler pitch angle (radians).
τ Variable used in convolution integrals (s).
Φ Euler roll angle (radians).
ω_e Encounter frequency (radians/second).

1. INTRODUCTION

High speed vessels have seen use in an increasing number of roles over the past few years. In particular they have been used extensively in passenger ferry applications. An important aspect in the operational viability of such high-speed passenger vessels is their seakeeping characteristics. Methods are required by which the seakeeping properties of vessels can be determined at the design stage. This allows for assessment of their suitability for particular tasks, with emphasis on the motions and their relationship to vessel availability and passenger safety/comfort.

Model testing programmes have been carried out for high speed vessels to determine their seakeeping characteristics, but such programmes are inherently expensive and limited in terms of the realism of the sea conditions they are able to replicate [1]. By developing a method suitable for performing simulations of ship motions in more realistic sea states, it is conceivable that the need for model tests could be reduced. This could lead to cost reductions in the design process as well as allowing for a more complete picture of the performance characteristics of a vessel.

Modelling of ship motions in the time domain allows for the evaluation of responses to arbitrary and/or transient excitation. Time domain methods offer many advantages over conventional frequency domain methods. Among these are the ability to account for the influence of control surfaces and excitation by random waves. In addition, the fluid memory effects, exemplified by the generation of motion induced surface waves, introduce a dependence of the fluid forces and moments on past motion/excitation.

The use of impulse response functions and a convolution integral formulation allows for the development of a time domain model that is capable of incorporating the influences and excitations mentioned earlier. A mathematical model for the simulation of manoeuvring in waves has been presented by Bailey et al [2], which is capable of simulating conventional seakeeping behaviour as well as manoeuvring in calm water. This method has been demonstrated for a Mariner type ship by Bailey et al. [3]. This method was further extended to include the influence of diffracted waves and applied to a Series 60 hull form [4]. These methods have been based on the use of frequency domain hydrodynamic data, determined using a suitable singularity distribution over the mean wetted surface of the ship. This hydrodynamic data is then used to create the required impulse response functions by the application of Fourier transformations and transforms between the equilibrium and body fixed axes of conventional seakeeping and manoeuvring theories, respectively, as shown by Bailey et al. [2,3].

The time domain simulation methods used in this investigation have used impulse response functions to describe the radiation and diffraction hydrodynamic actions. These impulse response functions have been calculated using two different frequency domain singularity methods. The first of these methods uses a pulsating source distribution to which a forward speed correction is applied. The second frequency domain method uses a translating, pulsating source distribution. Both frequency domain methods use a panelled idealisation of the mean underwater surface of the hull, with the sources being placed at the centre of the panels. Initially the hydrodynamic actions are calculated with respect to an equilibrium axis system, but this data is converted to a body fixed axis system afterwards to aid the calculation of the corresponding impulse response functions. The resultant equations of motion, referenced to a body fixed axis system, are solved in the time domain using a fourth order Runge-Kutta method of solution. At each time step the non-linear incident wave (Froude-Krylov) and restoring forces/moments are calculated using a panelled idealisation of the instantaneous underwater portion of the hull.

The results presented in this paper are for investigations of the heave and pitch characteristics of an NPL5b model

in regular head waves of varying amplitude. The model is examined in monohull configuration and catamaran configurations with hull separation to length (S/L) ratios of 0.2 and 0.4. Comparisons are made with experimental measurements, [1,5].

2. AXIS SYSTEM AND EQUATIONS OF MOTION

Traditionally, seakeeping studies have referenced the rigid body motions of a vessel to equilibrium axes. This axis system moves with the ship, but remains unaffected by the parasitic motions. However, it has been shown that the nature of the frequency domain added mass and damping calculated with respect to these axes makes accurate calculation of the corresponding impulse response functions difficult where forward speed is involved [4]. In particular, the tendency of certain frequency domain hydrodynamic coefficients, such as pitch damping, to tend to infinite values at low frequency results in difficulties in obtaining the impulse response functions using numerical transformation methods. Performing a transformation of the frequency domain data to a body fixed axis system [3] can circumvent this problem. The resultant oscillatory velocity derivatives do not tend to infinite values at low frequency, thus allowing accurate calculation of the impulse response functions.

For a ship travelling in regular waves at an arbitrary heading, the heave and pitch equations of motion referenced to a right-handed body fixed axis system can be written as

$$\begin{bmatrix} m & 0 \\ 0 & I_{yy} \end{bmatrix}\begin{bmatrix} \dot{w} \\ \dot{q} \end{bmatrix}+\begin{bmatrix} 0 & -m\overline{U} \\ 0 & 0 \end{bmatrix}\begin{bmatrix} w \\ q \end{bmatrix}= \begin{bmatrix} \tilde{Z}_{\dot{w}} & \tilde{Z}_{\dot{q}} \\ \tilde{M}_{\dot{w}} & \tilde{M}_{\dot{q}} \end{bmatrix}\begin{bmatrix} \dot{w} \\ \dot{q} \end{bmatrix}+\begin{bmatrix} \tilde{Z}_{w} & \tilde{Z}_{q} \\ \tilde{M}_{w} & \tilde{M}_{q} \end{bmatrix}\begin{bmatrix} w \\ q \end{bmatrix} +\begin{bmatrix} \tilde{Z}_{z^*} & \tilde{Z}_{\theta} \\ \tilde{M}_{z^*} & \tilde{M}_{\theta} \end{bmatrix}\begin{bmatrix} z^* \\ \theta \end{bmatrix}+\begin{bmatrix} Z(t) \\ M(t) \end{bmatrix}, \quad [1]$$

where $\tilde{Z}_{z^*}, \tilde{M}_{z^*}, \tilde{Z}_{\theta}$ and $\tilde{M}_{\theta}$ denote the restoring coefficients. Equation 1 represents another form of the conventional frequency domain analysis in regular waves, assuming excitation to be sinusoidal, but this time referenced to a body fixed axis system. In order for the motions to be determined in the time domain, this equation of motion is reformulated to incorporate convolution integrals. Accordingly Equation 1 can be rewritten in the following way [3]

$$\begin{bmatrix} \dot{w}(t) \\ \dot{q}(t) \end{bmatrix} = M^{-1}\begin{bmatrix} f_3(w,q,z^*,\theta,t) \\ f_5(w,q,z^*,\theta,t) \end{bmatrix} \quad [2]$$

where

$$f_3 = Z_\tau + Z^D\alpha + Z_\alpha + \tilde{Z}_w(\infty)w + \tilde{Z}_q(\infty)q + mq\overline{U}$$
$$f_5 = M_\tau + M^D\alpha + M_\alpha + \tilde{M}_w(\infty)w + \tilde{M}_q(\infty)q. \quad [3]$$

The mass matrix in Equation 2 is given by

$$M = \begin{bmatrix} m - \tilde{Z}_{\dot{w}}(\infty) & -\tilde{Z}_{\dot{q}}(\infty) \\ -\tilde{M}_{\dot{w}}(\infty) & I_{yy} - \tilde{M}_{\dot{q}}(\infty) \end{bmatrix}.$$

The terms with the subscript α in Equation 3 are those relating to the weight and buoyancy (i.e. restoring terms) and incident and diffracted wave excitation contributions, the latter denoted by superscript D. These are described in Sections 3.2 and 4.1. The terms with subscript τ in Equation 3 refer to the radiation forces and moments. In the case of the coupled heave and pitch motions considered in this paper, the radiation forces and moments are expressed fully as

$$Z_\tau = \int_0^t z_w^*(\tau)w(t-\tau)d\tau + \int_0^t z_q^*(\tau)q(t-\tau)d\tau$$
$$M_\tau = \int_0^t m_w^*(\tau)w(t-\tau)d\tau + \int_0^t m_q^*(\tau)q(t-\tau)d\tau, \quad [4]$$

where z_w^*, z_q^*, m_w^* and m_q^* are impulse response functions describing radiation actions (see Section 3.2).

3. CALCULATION OF IMPULSE RESPONSE FUNCTIONS

The representation of fluid actions using convolution integrals requires the calculation of impulse response functions. For this investigation the required impulse response functions are obtained from transforms of frequency domain data. Two frequency domain methods are used, both of which are based on a source distribution over the mean wetted surface of the hull.

3.1 FREQUENCY DOMAIN METHODS

The first method uses a pulsating source distribution with forward speed correction. This satisfies the zero speed linearised free surface condition. Forward speed effects are introduced in a simplified manner by way of corrections to the zero speed solution. These corrections are much the same as those used for strip theories [6]. While it has been shown that this method produces adequate results for moderately high speeds [5,7], a potentially more accurate solution is obtained by explicitly accounting for forward speed effects using a translating, pulsating source method.

The translating, pulsating source method used to obtain the second set of frequency domain data incorporates a velocity potential formulation that exactly satisfies the speed and frequency dependent linearised free surface condition [7]. Correctly accounting for forward speed effects is particularly necessary when examining catamaran vessels, as the interaction between the hulls is of considerable importance.

Hydrodynamic data from both frequency domain methods is initially referenced to an equilibrium axis system. Transformations are performed on this data in order to reference it to a body fixed axis system [2].

3.2 FUNCTIONAL REPRESENTATION OF FLUID ACTIONS

The use of a linear convolution integral formulation to describe the fluid actions acting on the vessel allows for the incorporation of fluid memory effects. The inclusion of such effects is important, as the flow conditions at a particular instant cannot uniquely determine the flow forces and moments occurring at that instant.

Convolution integral formulations have been widely used to model the response of a linear system to arbitrary or random input [8]. In its most general form, for an input *v(t)*, output *f(t)* and impulse response function *h(t)*, the convolution integral takes the form

$$f(t) = \int_{-\infty}^{\infty} h(\tau) v(t-\tau) d\tau .$$

The impulse response functions used to describe the fluid actions in this investigation are determined using Fourier transformations of the frequency domain hydrodynamic properties (oscillatory derivatives). It has been shown that the relationship between the impulse response function and the frequency domain transfer functions is given by the following equation [4]

$$h(\tau) = \frac{1}{\pi}\int_0^{\infty}\{H^R(\omega_e)\cos(\omega_e\tau) - H^I(\omega_e)\sin(\omega_e\tau)\}d\omega_e \text{ for all } \tau \quad [5]$$

where the superscript R and I refer to the real and imaginary parts of the transfer function H.

3.2(a) Radiation Impulse Response Functions

Working in the body fixed axis system, the acceleration and velocity derivatives can be equated to the real and imaginary parts of the transfer function respectively. By imposing the condition of realisability, i.e. $h(\tau) = 0$ for $\tau < 0$, whereby there can be no response prior to input and substituting $\tau = -\tau$, it is possible to show [2] that the impulse response function can be calculated from either the real or imaginary part of the frequency domain transfer function. For example, the heave-heave radiation impulse response function is,

$$z_w(\tau) = \frac{2}{\pi}\int_0^{\infty} \tilde{Z}_w(\omega_e)\cos(\omega_e\tau)d\omega_e$$

$$\text{or} \quad z_w(\tau) = -\frac{2}{\pi}\int_0^{\infty} \tilde{Z}_{\dot{w}}(\omega_e)\omega_e \sin(\omega_e\tau)d\omega_e \quad . [6]$$

These equations for the calculation of the impulse response functions are evaluated numerically using methods proposed initially by Solodovnikov [9] and later simplified by Burcher [10].

To account for the high frequency values of the frequency domain derivatives tending towards a non-zero value, they can be expressed for the heave-heave case as follows,

$$\tilde{Z}_{\dot{w}}(\omega_e) = \tilde{Z}_{\dot{w}}^{*}(\omega_e) + \tilde{Z}_{\dot{w}}(\infty)$$

$$\tilde{Z}_{w}(\omega_e) = \tilde{Z}_{w}^{*}(\omega_e) + \tilde{Z}_{w}(\infty)$$

where $\tilde{Z}_{\dot{w}}(\infty)$ and $\tilde{Z}_{w}(\infty)$ are the asymptotic values of the acceleration and velocity derivatives respectively. Hence the convolution integral representing, say, the heave-heave radiation contribution in Equation 4, can be expressed as

$$f(t) = \tilde{Z}_{\dot{w}}(\infty)\dot{w}(t) + \tilde{Z}_{w}(\infty)w(t) + \int_0^t z_w^{*}(\tau)w(t-\tau)d\tau$$

where $z_w^{*}(t)$ is obtained as per Equation 6, using $\tilde{Z}_{\dot{w}}^{*}(\omega_e)$ or $\tilde{Z}_{w}^{*}(\omega_e)$.

3.2(b) Diffraction Impulse Response Functions

The diffraction impulse response functions differ from the radiation impulse response functions in that they are not zero for $\tau < 0$. This is because the influence of a wave is apparent before it reaches the reference point (at t = 0). Physically this can be explained by describing an oncoming wave that reaches the bow and begins to exert exciting forces/moments on the vessel. This occurs before the wave reaches the midship reference point. To numerically account for this the impulse response functions must include a negative time component [11].

The fact that there must be a negative time component precludes the application of the condition of physical realisability. Hence the equation for the diffraction impulse response function maintains the general form of Equation 5. For example, the heave diffraction impulse response function $z_\alpha(t)$ used in the calculation of

$$Z_\alpha{}^D(t) = \int_0^t z_\alpha(\tau)\alpha(t-\tau)d\tau$$

is given by,

$$z_\alpha(\tau) = \frac{1}{\pi}\int_0^\infty \{Z^R(\omega_e)\cos(\omega_e\tau) - Z^I(\omega_e)\sin(\omega_e\tau)\}d\omega_e,$$

where $\alpha(t)$ denotes the wave elevation and $Z(i\omega_e)$ is the frequency domain complex heave diffraction excitation.

4. TIME DOMAIN METHODS

4.1 CALCULATION OF NON-LINEAR FROUDE-KRYLOV AND RESTORING CONTRIBUTIONS

The simulation of ship motions in the time domain provides the opportunity to incorporate non-linear effects into an otherwise linear system. In this study non-linear Froude-Krylov wave excitation and restoring contributions are included. Experimental measurements indicate differences between transfer functions obtained using varying wave amplitudes [12,13]. Accounting for the non-linearities associated with the incident wave and hydrostatic restoring contributions can be thought of as a plausible first step towards a fully non-linear method. It also gives the opportunity to assess the significance of the non-linear contributions for ships and operational conditions where the instantaneous underwater surface significantly differs from the mean wetted surface used in linear theories. Such contributions are bound to be significant for ships with large flare, large wave amplitudes, coupling between roll and heave and pitch in oblique waves etc.

The non-linear Froude-Krylov and restoring forces and moments are determined by the integration of the incident wave pressure over the instantaneous underwater portion of the hull together with the corresponding weight contributions. The determination of these forces/moments at each instant is a two step process.

The first step is the calculation of the instantaneous underwater portion of the hull. To achieve this, the entire surface of the ship's hull, including the part above the waterline, is discretised using quadrilateral panels. The panels are initially defined with reference to a body fixed axis system with its origin on the keel at amidships. At each time step the panels are placed in their perturbed position by first rotating them about the centre of mass and then translating them by the required amount. Having placed the hull in the perturbed position, the relationship between the panels and the wave elevation, both referenced to an earth fixed axis system, lying say, at the original still waterline, at that instant is examined. Panels that are entirely above the surface of the water are ignored. If the water surface is found to transect a panel, then special measures must be taken. Whilst such panels could simply be ignored, especially if the total number of panels defining the hull surface is high, it has been found that doing so causes step changes in the calculated excitation and hydrostatic actions [14]. Instead new quadrilateral panels are formed by either splitting the transected panels or replacing them with two smaller panels.

Having created the quadrilateral panel description of the instantaneous underwater portion of the hull, the centre of each panel is determined by averaging the co-ordinates of the panel corners. The pressure P acting on each panel is assumed uniform and equal to the pressure acting at the centre of the panel. The contribution of the pressure on each panel to the overall forces and moments is found using the normal of the panel. For example, for a panel of area A_n, unit normal $n_n = (n_{xn}, n_{yn}, n_{zn})$ and centre coordinates, $r^*_n = (x^*_n, y^*_n, z^*_n)$ in the earth fixed axis system, the heave force and pitch moment are given by summing up contributions over N panels defining the instantaneous wetted surface.

$$Z_\alpha(t) = \sum_{n=1}^{N} A_n P(x^*_n, y^*_n, z^*_n) n_{zn} + (-mg\cos\Theta\cos\Phi)$$

$$M_\alpha(t) = -\sum_{n=1}^{N} x_n A_n P(x^*_n, y^*_n, z^*_n) n_{zn} + \sum_{n=1}^{N} z_n A_n P(x^*_n, y^*_n, z^*_n) n_{xn}.$$

It should be noted that the assumption of the pressure acting on the centre of the panel is not entirely accurate. However, provided that a reasonable number of panels are used over the vessel, the effects of any such error are minimised.

Figure 1 shows an example of how the instantaneous underwater portion of the hull is extracted for the calculation of the non-linear Froude-Krylov and restoring forces/moments. In this case both the wavelength and

wave amplitude are out of the range of values considered in this study, but have been chosen simply to highlight the capabilities of the method.

4.2 TIME DOMAIN SIMULATION TECHNIQUES

The time domain simulation of the vessel's motions is carried out using a fourth order Runge-Kutta method of solution [3] in which the heave and pitch velocities (w,q) and displacements (z^*, θ) are calculated for a series of time steps of fixed increment. At each time step, the convolution integrals are evaluated using a numerical convolution method, in which the velocity and impulse response functions are represented using a series of discrete points. The convolution integrals are evaluated using a trapezoidal summation method. The numerical evaluation of the convolution integrals is complicated by the fact that the time steps of the velocity and impulse response functions may be different. Hence the time steps of the impulse response function are used in this evaluation and the velocity trace is linearly interpolated.

Fourier fitting a sinusoidal trace to the heave and pitch response data allows the response amplitude operators (RAOs) for the simulated motions in regular waves to be obtained.

4. DISCUSSION OF RESULTS

The model used in this investigation in both monohull and catamaran configuration was a 4.5m NPL5b round bilge type. Two quadrilateral panel representations of the hull surfaces were used [15]. For the calculation of the frequency domain radiation and diffraction actions, and corresponding impulse response functions, the mean wetted surface of the hull was discretised up to a draft of 0.2m using a total of 334 panels. In the cases of the catamaran models, this discretised hull form was simply mirrored, giving a total number of panels of 668. In addition, the hull surface was panelled up to a depth of 0.5m, essentially the entire hull up to the deck-line. The hull form panelled to the deck had a total of 906 panels on a single hull, giving double that number in the case of the catamaran models. The panelled idealisations of the hull have been made with regard to the aspect ratio of the panels [15]. When calculating the frequency domain data in particular it has been noted that the arrangement of the panels can affect the results, the aspect ratio being an important factor. All idealisations have a panel aspect ratio of 2, which provides a good compromise between economy in the total number of panels and sufficient accuracy [16]. The number and aspect ratio of the panels used in the second panel idealisation is of importance when generating the instantaneous wetted surface by comparing the wave elevation and the instantaneous attitude of the hull, both referenced to the earth fixed axis system.

Heave and pitch related velocity oscillatory derivatives obtained using pulsating and translating, pulsating source distributions are shown in Figures 2,4 and 6 for the NPL5b hull travelling at Fn=0.5 in monohull and catamaran (S/L=0.2 and 0.4) configurations respectively. Figures 3,5 and 7 contain the corresponding impulse response functions that have been calculated from the velocity derivatives. For the monohull it can be seen from Figure 2 that both the pulsating and translating, pulsating source methods produce derivatives that are relatively free from the effects of discontinuities. Nevertheless, the pulsating source velocity derivatives show notable irregularities at 10-12 and 15-17 radians/s and also at about 24 radians/s. Such effects are not apparent in the velocity derivatives calculated using the translating, pulsating source method. The two methods predict derivatives that are fairly similar for the radiation actions related to heave (Z_w and M_w), but there is lesser agreement for the actions linked to pitch (Z_q and M_q). The graphs in Figure 3 show that the impulse response functions calculated from the translating, pulsating source method display a smoother behaviour than those calculated from the pulsating source data, settling to zero more quickly. The oscillatory behaviour observed in the impulse response functions originating from the pulsating source method is most probably due to the presence of the irregularities observed at relatively high frequencies in the pulsating source velocity derivatives. These spikes in the frequency domain value give rise to transients in the impulse response function which, depending on the size of the irregular frequency value, may decay rather slowly. Calculations using an equivalent box technique verify that the first irregular frequency should occur at around 10.5 radians/s.

Examining the frequency domain derivatives for the S/L=0.2 catamaran model, presented in Figure 4, it is clear that the two frequency domain methods produce very different results when calculating the derivatives of a catamaran hull form. It can be seen that the pulsating source data suffers from large spikes in the vicinity of particular frequencies associated with interactions between component hulls. By comparison, the data from the translating, pulsating source method is well behaved throughout the frequency range. The contrast in the natures of the frequency domain data is reflected in the impulse response functions for the S/L=0.2 model that are shown in Figure 5. The impulse response functions calculated from the pulsating source data continue to exhibit large, slowly decaying oscillations long after those calculated from the translating, pulsating source frequency domain data have decayed to zero.

The frequency domain derivatives and corresponding impulse response functions for the S/L=0.4 catamaran model, shown in Figures 6 and 7, reinforce the trends observed in Figures 4 and 5. Figure 6 shows that the differences between the results from the two frequency domain methods noted for the S/L=0.2 model have become even greater as the separation between the hulls is increased. In particular, the discontinuities observed in the pulsating source velocity derivatives have become much larger. The derivatives calculated using the translating, pulsating source method continue to display a smooth behaviour over the range of frequencies calculated. The impulse response functions in Figure 7 display once again the effect of any discontinuities in the relevant frequency domain data. Thus, the oscillations that are seen in the impulse response functions calculated from the pulsating source data are of greater amplitude and decay slower than for the S/L=0.2 model. On the other hand, the impulse response functions calculated from the translating, pulsating frequency domain derivatives show similar characteristics to those calculated for the S/L=0.2 catamaran and the monohull, settling rapidly to zero with very little oscillation.

It should be noted that the trend of the velocity derivatives obtained for the catamarans using the translating, pulsating source method approaching the monohull condition as S/L is increased can be seen by comparing Figures 2,4 and 6. Conversely, increasing S/L when using the pulsating source method will result in an increasing number of discontinuities associated with the interaction between the component hulls, with consequent effects on the impulse response functions.

The predicted heave and pitch transfer functions for the monohull and catamaran (S/L=0.2 and 0.4) models travelling at Fn=0.5 in head waves are presented in Figures 8 to 13. The transfer functions (or RAOs) are defined as heave or pitch amplitude per wave amplitude. The time domain simulations were carried out at two amplitudes (0.001m and 0.05625m) using impulse response functions calculated using both of the frequency domain methods. These results are compared against experimental results obtained using a 1.6m model of the same hull form [5]. The larger of the two wave amplitudes used in the simulations with the 4.5m model is scaled so that it is equivalent to the wave amplitude in the experimental testing with a 1.6m model.

It has been shown [17,18], that when the wave amplitude used in the time domain simulation is low, i.e. commensurate with the concept of linearity, the time domain simulation method used produces results which match very closely those predicted by the frequency domain methods from which the hydrodynamic data originates. This was true for all of the results presented here, the frequency domain data not being included in the graphs to aid their clarity.

It can be seen in Figures 8 and 9 that, for the monohull, the pulsating source method gives the closest agreement to the experimental results in terms of amplitude of response. The translating, pulsating source method gives a better indication of the frequency of resonance. When the amplitude of the exciting waves is increased the resonance peak occurs at a lower frequency for both methods. The heave response determined using the pulsating source impulse response functions moves closer to the experimental results, while the results found using the translating, pulsating source impulse response functions increase in amplitude and become less similar. The monohull pitch amplitudes found using the pulsating source impulse response functions show good agreement with the experimental results, except at relatively high frequencies and, thus, the frequency of resonance is still dissimilar. The pitch responses found using the translating, pulsating source data have again shown that when the wave amplitude is increased, there is an increase in the amplitude and a reduction in the frequency at which the resonance peak occurs.

The responses predicted from the time domain simulations for the two catamaran models are shown in Figures 10 to 13. It can be seen that the responses predicted using the frequency domain data from the pulsating source method show little agreement with the experimental results, except at relatively low frequencies. The translating, pulsating source method by comparison shows reasonable agreement in heave, but less so in pitch and especially for S/L=0.2. For the S/L=0.2 model the simulated heave response using the translating, pulsating source data and the larger wave amplitude still shows good agreement with the experimental results in terms of amplitude, but the frequency at which the peak occurs is again incorrectly predicted. For the S/L=0.4 model the experimental results for heave are closely matched by the motions simulated using the translating, pulsating source data and the lower wave amplitude. Increasing the amplitude of the simulated waves causes the predicted peak in the heave response to increase in amplitude and become lower in frequency, moving it away from the experimental results. However, in pitch, increasing the simulated wave amplitude causes the results calculated using the translating, pulsating source data to better match the experimental results in terms of amplitude, though the resonance peak is still not predicted correctly.

5. CONCLUSIONS

A time domain simulation technique has been used to model the motions of a NPL5b hull form in monohull and catamaran configurations. This time domain

technique uses a convolution integral formulation to describe the radiation and diffraction actions. The Froude-Krylov and restoring forces/moments are calculated using a non-linear method whereby the incident wave pressure is integrated over the instantaneous underwater surface of the hull, also taking into account the corresponding weight contributions.

The impulse response functions used for the convolution integrals were determined using frequency domain velocity derivatives calculated from a pulsating source method, with forward speed correction and a translating, pulsating source method. It was found that the impulse response functions determined from data found using the pulsating source method were generally inferior to those determined using data from the translating, pulsating source method. This was particularly true for the catamaran models, where the impulse response functions calculated from the pulsating source velocity derivatives displayed considerable transient oscillations that took a long time to decay.

Heave and pitch RAOs obtained from the time domain simulations using a small wave amplitude, commensurate with the concept of linearity, produce results which are very close to the corresponding frequency domain analyses when using either pulsating or translating, pulsating source distribution methods. It is interesting to note that the resultant oscillations in the pulsating source impulse response functions do not affect this agreement, which is a sign of the robustness of the numerical methods employed in the current time domain analysis.

For the monohull at the Froude number (Fn=0.5) investigated, the pulsating source method predicts heave and pitch RAOs which, overall, are in closer agreement with experimental measurements than the corresponding predictions obtained from the translating, pulsating source method, although the latter produces a more accurate prediction of the frequency of resonance. Increasing the wave amplitude results in differences in the RAOs predicted by the time domain simulation (either pulsating or translating, pulsating) which are notable in the medium to relatively high frequency range. As a consequence of increasing the wave amplitude, the time domain predictions obtained using the pulsating source method display, in general, closer agreement with the experimental measurements, whilst those of the translating, pulsating source those show less agreement around the resonance. The problem with the translating, pulsating source method can be attributed to the pitch related velocity derivatives [5].

For the catamaran configurations the RAOs predicted by the pulsating source method do not agree with the experimental measurements, except at low frequencies. This is a result of the overestimation of the interactions between the component hulls and their consequent effects on the relevant impulse response functions. Increasing the wave amplitude only affects the RAOs at relatively high frequencies.

At the Froude number investigated, the catamaran RAOs predicted using the translating, pulsating source impulse response functions in the time domain simulation show reasonably good agreement with experimental measurements for the heave RAO and, in general, poor agreement for the pitch RAO. Increasing the wave amplitude results, in general, in poorer agreement with experimental measurements in the vicinity of resonance. There are exceptions, such as the pitch RAO for S/L=0.4. Nevertheless, this method is a superior prediction technique, compared to the pulsating source method, as it accounts more accurately for the interactions between the component hulls.

The results obtained so far from the time domain simulation method, incorporating impulse response functions for radiation and diffraction actions and non-linear contributions for incident wave and restoring force effects, demonstrate its potential. Future work will focus on investigations with higher Froude numbers, motions in oblique waves (six degrees of freedom) and increasing the amplitude of the incident waves used.

6. REFERENCES

1. MOLLAND, A.F., WELLICOME, J.F., TEMAREL, P., CIC, J., TAUNTON, D.J.. 'Experimental Investigation of the Seakeeping Characteristics of Fast Displacement Catamarans in Head and Oblique Seas', Trans. RINA, paper 255, 2000.

2. BAILEY, P.A., PRICE, W.G., TEMAREL, P., 'A Unified Mathematical Model Describing the Manoeuvring of a Ship Travelling in a Seaway'. Trans. RINA 140, 131-149, 1998.

3. BAILEY, P.A., HUDSON, D.A., PRICE, W.G., TEMAREL, P., 'Time Simulation of Manoeuvring and Seakeeping Assessments Using a Unified Mathematical Model'. Trans. RINA, Accepted for publication 2001.

4. BAILEY, P.A., BALLARD, E.J., HUDSON, D.A., TEMAREL, P., 'Time Domain Analysis of Vessels in Waves Accounting for Fluid Memory Effects'. In Proc. NAV2000, International Conference on Ship and Shipping Research, Volume II, pages 9.4.1-9.4.11, Venice, Italy, 2000.

5. BAILEY, P.A., HUDSON, D.A., PRICE, W.G., TEMAREL, P., 'Theoretical and Experimental Validation of the Seakeeping Characteristics of High Speed Mono and Multi-Hulled Vessels'. FAST'99: Fifth International Conference on Fast Sea Transportation, Seattle, 429-441, 1999.

6. BECK, R.F., CUMMINS, W.E., DALZELL, J.F., MANDEL, P., WEBSTER, W.C., 'Principles of Naval Architecture', Volume 3, Chapter 8, SNAME, 1989.

7. INGLIS, R.B. , PRICE, W.G., 'A Three Dimensional Ship Motion Theory: Comparison Between Theoretical Predictions and Experimental Data of the Hydrodynamic Coefficients with Forward Speed', Trans. RINA 124, 141-157, 1982.

8. MEIROVITCH, L., 'Elements of Vibration Analysis', McGraw Hill, 1986.

9. SOLODOVNIKOV, V.V., 'Statistical Dynamics of Linear Automatic Control Systems', D. Van Nostrand Co. Ltd., London, 1965.

10. BURCHER, R.K., 'Fluid Forces Acting on a Manoeuvring Ship', PhD. Thesis, University of London, 1974.

11. KING, B.K., BECK, R.F., MAGEE, A.R., 'Seakeeping Calculations with Forward Speed Using Time Domain Analysis'. In 17th Symposium on Naval Hydrodynamics, pages 557-596, The Hague, Netherlands, 1988.

12. McTAGGART, K., DATTA, I., STIRLING, A., GIBSON, S., GLEN, I., 'Motions and Loads of a Hydroelastic Frigate Model in Severe Seas, Trans. SNAME, 105, 427-454, 1997.

13. O'DEA, J., POWERS, E., ZSELECSKY, J., 'Theoretical and Experimental Study of the Non-Linearities in Vertical Plane Ship Motions'. Proc. 19th Symposium on Naval Hydrodynamics, 1992.

14. BAILEY, P.A., 'Manoeuvring of a Ship in a Seaway', PhD. Thesis, University of Southampton, 1999.

15. BAILEY, P.A., HUDSON, D.A., PRICE, W.G., TEMAREL, P., 'A Simple yet Rational Approach to the Panelling of a Hull Surface'. Trans. RINA, Accepted for publication 2001.

16. BAILEY, P.A., HUDSON, D.A., PRICE, W.G., TEMAREL, P., 'Comparisons Between Theory and Experiment in a Seakeeping Validation Study', Trans. RINA, paper 261, 2000.

17. BAILEY, P.A., BALLARD, E.J., HUDSON, D.A., TEMAREL, P., 'The Effect of Non-Linear Froude-Krylov Forces on the Seakeeping of Monohull Vessels Using a Novel Calculation Method', 3rd Numerical Towing Tank Symposium, 2000.

18. BAILEY, P.A., BALLARD, E.J., TEMAREL, P., 'Dynamic Behaviour of Rigid Mono- and Multi-Hulled Vessels in Waves, Incorporating Non-Linear Excitation', To be published in proceeding of PRADS 2001, 2001.

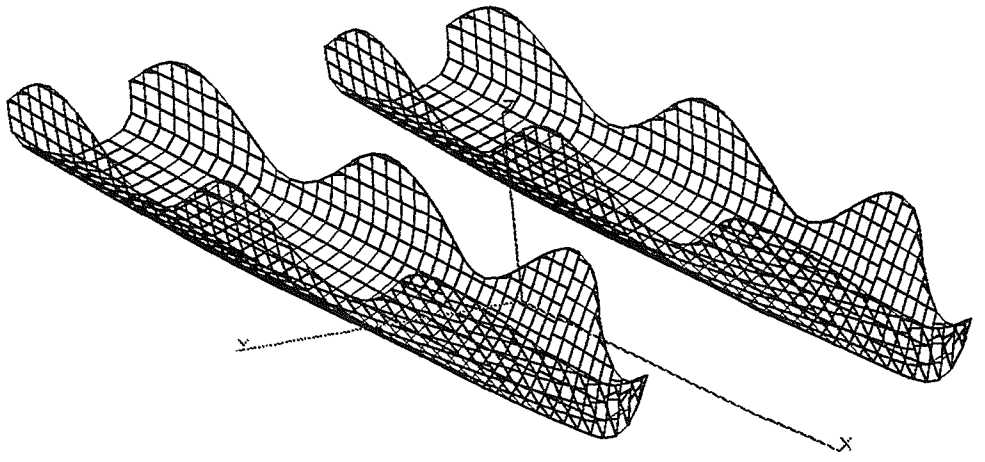

Figure 1: NPL5b 4.5m catamaran model, S/L=0.2, wavelength=1.53m, wave amplitude=0.1m, Fn=0.5.

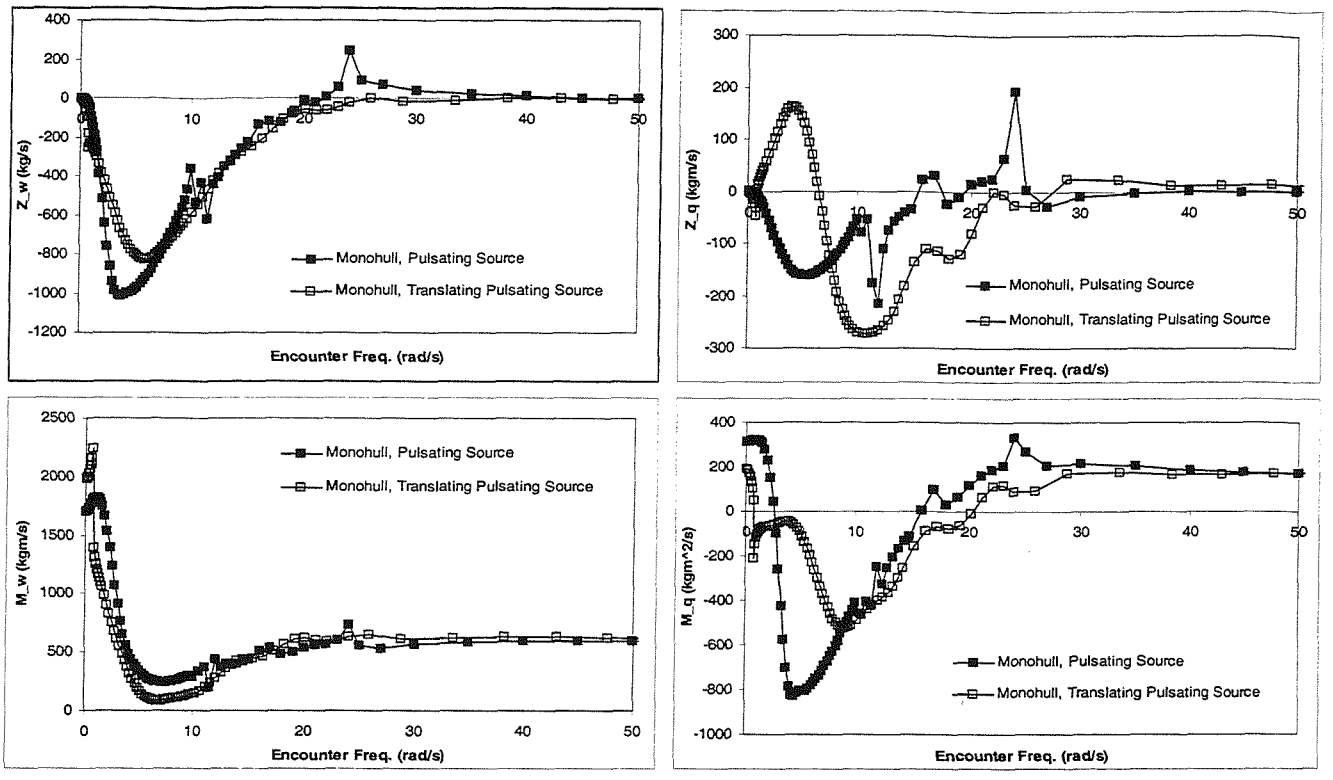

Figure 2: Frequency domain velocity derivatives calculated using pulsating and translating, pulsating source methods for NPL5b monohull, Fn=0.5.

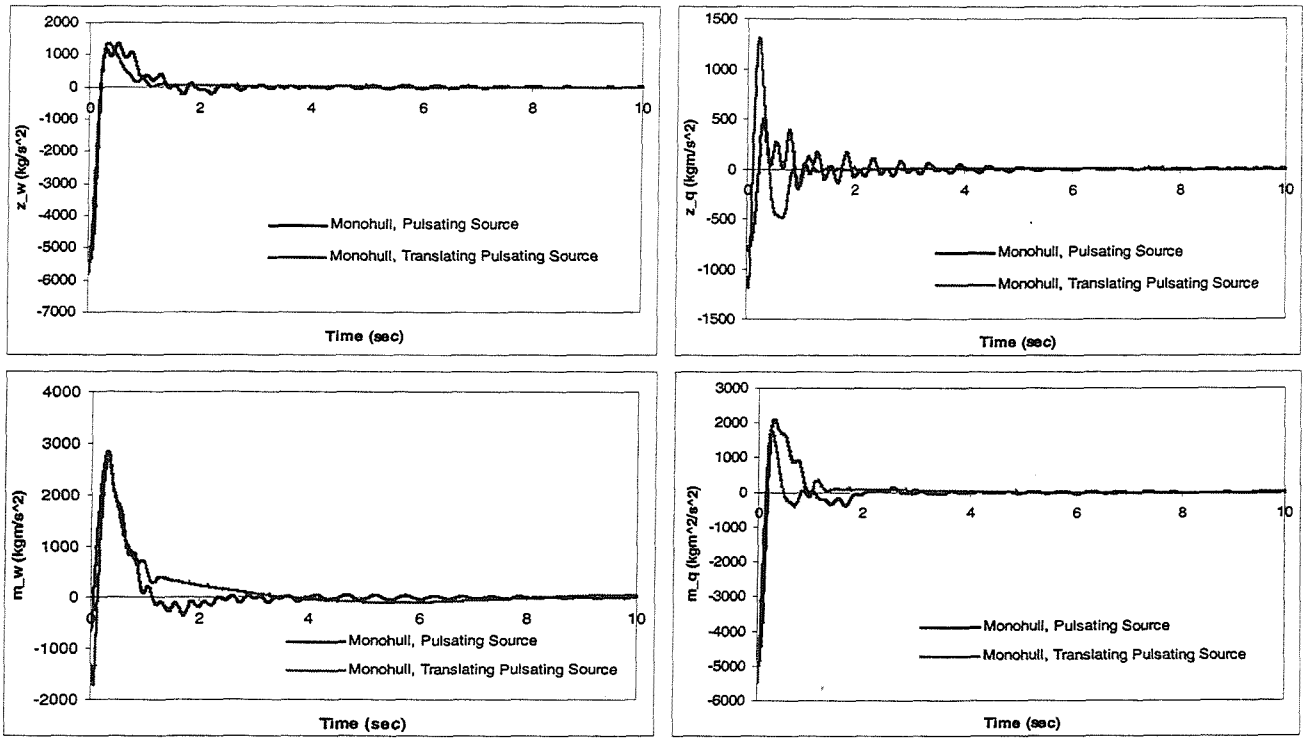

Figure 3: Radiation impulse response functions, calculated from frequency domain velocity derivatives for NPL5b monohull, Fn=0.5.

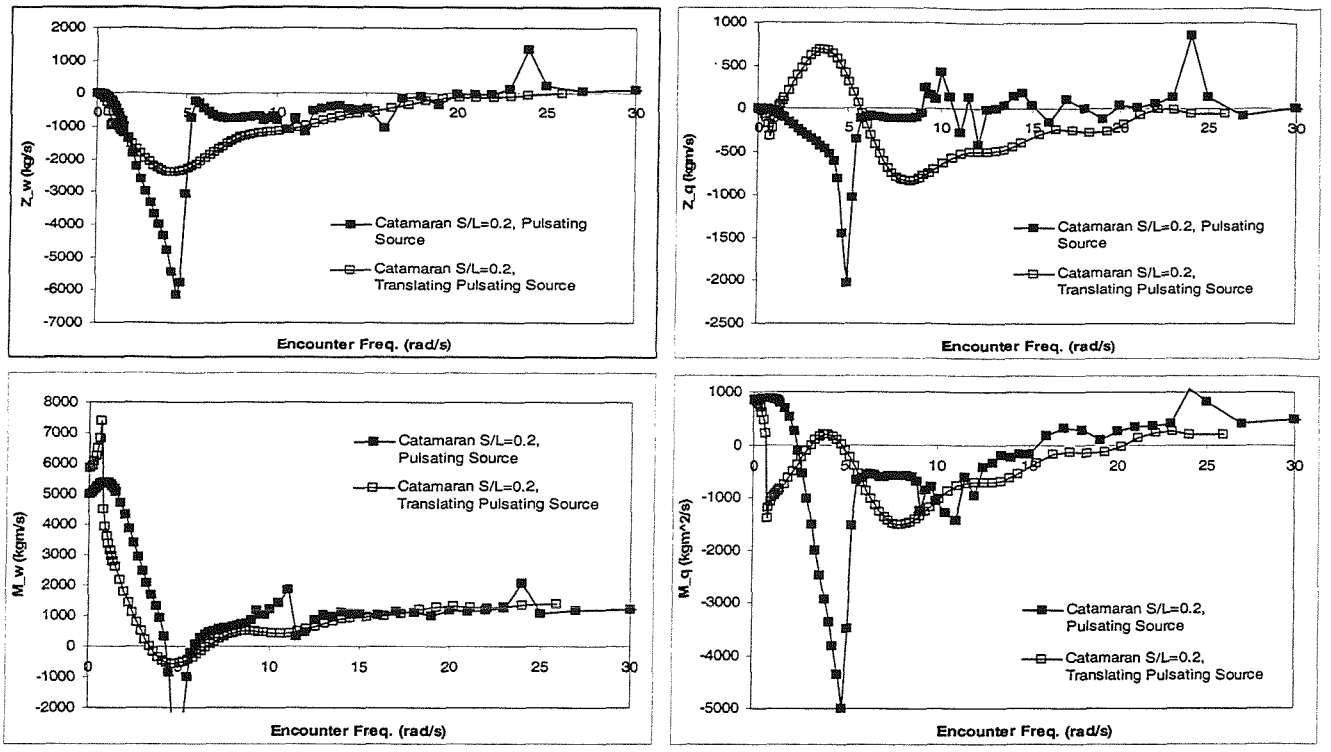

Figure 4: Frequency domain velocity derivatives calculated using pulsating and translating, pulsating source methods for NPL5b catamaran, S/L=0.2, Fn=0.5.

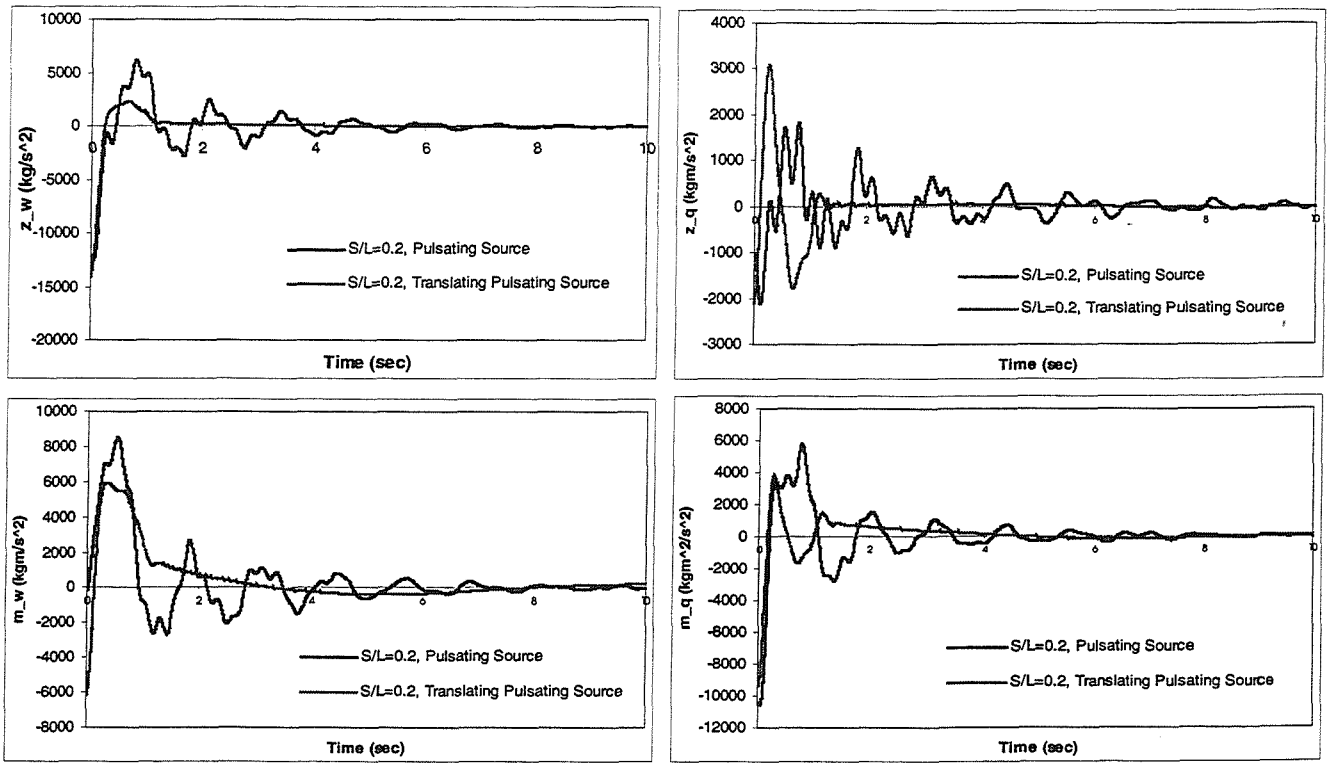

Figure 5: Radiation impulse response functions, calculated from frequency domain velocity derivatives for NPL5b catamaran, S/L=0.2, Fn=0.5.

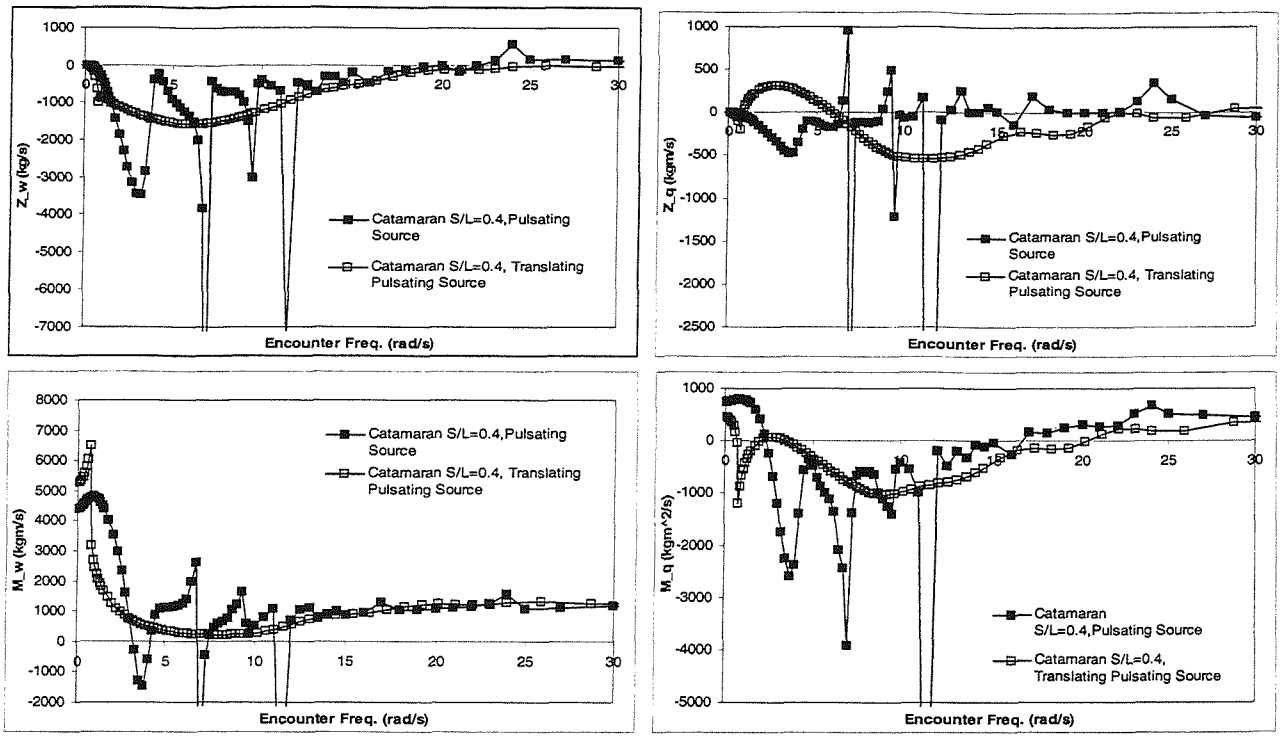

Figure 6: Frequency domain velocity derivative data calculated using pulsating and translating, pulsating source methods for NPL5b catamaran, S/L=0.4, Fn=0.5.

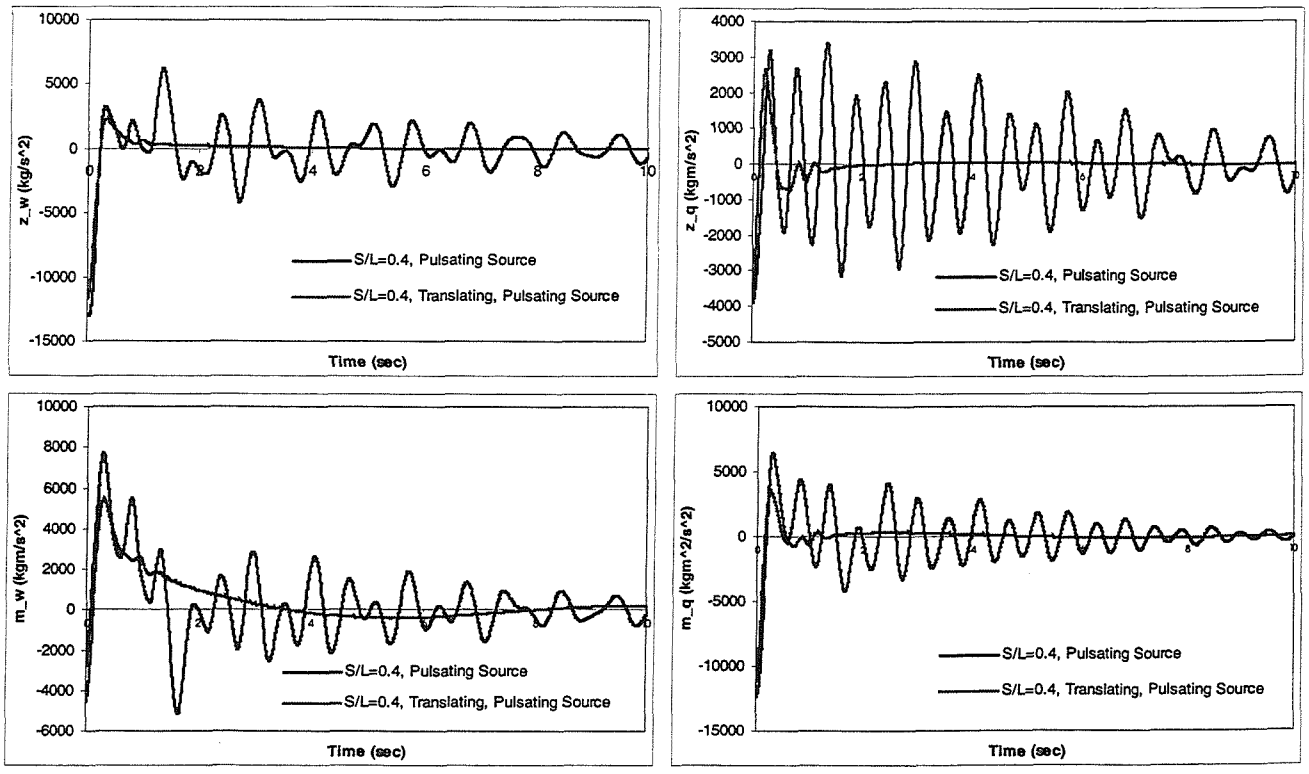

Figure 7: Radiation impulse response functions, calculated from frequency domain velocity derivative data for NPL5b catamaran, S/L=0.4, Fn=0.5.

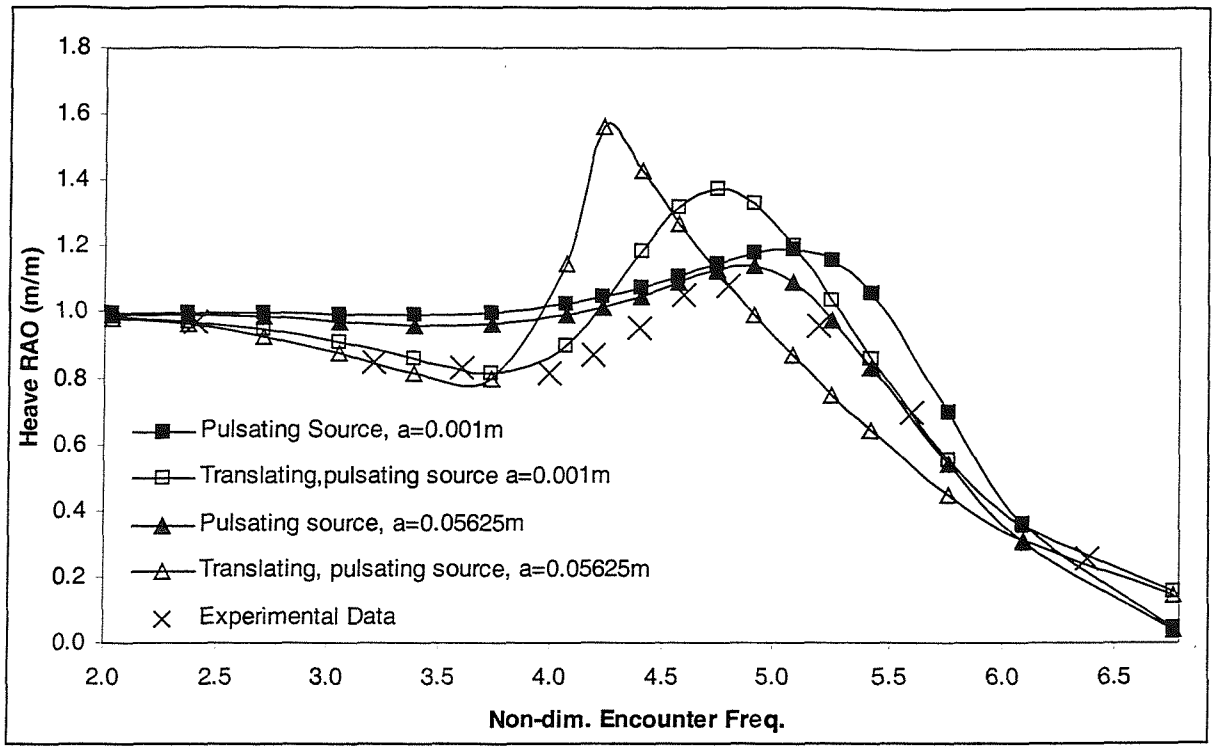

Figure 8: Heave response amplitude operators for NPL5b monohull, Fn=0.5, Heading=180 degrees.

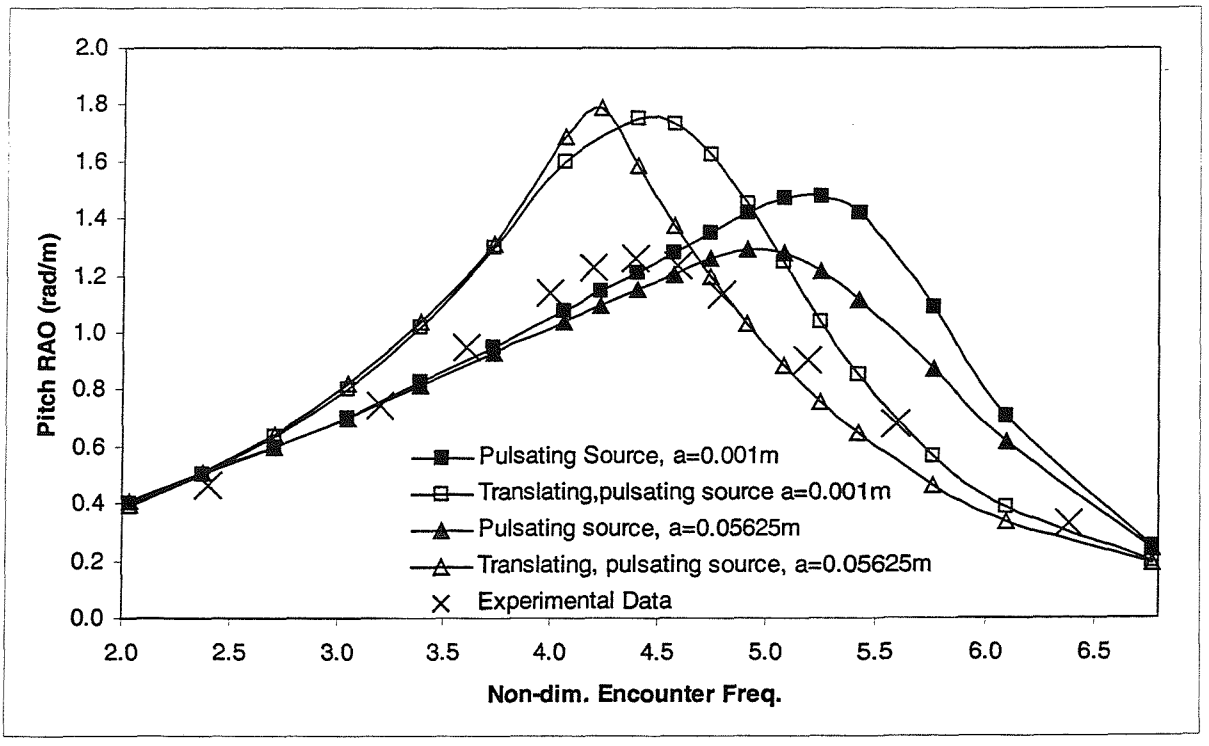

Figure 9: Pitch response amplitude operators for NPL5b monohull, Fn=0.5, Heading=180 degrees.

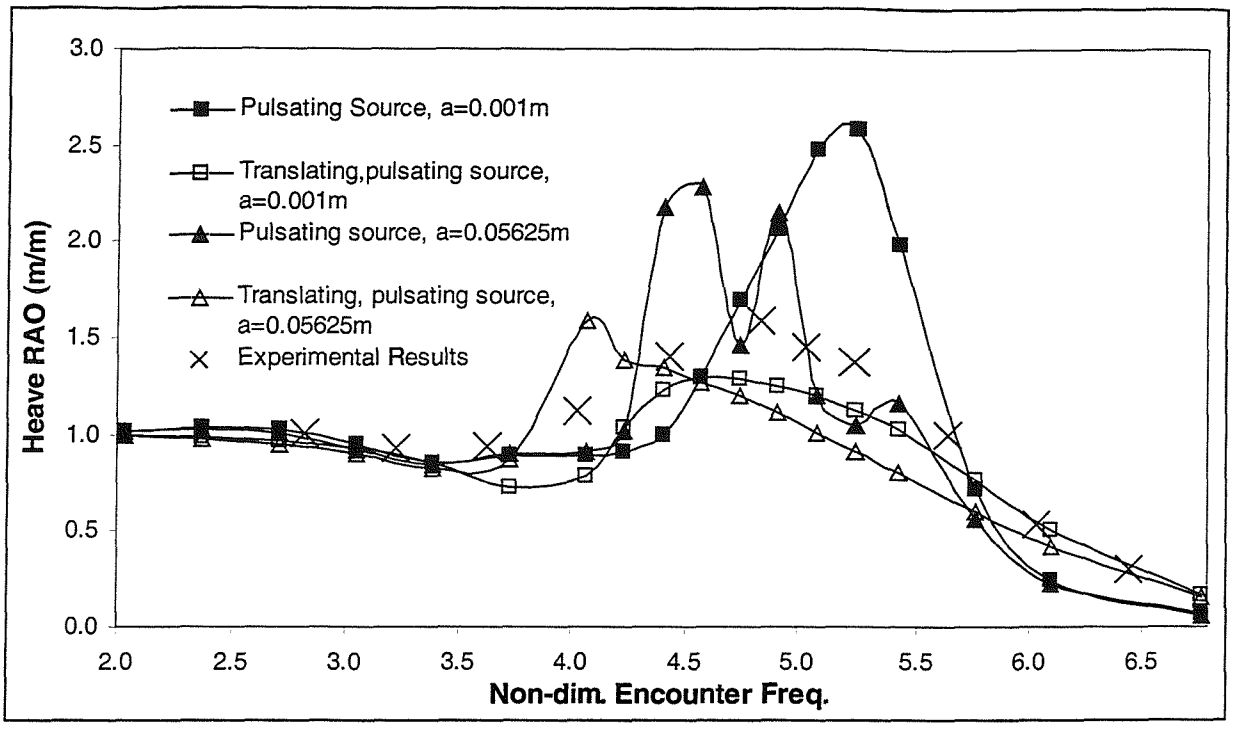

Figure 10: Heave response amplitude operators for NPL5b catamaran, S/L=0.2, Fn=0.5, Heading=180 degrees.

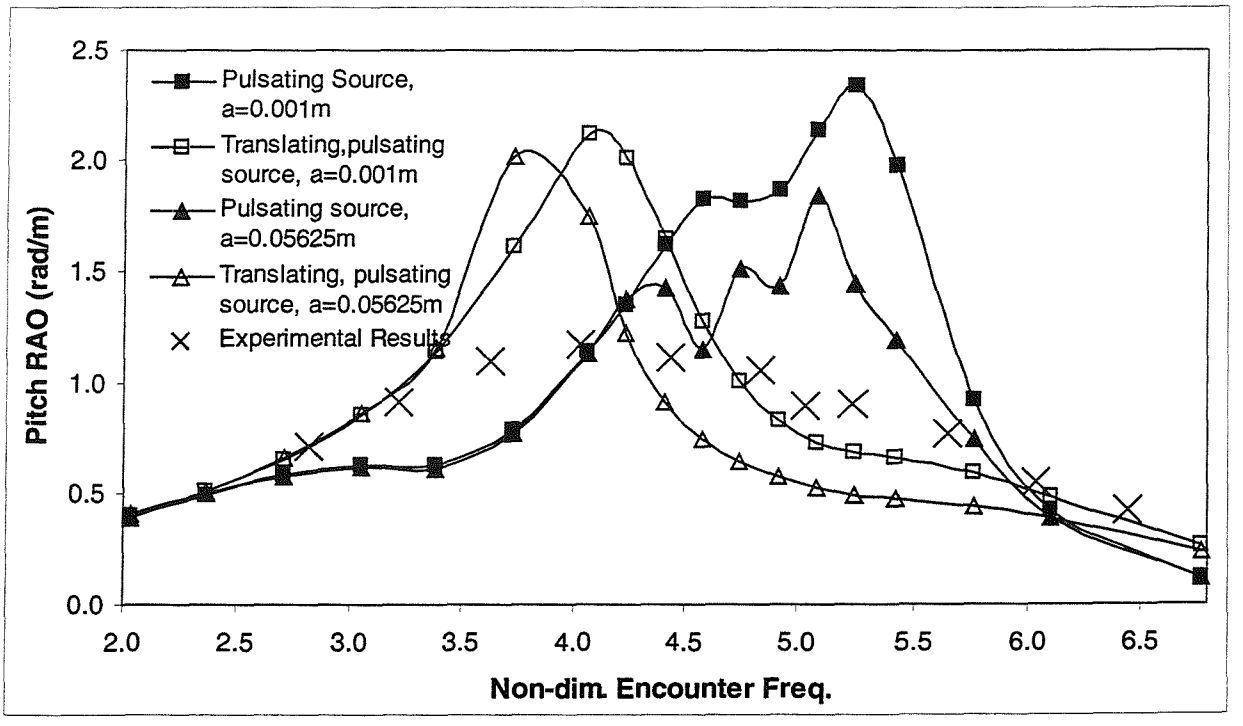

Figure 11: Pitch response amplitude operators for NPL5b catamaran, S/L=0.2, Fn=0.5, Heading=180 degrees.

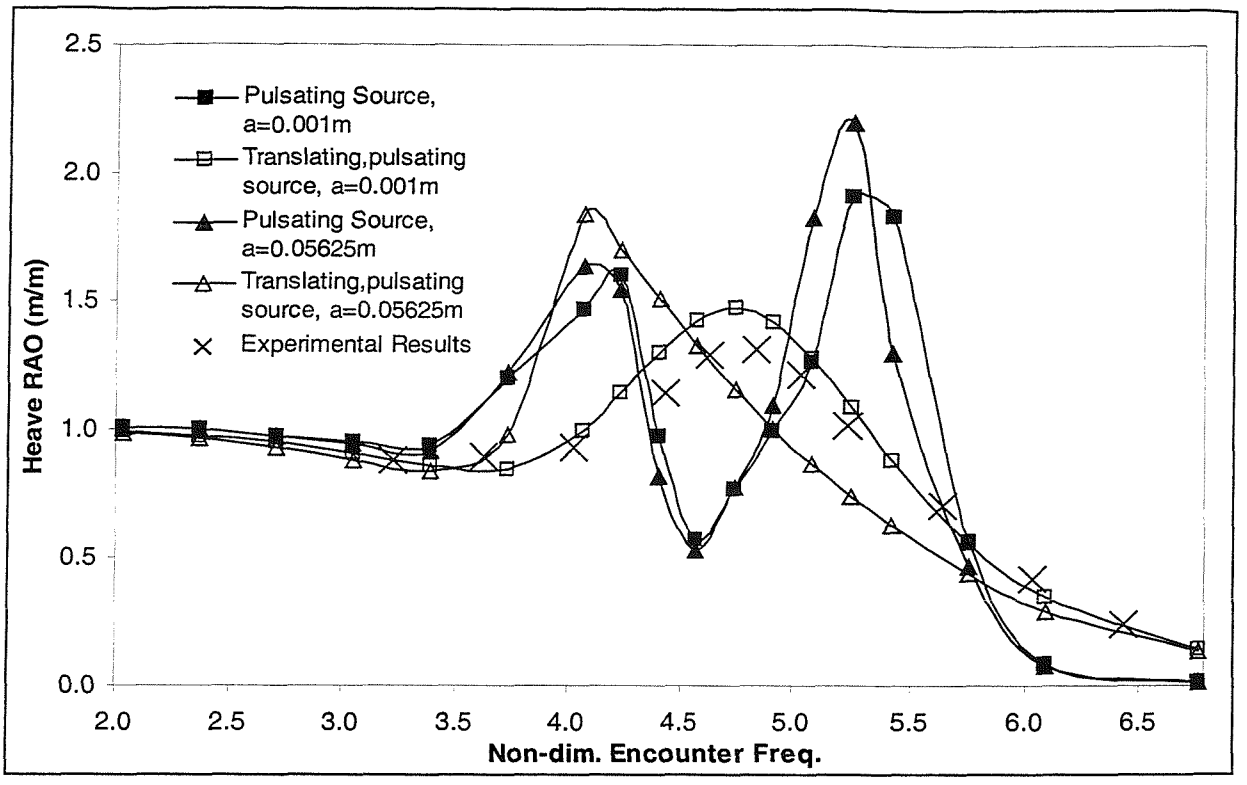

Figure 12: Heave response amplitude operators for NPL5b catamaran, S/L=0.4, Fn=0.5, Heading=180 degrees.

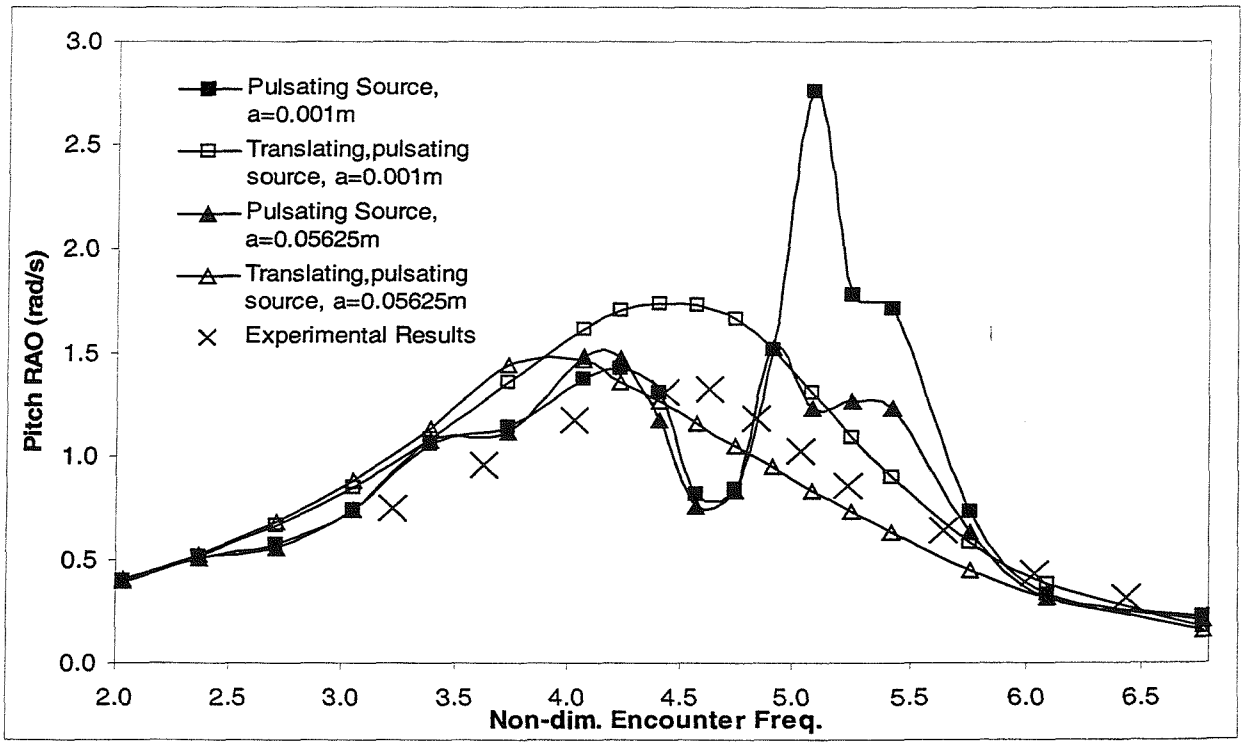

Figure 13: Heave response amplitude operators for NPL5b catamaran, S/L=0.4, Fn=0.5, Heading=180 degrees.

References

[1] P. A. Bailey, D. A. Hudson, W. G. Price, and P. Temarel. The measurement and prediction of fluid actions experienced by a manoeuvring vessel. In *Proc. Intl. Symposium and Workshop on Forces acting on a Manoeuvring Vessel, MAN '98*, pages 117–123, Val de Reuil, France, 1998.

[2] P. A. Bailey, D. A. Hudson, W. G. Price, and P. Temarel. Theoretical and experimental techniques for predicting seakeeping and manoeuvring ship characteristics. In *RINA Intl. Conf. on Ship Motions and Manoeuvrability, Paper No. 5*, London, 1998.

[3] P. A. Bailey, D. A. Hudson, W. G. Price, and P. Temarel. A validation of speed and frequency dependence in seakeeping. In *Proc. Intl. Shipbuilding Conf.*, St. Petersburg, 1998.

[4] P. A. Bailey, D. A. Hudson, W. G. Price, and P. Temarel. Time simulation of manoeuvring and seakeeping assessments using a unified mathematical model. *Trans. RINA*, 142, 2001.

[5] P. A. Bailey, D. A. Hudson, W. G. Price, and P. Temarel. A simple yet rational approach to the panelling of hull surfaces. *Trans. RINA*, (accepted for publication), 2002.

[6] P. A. Bailey, W. G. Price, and P. Temarel. A unified mathematical model describing the manoeuvring of a ship travelling in a seaway. *Trans. RINA*, 140:131–149, 1998.

[7] P.A. Bailey. *Manoeuvring of a Ship in a Seaway.* PhD Thesis, University of Southampton, 1999.

[8] P.A. Bailey, D.A. Hudson, W.G. Price, and P. Temarel. Comparison between theory and experiment in a seakeeping valication study. *Trans. RINA*, (accepted for publication), 2001.

[9] R. F. Beck, Y Cao, S. Scorpio, and W. Schultz. Nonlinear ship motion computations using the desingularized method. In *20th Symposium on Naval Hydrodynamics*, pages 227–247, Santa Barbara, California, USA, 1994.

[10] R.B Beck and S. Liapis. Transient motions of floating bodies at zero forward speed. *Journal of Ship Research*, 31(3):164–176, Sept. 1987.

[11] R.F. Beck, W.E. Cummins, J.F. Dalzell, P. Mandel, and W.C. Webster. *Principles of Naval Architecture*, volume 3, chapter 8. Trans. SNAME, 1989.

[12] M. Bessho. On the fundamental singularity in the theory of ship motions in a seaway. *Memoirs of the Defence Academy of Japan*, 17(3):95–105, 1977.

[13] H. Bingham, F. Korsmeyer, and J. N. Newman. Prediction of the seakeeping characteristics of ships. In *20th Symposium on Naval Hydrodynamics*, pages 27–47, Santa Barbara, California, USA, 1994.

[14] H. Bingham, F. T. Korsmeyer, J. N. Newman, and G. E. Osborne. The simulation of ship motions. In *Proceedings 6th International Conference on Numerical Ship Hydrodynamics*, pages 561–579, 1993.

[15] R. E. D. Bishop, R. K. Burcher, and W. G. Price. The fifth annual Fairey Lecture: on the linear representation of fluid forces and moments in unsteady flow. *Journal of Sound and Vibration*, 29(1):113–128, 1973.

[16] R. E. D. Bishop, R. K. Burcher, and W. G. Price. The uses of functional analysis in ship dynamics. *Proc. R. Soc. London*, A332:23–35, 1973.

[17] R. E. D. Bishop and A. G. Parkinson. Directional stability and control of rigid marine vehicles. Report 3/70, University College London, 1970.

[18] R. E. D. Bishop and W. G. Price. On the use of equilibrium axes and body axes in the dynamics of a rigid ship. *Journal of Mechanical Engineering Science*, 23(5):243–256, 1981.

[19] R. E. D. Bishop, W. G. Price, and P. K. Y. Tam. The representation of hull sections and its effects on estimated hydrodynamic actions and wave responses. *Trans. RINA*, 120:115–123, 1978.

[20] R.E.D. Bishop, W.G. Price, and P. Temarel. Hydrodynamic coefficients of some swaying and rolling cylinders of arbitrary shape. *International Shipbuilding Progress*, 27:54–65, 1980.

[21] R. Brard. A vortex theory for the manoeuvring ship with respect to the history of her motion. In *Fifth Symposium on Naval Hydrodynamics*, pages 815–911, Bergen, 1964.

[22] R. K. Burcher. *Fluid forces acting on a manoeuvring ship*. PhD Thesis, University of London, 1974.

[23] R. Centeno, K.S. Varyani, and C. Guedes Soares. Experimental study on the influence of hull spacing on hard-chine catamaran motions. *Journal of Ship Research*, 45:216–227, 2001.

[24] M. S. Chang. Computations of three-dimensional ship-motions with forward speed. In *2nd International Conference on Numerical Ship Hydrodynamics*, pages 124–135, Berkeley, USA, 1977.

[25] W. E. Cummins. The impulse response function and ship motions. *Schiffstechnik*, 9, 1962.

[26] S. X. Du. *A complete frequency domain analysis method of linear three-dimensional hydroelastic response of floating structures in waves*. PhD Thesis, China Ship Scientific Research Centre, Wuxi, China, 1996.

[27] S. X. Du, D. A. Hudson, W. G. Price, and P. Temarel. Comparison of numerical evaluation techniques for the hydrodynamic analysis of a ship travelling in waves. *Trans. RINA*, 141:236–258, 1999.

[28] S. X. Du, D. A. Hudson, W.G. Price, and P. Temarel. A validation study on mathematical models of speed and frequency dependence in seakeeping. *Proceedings of the Institution of Mechanical Engineers, Part C*, 214:181–202, 2000.

[29] J. Dudziak and M. Pawlowski. A simplified approach to time domain analysis of ship behaviour in head irregular seas. In *International Shipbuilding Conference*, pages 366–373, St. Petersburg, Russia, 1998.

[30] O. M. Faltinsen. *Sea Loads on Ships and Offshore Structures*. Cambridge Ocean Technology Series. Cambridge University Press, 1990.

[31] O. M. Faltinsen and F. C. Michelsen. Motions of large structures in waves at zero Froude number. In R. E. D. Bishop and W. G. Price, editors, *International Symposium on the Dynamics of Marine Vehicles and Structures in Waves*, pages 91–106, London, UK, April 1974. IMechE.

[32] O. M. Faltinsen and R. Zhao. Numerical prediction of ship motions at high forward speed. *Philosophical Transactions of The Royal Society*, 334:241–252, 1991.

[33] N. Fonseca and C. Guedes Soares. *Marine, Offshore and Ice Technology*, chapter Time Domain Analysis of Vertical Ship Motions, pages 225–242. Computational Mechanics Publication, 1994.

[34] N. Fonseca and C. Guedes Soares. Time-domain analysis of large-amplitude vertical ship motions and wave loads. *Journal of Ship Research*, 42:139–153, 1998.

[35] W. Frank. Oscillations of cylinders in or below the free surface of deep fluids. Technical Report 2375, NSRDC Report, 1967.

[36] W. Froude. On the rolling of ships. *Trans. INA*, 2:180–229, 1861.

[37] C. J. Garrison. Hydrodynamics of large objects in the sea part 1: Hydrodynamic analysis. *Journal of Hydronautics*, 8:5–12, 1974.

[38] J. Gerritsma and W. Beukelman. The distribution of the hydrodynamic forces on a heaving and pitching ship model in still water. In *Fifth Symposium on Naval Hydrodynamics*, pages 219–257, 1964.

[39] J. Gerritsma and W. Beukelman. Analysis of the modified strip theory for the calculation of ship motions and wave bending moments. *International Shipbuilding Progress*, 14:319–337, 1967.

[40] P. Guevel and J. Bougis. Ship motions with forward speed in infinite depth. *International Shipbuilding Progress*, 29:103–117, 1982.

[41] G. E. Hearn, W. Hills, and K. Sariöz. Practical seakeeping for design: A ship shape approach. *Trans. RINA*, 134:225–244, 1992.

[42] Y. Huang and P.D. Sclavounos. Nonlinear ship motions. *Journal of Ship Research*, 42:120–130, 1998.

[43] D.A. Hudson, W.G. Price, and P. Temarel. Seakeeping performance of high speed displacement craft. In *Fast '95*, pages 877–892, Lubeck, 1995.

[44] R. H. M. Huijsmans and A. J. Hermans. A fast algorithm for computation of 3-D ship motions at moderate forward speed. In *Proceedings 4th International Conference on Numerical Ship Hydrodynamics*, pages 124+, Washington, 1985.

[45] R. B. Inglis. *A Three Dimensional Analysis of the Motion of a Rigid Ship in Waves*. PhD thesis, University of London, 1980.

[46] R. B. Inglis and W. G. Price. Calculation of the velocity potential of a translating, pulsating source. *Trans. RINA*, 123:163–175, 1981.

[47] R. B. Inglis and W. G. Price. The influence of speed dependent boundary conditions in three dimensional ship motion problems. *Intl. Shipbuilding Progress*, 28(318):22–29, 1981.

[48] R. B. Inglis and W. G. Price. A three-dimensional ship motion theory: Calculation of wave loading and response with forward speed. *Trans. RINA*, 124:183–192, 1982.

[49] R. B. Inglis and W. G. Price. A three dimensional ship motions theory: Comparison between theoretical predictions and experimental data of the hydrodynamic data with forward speed. *Trans. RINA*, 124:141–157, 1982.

[50] F. John. On the motion of floating bodies. *Communications on Pure and Applied Maths*, 3:45–101, 1950.

[51] C.H. Kim. Motions and loads on a catamaran ship of arbitrary shape in a seaway. *Journal of Hydronautics*, 10:8–17, 1976.

[52] B. K. King, R. F. Beck, and A. R. Magee. Seakeeping calculations with forward speed using time-domain analysis. In *17th Symposium on Naval Hydrodynamics*, pages 577–596, The Hague, The Netherlands, 1988.

[53] F. T. Korsmeyer and H. B. Bingham. The forward speed diffraction problem. *Journal of Ship Research*, 42(2):99–112, 1998.

[54] B. V. Korvin-Kroukovsky. Investigation of ship motions in regular waves. *SNAME*, 63:386–435, 1955.

[55] B. V. Korvin-Kroukovsky and W. R. Jacobs. Pitching and heaving motions of a ship in regular waves. *SNAME*, 65:590–631, 1957.

[56] D. C. Kring, Y-F. Huang, and P. D. Sclavounos. Nonlinear ship motions and wave induced loads by Rankine method. In *21st Symposium of Naval Hydrodynamics*, 1997.

[57] D. C. Kring and P. D. Sclavounos. A time-domain seakeeping simulation for fast ships. In *FAST '97: Proceedings of the Fourth International Conference on Fast Sea Transportation*, pages 43–49, Sydney, Australia, 1997.

[58] A. Krylov. A general theory of the oscillations of a ship on waves. *Trans. INA*, 40:135–196, 1898.

[59] A. N. Krylov. A new theory of the pitching motions of the pitching of ships on waves and of the stresses produced by this motion. *Trans INA*, 37:326–359, 1896.

[60] L. Landweber and M. Macagno. Added masses of two-dimensional forms by conformal mapping. *Journal of Ship Research*, pages 109–116, 1967.

[61] C. M. Lee, H. D. Jones, and R. M. Curphey. Prediction of motion and hydrodynamic loads of catamarans. *Marine Technology*, 10(4):392–405, October 1973.

[62] F. M. Lewis. The inertia of water surrounding a vibrating ship. *Trans. SNAME*, 63:1–20, 1929.

[63] W. M. Lin, M. Meinhold, and N. Salvesen. Large-amplitude motions and wave-loads for ship design. In *20th Symposium on Naval Hydrodynamics*, pages 205–226, Santa Barbara, California, USA, 1994.

[64] W. M. Lin and D. Yue. Numerical solutions for large amplitude ship motions in the time domain. In *18th Symposium on Naval Hydrodynamics*, pages 41–66, University of Michigan, Ann Arbor, 1990.

[65] A. R. J. M. Lloyd. *Seakeeping, ship behaviour in rough weather.* Published by Lloyd, 26 Spithead Avenue, Gosport, Hamphire, UK., 1998.

[66] B. Maskew. Prediction of nonlinear wave/hull interactions on complex vessels. In *Proceedings 19th Symposium on Naval Hydrodynamics*, Seoul, Korea, August 1992.

[67] K. McTaggart, I. Datta, A. Stirling, S. Gibson, and I. Glen. Motions and loads of a hydroelastic frigate model in severe seas. *Trans. SNAME*, 105:427–454, 1997.

[68] L Meirovitch. *Elements of Vibration Analysis.* McGraw Hill, 1986.

[69] A.F. Molland, J.F. Wellicome, P. Temarel, J. Cic, and D.J. Taunton. Experimental investigation of the seakeeping characteristics of fast displacement catamarans and head and oblique seas. *Trans. RINA*, paper 261, 2000.

[70] S Nakamura. Comparison of measured ship motions and thrust increase of Series 60 ship models in reular head waves. In *11th ITTC Conference, Seakeeping Committee Report*, pages 420–426, Tokyo, 1966.

[71] S. Nakamura. *Applied Numerical Methods in C.* Prentice Hall, 1993.

[72] D. E. Nakos and P. D. Sclavounos. On steady and unsteady ship wave patterns. *Journal of Fluid Mechanics*, 215:263–288, 1990.

[73] J. N. Newman. A slender-body theory for ship oscillations in waves. *Journal of Fluid Mechanics*, 18:602–618, 1964.

[74] J. N. Newman. The exciting forces on a moving body in waves. *Journal of Ship Research*, 9:190–199, 1965.

[75] J. N. Newman. Applications of slender-body theory in ship hydrodynamics. *Ann. Rev. Fluid Mech.*, 2:67–94, 1970.

[76] J. N. Newman. *Marine Hydrodynamics*. The MIT Press, Cambridge, MA, 1977.

[77] J. N. Newman. The theory of ship motions. *Advances in Applied Mechanics*, 18:221–283, 1978.

[78] J. N. Newman and P. Sclavounos. The unified theory of ship motions. In *Thirteenth Symposium on Naval Hydrodynamics*, pages 373–394, Tokyo, 1980.

[79] J O'Dea, E. Powers, and J. Zselecsky. Theoretical and experimental study of the non-linearities in vertical plane ship motions. *Proc. 19th Symposium on Naval Hydrodynamics*, 1992.

[80] T. F. Ogilvie. Recent progress toward understanding and prediction of ship motions. In *5th Symp. on Naval Hydrodynamics*, pages 3–80, Bergen, 1964.

[81] T. F. Ogilvie and E. O. Tuck. A rational strip theory for ship motions. Technical Report 013, University of Michigan, Ann Arbor, 1969.

[82] M. Ohkusu. On the motion of twin hull ships in waves. *J. Society Naval Architects of Japan*, 129, 1971.

[83] M. Ohkusu and O. Faltinsen. Prediction of radiation forces on a catamaran at high froude number. In *Proc. 18th Intl. Symposium on Naval Hydrodynamics*, Ann Arbor, 1990.

[84] M. Ohkusu and H. Iwashita. Evaluation of the Green function for ship motions at forward speed and application to radiation and diffraction problems. In *Proceedings 4th International Workshop on Water Waves and Floating Bodies*, pages 195–199, Øystese, Norway, 1989.

[85] W. G. Price and R. E. D. Bishop. *Probabilistic Theory of Ship Dynamics*. Chapman and Hall, 1974.

[86] N. Salvesen, E. O. Tuck, and O. M. Faltinsen. Ship motions and sea loads. *SNAME*, 78:250–280, 1970.

[87] P. D. Sclavounos, D. E. Nakos, and Y. Huang. Seakeeping and wave induced loads on ships with flare by a Rankine panel method. In *6th International Conference on Numerical Ship Hydrodynamics*, pages 57–77, august 1993.

[88] P.D. Sclavounos. The unified slender-body theory: Ship motions in waves. In *15th Symposium on Naval Hydrodynamics*, pages 177–193, Hamburg, Germany, 1984.

[89] Manual for ShipShape. Wolfson Unit for Marine Technology and Indutrial Aerodynamics (WUMTIA), University of Southampton, UK., 1992.

[90] V. V. Solodovnikov. *Statistical Dynamics of Linear Automatic Control Systems*. D. Van Nostrand Company Ltd., London, England, 1965.

[91] M. A. Squires and P. A. Wilson. An investigation into the translating pulsating Green's function for ship motions prediction. In T.K.S. Murthy and J.A. Alaez, editors, *Design of Marine and Offshore Structures*, pages 305–322, 1992.

[92] R. Timman and J. N. Newman. The coupled damping coefficients of symmetrical ships. *Journal of Ship Research*, 5, 1962.

[93] F. H. Todd. Some further experiments on single-screw merchant ship forms- Series 60. *Trans. SNAME*, 61:516–589, 1953.

[94] F. Ursell. On the heaving motions of a circular cylinder on the surface of a fluid. *Quarterly Journal of Mechanics and Applied Mathematics*, 2:218–231, 1949.

[95] G. van Leeuwen. The lateral damping and added mass of an oscillating ship model. Report of Shipbuilding Laboratory 23, Delft University of Technology, 1964.

[96] A.P. Van't Veer and F.R.T Siregar. The interaction effects on a catamaran travelling with forward speed in waves. In *Fast '95*, pages 87–98, Seattle, 1995.

[97] G. Vossers, W.A. Swaan, and H. Rijken. Vertical and lateral bending moment measurements of Series 60 models. *International Shipbuilding Progress*, 8, 1961.

[98] J. H. Vugts. The hydrodynamic forces and ship motions in oblique waves. Report 150S, Research Centre TNO for Shipbuilding, Delft, The Netherlands, 1971.

[99] S. Wang and R. Wahab. Heaving oscillations of twin cylinders in a free surface. *Journal of Ship Research*, 15(1):33–48, 1971.

[100] J. Y. Wehausen and E. V. Laitone. Surface waves. In *Encyclopædia of Physics*, volume 9, pages 446–778. Springer Verlag, 1960.

[101] J.F. Wellicome, P. Temarel, A.F. Molland, and P.R. Couser. Experimental measurements of the seakeeping characteristics of fast displacement catamarans in long crested head seas. *Ship Science Report 113*, 1999.

[102] G. X. Wu and R. Eatock-Taylor. A Green's function form for ship motions at forward speed. *International Shipbuilding Progress*, 34(389):189–196, 1987.

[103] G. X. Wu and R. Eatock-Taylor. The hydrodynamic force on an oscillating ship with low forward speed. *Journal of Fluid Mechanics*, 211:333–353, 1990.

[104] H.K. Ye and C.C. Hsiung. Time-domain motion computations of twin- and monohull ships in head seas. *International Shipbuilding Progress*, 46:91–123, 1999.

[105] V. Zardi. A study on the influence of angle of entrance on the added resistance in waves and seakeeping performance of sailing yachts. MSc Thesis, University of Southampton, 2000.